

LBL-7811

SOME ANALYTIC MODELS OF PASSIVE SOLAR BUILDING PERFORMANCE:  
A THEORETICAL APPROACH TO THE DESIGN OF ENERGY-CONSERVING BUILDINGS

Copyright © 1978

by

David B. Goldstein

Energy and Environment Division  
Lawrence Berkeley Laboratory  
University of California  
Berkeley, California 94720

The United States Department of Energy has the right to use this report for any purpose whatsoever including the right to reproduce all or any part thereof.

## TABLE OF CONTENTS

Foreword . . . . .	.iii
List of Symbols . . . . .	vi
1. INTRODUCTION: ENERGY CONSERVATION IN BUILDINGS AND ANALYTIC MODELING . . . . .	1
Footnotes to Section 1 . . . . .	12
Figures for Section 1 . . . . .	14
2. PASSIVE SOLAR BUILDING MODELS . . . . .	18
2.1 Introduction . . . . .	18
2.2 The Passive Solar Building Model: The Basic Equations and Their Interpretation . . . . .	24
2.2.1 Heat Balance Equations . . . . .	25
2.2.2 Distributed Parameter Description . . . . .	28
2.2.3 Lumped Parameter Description . . . . .	29
2.2.4 Solution of the Equations . . . . .	31
2.2.5 Interpretation of the Equations . . . . .	33
2.3 Solution of the Lumped Parameter Model . . . . .	43
2.4 Solution of the Distributed Parameter Model . . . . .	49
2.4.1 Weather Response . . . . .	54
2.5 Evaluation of the Lumped Parameters . . . . .	59
2.6 Summary and Conclusions . . . . .	67
Footnotes to Section 2 . . . . .	69
Tables to Section 2 . . . . .	75
Figures for Section 2 . . . . .	93
3. EXPERIMENTAL VALIDATION OF THE MODELS . . . . .	104
3.1 Introduction and Overview of Results . . . . .	104
3.2 Determination of the Heat Capacity of LASL Concrete . . . . .	108

3.3	The Direct Gain Cell Comparisons . . . . .	120
3.3.1	Direct gain cell description . . . . .	120
3.3.2	Weather parameterization . . . . .	125
3.3.3	Constant weather experiment of 24 February 1978 .	128
3.3.4	Distributed parameter model . . . . .	133
3.3.5	Varying weather experiment of 8 March 1978, direct gain cell . . . . .	135
3.3.6	2½ week historic weather experiment . . . . .	139
3.4	Experiments on the LASL Trombe Wall Cell . . . . .	142
3.4.1	Trombe wall cell description . . . . .	142
3.4.2	Experimental results for 24 February 1978 . . . .	146
3.4.3	Weather variations: results for 8 March 1978 . .	150
3.5	The Sonoma House Model . . . . .	154
3.6	Conclusions . . . . .	172
	Footnotes to Section 3 . . . . .	173
	Tables for Section 3 . . . . .	175
	Figures for Section 3 . . . . .	189
4.	OVERALL SUMMARY . . . . .	203
	References . . . . .	206
	APPENDIX 2.3: The Lumped Parameter Model . . . . .	210
	APPENDIX 2.4: The Distributed Parameter Model . . . . .	237
	APPENDIX 2.5A: Evaluation of the Lumped Parameters . . . . .	271
	APPENDIX 2.5B: A Comparison Between an Exact Solution and Its Lumped Parameter Representation . . . . .	318

## FOREWORD

This paper describes an application of the fundamental methods of physics to solve a problem of environmental and economic interest: the description of the thermal performance of passive solar buildings. Such a description is of great practical interest to building designers; however, this paper is not intended to be of use to architects and engineers in its present form. Its intention is to provide a theoretical basis for understanding passive solar buildings; further effort is needed to develop rules of solar engineering.

The reader of this paper is assumed to have a background in physics and its application to buildings. Since building physicists have not yet developed analytic models of general applicability, this paper must derive its equations from first principles. This has resulted in a lengthy exposition. Because of the length, I have attempted to summarize the results of Section 2 early in the section. This summary is meant only as a guide to the reader, and so it presents many of its statements without proof or full explanation. More complete derivations are found later in the paper.

The passive solar problem has been of interest to physicists for several years. It was discussed in detail in the American Physical Society's summer study on efficient uses of energy (Ref. 1). Both of my advisors on this project (Prof. Sam Berman and Prof. Art Rosenfeld) were involved in the summer study and are highly interested in passive solar. Working with them provided many opportunities to look at passive solar buildings in more analytical detail.

Several approaches to modeling buildings were underway at Lawrence Berkeley Laboratory when I began work on this paper. Art Rosenfeld had developed a building model called TWOZONE which was intended to study the effect of south-facing windows on heating loads, while Sam Berman and Prof. Bob Richardson of New York University were working on analytic approaches to the study of thermostated furnace performance. My initial work with them led to this project.

In addition, the problem of passive solar heating arose in the context of the California residential energy-conservation building code. The 1975 code restricted windows to 20% of floor area, which would have severely discouraged passive solar building construction. Attempting to find conditions under which more glass could be allowed pointed out the lack of understanding of heat transfers in passive solar buildings, and suggested the approaches which are developed in this paper.

A number of people provided assistance and encouragement during the course of this project; I can only mention a few here. Stan Keniston worked with me on the California building code problem; this work provided some of the impetus to start on this project. Robert Sonderegger, now at LBL, has also been studying simplified building models; his work on a different form of lumped parameters was helpful in my research. Robert Clear discussed analytic building models with me during the earliest and most difficult part of this project, and helped to clarify the conceptual basis for these analytic models. Bob Richardson, in addition to his complementary work on analytic building models, read the earlier, less comprehensible versions of this write-up and helped me translate them into their present semblance of English. However, all present short-

comings in that regard remain the responsibility of the author.

I would like to thank Bob McFarland and Doug Balcomb of Los Alamos for the data they provided on their test buildings. There is a dearth of good hourly data on free-floating passive solar buildings; the LASL group has the only reliable and complete set of data I was able to find. I am also grateful to the Technical Information people at LBL for their help in the production of this paper from the original handwritten text and scrawled figures. Paula Bjork took responsibility for the typing with some assistance from Deberah Craig. Drawings were done by Antoinette Czerwinski.

Members of my thesis committee, Profs. Owen Chamberlain and John P. Holdren, supplied thoughtful comments on the content and exposition of this paper, which have been incorporated into its present form.

Finally, some mention is needed of the larger community of Berkeley. This community has been supportive of creativity and intellectual freedom throughout the nine years I have spent here; the feelings of acceptance and freedom that I have experienced were a crucial ingredient in the accomplishment of this project and others.

## LIST OF SYMBOLS

$A_x$ , $x = e, f, p, w$ :	area of a material surface
$A(\omega)$ :	a building response function
A (subscript) :	ambient
$B(\omega)$ :	a building response function
C :	heat capacity of a material
$\bar{C}$ :	heat capacity per unit area
$C(\omega)$ :	a building response function
H :	heater output
K :	thermal conductivity
N :	number of heavy materials in a building
Q :	heat flow
R :	thermal resistance
$R_1, R_2$ :	materials response functions
R (subscript) :	room
S :	solar gain
T :	temperature
T (subscript) :	Trombe wall
U :	heat transfer coefficient
$\hat{U}$ :	heat transfer coefficient times area
a (subscript) :	front surface of Trombe wall
$c_p$ :	heat capacity per unit mass (constant pressure)
c (subscript) :	Trombe wall air channel; also concrete (Sec. 3) or carpet (Appendix 2.5A and Table 2.3), or continuum model (Sec. 2.5)
d :	thickness of a material

$d_n$ :	Fourier expansion coefficients of the diurnal solar gain function
$d$ (subscript) :	day
$e$ (subscript) :	envelope walls
$f$ (subscript) :	floor
$h$ :	film heat transfer coefficient
$\hat{h}$ :	film heat transfer coefficient times area
$i$ :	imaginary number ( $\sqrt{-1}$ )
$i$ (subscript) :	inside of material (room side)
$j$ (subscript) :	indexing subscript
$k$ :	extinction coefficient
$\ell$ (subscript) :	lumped model
$n$ (subscript) :	night, also an index for summation
$o$ (subscript) :	outside of material
$p_n$ :	$n^{\text{th}}$ pole of a function
$p$ (subscript) :	partition wall
$q$ (subscript) :	quick
$r$ (subscript) :	thermal resistance
$s$ (subscript) :	surface
$t$ :	time
$t_d$ :	the time at which the building ceases to collect solar energy for the day
$t$ (subscript) :	thermostat
$w$ (subscript) :	wall; also weather-frequency
$x, y, z$ :	distance into a material
$z_n$ :	$n^{\text{th}}$ zero of a function
$\alpha$ :	fraction of solar gain absorbed on a given surface

$\bar{\alpha}$ :	flux of $\alpha$
$\Lambda, \lambda$ :	time constants
$\Lambda_1, \Lambda_2$ :	primary decay constants for a building
$\xi$ :	dimensionless distance into a material
$\rho$ :	mass density
$\Sigma$ :	an equivalent heat transfer coefficient
$\chi$ :	material response function for the lumped parameter model
$\omega$ :	frequency
$\omega_0$ :	the frequency $2\pi$ radians per 24 hours
$\omega_1$ :	the frequency of the solar gain function

## 1. INTRODUCTION

Energy is used in a wide variety of ways in the developed world, but in almost all its uses, the desired result is the accomplishment of some non-energy-related task. The physicist's approach to analyzing patterns of energy consumption has been to compare the energy requirements of present technologies or devices for accomplishing a task with the theoretical limits to energy use. This method reveals where present processes are inefficient and can suggest where new ideas might be sought.

Analysis of energy uses in the United States economy shows that almost all tasks that use significant amounts of energy are done very inefficiently, both thermodynamically and economically. The American Physical Society study on efficient energy use (Ref. 1) found that most processes have second-law efficiencies of 10% or less. Our research at Lawrence Berkeley Laboratory has shown more detailed examples of energy waste; we have never found any process for which the life cycle costs of energy use have been minimized. That is, in all tasks we have studied, the economic return on an additional investment in energy conservation (beyond existing practice) would have been justified at existing energy prices and interest rates.

To illustrate the conservation potential implied by present inefficiencies, we display in reference 22 a list of several dozen conservation measures all of which have acceptably large returns on investment which would, taken as a whole, save 25% of California's gas and electricity use in ten years. Collectively, they have an

annual return on investment of 40%. Most of these measures would have been economic at pre-1973 low energy prices, but to date very few of them have been implemented on a wide scale.

As an example, we note that in 1970, a typical owner of a new home in Northern California could have saved about \$50 a year on his heating bill by insulating his walls, while the cost of this improvement would have been \$125.<sup>1</sup> Despite this large return, very few new houses had insulated walls in California until 1975 when they were required by law. In similar fashion, the efficiency of other large energy users — home air conditioners and commercial chillers, refrigerators, lighting equipment, hot-water users, etc. — could be improved by a large amount (typically a factor of two) by readily available cost-effective conservation measures.

The study of energy-efficient methods to accomplish tasks is most easily organized by end-use ( e.g. space heating, refrigeration, etc.). As an example, we show in Fig. 1 the apportionment of California energy among residential end uses, as derived from Ref. 23. Residential electricity is about 40% of total electric consumption in California; residential gas is about one-third of the total for that fuel.

As illustrated in Fig. 1, energy consumption is divided among a number of relatively important end uses. Although some uses are larger than others, no single end use dominates the residential sector. So if one is interested in making large savings in overall energy requirements (or in reducing growth in energy use), conservation strategies must be studied for a variety of end uses.

Different strategies are applicable for different uses and for different time scales. In the short run, the properties of energy using equipment are fixed and one can save energy only by better management (e.g. turning off lights in unoccupied offices or rooms) or by changes in habit or comfort (such as turning down thermostats at night). These changes generally result in relatively small savings unless the operation was grossly mismanaged in the first place.

In the longer run, retrofits of existing equipment can be attempted, such as insulating the ceiling or walls of originally uninsulated structures. This process is more costly than it would be for new construction, but the savings can be large: 30% of original energy use for ceiling insulation and another 30% for walls, based on computer simulation of northern California climates.<sup>2</sup>

On a similar time-scale, replacement of appliances with the more efficient models currently on the market can save 40% or more of existing energy needs.<sup>3</sup> New buildings can be constructed in more energy-efficient ways. Mandatory efficiency standards in California will lead to a savings of 15% or more for commercial buildings<sup>4</sup> and as much as 60% for residential buildings.<sup>5</sup>

Over a longer time period, more fundamental design changes can be made. One recent study of refrigerator redesigns estimated potential savings of 2/3 through a few relatively simple and high-payback improvements.<sup>6</sup> The effects of adding some more advanced insulation measures for houses are shown in Fig. 2, which graphs space heating needs as a function of conservation expenditures for

Sacramento and Chicago climates. Although many of the measures are cost-effective in Sacramento only under the assumption of high future costs of gas, almost all the measures pay for themselves in Chicago.

Figure 2 raises some interesting questions, which we will discuss at length. Figure 2a on the Sacramento house shows that a sufficiently tight building requires essentially no heat at all. In other words, the accidental heat gains from sunshine and appliances balance the heat losses almost all the time. At some point one could substitute an occasional tolerance to cooler temperatures or more solar heating for one of the insulation steps and reduce costs, provided one could predict the results of the step.

Figure 2b on the Chicago house shows a potential reduction of heat load to 120 therms ( $120 \times 10^5$  Btu or  $12.7 \times 10^9$  Joules); this compares to more typical heat loads for that area of over 1000 therms. But further reductions in heat loss would tend to be less cost-effective than the measures described in the figure.

For both of these climates, the next step in the analysis would be to look at possible savings in heat load through the increased use of solar heat gains. As we have mentioned, the collection of sunlight through the windows is already contributing towards reducing the furnace load in both houses. Increasing the window area might further reduce space heat needs in Chicago, or lessen the requirements for insulation in Sacramento.

The trouble with this path of inquiry is that most present methods of modeling buildings are incapable of treating structures with large solar gain. Although the state-of-the-art building models

treat quite precisely the heat transfers driven by temperature differences, their treatment of solar gains is much more approximate.

In a real building, some fraction of sunlight incident on a window is transmitted into the interior. The direct beam component first strikes the floor or a piece of furniture, or perhaps an interior partition wall. Depending on the properties of the receiving surface, some portion of the energy is absorbed, and the rest is reflected. The reflected light, plus the diffuse sunshine from the window, strikes other surfaces in the room, is re-reflected, etc. Eventually all the sunshine is absorbed on some surface.

If the building models treated solar gain in detail, they would use their calculations of solar position in the sky to find the directly illuminated area within the building, and calculate solar absorption for each area of interior surface for each hour. They would then use these solar heat gains in calculating surface temperature for different sections of each material.

In fact, the current treatment of solar gains is highly simplified compared to this description. The U.S. National Bureau of Standards computer program NBSLD (Ref. 11) assumes that solar gain from a window is absorbed uniformly over all interior surfaces (floor, ceiling, etc.) for all hours of the day.<sup>8</sup> The Lawrence Berkeley Laboratory program DOE-1 (Cal/ERDA) (Ref. 18) is designed to simulate building model results in which the average solar gain for each surface is adjusted to be consistent with the exact modeling described above for only one specific hour and one specific building geometry and one set of surface reflectances. Only the thermal mass of the room is varied. Weighting factors are used to calibrate DOE-1 to these runs for light, medium, or heavy-weight

buildings. These three sets of weighting factors, which are appropriate for an office building with south-facing windows during the summer, are used to model the building response to all solar gains through all windows during all seasons.

While these simplifications are probably adequate for a building with relatively small solar gains (small in comparison with conduction losses or internal loads), they break down for passive solar buildings with large window areas.<sup>7</sup> So the greater the use of solar-collecting windows to design energy-conserving buildings, the more inadequate present building models become.

Furthermore, the response of the building varies greatly depending on the habits of the occupants. In Fig. 3 we plot temperature, both inside and outside the house, furnace output, and thermostat set points as a function of time for the first four days in January in Chicago. It describes the response of the best-insulated house at the right of Fig. 2. Notice that on day 1 and day 4, the furnace shuts off when the sun is out, even though ambient temperatures are below 21°F (-6°C) at all times. On day 4, the sun heats the house up from the thermostat setpoint of 70°F (21.1°C) to 76°F (24.4°C) during the afternoon. As window areas increase from the assumed 20% of wall area used in generating this figure to 40% or even 80%, further heating may occur.

Whether the house overheats or whether it stays within a comfortable range depends both on the heat storage ability of the house and on the thermal preferences of the occupants. For example, if the house is allowed to cool off more during the night, it can

store more solar heat before it reaches an unacceptably hot temperature the next day. This results in a tradeoff between comfort and amount of solar energy stored. Such tradeoffs are difficult to treat in general because one cannot measure comfort in units which are comparable to heat or cost. They can be treated in an individual way by a resident about to construct or buy a house, but only if he can understand the thermal performance of the building in advance.

### Outline

The rest of this paper is devoted to the derivation of an analytic model of building performance which can be used to develop an understanding of building response. Extensions and amplifications of this model can probably be developed as a design tool for new or retrofit buildings. The model is developed with the idea of describing buildings like the one discussed in Fig. 3 with large solar gain and tight insulation, but the theory should be generally applicable.

Section 2 describes the central equations and assumptions used in the model, and gives the solutions to a lumped-parameter and a distributed-parameter model. The derivations are performed in detail in a set of appendices whose numbers (2.3, 2.4, etc.) correspond to their analogous parts of Sec. 2.

Section 3 describes some experimental tests of the relationships derived in Sec. 2. Using data from the test buildings at Los Alamos Scientific Laboratory (LASL), we compute model response and compare it to measurements. Agreement between the data and the predictions is good.

The model described in this paper is self-contained and analytic — that is, it proceeds from fundamental laws of physics to its solution through analytic, as opposed to numerical, methods. All parameters used can be derived from physical data on materials properties or from weather data. Since numerical approaches are not needed, the calculations can be performed with pencil and paper and a hand calculator or slide rule.

Analytic models are not common in the building science literature. In fact, dynamic models as a whole are a relatively new development. Present building models are based on the concept of response factors, which describe the response of a component in a building (e.g., a wall surface temperature) at a time 't' in terms of temperatures at earlier times  $t$ ,  $t-\Delta t$ ,  $t-2\Delta t$ , ... (where  $\Delta t$  is usually taken to be one hour) multiplied by response factors for that hour. The response factors were first derived by modelling a slab of material as a chain of resistances and heat capacities in series. Currently, response factors are derived from numerically inverse-Laplace-transforming solutions to the diffusion equation.

Because of the amount of computation required to derive the response factors and then to solve the time series in which they appear for each hour and for each building component, response factor models are always handled on large computers. One side-effect of the computerization is that the models tend to function as a "black box". Since the effects of various elements of the building and of weather conditions are added together numerically,

there is no way to determine *a priori* which factors are responsible for the major features of a building's performance and which ones are unimportant. In addition, any errors in the model or approximations which are not accurate for a particular situation cannot readily be seen unless the model starts giving absurd results. One loses physical intuition in such an approach; the only way to find out what is really going on in the model is to make a large number of parametric runs, varying parameters which the modeller guesses will be important.

An analytic model, in contrast, will often show by its structure or the form of its equations which effects are dominant. For example, the distributed parameter model of Sec. 2.4 gives the response of room temperature in terms of relatively simple functions; the form of the key equation provides some insight into the expected results.

Also, a simple model of a building allows the determination of some of the parameters experimentally using a comparatively simple setup. Some of the linearities that show up in Sec. 2 can be exploited in reducing experimental complexity. In Sec. 3, we average over some large areas to obtain interesting theory vs. experiment comparisons with only a few measurements.

However, the models derived in this paper have more limitations than the computer models. The description of the building must be more elementary, and the response to complicated management schemes and even normal thermostatic control of a furnace cannot be handled. But, one can learn a lot about the heating and cooling needs

of a building by studying how its room temperature responds to solar and temperature inputs. Also, the intuition gained by studying the analytic models can be applied to writing better computer simulations. The mathematical formulation of the two types of model is parallel, so that understanding gained from studying the analytic model can be applied straightforwardly to improving the computer models. For example, programs like DOE-1(Cal-ERDA) currently model buildings by first computing heating and cooling energy needed to maintain a fixed thermostat setting, and then calculating the results for varying thermostats (e.g. night temperature setback) as a perturbation. The analytic models in Sec. 2 and 3 describe the response of a house which has freely floating temperature at all times. Application of this model to some well-insulated buildings shows that very little heating or cooling will be required for "typical" weather conditions. For more extreme weather, some climate control will be needed. But it will probably be more efficient to model the heating and cooling loads as perturbations to the floating-temperature solution, rather than vice versa.

Both analytic and computer-oriented passive solar building models are likely to be useful as tools in designing more efficient buildings.

The analytic methods are more suitable for designing simple buildings for a desired response to a design day, and perhaps for equipment sizing. As we have mentioned, they are also useful in developing a feel for how the building works. Computer models are more practical for estimating annual energy use, which can be employed in making economic tradeoffs, and for modelling complicated structures.

There is a large need for such improved modelling; very few new buildings are taking advantage of passive techniques, in part because of the lack of proven design rules.

Passive solar modelling is worthwhile as a tool for implementing one important conservative strategy — the use of building design to take advantage of "free" energy from the environment. As only one element of good energy-conserving design, it cannot be credited with a fixed or definable energy savings potential. However, the whole range of building energy strategies can reduce space-heating use to near zero, eliminating one of the major causes of energy demand.

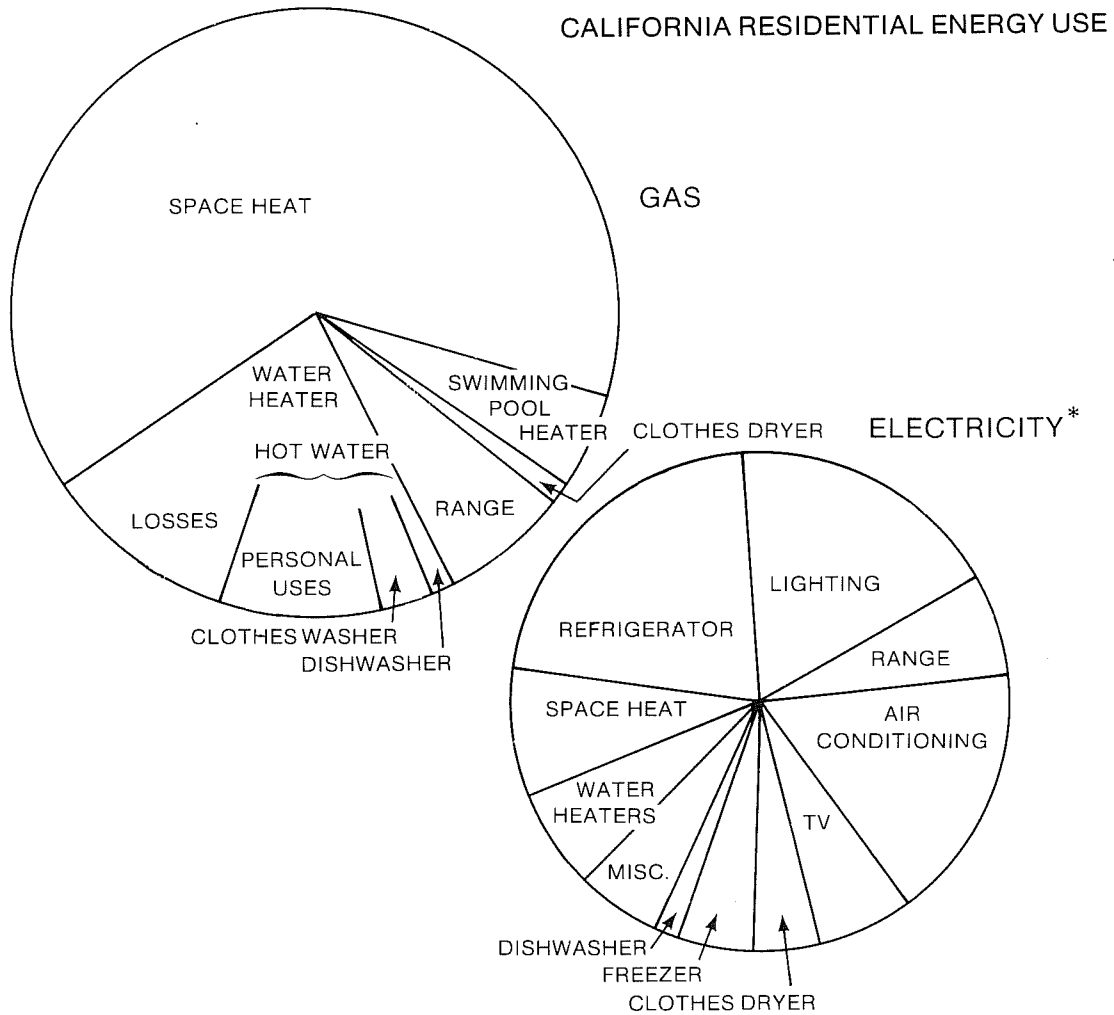
Section 1 Footnotes

1. We use the TWOZONE runs of Ref. 8 to predict heating energy savings for insulating the walls of a typical 1450 ft<sup>2</sup> single-floor house which is assumed to have ceiling insulation (R-19) already installed. At 1970 prices of 10¢ a therm (therm = 10<sup>5</sup> Btu) for natural gas fuel, the savings are about \$50 per year. We estimate costs for installing insulation in the walls of a new house from Means (Ref. 27) to be about 13¢ a square foot. The reference house has a wall area of about 1000 ft.<sup>2</sup> resulting in an extra cost of \$130.
2. Precise estimates of energy use before and after retrofit are found in Ref. 8. This modelling effort is based on the Oakland, California, climate, but runs for other California cities show similar percentage savings. Observation by California utilities have found energy savings of about 25% on the average for attic retrofits.
3. The 40% savings refers to the use of the most efficient existing refrigerator in each size and features class instead of a unit of average efficiency. Larger savings are possible by changing features, e.g. by switching from a fully automatic defrost system to a partial automatic defrost, or from a side-by-side style to a top-freezer arrangement.
4. The commercial building standards in California are formulated in terms of maximum lighting power levels or maximum annual energy use per unit area. Compliance with the code will result

Section 1 Footnotes (cont.)

in buildings which use 15% less energy than the average new building, based on simulations using DOE-1 (Ca1-ERDA) (see Ref. 18). However, some buildings will use less energy than the legal maximum (some already do), so actual savings will be much larger than 15%.

5. The 60% savings are for northern California climates where, in 1979, double glazed windows will be required. A double-glazed, insulated house uses 60% less heat than a pre-standards house with only attic insulation, according to Ref. 8.
6. The refrigerator study is listed as Ref. 26; its significance for overall patterns of energy demand is discussed in Ref. 24.
7. Personal communication, G. P. Mitalas, 4 July 1978.
8. Some recent versions of NBSLD allow the user to specify how much solar heat is absorbed on each surface. However, solar heat absorption on partition walls cannot be simulated.



\*Electricity converted to Resource Energy at 11,000 Btu/kWh

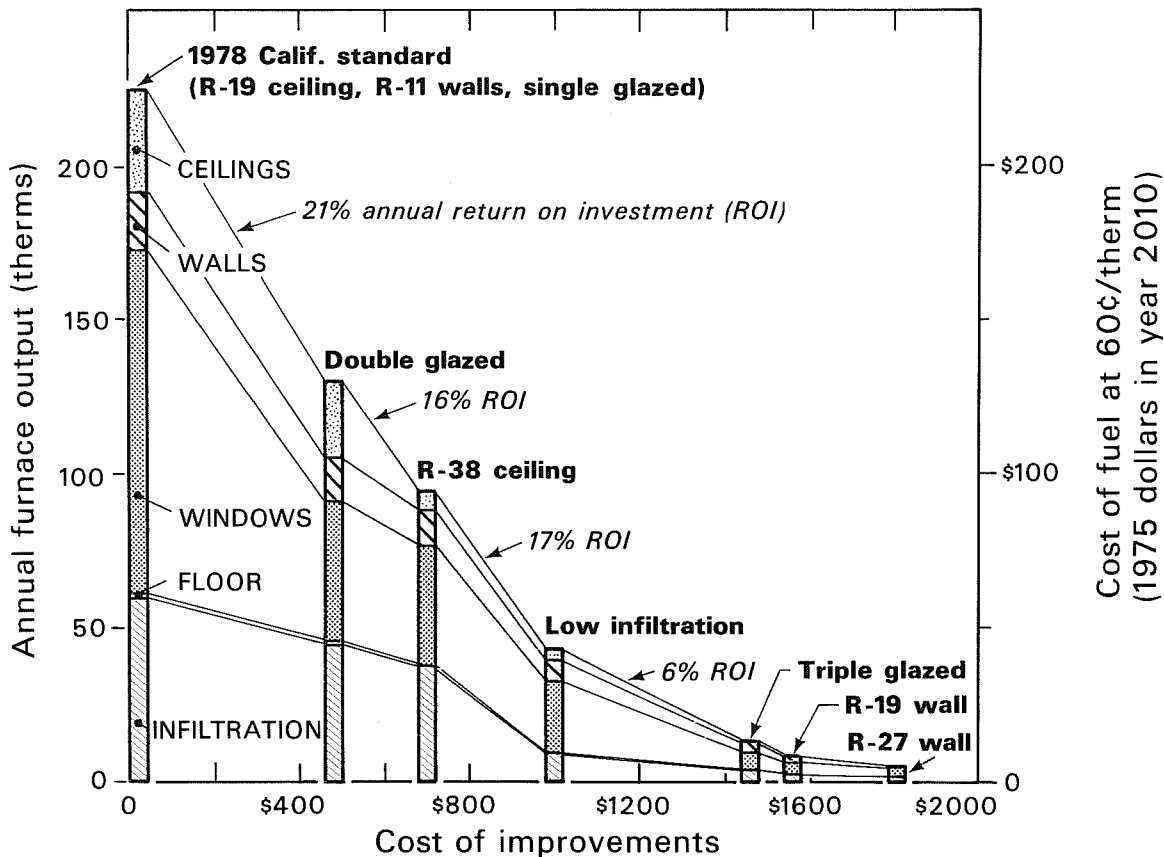
Sources:

"Electrical Energy use in California: Data Collection and Analysis", LBL Staff, UCID-3847

"Energy Extension in California, Context and Potential Impact", P. Craig, D. Goldstein, R. Kukula, A. Rosenfeld, LBL-5236

XBL 774-703B

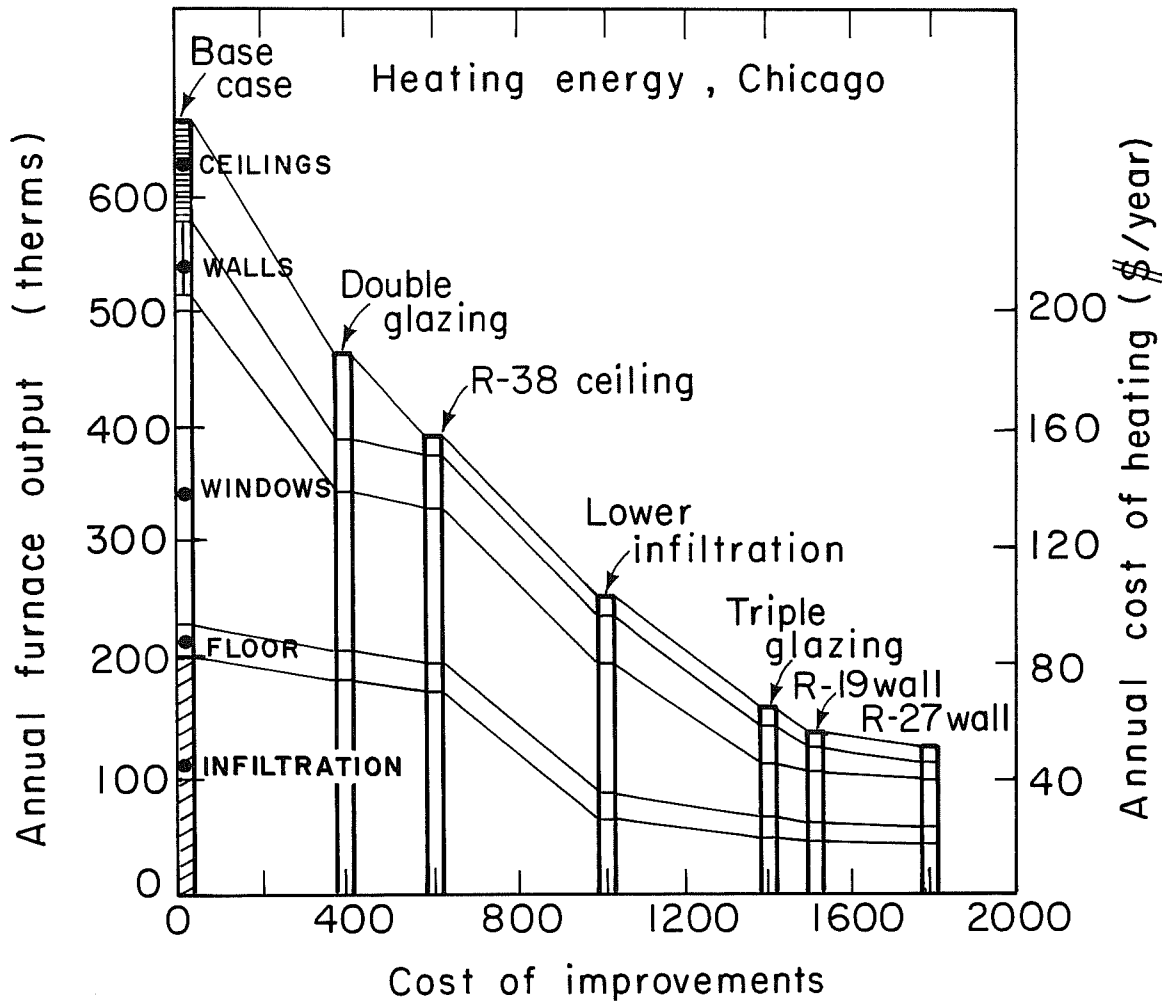
Fig. 1. Apportionment of California residential energy use among the major end-uses. Data are for the year 1975. Electricity is equated to resource energy using the conversion 11,000 Btu = 1 kWhr (31.0% efficiency) to account for average power plant efficiencies and transmission losses; except that air conditioner electricity is converted at 20,000 Btu/kWhr (17.1%) because of the lower efficiency of peaking power plants (e.g. gas turbines).



XBL 784-767

Figure 2 (A)  
Heating loads calculated for Sacramento

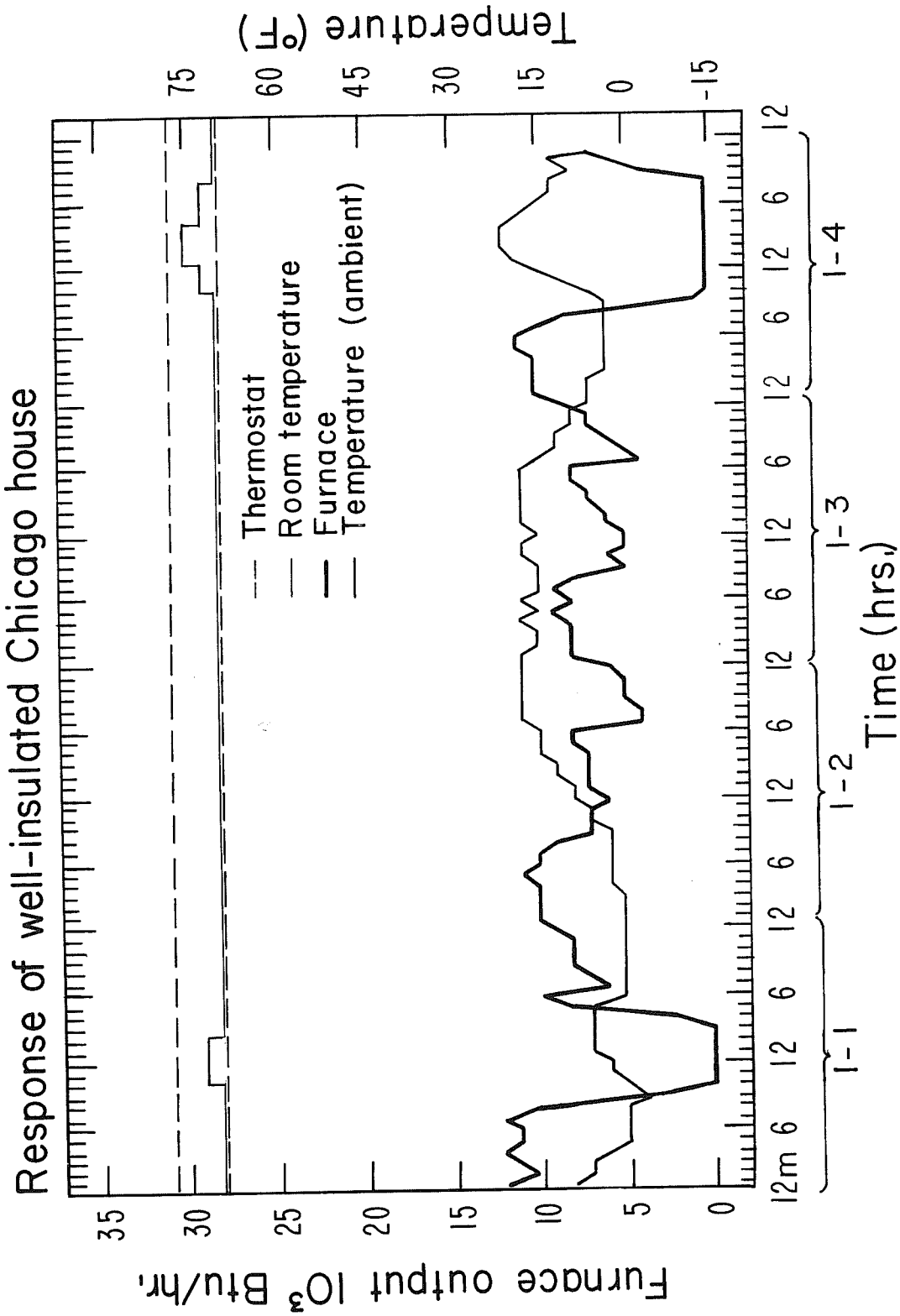
Fig. 2. Heating energy use for a new house as a function of expenditure on insulation. Heating loads are calculated for Sacramento (Fig. 2A) and Chicago (Fig. 2B). The bar at the left illustrates a house insulated with R-19 ceiling insulation, R-11 wall insulation, R-19 floor insulation, and with single-pane windows. The bar is divided into segments labelled "ceiling, walls", etc. to indicate which part of the house is responsible for what fraction of heating energy. The next bars progressively add insulation measures such as double-glazing, better sealing for lower air infiltration, etc. The right-hand scale gives the annual cost of heating; it is equal to heat load (left scale) divided by the furnace efficiency of 60% and multiplied by the cost of fuel. For Sacramento we use future fuel prices of 60¢ per therm (see Ref. 24); for Chicago we assume present fuel prices of 25¢ per therm. The heating loads were computed using TWOZONE (Ref. 8).



XBL 788-1468

Figure 2 (B).

Heating loads calculated for Chicago



XBL 789-11389

Fig. 3. Predicted furnace load as a function of time (hours) for the Chicago house at the right of Fig. 2b, for the first four days in January. We also display outside temperature, thermostat settings of  $70^{\circ}$ F for heating and  $78^{\circ}$ F to open the windows, and inside room temperature. This figure was generated by TWOZONE (Ref. 8).

## 2. PASSIVE SOLAR BUILDING MODELS

### 2.1 Introduction

Passive solar buildings are structures whose natural response to ambient sunlight and temperature conditions produces room temperatures which are within the comfort range of the building's occupants. An ideal passive solar building requires no heating or cooling at all; real passive buildings may require small amounts of climate control or may approach the ideal. Numerous ideas have been presented for the conceptual design of such buildings; the most easily understood schemes involve collecting sunlight through south facing windows.

Although windows are large sources of heat loss due to their high heat conductance, south-facing windows can collect more heat from sunlight than they lose by conduction over the course of the winter.<sup>1,2</sup> If all this heat can be used, increasing the amount of south-facing windows will reduce the amount of energy needed to heat the building.

A number of passive solar houses have been built over the past five years;<sup>3</sup> some of them are completely heated by sunlight. One example of passive solar construction is shown in Fig. 1. However, the design of most of these buildings is based on *ad hoc* rules of thumb or the intuition of the builder. These methods appear to work in many cases, but there are also many (poorly documented) failures. For example, one attempted passive solar house regularly heated up beyond 95°F (35°C) on sunny winter days and then rapidly cooled to uncomfortably low temperatures at night.<sup>22</sup>

Even the successful passive solar buildings cannot be considered to be optimal designs. For example, the Kelbaugh house in New Jersey

underwent several retrofits after the first winter to mitigate problems observed by its occupants.<sup>21</sup> Several other passive structures have required similar modification. This iterative approach is more costly than installing all the needed features during construction. Conversely, many passive houses have performed much better than expected. This, too, may be a problem if it results in oversizing the heating and cooling equipment. Additionally, the possibility that the building may not work "as planned" is a deterrent to the widespread application of passive solar designs.

To design a predictably well-performing passive building requires the use of an accurate model predicting building response, as well as an intuitive understanding of the heat transfers which are responsible for this performance. To this end, we present in this section a simple analytic model for calculating passive solar building response. The emphasis is on scientific clarity and simplicity. While it is our intent that the model be developed into a design tool for architects and building designers, in its present form it is not suitable for general use.

This model is most easily used to calculate "floating" or non-thermostated room temperature as a function of the driving forces of solar energy gain, ambient (outside air) temperature, and heater output (or internal heat generation from lights, appliances, etc.) It can also be used to calculate heater output needed to maintain a fixed room temperature, but this solution is generally of less interest. The mixed mode, in which room temperature floats between fixed thermostat positions, is much messier to handle and is not discussed in this paper.

Studying the floating temperature response of a room to different weather conditions can provide insight into the important parameters affecting building performance, and can suggest how to choose optimal values of building parameters to get a desired response.

Our model is developed from the basic equations of heat transfer and proceeds by analytic (as opposed to numerical) methods to the final form of the solution. Evaluation of a solution can be performed with a pencil and paper and hand calculator or slide rule; this is typically a one-hour operation with a 98-step programmable calculator, or 15 minutes with a card-reading calculator.

The central equations are heat balances for interior building surfaces (on which sunlight is absorbed) and conduction and diffusion equations for heat transfers through materials.

Our model parallels many computer models in terms of its basic equations; however, it differs in two significant ways. *First*, it solves the room heat balance algebraically, producing equations for room temperature in terms of building parameters and driving forces. In contrast, computer models solve the equations of heat transfer for each element of the building to produce sets of time series. The time series are added numerically yielding numerical expressions for the relationships between room temperature and the other weather variables. This type of expression tends to obscure the parametric dependences.

*Second*, while the computer models handle thermal radiation very precisely, they handle visible radiation (sunlight) in a very crude fashion. Typically, sunlight is assumed to be absorbed uniformly over

all interior surfaces in the room.<sup>16</sup> In contrast, our model allows the user to specify varying proportions of solar absorption on each surface (e.g. more sunlight absorbed on one wall than on another) or in the room air. This option makes a substantial difference in thermal response, as shown in Fig. 2.

Figure 2 graphs the room temperature of a passive solar building with wood frame walls and concrete floor under four sets of assumptions about solar energy absorption. The solid line labelled 'A' gives room temperature as a function of time for the case in which  $6/7$  of the sunlight is absorbed on the floor and  $1/7$  is absorbed on the walls and ceiling. Line 'B' describes the same house with only  $5/7$  of the sunlight absorbed on the floor and  $2/7$  on the walls; while in case 'C'  $3/7$  of the sunlight is absorbed on the floor and  $4/7$  on the walls. The dotted line labelled 'D' graphs the case in which all the sunlight is absorbed on light furniture or carpets.

As show in the figure, there is a noticeable difference between the four curves; this difference illustrates the importance of being able to specify where solar energy is absorbed. Any model which does not allow this specification (or calculate it) implicitly assumes that one of these curves is always correct.

The importance of correctly modelling where solar energy is absorbed comes about because the response of a passive solar building involves considerable amounts of heat storage. The quantity of heat stored by a building depends strongly on the heat capacity ("thermal mass") of the materials exposed to direct sunlight, (along with other properties). It is clear from the figure that solar absorption on surfaces of materials

with large thermal mass (such as concrete, water, brick, etc.) results in lower daily room temperature fluctuations; this result is also predicted by other theoretical work<sup>3a</sup> and has been observed in the field. One of the rules of thumb of passive solar design is to locate thermal mass so that it is exposed to direct sunlight; this rule is reflected in the Davis, California energy conservation building code.<sup>4</sup> However, this rule is only qualitative; there are no demonstrated relationships between amount of thermal mass used or degree of direct exposure to sunlight and the building response. Use of a simple building model may be helpful in the quantification of such rules.

Although much effort has gone into studying thermal response by numerical methods, simple analytic models for building performance are not often used. Sonderegger (Ref. 9) discusses building models using equivalent thermal parameters; although the model itself is simple and transparent, the analysis and the evaluation of the parameters is done numerically. Niles (Ref. 10) also looks at simple models to describe a specific passive solar house. But virtually all the rest of the modelling effort has gone into numerical simulations of building response,<sup>23</sup> usually response to historic weather.

In contrast, our model treats the response of buildings to idealized weather, such as typical sunny or cloudy days, or weather cycles of cloudy days following sunny days. This approach is useful in developing an understanding of the important parameters affecting the building response, and those which are not as significant. Since the form of our model parallels the computer models, improvements in the apportionment of solar energy among the various interior surfaces

can be studied using the simple model to determine which effects are significant enough to include in a revised computer model. For example, if it turns out that changing the solar radiation balance each hour as the sun moves across the sky does not strongly affect thermal response, then this feature need not appear in the computer models.

A simple model can also be used to decide what criteria to use in optimizing the thermal response of a building. As we will show, a building designed to minimize fluctuations in room temperature without heat input will be quite different from one designed to minimize annual energy use under fixed-thermostat conditions. When the various indices of thermal "quality" in a building disagree, a greater degree of understanding is needed to choose among alternate designs; a simple model can provide more insight into the physical process being modeled.

We now proceed to the derivation of the model. We will first present in Sec. 2.2 the basic equations of motion for the heat transfers within the building. These equations are developed along parallel paths for a "lumped-parameter" model and a "distributed-parameter" model. Next we will discuss the motivation for using each form of equation, and what the consequences and implications of the equations are. Finally, we solve the equations for the lumped parameter model in Sec. 2.3, and then for the distributed parameter or continuum model in Sec. 2.4. Comparisons between the lumped parameter and distributed parameter models are discussed in Sec. 2.5. The solution is sketched out in the text and redone with more technical detail in the appendices.

## 2.2 The Passive Solar Building Model: The Basic Equations and Their Interpretation

In this section we first describe very briefly the passive solar building to be modeled. We next present the basic equations of heat transfer for a passive solar building, without detailed explanation. Following this presentation, we will discuss some of the assumptions and consequences of these equations. Solution of the equations will be discussed in Sections 2.3 and 2.4.

We will consider in this paper passive solar buildings which are designed to make use of the solar energy input through their windows.<sup>4a</sup> The word "passive" is used to indicate that there are no active collector units or heat storage distinct from the structure of the building. (e.g., hot water storage tanks, rock beds, collector panels, etc.) We will study managed buildings (e.g. those with movable insulation panels) and will consider the buildings' response to backup heaters as well as sunlight.

The model has enough generality to describe a number of different designs of passive solar building, including direct gain systems, and Trombe wall<sup>4b</sup> or waterwall systems. The equations can be most easily understood if the reader imagines a direct gain system, that is, an ordinary building with large window area. The building is modeled as a small number of heavy elements, such as concrete floor or brick or solid wood walls, plus some light elements, such as windows, surrounding the room air.

Heat transfers *within* the heavy elements are treated either by a lumped-parameter approach or by a distributed-parameter model. The

lumped parameter approach is an approximation which is useful in describing the response of managed buildings, and in modelling irregular weather patterns. The distributed-parameter solution is more exact, and gives a more elegant solution, but is incapable of modelling managed buildings. Heat transfers through light elements, such as windows, insulation-filled wall cavities, and air leakage ("infiltration") are handled by steady-state methods which only consider inside and outside air temperatures.

We consider the large solar gains through south-facing windows. (Windows facing other directions can also be treated in the model). Sunlight enters the house through the window, and is absorbed, either directly or after one or more reflections, on the surfaces of heavy elements in the room (such as floors, partition walls, and envelope walls). This process is sketched in Fig. 3. This absorbed solar heat warms the room air in the manner described below.

### 2.2.1 Heat Balance Equations

The most central equations in this model are surface heat balances. After sunlight enters a window, it is absorbed on some inside surface (labelled 'j') which heats up to satisfy the following heat balance equation:

$$\hat{h}_j (T_{s_j} - T_R) - \alpha_j S + Q_{in_j} = 0 \quad (1)$$

where  $\hat{h}_j$  is the combined radiation/convection surface film coefficient times the area of the surface (for the  $j^{\text{th}}$  surface) (Btu/hr-°F or W/°C);

$T_{s_j}$  is the surface temperature (°F or °C) of the  $j^{\text{th}}$  surface;

$T_R$  is the room temperature (room *air* temperature) (°F or °C);

$S$  is the solar power entering the room ((Btu/hr) or W);  
 $\alpha_j$  is the fraction of sunlight absorbed on the  $j^{\text{th}}$  surface;  
 $Q_{in,j}$  is the heat transfer into the interior of the material  
from the  $j^{\text{th}}$  surface.

The first term represents the flow of heat from the  $j^{\text{th}}$  surface to the room air, given by a combined radiation/convection film coefficient (times area) multiplied by the temperature difference between the surface and the room air. The term  $-\alpha_j S$  is the heat transferred to the surface because of absorption of sunlight; the minus sign because solar heating is a heat gain while the other terms are losses. The final term is the heat transfer from the surface into the bulk of the material. The form of this term is different in the lumped parameter model and the distributed parameter model.

There are actually  $N$  different equations of the form (1); one for each surface of a heavy material. Note that in these equations we use the nomenclature  $\hat{U}$  or  $\hat{h}$  to denote a heat transfer coefficient or conductance times an area, while  $U$  or  $h$  would represent the usual heat transfer coefficients.

For simplicity, we usually describe the building using only 2 or 3 surfaces; typically we consider the floor, envelope walls, and possibly partition walls. In addition to the surface heat balance, we require a heat balance for the room air. We assume that the air has negligible heat capacity compared to the walls & floor, and divide heat transfers into two classes, quick and delayed. Quick heat transfers occur through pure conductive materials, with negligible heat capacity, such as windows, or through infiltration of outside air. Delayed heat transfers occur through

materials with nontrivial heat capacity, and involve heat transfers from the room to the material surface, and then from the surface through the material. These materials attenuate variations in outside air temperature and delay their influence on the room air. Delayed heat transfers will be discussed shortly; at present they are considered indirectly in the terms  $\hat{h}_j (T_{s_j} - T_R)$  describing heat transfers from the room air to the material surfaces, since the magnitude of  $T_{s_j}$  is determined by the internal heat flows.

The room heat balance is given by:

$$\sum_{j=1}^N \hat{h}_j (T_R - T_{s_j}) + \hat{U}_q (T_R - T_A) = H + \alpha_R S \quad (2)$$

where  $\hat{U}_q$  = heat transfer coefficient (Btu/(hr-°F) or W/°C) for quick heat transfers; the sum of the products of U-values times areas plus infiltration heat losses

$T_A$  = ambient temperature

$H$  = heater output (Btu/hr or W)

$\alpha_R$  = fraction of sunlight absorbed directly into the room air or on light materials

This equation states that the heat losses from the room always equal the heat gains. The first term is the sum of heat losses from the room air to each of the heavy material surfaces which surround it. Note that the surface temperature  $T_{s_j}$  will be influenced by both outside air ("ambient") temperature and sunlight. The second term combines into

a single term the heat losses to surfaces of light materials (including the characteristics of the entire conduction path to the outside), the heat losses through windows, and those due to infiltration of outside air. No other terms are needed, since the room air can lose heat only to solid surfaces or through infiltration. The terms on the right are heat gains; they are the heater output  $H$ , (which also includes the heat generated by lights and appliances), and  $\alpha_R S$ , the fraction of solar gain which is absorbed directly into the room air or on light surfaces such as carpets.  $\alpha_R$  is typically near zero, because most of the sunlight is absorbed on the surface of heavy materials.

To complete the description of the house, we must model the heat flows through heavy materials (those whose heat capacity can't be ignored). These heat flows can be described by either lumped parameter or distributed parameter models.

### 2.2.2 Distributed Parameter Description

In the distributed parameter case, we assume that the  $j^{\text{th}}$  material (wall or floor) is a slab of homogeneous isotropic material described by a conductivity  $K_j$ , a heat capacity  $(\rho C_p)_j$  per unit volume and a temperature distribution  $T_j(x,t)$ . For one-dimensional heat flow, the temperature is given by the solution to the diffusion equation

$$(\rho C_p)_j \frac{\partial T_j(x,t)}{\partial t} = K_j \frac{\partial^2 T_j(x,t)}{\partial x^2} \quad (3)$$

The heat flow from the surface into the material is given by

$$Q_{in_j} = -A_j K_j \left. \frac{\partial T_j(x,t)}{\partial x} \right|_{x=0} \quad (4)$$

where  $A_j$  is the area of the  $j^{\text{th}}$  surface ( $\text{ft}^2$  or  $\text{m}^2$ ). The fundamental solution to the diffusion equation (3) with frequency  $\omega$  can be written as (the real part of)

$$T_j(x,t) = \left( T_j^{(+)} e^{+k_j x} + T_j^{(-)} e^{-k_j x} \right) e^{i\omega t}$$

or

$$\left( T_j^{(c)} \cosh k_j x + T_j^{(s)} \sinh k_j x \right) e^{i\omega t} \tag{5}$$

where 
$$k_j = \sqrt{\frac{i\omega(\rho C_p)_j}{K_j}} = \sqrt{\frac{\omega(\rho C_p)_j}{2K_j}} (1+i)$$

The boundary conditions which determine the amplitudes  $T_j^{(+)}$  and  $T_j^{(-)}$  are the surface heat balance (1) and a condition on the outside surface; usually the condition is that the outside is coupled by a pure resistance to the ambient temperature or "sol-air" temperature.

The result can be visualized by looking at its limiting form for a very thick material. Only the negative sign in the exponential appears, and the solution is in the form of a traveling wave, exponentially damped in space.

The solution (5) assumes a single-layer wall or floor. Extension to two or more layers is straightforward, and is discussed in Appendix 2.4.

### 2.2.3 Lumped Parameter Description

For the lumped parameter case, we approximate the wall or floor as a sandwich of a lumped heat capacity  $C_j$  ( $\text{Btu}/^\circ\text{F}$  or  $\text{Joules}/^\circ\text{C}$ ) surrounded

by a lumped conductance  $\hat{U}_{i,j}$  (Btu/°F-hr or W/°C) on the inside and another lumped conductance  $\hat{U}_{o,j}$  on the outside, as shown in Fig. 4. The values of  $\hat{U}_{i,j}$ ,  $\hat{U}_{o,j}$  and  $C_j$  depend in a complicated way on the conductivity, heat capacity, and thickness of the material, as discussed in Sec. 2.5. The lumped heat capacity is characterized by a single temperature  $T_j$ . All heat transfers in the material are approximated by conductive heat transfers between the lumped heat capacity  $C_j$  and the inside and outside surfaces. The outside surface is taken to be at the ambient air temperature of  $T_A$ . (If the outside film coefficient is nonzero, its effects are incorporated into  $\hat{U}_{o,j}$ , as discussed in Sec. 2.5). The inside surface is at a temperature  $T_{s,j}$ , which is determined from Eq. (1).

Thus, the heat flow from the inside surface into the material,  $Q_{in,j}$ , is given by

$$Q_{in,j} = \hat{U}_{i,j} (T_{s,j} - T_j) \quad (6)$$

The diffusion equation is replaced by a simple differential equation

$$C_j \frac{\partial T_j}{\partial t} - Q_{in,j} + \hat{U}_{o,j} (T_j - T_A) = 0 \quad (7)$$

Equation (7) is simply a statement of conservation of energy: the amount of heat stored per unit time by the material  $\left(C_j \frac{\partial T_j}{\partial t}\right)$  plus the amount of heat lost to the surface  $(-Q_{in,j})$  plus the heat lost to the environment  $\left(\hat{U}_{o,j} (T_j - T_A)\right)$  must equal zero.

### 2.2.4 Solution of the Equations

The solutions for room temperature as a function of time are generally the most interesting. We briefly describe their form below. Solutions can be computed using Tables 1 and 2. These solutions are derived for typical daily weather conditions where the solar gain,  $S(t)$ , is given by (the real part of)

$$S(t) = \begin{cases} S_1 e^{i\omega_1 t} & \text{day } (0 \leq t < t_d) \\ 0 & \text{night } (t_d \leq t < 24 \text{ hrs}) \end{cases}$$

$S(t)$  is sketched in Fig. 5.<sup>17</sup> The ambient temperature  $T_A(t)$  is equal to (the real part of)  $\Delta T_A e^{i\omega_0 t} + \bar{T}_A$ , where  $\omega_0 = 2\pi/1$  day. The heater output is taken as  $H_0$ , a constant. (However, this constant can change values from day to night.) All temperatures are measured with respect to average ambient temperature, so we set  $\bar{T}_A = 0$ .

We use the lumped model primarily for buildings whose parameters change from day to night (e.g. because the collector windows are insulated at night). The model generates two solutions, one for the day period and one for the night period.

Solving the lumped parameter equations for  $N$  heavy materials ( $j = 1, N$ ) requires solving several sets of  $N$  simultaneous equations in  $N$  unknowns, so the solution becomes very difficult to compute by hand for  $N \geq 3$ . For  $N = 2$ , the result for room temperature can be written as

$$T_R(t) = \begin{cases} A_{1d} e^{-\Lambda_{1d}t} + A_{2d} e^{-\Lambda_{2d}t} + \chi_{A_d} \Delta T_A e^{i\omega_0 t} + \chi_s S_1 e^{i\omega_1 t} + T_{H_d} & \text{[day]} \\ A_{1n} e^{-\Lambda_{1n}t} + A_{2n} e^{-\Lambda_{2n}t} + \chi_{A_n} \Delta T_A e^{i\omega_0 t} + T_{H_n} & \text{[night]} \end{cases} \quad (8)$$

where the subscripts  $d$  and  $n$  indicate day or night values. The  $\chi$ 's

give the response of the building to solar and ambient temperature inputs. The first two terms of the solution are transients generated by the change of building parameters from day to night. The  $\Lambda$ 's are the characteristic decay constants of the house; the A's are coefficients whose values are determined by matching the daytime and nighttime solutions as described in Sec. 2.3. The values of all the coefficients in Eq. (8) can be determined from Table 1.

Table 1 for the lumped parameter model is arranged in the form of a program to calculate the numerical values of Eq. (8). If one begins with the lumped parameters for the wall:  $\hat{U}_{wi}$ ,  $\hat{U}_{wo}$ ,  $\hat{h}_w$  and  $\hat{C}_w$ ; and those for the floor:  $\hat{U}_{fo}$ ,  $\hat{U}_{fi}$ ,  $\hat{h}_f$  and  $C_f$ ; along with the quick heat loss coefficient  $\hat{U}_q$ , the radiation fractions  $\alpha_w$ ,  $\alpha_f$  and  $\alpha_R$ , and the weather variables  $\Delta T_A$ ,  $S_1$ ,  $t_d$  and  $\omega_1$ , one can evaluate each of the expressions in the table, in order, using only these parameters or the results of earlier steps. The final step is the numerical result for Eq. (8).

The distributed parameter model can easily model the response of the building to longer-range weather cycles. For weather occurring at a frequency  $\omega_w$ , it yields a solution of the form

$$T_R(t) = T_O + T_W e^{i\omega_w t} + \sum_{n=1}^3 T_n e^{i\omega_o nt} \quad (9)$$

This solution is a Fourier expansion of the response to the driving forces of all frequencies of importance; it is derived in Sec. 2.4.

Table 2 repeats this equation in a more detailed form and shows how to derive the coefficients in the room-temperature equation. Numerical evaluation of Eq. (9) would begin at the bottom of Table 2 and proceed to

the top of the table.

Descriptions of the solutions are provided in Sections 2.3 and 2.4. Modifications needed to describe Trombe wall or water-wall collectors are discussed in Appendices 2.3 and 2.4.

#### 2.2.5 Interpretation of the Equations

This set of equations (1-7) idealizes a building as a room with zero heat capacity, surrounded by a small number of materials of finite heat capacity, and a pathway for instantaneous conductive heat losses. Sunlight enters the room through windows, and is absorbed or reflected from the various surfaces in the room. The reflectances, absorptances, and room geometry produce a radiation balance; this balance is described by the  $\alpha$  parameters.

A fundamental difference between this model and most others is that the sunlight is absorbed in varying proportions on interior surfaces, rather than with uniform flux. Sunlight entering a south-facing window will first strike either the floor or a wall (or else a piece of furniture); that fraction of the energy which is not absorbed on that surface will reflect and strike a second surface. Eventually all the radiation will be absorbed on some material surface. If the absorption occurs on a heavy surface, then Eq. (1) applies. If the absorption is on a light surface (e.g. upholstery) then  $Q_{in}$  will quickly become zero, and all the solar heat gain will be transferred to the air. This is equivalent to assuming that the room air directly absorbs that fraction of the sunlight which falls on light surfaces: and is modeled by the term  $\alpha_R S$  in (2).

The values of the  $\alpha$ 's are not easy to determine by analytic calculation, since their determination involves tracing light rays through several diffuse reflections. The geometry is often complicated by the existence of furniture. Evaluating them from theory requires complicated computer modeling, (see Ref. 28).

The most direct way to evaluate the  $\alpha$ 's may be empirical; measuring incident light minus reflected light on a particular surface allows the calculation of absorption. This measurement must include not only the visible portion of the solar spectrum, but the near infrared. However, thermal radiation (that is, radiation caused when

a surface heats up due to absorption of sunlight) must be excluded from the measurement. In practice, one can measure all radiation at wavelengths shorter than  $3\mu$ , since longer-wave sunlight will be filtered out by the window glass.

As mentioned in the introduction, varying the fraction of the sunlight absorbed on each surface makes a large difference in the response of the building. Returning to Fig. 2 we see the difference in the response of a passive solar building with wood frame walls and concrete slab floor<sup>5</sup> for four different sets of  $\alpha$ 's. All four lines on the graph describe the same house. The solid line labeled A describes the case where  $\alpha_{\text{floor}} = 6/7$ ;  $\alpha_{\text{walls}} = 1/7$  and  $\alpha_{\text{R}} = 0$ . The lines labeled B and C successively double  $\alpha_{\text{w}}$  at the expense of  $\alpha_{\text{f}}$ , with  $\alpha_{\text{R}}$  remaining zero. The dotted line labeled D sets  $\alpha_{\text{f}} = \alpha_{\text{w}} = 0$  and  $\alpha_{\text{R}} = 1$ , corresponding to solar absorption in the room air.

As shown in the figure, the response of the building is noticeably different as we vary the  $\alpha$ 's. Going from case A to case B, the house is  $1^{\circ}\text{F}$  hotter during the afternoon but  $1/2^{\circ}\text{F}$  cooler at night. Moving to case C where 57% of the sunlight is absorbed on the light, wood-frame walls, the house overheats  $2-1/2^{\circ}\text{F}$  during the afternoon and is another  $1/2^{\circ}$  colder at night.

Case D with solar absorption in the room, differs most dramatically from any of the other cases; it overheats by almost  $8^{\circ}\text{F}$  compared to case A while cooling off  $2-1/2^{\circ}\text{F}$  more at night. Thus correctly accounting for solar absorption within the building makes a significant difference in the predictions of performance. Getting the exact radiation balance solved for a given house (i.e. evaluating the  $\alpha$ 's correctly) is

significant, but even a reasonable guess at the  $\alpha$ 's will be a better approximation than assuming some standard conditions. For a heavier house (e.g. brick walls rather than wood frame) the difference between case A and case D would be even larger.

The description of solar absorption as taking place on the surface of heavy materials also helps isolate some of the parameters which have important effects on the performance of passive solar buildings. Equations (1) and (2) imply that if  $Q_{in,j}$  is large, then the surface temperature will be low, and so the transfer of solar heat from the surface to the room will be small. This is a desirable feature; it tends to reduce overheating during the day. As will be shown in Sec. 2.4 and Appendix 2.5A, an important parameter for a surface will be the ratio of the conductivity into the surface ( $U_j$  or  $K_j k_j$ ) to the film coefficient  $h_j$ ; larger values of this ratio imply better performance (less overheating).

The model assumes that all the heat capacity is contained in the walls and floor. This assumption is really more of a definition; everything with nontrivial heat capacity is treated as a surface coupled to a bulk material (Eq. (1)); if furniture heat capacity is important, it must be treated as a separate surface.

The form of Eq. (1) also assumes that the sunlight is absorbed uniformly over each surface, in other words, that one unit area of a given surface receives exactly the same solar gain as another. This assumption is plausible due to the linearity of the Eqs. ((1), (3), (4), (6), and (7)): twice the sunlight absorbed over half the area should give roughly the same response, and is proven by the form of Eq. (14)

in Sec. 2.4. This equation shows that as long as heat transfers are linear in temperature difference, the distribution of sunlight received over a surface doesn't affect the solution; the only important parameter is the total amount of sunlight absorbed on the whole surface.

In fact, we assume that in general temperatures do not vary from one point on a surface to another; in other words, that the floor surface temperature  $T_{fs}$  represents an average over the whole floor surface. This assumption of 1-dimensional heat flows is common to all calculational methods; it is valid here as long as heat transfers are linear.

Linearity of the heat transfer equations is an assumption which is common to all building models; heat flows are taken as proportional to temperature differences. In fact, film coefficients are the sums of terms which involve the differences of fourth powers of temperature for radiation terms and roughly the 5/4 power of temperature difference for convective terms. These heat transfers can be approximated as linear because temperature differences are typically much smaller than absolute temperatures, so a Taylor expansion which drops all terms of higher order than 1 in  $\Delta T$  will not introduce serious error. For example for a room temperature of 300°K and a temperature difference of 10°K, the error in a linear approximation for radiative heat transfer is 5%.

It is interesting to compare the assumption of heat capacity in the walls and floor to the assumption of finite room heat capacity, (that is, to compare our assumption of heat capacity coupled to the room through finite conductances  $\hat{h}_j$  rather than perfect thermal contact between the room and the heat capacity). Figure 6 displays temperature versus time for the wood-frame, concrete floor house of Fig. 2 as calculated by our model for two choices of  $\alpha$ 's (solid lines) and as calculated assuming a finite room heat capacity (dashed line)<sup>6</sup>. As can be seen, there is nontrivial difference in the shape of the two types of curves.

Another simplifying assumption in the model is that of one-layer walls. In fact walls are composed of a sandwich of several materials: gypsum board, wood or insulation, building paper, perhaps sheathing, and siding. However, most of these materials either have negligible resistance and capacitance (e.g. building paper), or are not substantially different in properties from each other. For example, a section of wall composed of gypsum board 1/2" thick and wood 3-1/2"

thick, plus stucco siding, can be approximated as a 4" thick slice of wood for most purposes, since wood has<sup>8</sup>

$$\rho C_p \cong 9 \text{ Btu/}^\circ\text{F-ft}^3, \text{ and } K \cong 0.068 \text{ Btu/hr-}^\circ\text{F-ft},$$

while gypsum board has

$$\rho C_p \cong 13 \text{ Btu/ft}^3\text{-}^\circ\text{F}, \text{ and } K \cong 0.075 \text{ Btu/hr-}^\circ\text{F-ft},$$

not significantly different. This one-layer approximation yields a substantial reduction in algebraic manipulation needed to solve the equations. The response functions of Sections 2.4 and 2.5 can provide a check on the validity of this approximation. However, a two-layer model is used when there is substantial difference in material properties (e.g. wood slats over a concrete floor).

Similarly, materials of similar parameters are combined to form a single "surface"  $j$ ; this also reduces the amount of computation needed. For example, wood-frame walls can be treated together with the ceiling as a single surface. Combined or average parameters are used for this approximation.

Room heat capacity is taken as zero in Eq. (2), which says that heat losses from the room equal heat gains, with no heat storage term. This is a good approximation; even a light house has a heat capacity of about 2.25 Btu/ $^\circ$ F per square foot of floor area, while with 8-foot-high ceilings, the heat capacity of the air is only 0.14 Btu/ $^\circ$ F per ft.<sup>2</sup> A more realistic passive solar house<sup>7</sup> has 12 Btu/ $^\circ$ F of heat capacity per ft<sup>2</sup> of floor. To confirm that this assumption is unimportant, we calculated the 3 time constants for the lumped parameter model with

finite air heat capacity; for the one case we checked  $\Lambda_1$  and  $\Lambda_2$  agreed within 5% of their values for  $C_{\text{air}} = 0$ , while  $\Lambda_3$  was so much larger than  $\Lambda_1$  and  $\Lambda_2$  that terms involving it would decay rapidly to zero. A 5% error in the two decay constants  $\Lambda_1$  and  $\Lambda_2$  will produce an error of much less than 5% in room temperature.

Another assumption is buried in the use of film heat transfer coefficients. Film coefficients assume a conduction-like heat transfer between material surfaces and air. In fact, the heat transfers are the sum of two terms: a radiation term approx. 1 Btu/ft<sup>2</sup> - deg. F-hr and a convection term approx. 1/2 Btu/ft<sup>2</sup>-deg. F-hr. Actually only the convection term describes heat transfers from material surface to room air. The radiation term describes transfers directly between materials surfaces, between surfaces and clutter (light furniture, books, rugs, wall hangings, cabinets), etc. These other surfaces then transfer heat to the air by convection. It would be impossible to describe radiation exactly for a general case of an inhabited house, because of variations in geometry. However, one could attempt to separate each of the terms  $\hat{h}_j(T_{S_j} - T_R)$  into two terms; heat transfer from surface, to (eventually) room air  $\hat{h}'_j(T_{S_j} - T_R)$  and heat transfer from surface j to all other surfaces  $\sum_{\substack{i=1 \\ i \neq j}}^N \hat{h}_{ji}(T_{S_j} - T_{S_i})$  where the  $\hat{h}_{ji}$ 's include geometric form factors.

This approach is outlined in Appendix 2.4; it involves the inversion of an N x N matrix. This was attempted for one case; it greatly complicated the algebra without changing the results substantially.

In addition to these assumptions are the usual ones assumed in all building models -- no intra-zone temperature variations, one-dimensional heat flows, known materials properties, construction which follows designs (e.g. no forgotten insulation or air leaks), known behavior of thermostat, etc. In fact, the "standard" assumptions probably lead to about 10-20% uncertainty in any model, no matter how exact the mathematical modelling.<sup>19</sup> This "acceptability range" of  $\pm 10\%$ - $20\%$  justifies a number of the simplifications described above; if the description of the house is only correct within 10-20%, then 5% calculational errors are not crucial.

In addition to the simplifying assumptions about the building, an analytic model requires a different type of weather input than a numerical model. Weather data is available as a function of time only with 1-hour or 3-hour sampling periods. Numerical models use special forms of response functions to account for this.<sup>9</sup> An analytic model must be driven by continuous functions of time. Connecting data points with a smooth curve could lead to very long Fourier series for the weather and correspondingly messy solutions to the differential equations. In this model we approximate outside weather by simple, continuous functions of time, typically sinusoids. Weather conditions are usually treated by Fourier-analyzing the actual weather and only taking a few dominant frequencies in the series, typically  $\omega_0 = 2\pi/\text{day}$ ,  $2\omega_0$ ,  $3\omega_0$ , and 0.

This procedure is in line with the intended uses of the model as a design optimization tool and as a method for gaining an understanding of how the building works. For either of these two

objectives, it is more interesting to see how the building reacts to idealized weather, (such as a succession of cold, sunny cycles, or a cycle of sunny days followed by cloudy days) than to the more unpredictable fluctuations of historic weather.<sup>10</sup>

In summary, to allow analytic calculations of heat transfer, we have idealized a building consisting of a number of multi-layer walls, windows, etc., as a system of a few (e.g. 2) mono-layer walls and a quick heat transfer channel. We have assumed that sunlight is absorbed uniformly across the inside surface of each of these walls. All excitations are taken as simple functions of time.

### 2.3 Solution of the Lumped Model

This section discusses the solution of the lumped parameter model, using Eqs. (1), (2), (6), (7), and a simplified description of weather which is described below. In order to carry out this solution numerically one must first evaluate the lumped parameters. Evaluation is not trivial;  $C_w$  is not just the heat capacity of the bulk material which makes up the wall, neither is  $\hat{U}_{wi}$  or  $\hat{U}_{wo}$  equal to the U value times area. This problem is discussed in Sec. 2.5. The discussion in this section describes the solution of the lumped parameter model in general terms. The detailed algebraic manipulations are contained in Appendix 2.3. We first solve the equations for the free-floating (unheated) house.

We consider two surfaces with heavy materials behind them; call them "floor" and "walls". The floor and wall temperatures ( $T_f$  and  $T_w$ ) are the important variables in the calculation; they express the temperatures of massive elements. Thus we will derive differential equations which involve only  $T_w$  and  $T_f$ . The solution to these differential equations will then be used to derive room temperature  $T_R$ . The room temperature is usually the desired result of the calculation. It is given by Eq. (11) below.

We next describe the derivation, which is carried out in Appendix 2.3.

We use Eqs. (1) and (2) to derive a relationship between the room temperature and the dynamic temperatures  $T_w$  and  $T_f$ . This relationship shows that room temperature is a linear function of the dynamic temperatures and the driving forces S, H, and  $T_A$ ; it is given by

$$T_R = \frac{N_W}{N_R} T_W + \frac{N_f}{N_R} T_f + \frac{1}{N_R} T_A + \frac{N_s}{N_R} S + \frac{1}{\hat{U}_q N_R} H \quad (10)$$

where the N's are defined in Table 1.

We use this relationship, along with the surface heat balance equations (1) to rearrange the differential equations (7) until they contain only the dynamic temperatures  $T_W$  and  $T_f$  and the driving forces. The result can be written as

$$\dot{T}_W + \Lambda_p T_W - \Lambda_F T_f = a_1 H + a_2 S + a_3 T_A \quad (10a)$$

$$\dot{T}_f + \Lambda_G T_f - \Lambda_Q T_W = a_4 H + a_5 S + a_6 T_A$$

Again, the  $\Lambda$ 's and a's are defined in Table 1.

These are two coupled linear first-order differential equations for the dynamic temperatures. Their solutions, along with (10), will give us the room temperature. The solution to these equations can be written as the sum of a homogeneous solution and an inhomogeneous solution.

The homogeneous solution is

$$T_W = B_1 e^{-\Lambda_1 t} + B_2 e^{-\Lambda_2 t}$$

$$T_f = B_1 K_1 e^{-\Lambda_1 t} + B_2 K_2 e^{-\Lambda_2 t}$$

where the B's are arbitrary and the  $\Lambda$ 's and K's depend on the building parameters and are given in Table 1.

The inhomogeneous solution depends on the form of the driving functions. We approximate the driving forces by simple functions and then derive the inhomogeneous solution for each one.

The heater output is taken as a constant  $H_o$ , which may be different during the day and night (' $H_{o_d}$ ' and ' $H_{o_n}$ '). Then the inhomogeneous solution to the differential Eqs. (10a) is

$$T_w = T_{H_w}$$

$$T_f = T_{H_f}$$

These constant temperatures are given by Table 1.

The solar gain function  $S(t)$  is given by a sine wave during the day or zero at night.<sup>17</sup> We take  $t=0$  to be when the sunlight first enters the windows and  $t = t_d$  to be when it last enters. Then

$$S(t) = \begin{cases} S_1 e^{i\omega_1 t} & 0 \leq t < t_d \\ 0 & t_d \leq t < 24 \text{ hrs.} \end{cases}$$

We assume that  $S(t)$  is the same each day. Then the inhomogeneous solutions to (10a) is

$$T_w = \chi_{s_w} S_1 e^{i\omega_1 t} \quad 0 \leq t < t_d$$

$$T_f = \chi_{s_f} S_1 e^{i\omega_1 t} \quad 0 \leq t < t_d$$

and  $T_f = T_w = 0$  for  $t_d \leq t < 24$  hours (at night).

We take  $T_A(t) = \Delta T_A e^{i\omega_0 t}$  where  $\omega_0 = 2\pi/1$  day. This sets average ambient temperature equal to zero; that is, we measure all temperatures with respect to average ambient.

Then the inhomogeneous solution to (10a) is

$$T_w = \chi_{A_w} \Delta T_A e^{i\omega_0 t}$$

$$T_f = \chi_{A_f} \Delta T_A e^{i\omega_0 t}$$

The complete solution to (10a) is the sum of the homogeneous solution and the three inhomogeneous solutions. This solution still has two arbitrary constants  $B_1$  and  $B_2$ . We eliminate them by finding appropriate boundary conditions.

To do so, we note that there are different solutions to (10a) for the day and for the night. This is because the terms proportional to  $S$  only appear during the day, and also because the house parameters may change from day to night (e.g. if the windows are shuttered at night).

Although the *form* of solution may change from day to night, the actual *values* of  $T_w$  and  $T_f$  cannot change discontinuously, since this would require infinite heat flows. So the boundary conditions on the temperatures are that  $T_w(t)$  and  $T_f(t)$  are continuous functions of time.

The formulation of these boundary conditions will depend on the details of the problem. For the problem of constant weather conditions, where each day is precisely like the previous day, the boundary conditions are:

$$T_f(0^+) = T_f(0^-)$$

$$T_f(t_d^+) = T_f(t_d^-)$$

and

$$T_w(0^+) = T_w(0^-)$$

$$T_w(t_d^+) = T_w(t_d^-)$$

These four boundary conditions fix the four constants  $B_{1d}$ ,  $B_{2d}$ ,  $B_{1n}$  and  $B_{2n}$ . Knowing the B's, we now have the complete solution to (10a) for both day and night periods. We can finally use this solution with (10) to find room temperature.

The complete solution can be expressed as

$$T_w(t) = \begin{cases} B_{1d} e^{-\Lambda_{1d}t} + B_{2d} e^{-\Lambda_{2d}t} + \chi_{A_{wd}} \Delta T_A e^{i\omega_0 t} + \chi_{S_w} S_1 e^{i\omega_1 t} + T_{H_{wd}} & \text{[day]} \\ B_{1n} e^{-\Lambda_{1n}(t-t_d)} + B_{2n} e^{-\Lambda_{2n}(t-t_d)} + \chi_{A_{wn}} \Delta T_A e^{i\omega_0 t} + T_{H_{wn}} & \text{[night]} \end{cases} \quad (11a)$$

$$T_f(t) = \begin{cases} B_{1d} K_{1d} e^{-\Lambda_{1d}t} + B_{2d} K_{2d} e^{-\Lambda_{2d}t} + \chi_{A_{fd}} \Delta T_A e^{i\omega_0 t} + \chi_{S_f} S_1 e^{i\omega_1 t} + T_{H_{fd}} & \text{[day]} \\ B_{1n} K_{1n} e^{-\Lambda_{1n}(t-t_d)} + B_{2n} K_{2n} e^{-\Lambda_{2n}(t-t_d)} + \chi_{A_{fn}} \Delta T_A e^{i\omega_0 t} + T_{H_{fn}} & \text{[night]} \end{cases} \quad (11b)$$

$$T_R(t) = \frac{N_w}{N_R} T_w(t) + \frac{N_f}{N_R} T_f(t) + \frac{1}{N_R} \Delta T_A e^{i\omega_0 t} + \frac{N_s}{N_R} S_1 e^{i\omega_1 t} + \frac{1}{\hat{U}_q N_R} H \quad (11c)$$

The  $S_1$  term in the room temperature equation (11c) is omitted at night.

Table 1 below gives a program for calculating the functions described by (11) from building and weather parameters. In most cases, the interesting result of the calculation is the room temperature curve. Given design day weather conditions, the room temperature function describes whether the building will overheat during the day or cool off too much during the evening.

Wall and floor temperatures derived in (11) cannot be used directly, since they are not physically measurable temperatures. However, along with room temperature, they can be used to derive surface temperatures. The surface temperatures may be of interest either for experimental validation of the model or for calculating mean radiant temperatures.

The lumped parameter model is most useful for evaluating the response of managed passive solar buildings, since the calculational effort to solve the model does not increase noticeably if daytime and nighttime parameters differ. It can be most simply used to calculate the response of the building to steady diurnal weather variations which don't change from day to day, as detailed above. However, one can also predict the response of the building to a cold or less sunny day following the design day calculated above or to a succession of days with differing weather conditions, as described in Sec. 3.3.6.

Trombe walls or waterwalls can also be modelled using lumped parameters, with a slight change in some of the definitions of Table 1. The heat transfers for the Trombe wall are illustrated in Fig. 7; they involve the heat loss through the collector glazing, the heat transfer from the air channel to the room, and the heat transfer from the front surface of the Trombe wall to the channel air.

Table 1a lists the revised definitions needed to model the Trombe wall. Derivation of this model is left to Appendix 2.3.

## 2.4 Solution of the Distributed Parameter Model

This section discusses the solution of the continuum model at a similar level of overview to the previous section. Algebraic details are in Appendix 2.4A. The continuum model solves the heat transfer equations in Fourier-transform space. It can only be used when house parameters are time independent; time-dependent parameters generate extra terms which, although they can be calculated analytically (see Appendix 2.5B) are tedious to compute.

The continuum model is most useful in cases where the response of the building to several-day weather cycles is important. As we will show, the response to weather cycles can be derived relatively easily from the solution to daily cycles.

This model also handles more than two material surfaces without undue complication of the algebra. We will therefore display the equations of heat transfer for a slightly more complicated system than used in the lumped parameter model. We will use three material surfaces in this derivation, with subscript "e" for envelope walls, "p" for partition walls, and "f" for floor. Extension to a larger number of surfaces is straightforward.

The continuum model is solved in Fourier transform space; instead of looking at, say, the room temperature  $T_R(t)$ , we look at its Fourier transform  $\tilde{T}_R(\omega) = 1/(2\pi) \int_{-\infty}^{\infty} dt T_R(t) e^{-i\omega t}$ .  $\tilde{T}_R(\omega)$  is a function of the driving forces of solar gain  $\tilde{S}(\omega)$ , ambient temperature  $\tilde{T}_A(\omega)$  and heater output  $\tilde{H}(\omega)$ . If these driving forces can be expressed as sums over only a few frequencies, then we can write  $T_R(t)$  as a Fourier sum over a small number of frequencies. These relationships are summarized in Table 2. We derive them below:

Heat transfers in each heavy material  $j$  are described by the diffusion equation (3). This solution can be expressed as a temperature distribution

$$\tilde{T}_j(\omega, x) = A_j \cosh k_j d_j (1-\xi) + B_j \sinh k_j d_j (1-\xi)$$

where  $k_j = \sqrt{\frac{i\omega(\rho c_p)_j}{K_j}}$

$$\xi = x/d_j$$

$d_j$  = the thickness of the  $j^{\text{th}}$  material.

$A_j$  and  $B_j$  can be evaluated using boundary conditions for the two surfaces of the material.

The outside surface of an envelope wall is coupled to ambient temperature by a pure resistance, so the outside boundary condition is conservation of heat flux at the boundary between the heavy material and the resistance, as in Eq. A2.4-(9-11). The inside boundary condition is the surface heat balance (1).

We can evaluate this expression for surface temperature

$\tilde{T}_j(\omega, x=0) \equiv T_{s_j}$ ; the result is

$$T_{s_j} = (\bar{\alpha}_j S + h_j T_R) R_{1j} + T_A R_{2j} \quad (13)$$

where  $\alpha_j = \alpha_j$  per unit area and  $R_{1j}$  and  $R_{2j}$  are linear response functions of  $\omega$  which describe the response of the indoor surface of material 'j' to thermal inputs.  $R_{1j}$  describes the response to heat flows directed toward the inside surface, while  $R_{2j}$  gives the response to varying temperatures on the outside surface. The response functions are monotonically decreasing functions of  $\omega$ . For one- or two-layer materials, they have relatively simple forms, and are given for

several types of materials (e.g. envelope walls, partition walls, and semi-infinite floor slab) in Table 2 and Eq. (A2.4-21). Some typical  $R_1$  functions are plotted in Figs. 8, 9, A2.5-2 and A2.5-3.  $R_1$  has dimensions of thermal resistance, °F-ft<sup>2</sup>-hr/Btu or °C-m<sup>2</sup>/W, while  $R_2$  is dimensionless. With slight redefinitions, these response functions are the Fourier form of the response factors used in computer models.

The response functions will also be important in choosing values for the lumped parameters; they are plotted and tabulated for several representative materials in Sec. 2.5 and Appendix 2.5A.

The expressions for surface temperature (Eq. (13)) can be used in the room heat balance to produce the equation

$$\begin{aligned}
 T_R(\omega) & \left\{ \hat{U}_q + \hat{h}_e(1-h_e R_{1e}) + \hat{h}_p(1-h_p R_{1p}) + \hat{h}_f(1-h_f R_{1f}) \right\} \\
 & = S(\omega) (\alpha_R + h_e \alpha_e R_{1e} + h_p \alpha_p R_{1p} + h_f \alpha_f R_{1f}) \\
 & + T_A(\omega) (\hat{U}_q + \hat{h}_e R_{2e}) + H(\omega)
 \end{aligned} \tag{14}$$

This equation relates the Fourier transform of the room temperature to those of the driving forces  $S$ ,  $T_A$  and  $H$ . It can be written simply in the form

$$T_R(\omega) \cdot A(\omega) = S(\omega) \cdot B(\omega) + T_A(\omega) \cdot C(\omega) + H(\omega) \tag{14a}$$

where  $A$ ,  $B$ , and  $C$  are frequency dependent functions given by (14). All of the building response functions  $A$ ,  $B$ , and  $C$  are linear combinations of heat transfer coefficients times materials response functions. All the frequency dependence is contained in the materials response functions  $R_1$ ,  $R_2$ ; materials properties such as conductivity do not appear except in these functions.

The response of the building is driven by the Fourier transforms of ambient temperature  $T_A(t)$  and solar gain  $S(t)$ . Fourier transformation

produces very short series, since  $T_A$  can be modelled acceptably by 1 to 3 terms. If we take the same function for  $S$  as in the lumped-parameter model:

$$S = \begin{cases} |S_1| \sin \omega_1 t & 0 \leq t < t_d \\ 0 & t_d \leq t < 24 \text{ hrs.} \end{cases}$$

where  $\omega_1 = \pi/t_d$ ; then  $S$  can be written as

$$S = |S_1| \sum_{n=0}^{\infty} d_n e^{in\omega_0 t} \quad \text{where } \omega_0 = 2\pi/\text{day}$$

where the real part of the complex quantity is implied, and

$$d_n = \begin{cases} \frac{\omega_0}{\pi\omega_1} & \dots \dots \dots n = 0 \\ \frac{\omega_0}{2\pi} \frac{2\omega_1}{\omega_1^2 - (n\omega_0)^2} \left( e^{-in\omega_0 t_d} + 1 \right) & \dots \dots \dots n \neq 0 \end{cases}$$

For large  $n$ ,  $d_n \rightarrow 0$  as  $1/n^2$ : for  $t_d \sim 7-9$  hrs,  $|d_4| \lesssim 0.08$  and  $|d_5| \lesssim 0.02$ . Thus for 10% accuracy, we can ignore harmonics of  $S$  higher than  $3 \omega_0$ .

The solution of the model for constant weather is then

$$T_R = |S_1| \sum_{n=1}^3 \frac{B(n\omega_0)}{A(n\omega_0)} d_n e^{in\omega_0 t} + |S_1| \frac{B(0)}{A(0)} d_0 + \frac{C(\omega_0)}{A(\omega_0)} \Delta T_A e^{i\omega_0 t} + \bar{T}_A + \frac{H}{A(0)} \tag{15}$$

This gives the response of room temperature to daily weather fluctuations.

A similar form of equation applies for a Trombe wall building, with  $A$ ,  $B$ , and  $C$  given by Eq. (A2.4-39).

The form of Eq. (15) tells us something about the desired frequency dependence of  $A$ ,  $B$ , and  $C$  for a floating-temperature passive house. We want the house to sit at a considerably warmer room temperature than  $T_A$ , but we don't want its temperature to fluctuate rapidly over the course of a day. Therefore we want to choose materials

such that  $\frac{B(0)}{A(0)}$  is large but  $\frac{B(\omega_0)}{A(\omega_0)}$  and  $\frac{C(\omega_0)}{A(\omega_0)}$  are small.

We can also see what design criteria apply to a constant-thermostat house which is continuously heated for constant room temperature  $T_R(\omega) = 0$  for  $\omega \neq 0$ . In that case, we can write (14a) as

$$H(\omega) = T_R(\omega) A(\omega) - S(\omega) B(\omega) - T_A(\omega) C(\omega)$$

We note that  $H(\omega)$  integrates to zero unless  $\omega = 0$ , so that to minimize heating requirements, we want  $B(0)$  large and  $C(0)$  small. (Of course, if  $H(t)$  goes negative in this solution, it means that air conditioning is required and our model is then unrealistic). We show in Appendix 2.4 that  $C(0)$  is just the steady-state heat transfer coefficient of the house; so the strategy of minimizing  $C(0)$  is satisfied by simply insulating the building.

Thus we see that the design strategy for optimizing thermal performance of a house depends on whether the house is free-floating or thermostated. Design strategies for the thermostated house will not differ radically from those implied by the degree-day method, while those for the free-floating house will be more complex.

We can also use Eqs. (14) and (14a) to see some of the physical significance of the response functions. To get  $A(\omega)$ , we add the quick heat transfer coefficient  $\hat{U}_q$  to terms of the form  $\hat{h}_j(1-h_jR_{1j})$ . These terms act as heat transfer coefficients (or U-values times areas) for their heavy materials. For  $\omega \rightarrow 0$ , they reduce to the conventional steady-state heat transfer coefficients, as shown in Appendix 2.4. For

typical wall sections the U-value is much less than  $1 \text{ Btu}/^\circ\text{F-hr-ft}^2$ , so  $h_j(1 - h_j R_{1j}) \ll 1 \text{ Btu/hr-ft}^2\text{-}^\circ\text{F}$  for  $\omega \rightarrow 0$ .

Typical  $R_1$  functions begin to decline slowly as  $\omega$  becomes finite. Since  $h_j \sim 1 \text{ Btu/ft}^2\text{-}^\circ\text{F-hr}$  and  $h_j(1 - h_j R_{1j}) \ll 1 \text{ Btu/ft}^2\text{-}^\circ\text{F-hr}$ ,  $h_j R_{1j}$  is very close to 1 for small values of  $\omega$ . Thus small decreases in  $R_{1j}$  will result in large relative increases in  $h_j(1 - h_j R_{1j})$ . This allows  $A(\omega)$  to increase, so that oscillations in room temperature  $T_R$  will be damped, regardless of whether they are a response to sunlight, temperature, or heater output.

Similarly, the form of  $C(\omega)$  involves adding  $\hat{U}_q$  to terms like  $\hat{h}_j R_{2j}$ . Evidently these terms also act like heat transfer coefficients; in the limit of  $\omega \rightarrow 0$ ,  $\hat{h}_j R_{2j} = \hat{h}_j(1 - h_j R_{1j}) = \hat{U}_j$ . The function  $R_{2j}$  is nearly constant for small  $\omega$  and decreases monotonically with more and more slope as  $\omega$  increases. Thus  $C(\omega)$  decreases monotonically with  $\omega$ , resulting in less and less response to faster air temperature oscillations.

#### 2.4.1 Weather Response

The distributed parameter model can easily be used to study the response of a building to several-day-long fluctuations in sunshine or temperature. Adding slowly-varying ambient temperature to the model is trivial; for  $T_A$  varying at weather frequency  $\omega_w$ , we simply add

$$\Delta T_{A_w} \frac{C(\omega_w)}{A(\omega_w)} e^{i\omega_w t} \text{ to the solution for } T_R.$$

To add slowly varying insolation, we assume that solar gain is still sinusoidal every day, but that the amplitude of the solar gain varies sinusoidally over a weather cycle. That is, we express  $S(t)$  as

$$S(t) = \begin{cases} (\bar{S} + \Delta S_w \cos \omega_w t) \sin \omega_1 (t - t_{sr}) & , \quad \text{daytime} \\ 0 & \dots \dots \dots \text{nighttime} \end{cases}$$

where  $t_{sr}$  is the time of the most recent sunrise.

We assume that  $\omega_o/\omega_w$  is an integer for simplicity. Thus solar intensity is approximately  $\bar{S} + \Delta S_w$  at noon on the sunniest day and  $\bar{S} - \Delta S_w$  at noon on the cloudiest day.

$S(t)$  can be Fourier analyzed into relatively few frequencies (in principle, all integer multiples of  $\omega_w$  are possible). We show in Appendix 2.4 that the only frequencies which appear are  $\omega_w, \omega_o, \omega_o \pm \omega_w, 2\omega_o \pm \omega_w \dots$ . The amplitudes are found as follows:

The amplitude at frequency	0	is	$d_o \times \bar{S}$
	$\omega_w$		$d_o \times \Delta S_w$
	$\omega_o$		$d_1 \times \bar{S}$
	$\omega_o \pm \omega_w$		$d_1 \times \frac{\Delta S_w}{2}$
	$n\omega_o$		$d_n \times \bar{S}$
	$n\omega_o \pm \omega_w$		$d_n \times \frac{\Delta S_w}{2}$

This can be understood as follows: a term  $|S_1| d_n e^{i\omega_n t}$  from the Fourier expansion of the daily solar gain function is replaced by the terms

$\bar{S}d_n e^{i\omega_n t} + \frac{\Delta S_w}{2} d_n e^{i(\omega_n - \omega_w)t} + \frac{\Delta S_w}{2} d_n e^{i(\omega_n + \omega_w)t}$  . These three terms  
add to  $(\bar{S} + \Delta S_w \cos \omega_w t) d_n e^{i\omega_n t}$  .

The solution can be written as the steady-state term and the  $\omega_w$  term plus triplets of terms of the form  $\bar{S} \frac{B(n\omega_o)}{A(n\omega_o)} d_n e^{in\omega_o t} +$

$$\frac{\Delta S_w}{2} \frac{B(n\omega_o + \omega_w)}{A(n\omega_o + \omega_w)} d_n e^{i(n\omega_o + \omega_w)t} + \frac{\Delta S_w}{2} \frac{B(n\omega_o - \omega_w)}{A(n\omega_o - \omega_w)} d_n e^{i(n\omega_o - \omega_w)t}$$

These are approximately equal to<sup>12</sup>  $\bar{S} + \Delta S_w \cos \omega_w t$  times the solar gain term at frequency  $n\omega_o$  in the daily solution.

Thus, the only term added to the daily solution by the addition of weather-varying solar gain is the weather frequency term itself:

$\Delta S_w \frac{B(\omega_w)}{A(\omega_w)} d_o e^{i\omega_w t}$  . The daily solution is exactly what we derived previously in Eq. (15) except that  $|S_1|$  is replaced by  $\bar{S} + \Delta S_w \cos \omega_w t$ . The full solution is displayed below:

$$\begin{aligned} T_R(t) = & \left( \bar{S} + \Delta S_w \cos \omega_w t \right) \left\{ \sum_{n=1}^3 \frac{B(n\omega_o)}{A(n\omega_o)} d_n e^{in\omega_o t} \right\} + \\ & + \bar{S} \frac{B(0)}{A(0)} d_o + \Delta S_w \frac{B(\omega_w)}{A(\omega_w)} d_o e^{i\omega_w t} + \bar{T}_A + \Delta T_{A_w} \frac{C(\omega_w)}{A(\omega_w)} e^{i\omega_w t} + \\ & + \Delta T_A \frac{C(\omega_o)}{A(\omega_o)} e^{i\omega_o t} + H \frac{1}{A(0)} \end{aligned} \tag{16}$$

We have derived in this section a simple expression for room temperature response to ambient temperature and solar gain, which uses truncated Fourier series. A model which considers approximately weekly weather variations will express  $T_R$  as a sum of 8 terms, which can be computed by hand.

As mentioned earlier, this model will only work for unmanaged passive buildings; that is, buildings which do not open windows or add insulation in response to weather conditions or time of day. However, for these unmanaged buildings, the solution derived is an exact solution of the heat transfer equations (to arbitrary accuracy depending on how many terms of the Fourier expansion are retained). In other words, all the simplifications in the model occur in the writing of Eqs. ((1), (2), (3), and (4)), not in their solution.

Also, it is often possible to produce an approximate solution to a managed building by changing the value of  $H(t)$ , the heater output function. For example, suppose we assume that a window is insulated at night. We estimate the expected reduction in heat loss due to this increase in insulation, and assume that much energy is released to the room air by the heater. An exact solution would require equivalent heater output to equal  $\Delta UA(T_R - T_A)$  where  $\Delta U$  is the change in conductance of the windows. The approximate solution (or iterative approach to the exact solution) assumes that we already know  $(T_R - T_A)$  and adjusts  $H(t)$  to equal the guessed value of  $\Delta UA(T_R - T_A)$ . This approximation moves the time-dependence from the building parameters (which we can't handle) to the input functions.

The form of the equations in this section assume single-layer heavy materials; however, the use of multi-layer materials will only produce

messier expressions for the response functions. Some two-layer material response functions are given in Appendix 2.4 and Appendix 2.5. As in the lumped case, we do not model direct radiant heat exchange between material surfaces. Including this effect greatly complicates the computations, as shown in Appendix 2.4.

## 2.5 Evaluation of the Lumped Parameters

The section on the lumped parameter model (Sec. 2.3) shows how to calculate the response of a building as a function of a few lumped parameters. However, it did not describe how to calculate values for these parameters if they were to be used to model a continuous wall. In this section, we derive methods for choosing values of lumped parameters which optimally simulate the response of continuum materials. The purpose of this exercise is to provide a way of simulating a managed building whose parameters change from day to night or as a function of weather.

Lumped parameters are a mathematical construct used to simplify solution of the equations. A continuum wall's temperature is described by a function of position  $T_w(x,t)$ ; to describe it by a single temperature  $T_w$  is not physically meaningful. That is, the lumped temperature  $T_w$  cannot be measured. However,  $T_w$ , along with the lumped parameters  $\hat{U}_{wi}$ ,  $\hat{U}_{wo}$  and  $C_w$ , will determine a wall surface temperature which can be measured. If  $\hat{U}_{wi}$ ,  $\hat{U}_{wo}$ , and  $C_w$  can be chosen such that this wall surface temperature agrees with that derived from the exact solution, then the lumped model will be useful.

We derive optimal values for the lumped parameters by calculating surface temperatures for an isolated material (floor or wall) in both the lumped and continuum models.

The calculation proceeds along the same lines as that used to derive the response functions of Sec. 2.4. The result is an expression for response functions for the lumped model, along with the previously-derived response functions.

Thus we find that in the lumped model, the surface temperature  $T_s$  is given by:

$$T_s = R_{1\ell} (hT_R + \bar{\alpha} S) + R_{2\ell} T_A \quad (18)$$

where

$$R_{1\ell} = \frac{U_o + U_i + i\omega\bar{C}}{(U_o + U_i + i\omega\bar{C})(h + U_i) - U_i^2}$$

$$R_{2\ell} = \frac{U_o U_i}{(U_o + U_i + i\omega\bar{C})(h + U_i) - U_i^2}$$

while for the continuum model

$$T_s = R_{1c} (hT_R + \bar{\alpha} S) + R_{2c} T_A \quad (19)$$

where

$$R_{1c} = \frac{\sinh kd}{Kk \cosh kd + h \sinh kd}, \quad R_{2c} = \frac{Kk}{Kk \cosh kd + h \sinh kd}$$

The lumped parameters are then chosen to provide the best fit between  $R_{1c}$  and  $R_{1\ell}$  and between  $R_{2c}$  and  $R_{2\ell}$ . This will also provide the best match between the surface temperatures predicted by the two models. It is apparent from Eq. (14) that accurately simulating the response functions or surface temperatures for each material will provide a good simulation of the response of the entire building.

From the form of (18) and (19) we see that the lumped response functions cannot agree with the continuum response functions for all  $\omega$ . For example,  $R_{1\ell}$  approaches a finite constant for large  $\omega$ , while  $R_{1c}$  decreases steadily as  $\omega$  increases. However, not all frequencies are of

interest in the passive solar heating problem. The driving functions  $T_A$  and  $S$  have spectra which are large for  $\omega = 0$  or  $\omega = 2\pi/\text{yr}$  and for frequencies around  $\omega_0 = 2\pi/\text{day}$ . However, their components at high frequency ( $\omega > 3 \omega_0$ ) are generally not very large, so if we can choose the lumped parameters such that  $R_{1\ell}$  and  $R_{1c}$  agree  $0 \leq \omega \lesssim 3 \omega_0$  we should expect good agreement for the lumped and continuum models.

We present two methods for simulating the lumped parameters, one for thin walls and one for thick walls. The definitions of thin and thick will become clear from the analysis; in practice walls thinner than 5" of wood or 10" of concrete are "thin".

For the thin wall model, we use an adaptation of a method suggested by Sonderegger.<sup>13</sup> We look at the poles and zeroes of the response functions. Noting that the  $R_2$  functions have no zeroes, and that their poles are the same as those of the  $R_1$  functions, we can look at  $R_1$  only. Functions of a complex variable can be expanded as

a ratio infinite products 
$$F \cdot \frac{\prod_{i=1}^{\infty} \left(1 - \frac{z}{z_i}\right)}{\prod_{i=1}^{\infty} \left(1 - \frac{z}{p_i}\right)}$$
 where the  $z$ 's and  $p$ 's are

zeroes and poles and  $F$  is the value of the function for  $z = 0$ .

If  $z \ll z_i$  the term  $\left(1 - \frac{z}{z_i}\right)$  will be close to 1. Thus if we look at the function for  $z \ll z_i$  and  $p_i$  we can approximate the function by truncating the product with  $i$  terms, since all terms of higher order than  $i$  will equal 1.

The function  $R_{1\ell}$  has only one pole and one zero, while  $R_{1c}$  has an infinite string of alternating poles and zeroes. All poles and zeroes of all four functions occur along the positive imaginary

$\omega$  axis. If the first pole and zero of  $R_{1c}$  occur at values of  $|\omega|$  much larger than  $3 \omega_0$ , then we can truncate the products for  $R_{1c}$  at one term and get a good approximation<sup>14</sup> for  $R_{1c}$  using  $R_{1\ell}$ . Such a truncation will give us three equations in the three unknowns  $\hat{U}_i$ ,  $\hat{U}_o$  and  $C$ .

These equations are:

$$1) \text{ pole of } R_{1\ell} = \text{first pole of } R_{1c}$$

$$2) \text{ zero of } R_{1\ell} = \text{first zero of } R_{1c}$$

and also 
$$3) R_{1\ell}(\omega = 0) = R_{1c}(\omega = 0)$$

Solving these three equations (see Appendix 2.5A) gives the following results for  $U_i$ ,  $U_o$  and  $\bar{C}$ , which are also summarized in Table 3.

$$U_i = \frac{\Pi^2}{p_1^2} \frac{K}{d} + \left( \frac{\Pi^2}{p_1^2} - 1 \right) h$$

$$U_o = \frac{\frac{K^2}{d} + \left( 1 - \frac{p_1^2}{\Pi^2} \right) K h}{\left( 1 - \frac{p_1^2}{\Pi^2} \right) (K + dh)} \quad (20)$$

$$\bar{C} = \frac{d^2 \rho C_p (U_o + U_i)}{\Pi^2 K}$$

where  $p_1$  is the first solution of  $\tan p_1 = \frac{-p_1 K}{dh}$ .

For the case where the continuum wall is in series with a resistance  $R$ , we cannot simply add the lumped resistance  $\frac{1}{U_i}$  or  $\frac{1}{U_o}$  to the

resistance  $R$  to get the new value of  $\frac{1}{U_i}$  or  $\frac{1}{U_o}$  ; instead the whole process of matching poles and zeroes of response functions must be repeated. The results for inside insulation, outside insulation, and partition walls are shown in Table 3. The derivation is shown in Appendix 2.5A.

As mentioned earlier, the thin wall approximation only works for  $\omega \ll p_1$  or  $z_1$ . Sonderegger shows that this will be true for all

$$\omega \leq \omega_{\max} \quad \text{when} \quad d \lesssim \sqrt{\frac{3K}{\rho C_p \omega_o}} \quad (\omega_{\max} \cong 3 \omega_o), \quad (\text{see Appendix 2.5A}).$$

As an example, we present the comparison between the exact (continuum) response functions and the lumped response functions for 2" concrete in Table 4. This table shows good agreement for both response functions for  $\omega \leq 8 \omega_o$ . Table 5 for 4" wood also shows good agreement for  $\omega \lesssim 3 \omega_o$ , except for some loss of phase lag in the lumped functions. The magnitude of  $R_1$  is graphed for this case in Fig. 8; the solid line represents  $|R_{1c}|$  while the light dashed line represents  $|R_{1l}|$ .

But the agreement worsens for thick materials. Table 6 lists the continuum and lumped response functions for 1½ - foot concrete; and Fig. 9 graphs  $|R_{1c}|$  and  $|R_{1l}|$ . As shown, the agreement becomes poor for  $\omega \gtrsim \omega_o$ .

For thick walls, a number of poles and zeroes of  $R_{1C}$  occur whose magnitude is less than  $3\omega_o$ . Since  $R_1$  has only 1 pole and zero, the locations of these points must be chosen to approximately simulate

the behavior of the many poles and zeroes of  $R_{1c}$ . To do this we require that in the semi-infinite wall limit (the limit of  $d \rightarrow \infty$  and  $U_o \rightarrow 0$ ) that  $R_{1\ell} = R_{1c}$  exactly for some arbitrary frequency  $\omega$ . We chose the frequency to be  $\omega_o$ , since the need for accurate simulation is highest at this frequency. This condition can be expressed as one complex equation in two unknowns  $U_i$  and  $\bar{C}$ . We also require that  $U_i$  and  $\bar{C}$  are real, which ensures that the pole and zero of  $R_{1\ell}$  will be on the positive imaginary  $\omega$  axis. This yields results for  $U_i$  and  $\bar{C}$  for the semi-infinite wall:

$$U_i = \sqrt{2} K |k| \quad (2.21a)$$

$$\bar{C} = \frac{\sqrt{2} \rho C_p}{|k|} \quad (2.21b)$$

Physically, these equations tell us that the effective heat capacity is that contained in the skin depth of thickness  $\frac{\sqrt{2}}{|k|}$  while the effective

inside U-value is just the conductivity K divided by half this skin depth.

For finite thickness walls, we let  $U_o$  be finite and adjust its value to give the correct steady-state U-value  $\left(\frac{K}{d}\right)$  when in series with  $U_i$  :

$$U_o = \left\{ \frac{d}{AK} - (U_i)^{-1} \right\} \quad (2.21c)$$

This method gives functions  $R_{1\ell}$  which agree well with  $R_{1c}$  for several sample materials. Figure 8 shows the comparison between  $|R_{1c}|$  and

$|R_{1\ell}|$  for 6" wood; while Fig. 9 is for 1½' concrete. In both figures, the continuum response functions are plotted with solid lines, while the thick-wall lumped parameter functions are plotted with heavily dashed lines. For comparison, the thin-wall functions are plotted with lightly dashed lines. Figure 9 also shows the comparison in the limit of a semi-infinite concrete slab. The comparisons between both  $R_1$  and  $R_2$  are also listed in Tables 7, 8, and 9, respectively.

Another feature of the thick-wall method is that its values for the lumped parameters join smoothly with those given by the thin wall model. That is, when  $\bar{C}_{thin} = \bar{C}_{thick}$ ,  $U_{i thin} \cong U_{i thick}$  for both wood and concrete. Figure 10 graphs the values of lumped parameters as a function of wall thickness for concrete, and illustrates this smooth transition. The numerical values for the lumped parameters are tabulated in Table 10 for concrete and Table 11 for wood. Because of this transition, we can provide a rule for distinguishing thin walls from thick: whenever  $C_{thin model} > C_{thick model}$ , we use the thick model. Physically, this is because the effective heat capacity of a finite-thickness wall can never exceed that of a semi-infinite wall.<sup>15</sup>

The thick-wall parameters of (21) are chosen to represent a single-layer thick wall. Extension to two-layer walls is done in Appendix 2.5A; the results are summarized in Table 3. Because of the use of the penetration depth in the equations for the lumped parameters, the thick wall approximation should be valid only for  $d > \frac{\sqrt{2}}{|k|}$ . But the thin wall model is valid for  $d < \sqrt{\frac{3}{2}} \frac{\sqrt{2}}{|k|}$ . Thus, the two models overlap and either one or the other should be valid for all thicknesses

of wall. We note, however, that the thick wall model is based on an arbitrary choice of match frequency. Although it appears valid for common building material parameters (such as those for wood or concrete), we have not provided a general demonstration of validity.

The purpose of this section has been to present a methodology for selecting lumped parameters to approximate the performance of a continuum wall with a sandwich wall model. This methodology is summarized in Table 3: for each combination of materials parameters ( $K$ ,  $\rho C_p$ , etc.) one calculates  $C$  for both thick and thin models. Whichever model generates the smaller estimate of  $C$  is used to evaluate  $\hat{U}_i$  and  $\hat{U}_o$ . For a sample of building materials, the lumped-parameter  $R_1$  generally simulate the distributed-parameter  $R_1$  to within 10%; the maximum error observed was less than 30% at  $\omega = 2\pi/\text{week}$  for semi-infinite concrete.

The lumped parameter solution for a whole building is compared to an exact solution in Appendix 2.5B. This Appendix shows the agreement, for one choice of house characteristics, between the lumped parameter solution and the exact solution. The results are summarized in Fig. 11, which compares the room temperature of a house with one continuum wall, first as approximated by the optimal choice of lumped parameters and then with an exact solution. As shown in the figure, the lumped parameters (solid line) provide a good simulation of the exact solution (dashed line).

## 2.6 Summary and Conclusions

This section is intended to present a method for calculating the response of a simple passive solar building to idealized weather. Such a calculation can be used in finding optimum window areas, insulation levels, amounts of heat capacity, etc., for a given climate.

We have described two approaches: a distributed parameter model, which is useful in developing an intuitive understanding of the building, and which works only for unmanaged buildings; and a lumped parameter model, which provides a more approximate solution, but is capable of handling time-dependent building parameters (e.g. night insulation). The results of these approaches are summarized in Tables 1 and 2.

We have developed arguments to show that the approximations made in deriving our results appear to be justified and have shown that for one test case, the results of the lumped parameter approach agree with the exact solution. We will show the agreement with experiment in Sec. 3.

However, much work remains to be done before these models can be used for practical design applications.

First, sample optimization calculations should be done for a few typical climate areas to see which parameters change dramatically with climate and which are relatively unaffected. Optimum free-floating houses should be compared with optimum thermostated units; the habits of the occupants will apparently change the optimal window areas.

Second, further approximations should be made to simplify the arithmetic. The end-product should be a model which can be used by

architects and non-technically-trained building designers. This simplification might generate some simple rules of thumb for design trade-offs.

Third, realistic models of weather should be developed. Computer Fourier transform techniques may be usable to generate best estimates for the weather-frequency  $\omega_w$ , the expected fluctuations in sunlight, and the correlation between cold weather and cloudy weather.

These problems will be discussed in future papers.

We conclude that analytic models can be used, with reasonable accuracy, to model the dynamic thermal response of passive solar buildings, given design weather conditions. These models can be solved in less than an hour with pencil and paper and a slide rule or electronic calculator.

Footnotes to Section 2

1. Ref. 1 describes the heat balance (solar radiation in minus conduction/convection out) on a south-facing window for several typical U.S. climates.
2. Ref. 2 discusses heat balances for different types of glazing.
3. These houses are described in Refs. 5, 10 and 20, and are catalogued in Ref. 6. Ref. 7 contains several-page write-ups of the architecture and thermal performance of 5 passive buildings.
- 3a. See Ref. 3a and the discussion in the beginning of Ref. 4.
4. Ref. 4.
- 4a. Balcomb defines passive solar buildings as those in which energy flows by natural means (Ref. 3c). Our definition of passive is a little more restrictive: we exclude systems which use collectors which are distinct from the building itself.
- 4b. A Trombe wall is a south-facing heavy wall with one or more layers of glazing covering the south or outside surface. The sunlight is absorbed after passing through the glazing (see Fig. 7). The air in the channel between the wall surface and the glazing may be coupled convectively to the room air through slots in the bottom of the wall. The inventor of the Trombe wall discusses some of its attributes in Ref. 20.
5. See next page.
6. The method for deriving lumped parameters is specific to the surface-absorption model, so it is not clear what values of heat capacity to use for  $C_{\text{room}}$ . But the form of the two curves is

5. The thermal properties of dry soil are not much different from those of concrete (see Table F-1) so we can model the system of floor + soil as a homogeneous material. The actual diffusion problem for a concrete slab with soil underneath is three dimensional. Heat flows along curved paths from the inside floor surface to ground surface and then to the air.

To first approximation, we can model this system as a one-dimensional heat flow problem through a thickness of about half the diameter of the floor, particularly if the slab edge is insulated. The exact thickness is unimportant, since most of the heat transfer occurs in the first foot from the floor surface. The penetration depth for a sinusoidal temperature variation in concrete is about 6" for daily cycles and 8 feet for annual cycles.

---

Table F-1  
Thermal Properties of Concrete and Soil

	$\rho$ (lb/ft <sup>3</sup> )	$C_p$ (Btu/lb)	$K$ ( $\frac{\text{Btu}}{\text{F}^\circ\text{-hr-ft}}$ )	$\alpha = \frac{K}{\rho C_p}$ ( $\frac{\text{ft}^2}{\text{hr}}$ )
Concrete (Ashrae) (Ref. 15)	144	.156	.54	.024
Concrete (LASL) (measured)	$\rho C_p = 18.$		.8	.044
Concrete (Neville) (Ref. 16)	140	.20-.28	.98	.02- .06
Dry Soil (Rose) (Ref. 17)	~60	~.20	~.5	~.020-.045

---

sufficiently different that even if we were to choose a different value for  $C_{\text{room}}$ , the agreement would still be poor. (Note that the value of  $U$  that is used is not ambiguous. The model must always give the same steady-state heat loss as the exact solution).

7. See Appendix 2.3 for description of house parameters.
8. Values are from Ashrae Handbook of Fundamentals, Ref. 15, for gypsum board  $\rho = 50 \text{ lbs/ft}^3$ ;  $K = 0.075 \text{ Btu/}^\circ\text{F-ft-hr}$ . Heat capacity  $C_p$  is not listed, so we use the value of  $0.259 \text{ Btu/}^\circ\text{F}$  for gypsum.
9. The discrete form of the Laplace transform is called the z-transform; it is described in some detail for building models in Ref. 29.
10. This is apparent from looking at the output of the TWOZONE program (for a description of the program see Ref. 8). TWOZONE provides as output a graph of room temperature, ambient temperature, furnace output, and thermostat setting as a function of time. (see Fig. 1.3) The graph covers the first four days of each month.

One can get an idea of the passive performance of the TWOZONE house by setting the thermostat very low (e.g. 55 or even 40 F) and looking at the fluctuations in room temperature. But to do so, requires first trying to find typical circumstances of outside weather - which hopefully occur during the first four days of the month - and then looking at the response of the building to custom-selected typical weather. It would be much easier to simply program in the desired "typical" weather.

11. Concrete and soil both have thermal properties which depend on the detailed description of the individual specimen. Moisture

content and density are properties which strongly affect the thermal transmission of both soil and concrete, and which are highly variable.

Typical values for the properties lead to thermal parameters which are roughly the same, as shown in footnote 5; thus for simplicity we model the floor and soil as a single entity. This approximation will break down if there is moisture transport through the soil under the house.

12. This is the case if  $\frac{B}{A}$  varies slowly with  $\omega$ , as shown in Appendix 2.4.
13. See Ref. 9, Chapter III.
14. A truncated infinite product expansion of a response function does not minimize the mean-square error of the result; however, it does maintain the correct location of poles and zeroes and it also apparently preserves minima and maxima of the resulting function in the time domain (see Ref. (19)). These last properties are important in the case of a passive solar house. One important criterion of a good model is that the hottest and coldest temperatures be predicted correctly. A minimum-least-square-error fit of the response functions may allow the extreme temperatures of the approximate solution to overshoot the correct answer, while the product expansion method will preserve the correct temperature extrema.
15. Actually, at a fixed frequency, there is an optimum thickness of wall which maximizes the heat storage in the wall. This thickness

15. is  $\frac{1}{|k|}$ , since for  $\Pi > \left| \frac{kd}{\sqrt{2}} \right| > \frac{\Pi}{2}$ ,  $T(x)$  is negative and the  
cont. increasing thickness slightly diminishes the heat stored in the wall. However, this optimum thickness varies with frequency, so for a range of frequencies, a thicker wall should always store slightly more heat than a thinner wall.
16. The NBSLD program (see Ref. 11 for program description) assumes that the solar gain is spread uniformly over all interior surfaces. The Cal/ERDA or DOE-1 program (see Ref. 18) and NECAP (see Ref. 12) both use the weighting factors given by ASHRAE (Ref. 15). The derivation of these weighting factors has never been described in a paper, but is based on some computer runs by G. P. Mitalas, assuming typical office building conditions, such as light-colored floors, relatively small windows (less than half of wall area). These conditions would not be appropriate for simulating passive solar buildings (personal communication, G. P. Mitalas, telephone 4 July 1978). The TWOZONE program (see Ref. 8) uses weighting factors for solar absorption based on the above results, also. In addition, the results used in the programs simply distinguish between light, medium, or heavy-weight rooms; they do not consider the precise materials properties (conductivity, heat capacity, etc.) of the walls.
17. This sinusoidal solar gain function is shown to be a good approximation to the data for at least one particular climate in Ref. 21.
18. See Ref. 9, Chapter IV.

19. Measurements performed on identical townhouses by the Princeton Center for Environmental Studies show a 2:1 variation in energy consumption between different houses. Only about 2/3 of this variation can be accounted for by the behavior of the occupants. See Refs. 9 and 14 for details.
20. See Ref. 19 for a discussion of simulating Fourier or Laplace response functions using infinite product expansions.
21. See the discussion of the Kelbaugh house in Ref. 7.
22. As mentioned, the failures are not usually written up, so there is no written citation for this case. This example is based on conversations with Philip Caesar of the Solar Center, 62 Townsend Street, San Francisco. Both he and Professor Marshall Merriam of the University of California have said that there are many such houses in existence.
23. The British "Admittance Procedure" can be used to model building response to simplified "design-condition" weather, as is done in Ref. 33. However, the procedure is of more limited applicability than our model; it is intended for use in describing summer conditions only.

Table 1

A PROGRAM FOR EVALUATING THE LUMPED PARAMETER EQUATIONS

$$N_w = \frac{1}{\hat{U}_q} \frac{\hat{h}_w \hat{U}_{wi}}{\hat{h}_w + \hat{U}_{wi}}$$

$$N_f = \frac{1}{\hat{U}_q} \frac{\hat{h}_f \hat{U}_{fi}}{\hat{h}_f + \hat{U}_{fi}}$$

$$N_R = 1 + N_w + N_f$$

$$N_s = \frac{N_w \alpha_w}{\hat{U}_{wi}} + \frac{N_f \alpha_f}{\hat{U}_{fi}} + \frac{\alpha_R}{\hat{U}_q}$$

$$\lambda_w = \frac{\hat{U}_q}{C_w} N_w$$

$$\lambda_f = \frac{\hat{U}_q}{C_f} N_f$$

$$\Lambda_P = \lambda_w \left( 1 - \frac{N_w}{N_R} \right) + \frac{\hat{U}_{wo}}{C_w}$$

$$\Lambda_G = \lambda_f \left( 1 - \frac{N_f}{N_R} \right) + \frac{\hat{U}_{fo}}{C_f}$$

$$\Lambda_F = \frac{\lambda_w N_f}{N_R} = \frac{\hat{U}_q N_f N_w}{C_w N_R}$$

Table 1 (cont'd) pg.2

$$\Lambda_Q = \frac{\lambda_f N_w}{N_R} = \frac{\hat{U}_q N_f N_w}{C_f N_R}$$

$$a_1 = \frac{\lambda_w}{N_R \hat{U}_q}$$

$$a_2 = \lambda_w \left( \frac{\alpha_w}{\hat{h}_w} + \frac{N_s}{N_R} \right)$$

$$a_3 = \frac{\lambda_w}{N_R} + \frac{\hat{U}_{wo}}{C_w}$$

$$a_4 = \frac{\lambda_f}{N_R \hat{U}_q}$$

$$a_r = \lambda_f \left( \frac{\alpha_f}{\hat{h}_f} + \frac{N_s}{N_R} \right)$$

$$a_6 = \frac{\lambda_f}{N_R} + \frac{\hat{U}_{fo}}{C_f}$$

$$\Lambda_X = \Lambda_P \Lambda_G - \Lambda_F \Lambda_Q$$

Table 1 (cont.) p.3

$$\chi_{A_w} = \frac{a_3(\Lambda_G + i\omega_0) + a_6 \Lambda_F}{(\Lambda_P + i\omega_0)(\Lambda_G + i\omega_0) - \Lambda_F \Lambda_Q}$$

$$\chi_{A_f} = \frac{a_6(\Lambda_P + i\omega_0) + a_3 \Lambda_Q}{(\Lambda_P + i\omega_0)(\Lambda_G + i\omega_0) - \Lambda_F \Lambda_Q}$$

$$\chi_{S_w} = \frac{a_2(\Lambda_G + i\omega_1) + a_5 \Lambda_F}{(\Lambda_P + i\omega_1)(\Lambda_G + i\omega_1) - \Lambda_F \Lambda_Q}$$

$$\chi_{S_f} = \frac{a_5(\Lambda_P + i\omega_1) + a_2 \Lambda_Q}{(\Lambda_P + i\omega_1)(\Lambda_G + i\omega_1) - \Lambda_F \Lambda_Q}$$

$$T_{H_w} = \frac{a_1 \Lambda_G + a_4 \Lambda_F}{\Lambda_X} H_0$$

$$T_{H_f} = \frac{a_4 \Lambda_P + a_1 \Lambda_Q}{\Lambda_X} H_0$$

$$\Lambda_{1_2} = \frac{1}{2}(\Lambda_P + \Lambda_G) \mp \frac{1}{2} \sqrt{(\Lambda_P + \Lambda_G)^2 - 4\Lambda_X}$$

$$K_{1_2} = \frac{-\Lambda_{1_2} + \Lambda_P}{\Lambda_F}$$

$$t_n = 24 \text{ hours} - t_d$$

Table 1 (cont.) p. 4

$$Y_4 = (e^{-\Lambda_{2n}t_n} - e^{-\Lambda_{1n}t_n})^{-1} \left( 1 - e^{-(\Lambda_{1d}t_d + \Lambda_{1n}t_n)} \right)$$

$$Y_5 = (e^{-\Lambda_{2n}t_n} - e^{-\Lambda_{1n}t_n})^{-1} \left( 1 - e^{-(\Lambda_{2d}t_d + \Lambda_{1n}t_n)} \right)$$

$$Y_6 = (e^{-\Lambda_{2n}t_n} - e^{-\Lambda_{1n}t_n})^{-1} \left\{ (\chi_{A_{wd}} - \chi_{A_{wn}}) (1 - e^{i\omega_0 t_d} e^{-\Lambda_{1n}t_n}) \right. \\ \left. + \chi_{S_w} (1 - e^{i\omega_1 t_d} e^{-\Lambda_{1n}t_n}) + (T_{H_{wd}} - T_{H_{wn}}) (1 - e^{-\Lambda_{1n}t_n}) \right\}$$

$$Y_1 = e^{-\Lambda_{1d}t_d} - Y_4$$

$$Y_2 = e^{-\Lambda_{2d}t_d} - Y_5$$

$$Y_1 = (\chi_{A_{wd}} - \chi_{A_{wn}}) e^{i\omega_0 t_d} + \chi_{S_w} e^{i\omega_1 t_d} + (T_{H_{wd}} - T_{H_{wn}}) - Y_6$$

$$Q_1 = Y_3 K_{1n} + Y_6 K_{2n} - \left\{ (\chi_{A_{fd}} - \chi_{A_{fn}}) e^{i\omega_0 t_d} + \chi_{S_f} e^{i\omega_1 t_d} + (T_{H_{fd}} - T_{H_{fn}}) \right\}$$

$$Q_2 = K_{1d} e^{-\Lambda_{1d}t_d} - Y_1 K_{1n} - Y_4 K_{2n}$$

$$Q_3 = K_{2d} e^{-\Lambda_{2d}t_d} - Y_2 K_{1n} - Y_5 K_{2n}$$

$$Q_4 = (\chi_{A_{fd}} - \chi_{A_{fn}}) + \chi_{S_f} + (T_{H_{fd}} - T_{H_{fn}}) - Y_3 K_{1n} e^{-\Lambda_{1n}t_n} - Y_6 e^{-\Lambda_{2n}t_n}$$

Table 1 (cont.)p.5

$$Q_5 = K_{2d} - Y_2 K_{1n} e^{-\Lambda_{1n} t_n} - Y_5 K_{2n} e^{-\Lambda_{2n} t_n}$$

$$Q_6 = K_{1d} - Y_1 K_{1n} e^{-\Lambda_{1n} t_n} - Y_4 K_{2n} e^{-\Lambda_{2n} t_n}$$

$$B_{1d} = \frac{Q_3 Q_4 + Q_1 Q_5}{Q_2 Q_5 - Q_3 Q_6}$$

$$B_{2d} = \frac{Q_1 - Q_2 B_{1d}}{Q_3}$$

$$B_{1n} = Y_1 B_{1d} + Y_2 B_{2d} + Y_3$$

$$B_{2n} = Y_4 B_{1d} + Y_5 B_{2d} + Y_6$$

$$T_w = \begin{cases} B_{1d} e^{-\Lambda_{1n} t} + B_{2d} e^{-\Lambda_{2d} t} + \chi_{A_{wd}} \Delta T_A e^{i\omega_o t} + \chi_{Sw} S_1 e^{i\omega_1 t} + T_{H_{wd}} & 0 \leq t < t_d \\ B_{1n} e^{-\Lambda_{1n} (t-t_d)} + B_{2n} e^{-\Lambda_{2n} (t-t_d)} + \chi_{A_{wn}} \Delta T_A e^{i\omega_o t} + T_{H_{wn}} & t \leq t_d < + 24 \text{ hours} \end{cases}$$

Table 1 (cont.) p.6

$$T_f = B_{1d} K_{1d} e^{-\Lambda_{1d} t} + B_{2d} K_{2d} e^{-\Lambda_{2d} t} + \chi_{A_{fd}} \Delta T_A e^{i\omega_0 t} + \chi_{Sf} S_1 e^{i\omega_1 t} + T_{H_{fd}} \quad 0 \leq t < t_d$$

$$B_{1n} K_{1n} e^{-\Lambda_{1n}(t-t_d)} + B_{2n} K_{2n} e^{-\Lambda_{2n}(t-t_d)} + \chi_{A_{fn}} \Delta T_A e^{i\omega_0 t} + T_{H_{fn}} \quad t_d \leq t < 24 \text{ hrs}$$

$$T_R(t) = \frac{N_w}{N_R} T_w + \frac{N_f}{N_R} T_f + \frac{1}{N_R} \Delta T_A e^{i\omega_0 t} + \frac{N_s}{N_R} S_1 e^{i\omega_1 t} + \frac{1}{N_R \hat{U}_q} H_o$$

Table 1a

Definitions: Trombe Wall Case

$$N_w = \frac{\hat{h}_{wc} \hat{U}_{CR} \hat{U}_{wi}}{\hat{U}_q \hat{\Sigma} (\hat{U}_{wi} + \hat{U}_a)} + \frac{\hat{U}_{wo}}{\hat{U}_q}$$

$$N_f = \frac{1}{\hat{U}_q} \frac{\hat{h}_f \hat{U}_{fi}}{\hat{h}_f + \hat{U}_{fi}}$$

$$N_R = 1 + N_f + \frac{\hat{U}_{wo}}{\hat{U}_q} + \frac{\hat{U}_{CR}}{\hat{\Sigma} \hat{U}_q} \left( \hat{h}_{wc} + \hat{U}_{CA} - \frac{\hat{h}_{wc}^2 \hat{U}_{CR}}{\hat{\Sigma} (\hat{U}_{wi} + \hat{U}_a)} \right)$$

$$N_S = \frac{\alpha_w \hat{h}_{wc} \hat{U}_{CR}}{\hat{U}_q (\hat{U}_{wi} + \hat{U}_a) \hat{\Sigma}} + \frac{\alpha_f N_f}{\hat{U}_{fi}} + \frac{\alpha_R}{\hat{U}_q}$$

$$N_A = 1 + \frac{\hat{U}_{CA} \hat{U}_{CR}}{\hat{U}_q \hat{\Sigma}} + \frac{\hat{h}_{wc}^2 \hat{U}_{CA} \hat{U}_{CR}}{\hat{\Sigma}^2 (\hat{U}_{wi} + \hat{U}_a)}$$

$$\lambda_f = \frac{1}{C_w} \left( \frac{\hat{U}_{fi} \hat{h}_f}{\hat{U}_{fi} + \hat{h}_f} \right)$$

$$\lambda_R = \frac{1}{C_w} \left( \hat{U}_{wo} + \frac{\hat{h}_{wo} \hat{U}_{CR} \hat{U}_{wi}}{\hat{\Sigma} (\hat{U}_{wi} + \hat{U}_a)} \right)$$

$$\Lambda_P = \frac{1}{C_w} \left[ \frac{\hat{U}_{wi} \hat{U}_a}{\hat{U}_{wi} + \hat{U}_a} + \hat{U}_{wo} \right] - \lambda_R \frac{N_w}{N_R}$$

Table 1a (cont.) p.2

$$\Lambda_G = \lambda_f \left( 1 - \frac{N_f}{N_R} \right) + \frac{\hat{U}_{fo}}{C_f}$$

$$\Lambda_F = \lambda_R \frac{N_f}{N_R}$$

$$\Lambda_Q = \lambda_f \frac{N_w}{N_R}$$

$$a_1 = \frac{\lambda_R}{N_R \hat{U}_q}$$

$$a_2 = \frac{\alpha_w}{C_w} \frac{\hat{U}_{wi}}{\hat{U}_{wi} + \hat{U}_a} + \lambda_R \frac{N_s}{N_R}$$

$$a_3 = \lambda_R \frac{N_A}{N_R} + \frac{\hat{U}_{wi} \hat{h}_{wc} \hat{U}_{CA}}{C_w \hat{\Sigma} (\hat{U}_{wi} + \hat{U}_a)}$$

$$a_4 = \frac{\lambda_f}{N_R \hat{U}_q}$$

$$a_5 = \lambda_f \left( \frac{\alpha_f}{\hat{h}_f} + \frac{N_s}{N_R} \right)$$

$$a_6 = \lambda_f \frac{N_A}{N_R} + \frac{\hat{U}_{fo}}{C_f}$$

Table 2. Solution to the Distributed Parameter Model

$$T_R(t) = \left( \bar{S} + \Delta S_w \cos \omega_w t \right) \left\{ \sum_{n=1}^3 \frac{B(n\omega_o)}{A(n\omega_o)} d_n e^{in\omega_o t} \right\} + \bar{S} \frac{B(0)}{A(0)} d_o + \Delta S_w \frac{B(\omega_w)}{A(\omega_w)} d_o e^{i\omega_w t}$$

$\leftarrow$  diurnal solar term  $\rightarrow$        $\leftarrow$  steady-state solar  $\rightarrow$        $\leftarrow$  weather varying solar  $\rightarrow$

$$+ \bar{T}_A + \Delta T_A \frac{C(\omega_w)}{A(\omega_w)} e^{i\omega_w t} + \Delta T_A \frac{C(\omega_o)}{A(\omega_o)} e^{i\omega_o t} + \frac{H}{A(0)}$$

$\nearrow$  steady state temperature       $\leftarrow$  weather varying temperature  $\rightarrow$        $\leftarrow$  diurnal temperature  $\rightarrow$        $\nwarrow$  steady-state heater

where  $\bar{S}$  is the average solar gain amplitude

$\Delta S_w$  is the weather-variation of solar gain amplitude

$\omega_w$  is the weather frequency

$$d_o = \frac{\omega_o}{\pi\omega_1}$$

$$d_n = \begin{cases} \frac{\omega_o}{\pi} \frac{\omega_1}{\omega_1^2 - (n\omega_o)^2} (1 + e^{-in\omega_o t_d}) & n\omega_o \neq \omega_1 \\ \frac{\omega_o}{2\pi} \frac{t_d}{i} & n\omega_o = \omega_1 \end{cases}$$

$\bar{T}_A$  is average ambient temperature

$\Delta T_A$  is the complex amplitude of diurnal ambient temperature

variation and A, B and C are functions of frequency

defined below:

$$A(\omega) = \hat{U}_q + \hat{h}_e (1 - h_e R_{1e}) + \hat{h}_p (1 - h_p R_{1p}) + \hat{h}_f (1 - h_f R_{1f})$$

Table 2 (cont.) p.2

$$B(\omega) = \alpha_R + \alpha_e h_e R_{1e} + \alpha_p h_p R_{1p} + \alpha_f h_f R_{1f}$$

$$C(\omega) = \hat{U}_q + \hat{h}_e R_{2e} + \hat{h}_f R_{2f}$$

where the subscripts e, p, and f stand for envelope walls, partition walls, and floor

The response functions  $R_{1j}$  and  $R_{2j}$  are functions of frequency which depend on materials properties. They are:

$$R_{1,e \text{ or } f} = \frac{\cosh kd + \frac{1}{Rk} \sinh kd}{(h + \frac{1}{R}) \cosh kd + (Kk + \frac{h}{Rk}) \sinh kd}$$

$$R_{2,e \text{ or } f} = \frac{\frac{1}{R}}{(h + \frac{1}{R}) \cosh kd + (Kk + \frac{h}{Rk}) \sinh kd}$$

where  $k = \sqrt{\frac{i\omega\rho c_p}{K}} = \sqrt{\frac{\omega\rho c_p}{2K}} (1+i)$

$R$  is the thermal resistance of the insulation on the outside of the wall,

$R_{1p}$  has the same form for  $R \rightarrow \infty$ ,

$$R_{2p} = 0,$$

and  $\cosh x(1+i) = \cosh x \cos x + i \sinh x \sin x$

$$\sinh x(1+i) = \sinh x \cos x + i \cosh x \sin x$$

for  $x$  real

Table 3 Equations for the Lumped Parameters

Case	$z_1$	$P_1$	$\hat{U}_i$	$\hat{U}_o$	C
Base Wall		$\tan P_1 = \frac{-P_1 K}{dh}$	$\frac{\pi^2}{P_1^2} \frac{AK}{d} + \left(\frac{\pi^2}{P_1^2} - 1\right) \hat{h}$	$\left(\frac{d}{AK} - \hat{U}_i\right)^{-1}$	$\frac{d^2 \rho c_p (\hat{U}_i + \hat{U}_o)}{\pi^2 K}$
					$\frac{\sqrt{2} \rho c_p A}{ k }$
Outside Insulation	$\tan z_1 = \frac{-z_1 K}{U_r d}$	$\tan P_1 = \frac{P_1 (U_r + h)}{K P_1 \frac{U_r h d}{d} - \frac{K}{d}}$	$\frac{z_1^2}{P_1^2} \frac{AK \hat{U}_r}{dU_r + AK} + \left(\frac{z_1^2}{P_1^2} - 1\right) \hat{h}$	$\left(\frac{d}{AK} - \hat{U}_i^{-1} + \hat{U}_r\right)^{-1}$	$\frac{d^2 \rho c_p (\hat{U}_i + \hat{U}_o)}{z_1^2 K}$
					$\frac{\sqrt{2} AK  k }{ k }$
Inside Insulation	$\tan z_1 = \frac{-z_1 K}{U_c d}$	$\tan P_1 = \frac{-P_1 K (h + U_c)}{h U_c d}$	$\frac{z_1^2}{P_1^2} \frac{AK \hat{U}_c}{AK + d\hat{U}_c} + \left(\frac{z_1^2}{P_1^2} - 1\right) \hat{h}$	$\left(\frac{d}{AK} - \hat{U}_i^{-1} + \hat{U}_c\right)^{-1}$	$\frac{d^2 \rho c_p (\hat{U}_i + \hat{U}_o)}{z_1^2 K}$
					$\frac{\sqrt{2} \rho c_p A}{ k }$
Partition Wall		$\tan P_1 = \frac{hd}{K P_1}$	$h \left(\frac{\pi^2}{4 P_1^2} - 1\right)$	0	$\frac{4 \rho c_p d^2 \hat{U}_i}{\pi^2 K}$
					$\frac{\sqrt{2} \rho c_p A}{ k }$

Table 4  
Response Functions for 2" Thick Concrete\*

$\omega$	Continuum Model		Lumped Model	
	$R_1 \left( \frac{\text{hr-ft}^2-\text{°F}}{\text{Btu}} \right) R_2$			
0	.211	.684	.211	.684
$2\pi/\text{month}$	.211 $e^{-.002i}$	.684 $e^{-.004i}$	.211 $e^{-.002i}$	.684 $e^{-.003i}$
$2\pi/\text{week}$	.211 $e^{-.010i}$	.683 $e^{-.017i}$	.211 $e^{-.009i}$	.683 $e^{-.013i}$
$2\pi/\text{day}$	.210 $e^{-.064i}$	.681 $e^{-.119i}$	.210 $e^{-.060i}$	.681 $e^{-.091i}$
$2\pi/12 \text{ hrs}$	.208 $e^{-.136i}$	.672 $e^{-.236i}$	.208 $e^{-.119i}$	.672 $e^{-.181i}$
$2\pi/ 8 \text{ hrs}$	.204 $e^{-.200i}$	.659 $e^{-.351i}$	.204 $e^{-.176i}$	.659 $e^{-.267i}$
$2\pi/ 3 \text{ hrs}$	.175 $e^{-.456i}$	.548 $e^{-.855i}$	.175 $e^{-.391i}$	.552 $e^{-.631i}$

\* Assumes ASHRAE properties:  $\rho = 144 \text{ lbs/ft}^3$ ,  $C_p = .156 \frac{\text{Btu}}{\text{lb } \text{°F}}$ ,

$$h = 1.5 \frac{\text{Btu}}{\text{ft}^2\text{-hr-deg F}}, \quad K = .54 \frac{\text{Btu}}{\text{°F-hr-ft}}$$

Table 5  
Response Functions for 4" Thick Wood\*

$\omega$	Continuum Model		Lumped Model	
	$R_1 \left( \frac{\text{hr-ft}^2-\text{°F}}{\text{Btu}} \right)$	$R_2$	$R_1 \left( \frac{\text{hr-ft}^2-\text{°F}}{\text{Btu}} \right)$	$R_2$
0	.587	.120	.587	.120
$2\pi/\text{month}$	$.587 e^{-.005i}$	$.120 e^{-.027i}$	$.587 e^{-.004i}$	$.120 e^{-.017i}$
$2\pi/\text{week}$	$.586 e^{-.022i}$	$.119 e^{-.113i}$	$.586 e^{-.015i}$	$.119 e^{-.071i}$
$2\pi/\text{day}$	$.562 e^{-.136i}$	$.106 e^{-.759i}$	$.564 e^{-.090i}$	$.107 e^{-.462i}$
$2\pi/8 \text{ hrs}$	$.489 e^{-.246i}$	$.061 e^{-1.856i}$	$.502 e^{-.117i}$	$.067 e^{-.981i}$
$2\pi/3 \text{ hrs}$	$.410 e^{-.335i}$	$.018 e^{-3.474i}$	$.468 e^{-.064i}$	$.029 e^{-1.325i}$

\* Assumes materials properties of  $\rho C_p = 9 \text{ Btu/ft}^3-\text{°F}$ ,

$$K = 0.068 \text{ Btu/°F-hr-ft} ,$$

$$h = 1.5 \text{ Btu/°F-hr-ft}^2 .$$

Table 6  
Response Functions for 1½-ft Thick Concrete

$\omega$	Continuum Model		Lumped Model (thin wall)	
	$R_1 \left( \frac{\text{hr-ft}^2-\text{°F}}{\text{Btu}} \right)$	$R_2$	$R_1 \left( \frac{\text{hr-ft}^2-\text{°F}}{\text{Btu}} \right)$	$R_2$
0	.538.	.194	.538	.194
2 $\pi$ /month	.535 e <sup>-.052i</sup>	.192 e <sup>-.188i</sup>	.536 e <sup>-.039i</sup>	.192 e <sup>-.122i</sup>
2 $\pi$ /week	.503 e <sup>-.198i</sup>	.170 e <sup>-.768i</sup>	.505 e <sup>-.142i</sup>	.171 e <sup>-.483i</sup>
2 $\pi$ /day	.329 e <sup>-.428i</sup>	.035 e <sup>+3.137i</sup>	.379 e <sup>-.116i</sup>	.051 e <sup>-1.305i</sup>
2 $\pi$ /8 hrs.	.233 e <sup>-.535i</sup>	.003 e <sup>+4.467i</sup>	.366 e <sup>-.043i</sup>	.017 e <sup>-1.480i</sup>

\* Assumes ASHRAE properties  $\rho = 144 \frac{\text{lbs}}{\text{ft}^3}$ ,  $C_P = .156 \frac{\text{Btu}}{\text{lb-°F}}$ ,

$$K = .54 \frac{\text{Btu}}{\text{°F-hr-ft}}, \quad h = 1.5 \frac{\text{Btu}}{\text{°F-ft}^2\text{-hr}}$$

Table 7

Response Functions for 6-inch Thick Wood\*

$\omega$	Continuum Model		Lumped Model	
	Thick Wall	Thin Wall	Thick Wall	Thin Wall
	$R_1 \left( \frac{\text{hr-ft}^2-\text{°F}}{\text{Btu}} \right) R_2$			
0	.611	.083	.611	.083
2 $\pi$ /week	.609 e <sup>-.034i</sup>	.082 e <sup>-.238i</sup>	.609 e <sup>-.028i</sup>	.610 e <sup>-.023i</sup>
2 $\pi$ /day	.558 e <sup>-.159i</sup>	.055 e <sup>-1.436i</sup>	.554 e <sup>-.115i</sup>	.563 e <sup>-.085i</sup>
2 $\pi$ /8 hrs	.488 e <sup>-.241i</sup>	.019 e <sup>-3.233i</sup>	.500 e <sup>-.078i</sup>	.525 e <sup>-.053i</sup>

\*Assumes  $\rho C_p = 9 \frac{\text{Btu}}{\text{°F-ft}^3}$ ,  $K = .068 \frac{\text{Btu}}{\text{°F-ft-hr}}$ ,  $h = 1.5 \frac{\text{Btu}}{\text{ft}^2\text{-deg F-hr}}$

Table 8  
RESPONSE FUNCTIONS FOR 1½-FOOT THICK CONCRETE\*

$\omega$	Continuum Model		Lumped Model	
	$R_1 \left( \frac{\text{hr-ft}^2-\text{°F}}{\text{Btu}} \right)$	$R_2$	$R_1 \left( \frac{\text{hr-ft}^2-\text{°F}}{\text{Btu}} \right)$	$R_2$
0	.538	.194	.538	.194
$2\pi/\text{month}$	.535 $e^{-.052i}$	.192 $e^{-.188i}$	.537 $e^{-.933i}$	.193 $e^{-.062i}$
$2\pi/\text{week}$	.503 $e^{-.198i}$	.170 $e^{-.768i}$	.524 $e^{-.137i}$	.187 $e^{-.259i}$
$2\pi/2\text{-days}$	.392 $e^{-.364i}$	.083 $e^{-2.045i}$	.429 $e^{-.343i}$	.142 $e^{-.748i}$
$2\pi/\text{day}$	.329 $e^{-.428i}$	.035 $e^{+3.137i}$	.336 $e^{-.367i}$	.092 $e^{-1.076i}$
$2\pi/8\text{ hours}$	.233 $e^{-.535i}$	.003 $e^{+.467i}$	.262 $e^{-.193i}$	.034 $e^{-1.343i}$

\* Assumes ASHRAE materials properties of  $\rho = 144 \frac{\text{lbs}}{\text{ft}^3}$ ,  $C_p = .156 \frac{\text{Btu}}{\text{lb-°F}}$ ,

$$K = .54 \frac{\text{Btu}}{\text{ft-°F-hr}}, \quad h = 1.5 \frac{\text{Btu}}{\text{ft}^2-\text{°F-hr}}$$

Table 9  
RESPONSE FUNCTIONS FOR 20-FOOT (SEMI-INFINITE) CONCRETE\*

$R_1$  ONLY;  $R_2 \sim 0$

$\omega$	continuum model $R_1^{**}$	lumped model $R_1^{**}$
0	.655 (.667)	.655 (.667)
$2\pi/\text{yr}$	.638 $e^{-.043i}$ (.638 $e^{-.042i}$ )	.655 $e^{-.004i}$ (.667 $e^{-.005i}$ )
$2\pi/\text{month}$	.573 $e^{-.132i}$	.653 $e^{-.054i}$ (.664 $e^{-.056i}$ )
$2\pi/\text{week}$	.492 $e^{-.237i}$	.620 $e^{-.216i}$ (.629 $e^{-.224i}$ )
$2\pi/\text{day}$	.329 $e^{-.428i}$	.330 $e^{-.424i}$ (.329 $e^{-.428i}$ )
$2\pi/8\text{-hr}$	.234 $e^{-.535i}$	.260 $e^{-.197i}$ (.260 $e^{-.198i}$ )

\* Assumes ASHRAE materials properties of  $\rho = 144 \frac{\text{lbs}}{\text{ft}^3}$ ,  $C_p = .156 \frac{\text{Btu}}{\text{°F-lb}}$

$$K = .54 \frac{\text{Btu}}{\text{degF-hr-ft}} \quad h = 1.5 \frac{\text{Btu}}{\text{°F-hr-ft}^2}$$

\*\* Dimensions of  $R_1$  are  $\text{°F-ft}^2\text{-hr/Btu}$ .

Table 10  
VALUES OF THE LUMPED PARAMETERS, CONCRETE\*

d	$U_i$ (Btu/°F-hr-ft <sup>2</sup> )		$U_o$ (Btu/°F-hr-ft <sup>2</sup> )		C (Btu/°F-ft <sup>2</sup> )	
	Thin wall model	Thick wall model	thin	thick	thin	thick
$\frac{1}{2}$ inch	51.8		17.3		.51	
1 inch	25.6		8.68		1.00	
2 inch	12.62		4.36		1.99	
3 inch	8.30		2.92		2.96	
8 inch	2.97	2.52	1.114	1.194	7.65	9.64
$10^{\frac{1}{4}}$ inch	2.28	2.52	.875	.844	9.70	9.64
1 foot	1.93	2.52	.750	.687	11.28	9.64
$1\frac{1}{2}$ foot	1.245	2.52	.506	.420	16.61	9.64
3 foot		2.52		.194		9.64
$\infty$		2.52		0		9.64

\* Assumes ASHRAE materials properties  $\rho = 144 \frac{\text{lbs}}{\text{ft}^3}$ ,  $C_p = .156 \frac{\text{Btu}}{\text{°F-lb}}$

$$K = .54 \frac{\text{Btu}}{\text{°F-ft-hr}}, h = 1.5 \frac{\text{Btu}}{\text{°F-ft}^2\text{-hr}}$$

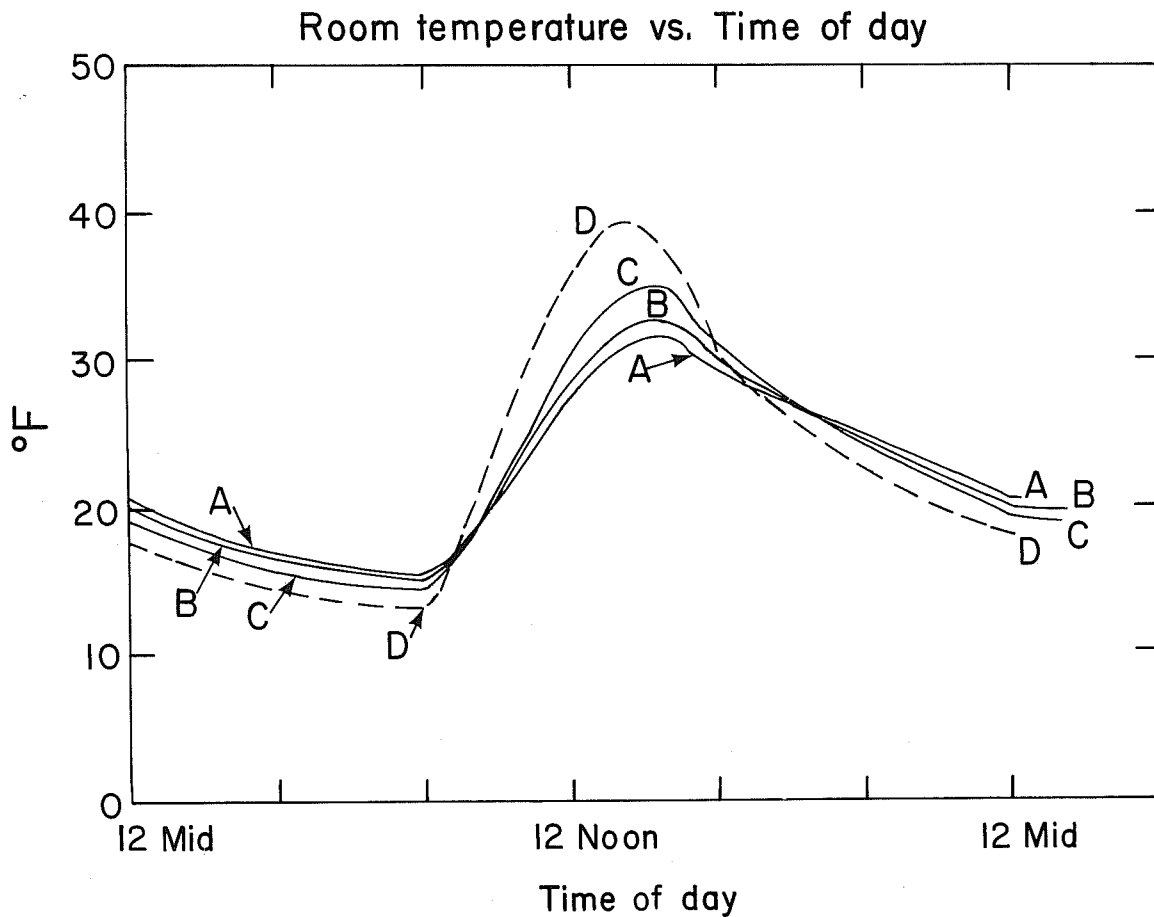
Table 11  
VALUES OF THE LUMPED PARAMETERS, WOOD\*

d	$U_i$ (Btu/°F-hr-ft <sup>2</sup> )		$U_o$ (Btu/°F-ft <sup>2</sup> -hr)		C (Btu/°F-ft <sup>2</sup> )	
	thin wall model	thick wall model	thin	thick	thin	thick
$\frac{1}{4}$ inch	12.73		4.393		.100	
1 inch	2.995		1.121		.383	
2 inch	1.426		.5713		.744	
4 inch	.676	.564	.292	.320	1.442	2.164
5 inch	.534	.564	.235	.230	1.790	2.164
6 inch	.440	.564	.197	.179	2.135	2.164
9 inch	.287	.564	.133	.108	3.167	2.164
1 foot		.564		.0773		2.164
		.564		0		2.164

\* Assumes materials properties of  $\rho C_p = 9$  Btu/°F-ft<sup>3</sup>,  $K = .068$  Btu/°F-ft-hr ,  
 $h = 1.5$  Btu/°F-ft<sup>2</sup>-hr

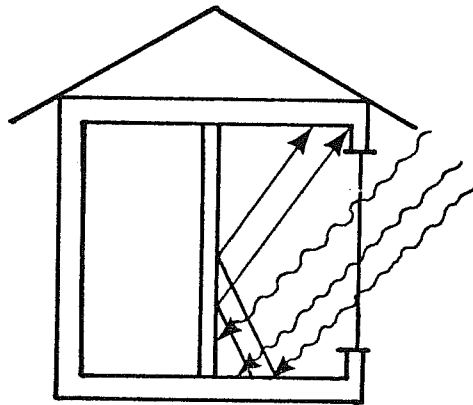


Fig. 1. Interior and exterior photographs of a passive solar house at First Village in Santa Fe, New Mexico. Some of the windows seen in the exterior view provide direct solar gain to the inside, where the sunlight falls on the brick floor. Other windows illuminate Trombe walls of  $1\frac{1}{2}$  foot concrete. (Photos by the author.)



XBL 786-1100

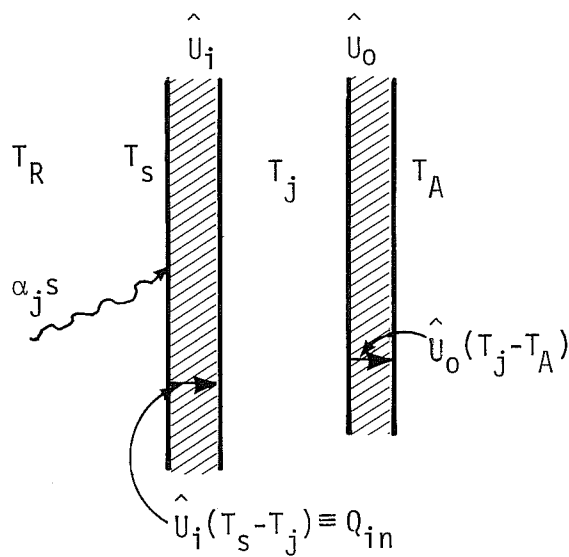
Fig. 2. Room temperature vs. time of day for a passive solar house under four different cases of solar energy absorption. In case A,  $6/7$  of the solar energy is absorbed on the floor and  $1/7$  is absorbed on the walls ( $\alpha_{\text{floor}} = 6/7$ ;  $\alpha_{\text{walls}} = 1/7$ , and  $\alpha_{\text{room}} = 0$ ). Cases B and C successively double the solar absorption on the walls ( $\alpha_{\text{walls}}$ ) and decrease the absorption on the floor ( $\alpha_{\text{floor}}$ ). In case D all sunlight is absorbed in the air or on light furniture or carpets ( $\alpha_{\text{floor}} = \alpha_{\text{walls}} = 0$  and  $\alpha_{\text{room}} = 1$ ). All temperatures are measured with respect to average ambient temperature. The house is described in Appendix 2.3.



XBL 787-1267

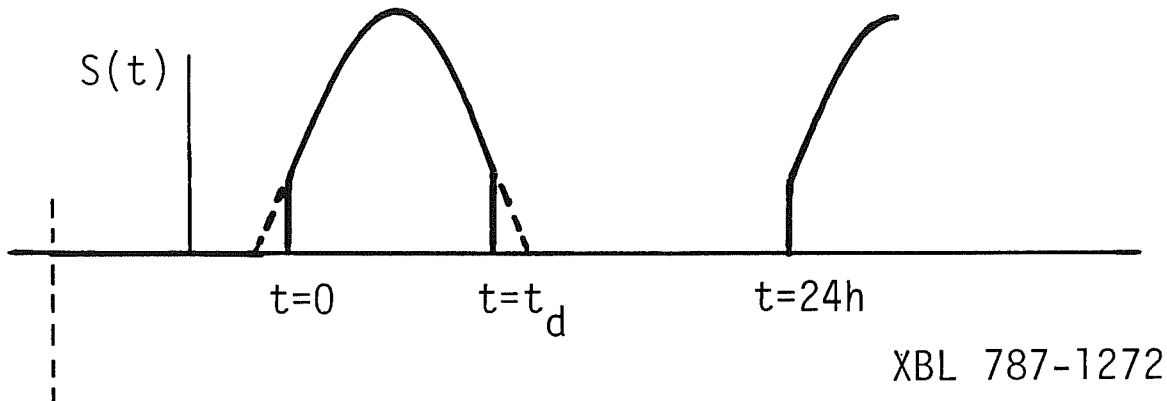
Fig. 3. Sketch of the path of solar energy as it is absorbed and reflected from surfaces in a direct gain building. Actual reflections are likely to be diffuse rather than specular.

Heat Transfers for the Lumped Parameter Model



XBL 787-1269

Fig. 4. Inside the room at the left the temperature is  $T_R$ . Solar energy strikes the inside surface of the  $j^{\text{th}}$  material; the resulting surface temperature is  $T_{Sj}$ . Heat is transferred from the surface to the inside of the wall; the heat flow is given by  $\hat{U}_{ij} (T_{Sj} - T_j)$  or  $Q_{in}$ . The interior of the wall is at a temperature  $T_j$ . Heat flows from the interior to the ambient air at right; this heat flow is given by  $\hat{U}_{oj} (T_j - T_A)$ .



XBL 787-1272

Fig. 5. Assumed form of the solar gain through a south window as a function of time. The same function repeats every day. In this sketch the function jumps discontinuously from zero to a finite value at  $t=0$  and jumps back at  $t=t_d$ . In most cases the curve begins and ends smoothly at zero at these times.

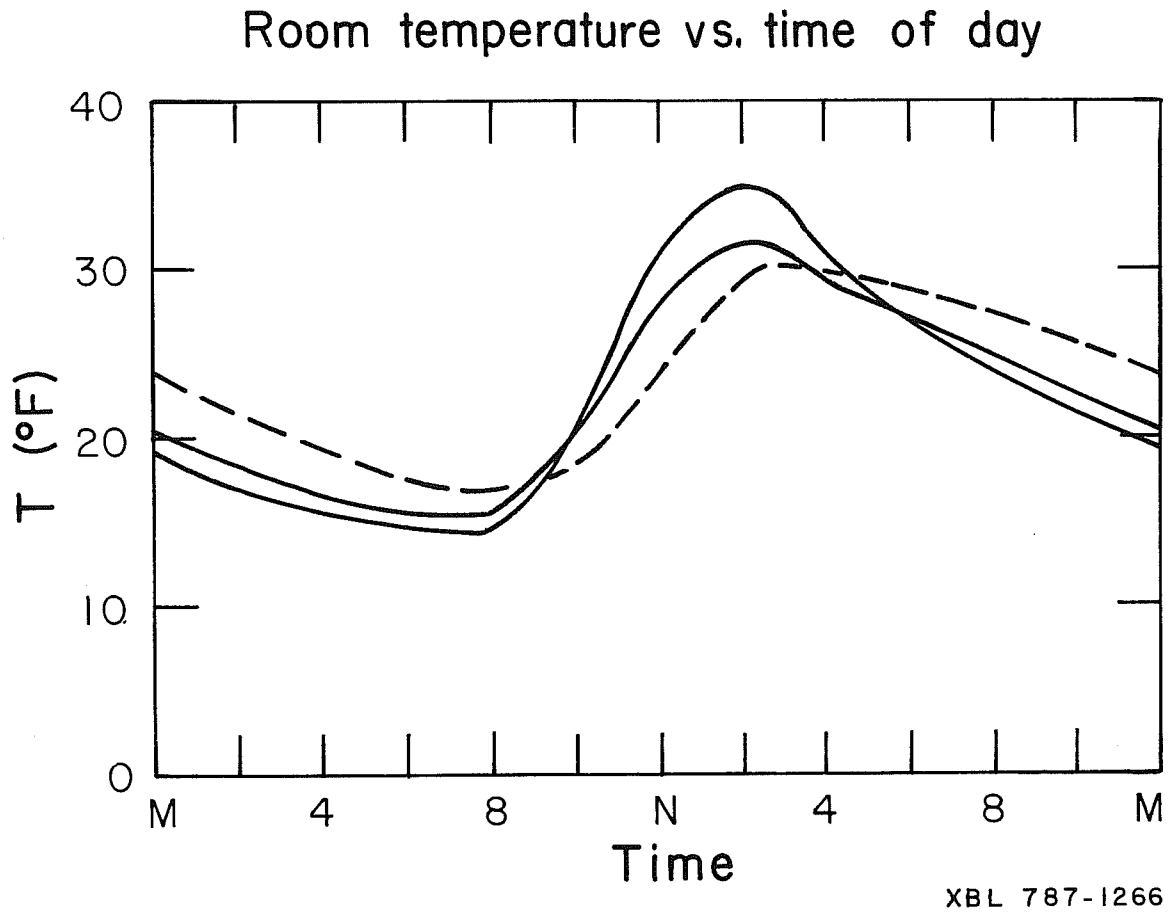
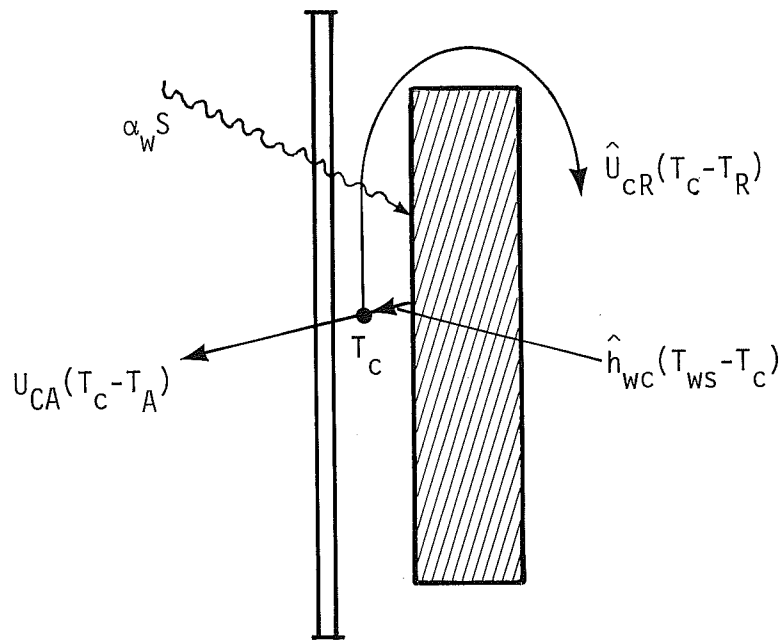
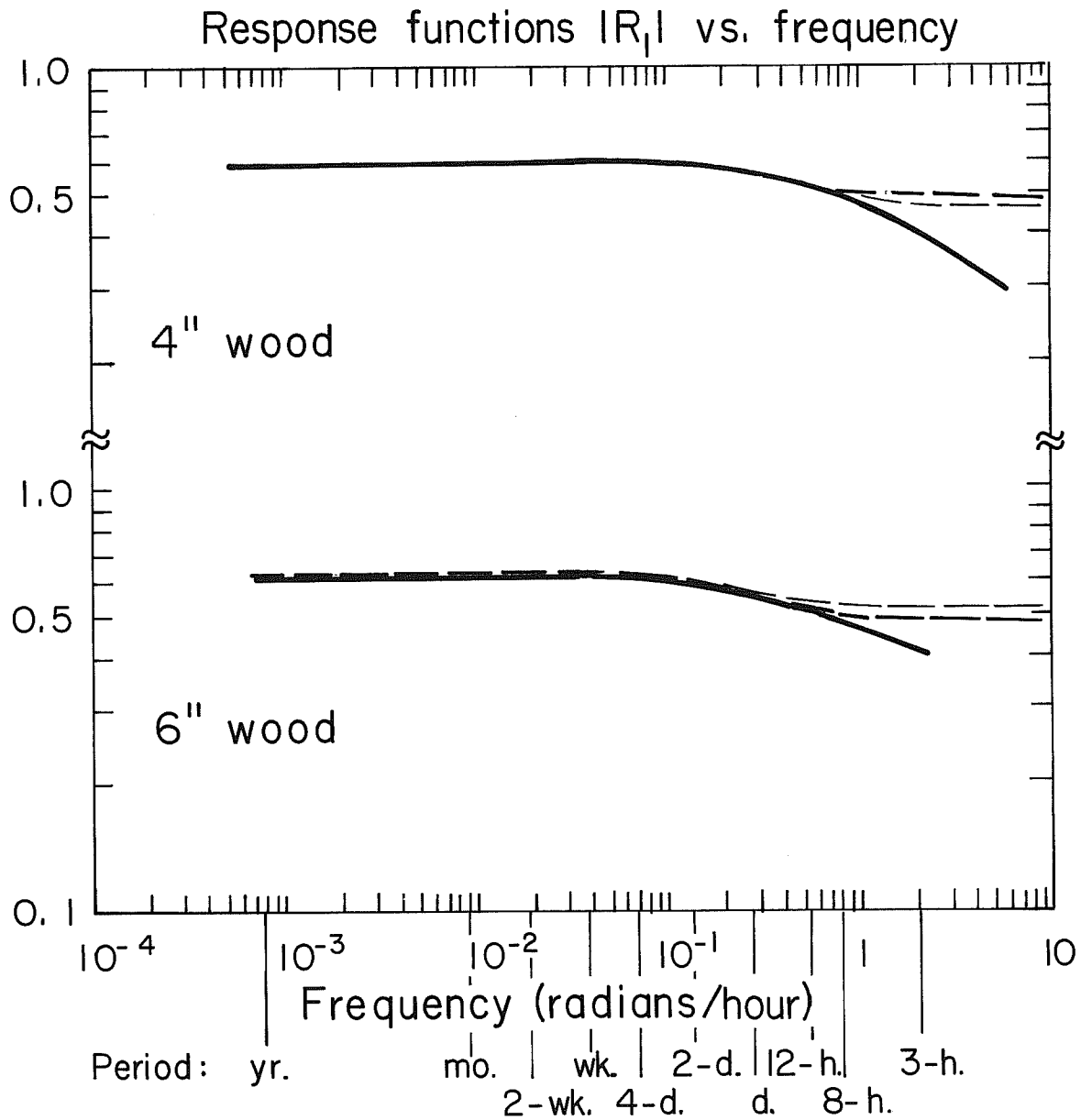


Fig. 6. Room temperature elevation as a function of time of day for different models of solar absorption. The dashed line describes the case where solar heat is absorbed in a massive room; the solid lines graph the response when sunlight is absorbed on material surfaces and transferred to massless room air. The two solid lines represent two different proportions of solar absorption on different material surfaces.



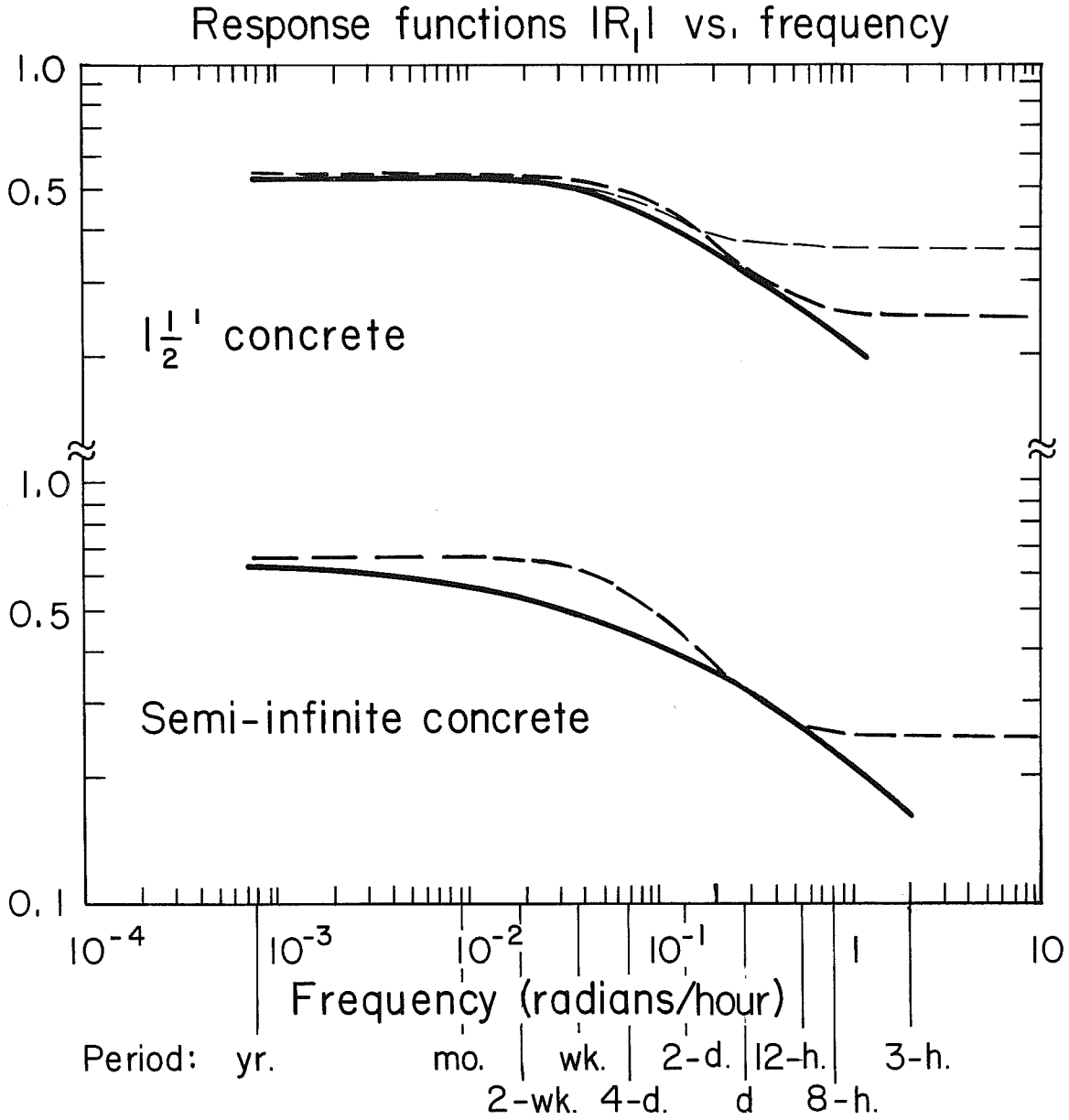
XBL 787-1268

Fig. 7. Heat transfers for the Trombe wall model. Sunlight enters through the window at left and is absorbed on the left-hand surface of the Trombe wall. This wall surface is in thermal contact with the channel air which is at a temperature of  $T_c$ . The channel can lose heat to the outside air at left or to the room at at right.



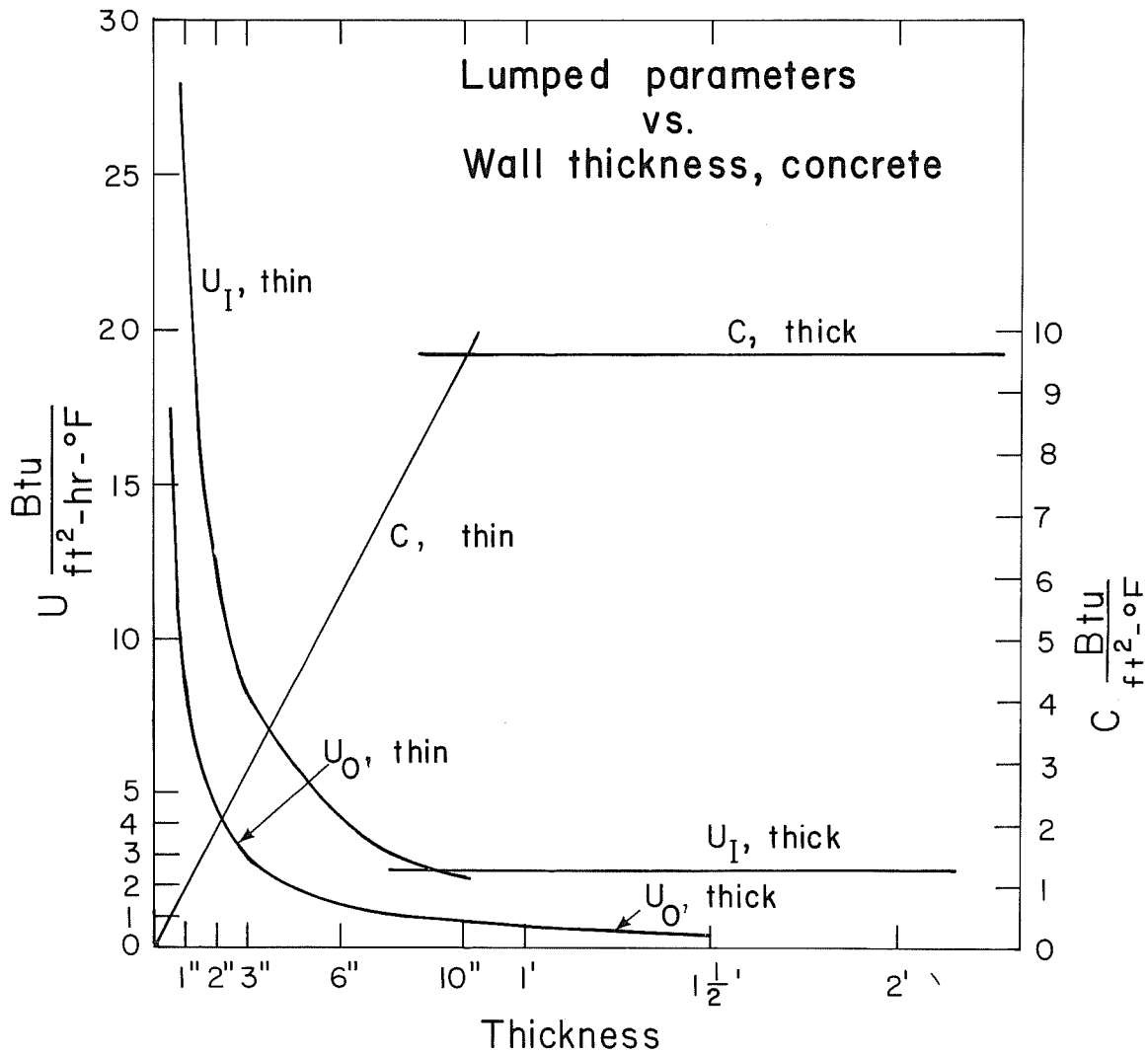
XBL 786 - 1105A

Fig. 8. Response functions as a function of frequency. This figure plots  $\log|R_1|$  vs.  $\log \omega$  for 4" and 6" wood. The solid lines represent the continuum response functions. The heavy dashed lines describe the thick-wall lumped model response functions, while the light dashed lines represent thin-wall functions.



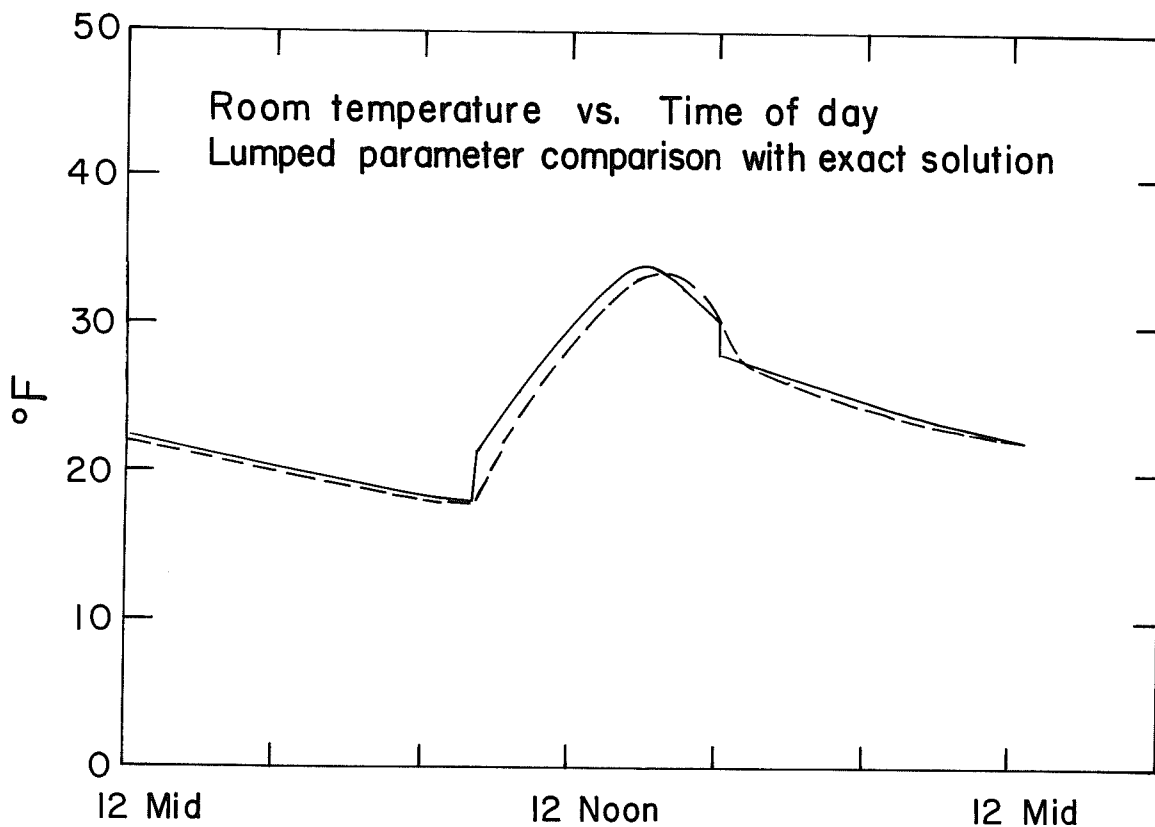
XBL 786 - 1103A

Fig. 9. Response functions as a function of frequency. This figure plots  $\log|R_1|$  vs.  $\log \omega$  for  $1\frac{1}{2}$  foot thick and semi-infinite concrete. The solid lines represent the continuum response functions; the heavy dashed lines describe the thick-wall lumped model response functions; and the light dashed lines represent thin-wall functions.



XBL 786-III3

Fig. 10. Values of the lumped parameters as a function of wall thickness (d) for concrete. Values are tabulated in Table 10.



XBL 786 - 1101A

Fig. 11. Room temperature elevation vs. time for comparing the lumped parameter approximation to an exact solution. The exact solution for room temperature of the building described in Appendix 2.5B is graphed as a dotted line; the lumped parameter approximation is plotted as a solid line.

non-circulating Trombe wall — a thick concrete wall which is located directly behind the window. The air channel between the wall and the window is sealed to prevent air exchange between the channel and the room; thus the path for solar heat gain into the house requires absorption on the front surface of the Trombe wall and diffusion through the wall into the room.

Accurate modelling of the test buildings requires knowledge of the materials properties of the concrete. This is not a trivial look-up exercise, since the conductivity and heat capacity of concrete can vary over a factor of two range even at fixed density.<sup>1</sup> Los Alamos staff measured the conductivity; their estimate appears to be consistent with the data to high accuracy. However, the heat capacity was not measured, and handbook values appear to give inaccurate results.

We therefore begin our discussion of data analysis with a derivation of the heat capacity of Los Alamos concrete from data obtained using thermocouples buried inside the concrete. We conclude that the heat capacity per unit volume is  $18 \text{ Btu}/^\circ\text{F}\text{-ft}^3$  to within about 7%. This determination is described in Sec. 3.2.

In Sec. 3.3, we discuss modelling the direct gain test cell. We first describe the cell, and then evaluate model parameters. Using these parameters, and a design day chosen for time-independent weather patterns, we compare room temperature measurements with predictions of

the lumped parameter and distributed parameter models. We then use another design day chosen for having weather history which could be described by one sinusoidal weather term as in Sec. 2.4. Data for that day are compared with the predictions of Eq. (2.16). Finally, we use a lumped-parameter approach to model the building's response to 18 days of observed weather; this result is compared to measured room temperatures.

We model the Trombe wall cell in Sec. 3.4. As before, we first describe the cell and evaluate its parameters. We note that the lumped parameter approach breaks down for this thick a wall with no thermocirculation, as shown in Appendix 2.5A, and consequently we use only the distributed parameter model. For the two test days described above, we calculate model predictions and compare these with measurements.

In the following section, 3.5, we discuss the Sonoma house experiment. This house used night insulation of its collector window, so it can only be modelled using the lumped parameter approach.

The results of these experiments show excellent agreement between data and experiment. This agreement was obtained, at least in the case of the Los Alamos buildings, using "first guess" values of quantities not directly measured (eg. transmissivities of the windows, air exchange rates); that is, we did not adjust building parameter values to get a better fit.

These results, along with the mathematical similarity between our model and computer codes such as NBSLD, provide some credibility to the model. It remains to be seen whether real buildings

(~ 150 m<sup>2</sup> in floor area) can be adequately described by single-zone models. However, the application of our model to the small buildings described here should provide some insight into what temperatures should be measured to make that comparison efficiently.

### 3.2 Determination of the Heat Capacity of LASL Concrete

In this section, we use temperature data collected from thermocouples located at different positions within the concrete in the LASL test cells to find the heat capacity of LASL concrete. We conclude that its heat capacity is  $18 \pm 1 \text{ Btu}/^\circ\text{F-ft}^3$ ; considerably lower than many handbook estimates but still within the range of values observed in the literature.<sup>2</sup>

The determination is based on measuring the diffusivity of temperature in the concrete. Based on the diffusion equation (2.1), we expect to find temperature distributions inside a slab of concrete which can be expressed as in Eq. (2.5) as

$$T(x,t) = \left\{ A \cosh kd(1-\xi) + B \sinh kd(1-\xi) \right\} e^{i\omega t} \quad (1)$$

where  $k = \sqrt{\frac{i\omega\rho c_p}{K}}$

$$\xi = \frac{x}{d}$$

$K$  = the conductivity of the concrete

$\rho c_p$  = the heat capacity per unit volume

The coefficients  $A$  and  $B$  are determined by the boundary conditions.

Based on Eq. (1), if we Fourier-analyze temperature data, we should find that for any frequency  $\omega$ ,

---

$$T(x,\omega) = A \cosh kd(1-\xi) + B \sinh kd(1-\xi) \quad (2)$$

If we know the temperature  $T(\omega)$  for the front and back surfaces of the material, we can determine A and B from (2) evaluated at  $\xi = 0$  and  $\xi = 1$ , respectively. If we then know  $T(\omega)$  for some intermediate value of  $\xi$ , we can determine k such that the prediction from (2) most closely agrees with the measurement. Knowing k gives us the heat capacity  $\rho c_p$  provided that K, the conductivity, is known.

In fact, K was measured at Los Alamos, it is equal to .80 Btu/°F-hr-ft, which is consistent with our model. Thus we will use the interior temperature data from the LASL concrete walls to find  $\rho c_p$  as described.

We perform the experiments using the component of temperature at frequency  $\omega_0 = 2\pi/24$  hours since there is a large signal at that frequency. The Fourier-transformed temperature for a cycle of length P is given by

$$T(\omega) = \frac{2}{P} \int_{t=0}^{t=P} T(t) e^{-i\omega t} dt \quad (3)$$

Our data is available only at hourly intervals, so we use the approximation

$$T(\omega_0) \cong \frac{2}{P} \sum_{n=0}^{P-1 \text{ hr}} T(t) e^{-i\omega_0 t} \quad (4)$$

We describe four experiments, one using the Trombe cell data for 24 February 1978, which was chosen for having time-independent weather patterns; the second uses the direct gain cell for the same date; the third uses the Trombe cell data for 8 March 1978; and the

fourth uses the Trombe cell data for the 9-day period 21 February to 1 March 1978. Following these experiments is a discussion of results.

Trombe Wall Test: 24 February 1978

The Trombe wall has four thermocouples hooked up to different depths of wall at mid-height. Channel 41 is attached to the front (window-side) surface, Channel 43 is buried 8 inches into the concrete from the front, Channel 44 is 14 inches into the material, and Channel 45 measures back surface (room side) temperature.

Using (4) for the Fourier transform temperatures, we find that

$$\begin{aligned}T_{41} &= 28.09e^{-i3.9872} \\T_{43} &= 9.22e^{-i5.1941} \\T_{44} &= 6.01e^{-i5.8565} \\T_{45} &= 5.68e^{-i5.8067}\end{aligned}$$

Using (2) to find A and B from  $T_{41}$  and  $T_{45}$ , we find that  $A = T_{45}$ . B will then depend on the choice of  $\rho c_p$ . We choose several test values of  $\rho c_p$ , calculate B, and then use A and B to predict  $T_{43}$  and  $T_{44}$ . The results are:

For  $\rho c_p = 28 \text{ Btu/ft}^3\text{-}^\circ\text{F}$  - the LASL handbook-estimate, we find

$$\begin{aligned}T_{43} &= 7.042e^{-5.603i} \\T_{44} &= 5.667e^{-6.065i}\end{aligned}$$

This is relatively poor agreement with the data.

For  $\rho c_p = 20 \text{ Btu/ft}^3\text{-}^\circ\text{F}$ , we find

$$\begin{aligned}T_{43} &= 8.80e^{-5.3276i} \\T_{44} &= 6.14e^{-5.9036i}\end{aligned}$$

These are apparently pretty close; we shall measure closeness of fit by calculating the squared fractional error for each temperature and adding. We find that  $\Delta_{43}^2 = 0.0191$ ;  $\Delta_{44}^2 = 0.0027$ , so  $\Delta^2 = 0.0217$

For  $\rho c_p = 18 \text{ Btu/ft}^3\text{-}^\circ\text{F}$ , we calculate

$$T_{43} = 9.325e^{-5.2491i}$$

$$T_{44} = 6.24e^{-5.8512i}$$

The errors are:  $\Delta_{43}^2 = 0.00319$ ;  $\Delta_{44}^2 = 0.00145$ , so  $\Delta^2 = 0.00464$ , considerably smaller than for  $\rho c_p = 20$ .

For  $\rho c_p = 17 \text{ Btu/ft}^3\text{-}^\circ\text{F}$ ,

$$T_{43} = 9.60e^{-5.2072i}$$

$$T_{44} = 6.28e^{-5.8276i}$$

The errors are:  $\Delta_{43}^2 = 0.00187$ ;  $\Delta_{44}^2 = 0.00288$  so  $\Delta^2 = 0.00475$ .

We see that reducing  $\rho c_p$  from 18 to 17 improves the fit for  $T_{43}$  but worsens it for  $T_{44}$ ; the total squared error is slightly larger for  $\rho c_p = 17$ .

As a check on this experiment, if we really have a day with no long-term weather trends, the average temperatures (that is, the Fourier coefficient for  $\omega = 0$ ) should be along a straight line. We calculate the steady state terms  $\bar{T}$ ; they are

$$\bar{T}_{41} = 108.33$$

$$\bar{T}_{43} = 96.48$$

$$\bar{T}_{44} = 89.17$$

$$\bar{T}_{45} = 86.94$$

These temperatures are graphed in Fig. 1; as shown, the intermediate temperatures  $T_{43}$  and  $T_{44}$  are either on or very close to a straight line between the surface temperatures.

Thus we conclude from this experiment that  $\rho c_p$  is between 17 and 18 Btu/°F-ft<sup>3</sup> and slightly closer to 18.

Direct Gain Cell Test: 24 February 1978

The direct gain cell has thermocouples on both inside (room side) and outside surfaces of the concrete and one in the interior. There are sets of thermocouples in 3 positions on the floor. We look at data from the set at the south end of the floor to get the largest signal (largest oscillations in temperature).

Since we do not know from direct measurement how deep into the material the interior thermocouple is located, we determine its depth using average temperatures. We calculate average and daily Fourier components of the temperatures for Channel 54, the top (room) surface temperature; Channel 53, the interior temperature; and Channel 52, the bottom surface temperature, as follows:

$$\bar{T}_{54} = 93.625$$

$$\bar{T}_{53} = 92.77$$

$$\bar{T}_{52} = 91.44$$

$$T_{54} = 23.32e^{+i2.0453}$$

$$T_{53} = 21.59e^{+i1.730}$$

$$T_{52} = 20.82e^{+i1.5803}$$

Using the average temperature data, we find that the depth of the Channel 53 thermocouple is 2.20 inches into the  $5^{5/8}$ -inch-thick concrete, so  $\xi = 0.3913$  for this measurement.

We next use  $T_{54}$  and  $T_{52}$  and our guesses for  $\rho c_p$  to determine A and B from (2) and use (2) to predict  $T_{53}$ .

We first check  $\rho c_p = 28 \text{ Btu}/^\circ\text{F-ft}^3$ . We find that the prediction for  $T_{53}$  is  $T_{53} = 21.165e^{+i1.6445}$ . This is off in both magnitude and phase; the fractional error squared is  $7.55 \times 10^{-3}$ .

Our next guess for  $\rho c_p$  is  $18 \text{ Btu}/^\circ\text{F-ft}^3$ . Then our prediction is  $T_{53} = 21.480e^{+i1.727}$ . The fractional squared error is  $3.49 \times 10^{-5}$ ; considerably smaller than the previous estimate.

We next try  $\rho c_p = 17.5 \text{ Btu}/^\circ\text{F-ft}^3$  based on the results of the previous experiment. We find that

$$T_{53} = 21.494e^{+i1.7312}$$

The error-squared  $\Delta^2 = 2.14 \times 10^{-5}$ , slightly smaller than the previous case.

$$\text{For } \rho c_p = 17 \text{ Btu}/^\circ\text{F-ft}^3, T_{53} = 21.506e^{+i1.7354} \text{ and } \Delta^2 = 4.39 \times 10^{-5}$$

(We also note that if we had assumed  $\xi = 1/2$  or the interior thermocouple located in the exact center of the concrete, the fits would not be very good until  $\rho c_p \sim 12 \text{ Btu}/\text{ft}^3\text{-}^\circ\text{F}$ , which is implausibly small.)

From this test, we conclude that  $\rho c_p$  is between 17.5 and 18  $\text{Btu}/^\circ\text{F-ft}^3$ ; and much closer to 17.5. This agrees with the previous result.

Trombe Cell Data, 8 March 1978

We use the same test points as for the previous Trombe wall experiment, but for a different day. March 8 had large solar gain on the wall (large signal) but the weather was varying from day to day.

We display the data for  $\bar{T}$  and  $T$  below:

$$\bar{T}_{41} = 92.29$$

$$\bar{T}_{43} = 80.92$$

$$\bar{T}_{44} = 75.17$$

$$\bar{T}_{45} = 73.71$$

$$T_{41} = 26.507e^{i2.2591}$$

$$T_{43} = 9.904e^{i1.233}$$

$$T_{44} = 6.250e^{i0.7182}$$

$$T_{45} = 6.028e^{i0.7274}$$

Note that the relationship between the  $\bar{T}$ 's is not as linear as it was for the 24th of February.

We again calculate  $T_{43}$  and  $T_{44}$  from (2) using  $T_{41}$  and  $T_{45}$  to find A and B, as before.

For  $\rho c_p = 28$ ,

$$T_{43} = 7.113e^{0.6289i}$$

$$T_{44} = 5.847e^{0.4001i}$$

These are again clearly in error.

For  $\rho c_p = 18$

$$T_{43} = 9.414e^{i0.9820}$$

$$T_{44} = 6.601e^{i0.5882}$$

Here  $\Delta_{43}^2 = 0.062$  and  $\Delta_{44}^2 = 0.021$  so  $\Delta^2 = 0.083$

For  $\rho c_p = 16$

Then  $T_{43} = 9.970 e^{i1.0689}$

$$T_{44} = 6.733e^{i0.6387}$$

$\Delta_{43}^2 = 0.0271$  and  $\Delta_{44}^2 = 0.0128$  so  $\Delta^2 = 0.0399$ . Since  $\Delta^2$  is still decreasing, we check  $\rho c_p = 15$ .

Then  $T_{43} = 10.257e^{i1.1150}$

$$T_{44} = 6.792e^{i0.6658}$$

$\Delta_{43}^2 = 0.0157$ ;  $\Delta_{44}^2 = 0.0105$  so  $\Delta^2 = 0.0257$ .

We next try  $\rho c_p = 14$  :

$$T_{43} = 10.547e^{i1.1628}$$

$$T_{44} = 6.845e^{i0.6943}$$

$\Delta_{43}^2 = 0.00946$ ;  $\Delta_{44}^2 = 0.00969$ ;  $\Delta^2 = 0.01915$

For  $\rho c_p = 13$

$$T_{43} = 10.841e^{i1.2126}$$

$$T_{44} = 6.891e^{i0.7241}$$

$\Delta_{43}^2 = 0.00941$ ;  $\Delta_{44}^2 = 0.01055$  so  $\Delta^2 = 0.01996$

Thus from this experiment  $\rho c_p$  is somewhat less than  $14 \text{ Btu}/^\circ\text{F-ft}^3$  but greater than 13. Why the discrepancy with the other experiments? The apparent reason is that the Fourier transform formula ((3) or (4)) is only accurate in picking out the daily component when there are no components longer than  $P$ , the length of the data record, present. This is certainly not true for 8 March. Table 1 shows average temperatures and insolation estimates for Los Alamos. While the days before the 24th of February are relatively alike, the days before and after the 8th of March show much variation.

This will affect the Fourier transform as follows: Suppose that in addition to the daily-cycling temperatures there is an error term resulting from a long weather cycle of  $T_e e^{i\omega_w t}$ . Thus  $T = T_o(t) + T_e e^{i\omega_w t}$ .

Then (3) says that

$$T(\omega_o) = \frac{2}{P} \int_{t=0}^{t=P} T_o(t) e^{-i\omega_o t} dt + \frac{2}{P} \int_{t=0}^{t=P} T_e e^{+i(\omega_w - \omega_o)t} dt \quad (5)$$

The second term of (5) is equal to  $\frac{2T_e}{P(\omega_w - \omega_o)} [e^{i\omega_w P} - 1]$ .

This is an error term: a term that comes up because we tried to Fourier-analyze a long-period phenomenon in terms of harmonics of a short period  $P$ .

The fact that an error term is present is clear from looking at the values of  $T_{41}(t)$ ,  $T_{43}(t)$ ,  $T_{44}(t)$ , and  $T_{45}(t)$  at the beginning and end of March 8. In principle, these temperatures should be equal at

both times, but for March 8, they are 8 or 9° F higher at the end of the day than at the beginning.

Trombe Cell Data, 9-day period

We attempt to correct for the errors in the previous experiment caused by long-term weather variations in two ways. First, we use a longer test period P, and second, we end the period such that the final period temperatures are lower than the initial temperatures, in contrast to the previous cases.

This will produce a higher estimate for  $\rho c_p$ . This high estimate allows the estimation of upper and lower bounds for  $\rho c_p$ : the estimate for 24 February when temperatures were slowly rising provides a lower bound and the one for this period will provide an upper bound.

We find that

$$\begin{aligned}T_{41} &= 19.767e^{i2.31954} \\T_{43} &= 6.0351e^{i0.98950} \\T_{44} &= 4.3015e^{i0.25921} \\T_{41} &= 3.9946e^{i0.26404}\end{aligned}$$

We check  $\rho c_p = 28$  to confirm that it gives unrealistic results in this case; we then try  $\rho c_p = 18, 19$ , and 20.

$$\text{For } \rho c_p = 18 \text{ Btu/}^\circ\text{F-ft}^3$$

$$\begin{aligned}T_{43} &= 6.227e^{i1.0643} \\T_{44} &= 4.224e^{i0.2828}\end{aligned}$$

$$\Delta_{41}^2 = 0.0067; \quad \Delta_{44}^2 = 0.00087; \quad \Delta^2 = 0.00766.$$

For  $\rho c_p = 19$

$$T_{43} = 6.050e^{i1.023}$$

$$T_{44} = 4.206e^{i0.2566}$$

$$\Delta_{43}^2 = .00113 ; \Delta_{44}^2 = .00050 \quad \Delta^2 = .00163$$

For  $\rho c_p = 20$

$$T_{43} = 5.878e^{i0.9832}$$

$$T_{44} = 4.185e^{i0.2315}$$

$$\Delta_{43}^2 = .00071 ; \Delta_{44}^2 = .00149 \quad \Delta^2 = .00220$$

Thus from this experiment, we find  $\rho c_p \sim 19.3$  .

### Conclusions

From the four experiments described here, we can observe that a rising secular trend of temperature whose timescale is much longer than the period of integration P will result in too low an estimate of  $\rho c_p$ , while a falling trend will result in too high an estimate. Based on our data, we can conclude that  $17.5 < \rho c_p < 19.3$  .

Since the conductivity of the concrete is only accurate to two significant figures, we will choose a 2-digit estimate for  $\rho c_p$ . We take  $\rho c_p = 18 \text{ Btu}/^\circ\text{F}\text{-ft}^3$  because two of the experiments support 18 as the closer estimate and because despite a slow secular increase in temperature, the weather seems closer to being periodic on the day for which  $\rho c_p = 17.5$  was derived. Further, we would expect that since the direct gain wall is only about 1/3 as thick as the Trombe wall, secular

changes in weather would affect the response of these two walls in different ways. The fact that both produce nearly identical estimates of  $\rho c_p$  (to 1%) suggests that their value is close to the truth.

Thus we conclude that heat capacity per unit volume of the Los Alamos concrete is  $18 \pm 1$  Btu/°F-ft<sup>2</sup> with the error most likely occurring on the high side, and use this value in subsequent calculations. We note that 5-10% errors in  $\rho c_p$  will introduce imperceptibly small errors into the predictions that follow; however, larger errors (~ 50%) will produce noticeable disagreements.

### 3. EXPERIMENTAL VALIDATION OF THE MODELS

#### 3.1 Introduction and Overview of Results

The passive solar building models of Sec. 2 were derived from theory, with no reference to measurements of temperatures in real buildings. Since the theory is based on well-established relationships and relatively straightforward mathematics, we expect that the models should bear a close relationship to experiments, at least for simple buildings.

This expectation is borne out by comparisons described in this section with three small test buildings. There is very little hour-by-hour temperature data available on passive solar buildings; these three buildings were chosen primarily because data existed. Two of the buildings are located at Los Alamos Scientific Laboratory (LASL) in New Mexico. We obtained detailed data for a three-week period in February-March 1978 for these two structures; comparisons with model predictions are shown in Figs. 5, 6, 7, 9, and 10.

The third building was a poorly-instrumented demonstration-house constructed at California State University at Sonoma and since demolished. Data and descriptive material for this building are less accurate, but we still obtain reasonable agreement between model and data, as shown in Fig. 12.

The Los Alamos buildings are small ( $\sim 2\text{m} \times 2\text{m}$ ) well-insulated boxes with large south windows. Thermal storage is provided by solid concrete blocks. One of the cells is a direct-gain building; it has concrete on the inside of its envelope walls. The other contains a

### 3.3 The Direct Gain Cell Comparisons

We describe in this section the experiments performed on the LASL direct gain test cell. We first derive the thermal parameters from the description of the cell; we then choose appropriate weather to model and parameterize the weather. Using these results as input to the model, we compare model predictions with room temperature data.

Comparisons are performed using both the lumped parameter approach and the distributed parameter approach. When they are both applicable, they agree almost perfectly; however, there are some experiments where only one of the models can be used. The results of the experiments are summarized in Figs. 5, 6 and 7.

#### 3.3.1 Direct Gain Cell Description

The direct gain cell is a closet-sized box about 5' × 7' (~1.5 × 2m) in floor area and 10 feet (3m) high. The south wall is almost entirely glazed, while the remaining walls are covered in many places by 5-5/8 inch thick (14.3 cm) concrete blocks. The walls themselves are constructed of standard 2 × 4 wood framing with fiberglass insulation; the thermal resistance of the insulation is R-11 (11°F-ft<sup>2</sup>-hr/Btu or 1.94 °C-m<sup>2</sup>/W). Inside the framing is an inch (2.54 cm) of polystyrene board insulation with a thermal resistance of R-5. Thus a wall section, going from inside to outside, consists of concrete block, styrofoam board and wood framing.

A sketch of the cell is presented in Fig. 2; it provides the dimensions of the cell, based on measurements by the author. As shown in the figure, only part of the inside wall surface area is concrete blocks. The blocks cover an irregular area which intercepts all the direct

sunlight on a winter day near the solstice . Thus all the direct sunlight hits the concrete at all times.

There are only four channels for heat loss from the room air: infiltration, loss through the glass (collector), heat transfer to the styrofoam envelope wall surfaces, and heat transfer to the concrete. The first three channels are all relatively fast heat transfers, so we lump their effects into  $\hat{U}_q$ . We treat the concrete as being the only heavy material, since the properties of the blocks lining the walls are identical to those of the concrete on the floor. (The film coefficients may be slightly different, but the results are not very sensitive to the exact value of h chosen, as shown later in this section.)

#### Evaluation of Building Parameter

We next use the materials properties of the elements used in construction of the cell along with the measurements in Fig. 2 to derive building parameters for the lumped parameter and for the distributed parameter models.

We first evaluate the parameters for the concrete. We consider as concrete surface area only those areas which face the inside of the cell; that is, we ignore the small areas of concrete which are parallel to the glazing and only two inches behind it. Thus the surface areas of concrete are:

$$\begin{array}{l r r} \text{side walls:} & 2 \text{ walls} \times \{8.92' \times 3.92' + 1.30' \times 4.49'\} & = 80.60 \text{ ft}^2 \\ \text{back walls:} & 4.50' \times 5.25' & = 22.57 \text{ ft}^2 \\ \text{floor} & : 4.30' \times 6.88' & = 29.58 \text{ ft}^2 \\ \text{Total concrete surface area} & & \underline{133.75 \text{ ft}^2} \end{array}$$

The lumped parameters for the concrete are given by Table 2.3 with  $K = 0.8 \text{ Btu}/^\circ\text{F}\text{-ft} \text{-hr}$ ;  $\rho c_p = 18 \text{ Btu}/^\circ\text{F}\text{-ft}^3$ ;  $d = 0.4688 \text{ ft}$ . We assume  $h = 1.0 \text{ Btu}/^\circ\text{F}\text{-ft}^2\text{-hr}$ ; this low value is chosen because radiation heat exchange with the room air is retarded by the simple geometry of the room. Radiation from one part of the concrete has a large probability of striking another part of the concrete, while some of the radiant heat striking the styrofoam will simply reradiate to the concrete. Since the radiative part of  $h$  is usually about  $1 \text{ Btu}/\text{ft}^2\text{-degF}\text{-hr}$ , we reduce this value by 50%; together with the convective contribution of about  $1/2 \text{ Btu}/\text{ft}^2\text{-degF}\text{-hr}$ , we get  $h \cong 1$ . We take the outside insulation to be R-15, corresponding to R-5 for one inch of styrofoam and R-10 for a frame wall with 20% wood and 80% insulation (R-11), with plywood exterior siding.

The assumptions set  $U_i$  equal to  $4.082 \text{ Btu}/\text{ft}^2\text{-}^\circ\text{F}\text{-hr}$ ,  $U_o = 0.06518 \text{ Btu}/\text{ft}^2\text{-degF}\text{-hr}$ , and  $\bar{C} = 8.055 \text{ Btu}/\text{ft}^2\text{-}^\circ\text{F}$ . (These are derived from the thin-wall model; the thick-wall model would have set  $\bar{C} = 8.41$ ). Thus for the concrete,  $\hat{U}_{ci} = 546 \text{ Btu}/\text{degF}\text{-hr}$ ,  $\hat{U}_{co} = 8.718 \text{ Btu}/^\circ\text{F}\text{-hr}$ , and  $C_c = 1077.4 \text{ Btu}/^\circ\text{F}$ .

We next look at the collector window. The gross area of the window, including wooden supports, is  $4'11'' \times 9' 3\text{-}3/8'' = 45.63 \text{ ft}^2$ . This area is relevant to calculating heat losses; using a handbook U-value of  $0.55 \text{ Btu}/\text{ft}^2\text{-deg}\text{-hr}$  for double pane glass, the heat transfer coefficient is  $25.10 \text{ Btu}/\text{deg}\text{-hr}$ ; this is part of the quick heat transfer coefficient  $\hat{U}_q$ . The area which actually collects sunlight is smaller. The effective width is the area between the concrete on the side walls:  $4.30 \text{ ft}$ ; while the effective height is the distance from the concrete

floor to the top of the glass less the 2-7/8" of horizontal wood framing in the window: 8.885 ft. Thus the effective collector area is 38.2 ft<sup>2</sup>.

We calculate the rest of  $\hat{U}_q$  by adding infiltration losses to conduction losses through the styrofoam. Infiltration losses are calculated by assuming 1/4 air change per hour, and multiplying by the volume times the heat capacity of air at Los Alamos elevation: 0.014 Btu/°F-ft<sup>3</sup>. We use 1/4 air change as a guess based on the LASL scientists' feeling that the house was "very tight" and a comparison with a very tight Princeton retrofit townhouse (see Ref. 25 ) which had 1/4 air change per hour in ~ 5 mph winds. The approximate volume is equal to the volume of a parallelepiped whose sides correspond to the surfaces of concrete, plus a set of irregular volumes one concrete block in thickness where no concrete is present:

Volume  $\cong 9.67' \times 4.30' \times 7.04' + 2 \times [(9.67' \times 7.04' - 40.80 \text{ ft}^2) \times .469 \text{ ft}] + [(5.25' \times 9.67' - 22.57 \text{ ft}^2) \times 4.69 \text{ ft}] \cong 331.5 \text{ ft}^3$ ; thus the heat transfer coefficient is 1.16 Btu/degF-hr.

Finally, the heat losses for the styrofoam are equal to the area of styrofoam times the U-value of 1/16. (The resistance is 15 for the styrofoam-plus-wood-frame and 1 for the film coefficient). The area of styrofoam includes only one side wall (since the other is a party wall with the adjoining cell). It is:

ceiling	$5.25' \times 7.56'$	=	$39.69 \text{ ft}^2$
side wall	$(9.67' \times 7.04' - 40.80 \text{ ft}^2) + (9.67' - 4.50') \times 0.469 \text{ ft}^2$	=	$29.70 \text{ ft}^2$
back wall	$5.25' \times 9.67' - 22.57 \text{ ft}^2$	=	$28.20 \text{ ft}^2$
Total styrofoam area is			<hr/> $97.59 \text{ ft}^2$

Thus total quick heat transfer coefficient in  $25.10 \text{ Btu}/^\circ\text{F}\text{-hr} + 1.16 + (97.59 \text{ ft}^2 \times (1/16) \text{ Btu}/\text{ft}^2\text{-degF}\text{-hr}) = 32.4 \text{ Btu}/^\circ\text{F}\text{-hr} \equiv \hat{U}_q$ .

We next estimate radiation balance. The estimate is very crude but should give an approximate idea of the values of the radiation balance parameters  $\alpha_c$  and  $\alpha_R$ . All the direct sunlight hits concrete, so  $\alpha_R$  consists of that portion of sunlight which is diffusely reflected from the concrete and absorbed on the styrofoam.

We assume that the concrete has about the same reflectivity as the styrofoam (this appeared to be true); it also had approximately the same area (including  $29.70 \text{ ft}^2$  of styrofoam party-wall). We roughly measured reflected intensities as seven times larger over the illuminated portions of the concrete compared to the shaded portion (using a photographic light meter). If we assume that half the concrete is illuminated and half shaded, then the 7:1 ratio of intensities implies that 70% of the light is absorbed in the illuminated area and 30% in the shaded area. Since the shaded area is  $2/3$  styrofoam, 20% of the light is absorbed on the styrofoam and 80% on the concrete. Thus  $\alpha_c = 0.8$  and  $\alpha_R = 0.2$ . This is a very rough estimate, so we also calculate the response for  $\alpha_R = 0.1$  and  $\alpha_c = 0.9$ . The difference between these assumptions does not affect the building response very strongly.

We must also determine how much of the incident sunlight is involved in this radiation balance. The transmissivity of double-pane glass is approximately 75% averaged over typical angles of incidence. But some of the sunlight is reflected inside the test cell and comes back out through the window. The cell appears bright to the eye when viewed from the outside; we assume that 5% of the incident light is

re-reflected out the window. This 5% loss is consistent with the fluxes calculated in determining the  $\alpha$ 's. So the net transmissivity of the collector is 70%. Since the transmission was not measured, this estimate could be in error by 5-10%.

### 3.3.2 Weather Parameterization

As input to the models, we need weather which has sinusoidal form. We will fit ambient temperature to the form  $T_A(t) = \bar{T}_A + \Delta T_A e^{i\omega_0 t}$  or else to the form  $T_A(t) = \bar{T}_A + \Delta T_A e^{i\omega_0 t} + \Delta T_{A_w} e^{i\omega_w t}$ . The first form can be calculated using Eq. (4) for each day; the results for  $\bar{T}_A$  and  $\Delta T_A$  are given for each day in Table 1. The term  $\Delta T_{A_w}$  can be found by guessing at  $\omega_w$  and then using (4) on the daily estimates of  $\bar{T}_A$  to find  $\Delta T_{A_w}$ . This process of fitting a sinusoidal model to the observed data is illustrated in Fig. 3.

Solar gain is also assumed to be sinusoidal: 
$$S(t) = \begin{cases} S_1 e^{i\omega_1 t} & \text{day} \\ 0 & \text{night} \end{cases}$$

We have as input data LASL measurements of solar flux incident on a south-facing vertical plane; the measurements were taken each hour. We first add all the solar gain values for the whole day; this gives an estimate of daily solar gain. These values are listed in Table 1 and graphed in Fig. 3.

We use this data to pick test days. We first look for a day with little change in weather patterns from previous days. From Table 1, the best choice is apparently February 24. We see this more clearly from Fig. 4, which graphs solar gain as a function of time for several days around the 24th of February. As seen in the figure, there have

been several days of regular sunshine preceding this choice of test date. (Sunshine is by far the most important driving force for these buildings as seen below).

For the 24th of February, we fit  $S_1$  and  $\omega_1$  and find sunrise and sunset by looking at the hourly data. Using the first and last observations, 68 Btu/hr-ft<sup>2</sup> at 8 a.m. and 36 at 6 p.m. and the peak value of 252 Btu/hr-ft<sup>2</sup> at 1 p.m., we can approximate the data by setting  $S_1 = 255$  Btu/hr-ft<sup>2</sup>,  $\omega_1 = 0.273$  radians/hour, sunrise ( $t = 0$ ) at 7 a.m. and sunset ( $t = t_d$ ) at 18.52:00 or 6:31 p.m.

Thus for 78/02/24 we set

$$S(t) = \begin{cases} 255 e^{i\omega_0(t-5.763)} & 0 \leq t < 11.52 \text{ hrs} \\ 0 & 11.52 \leq t < 24 \text{ hrs} \end{cases}$$

where  $t$  is measured in hours

Note that the time 5.763 (solar noon) is defined with respect to 7 a.m. sunrise; the entries in Table 1 have times defined with respect to midnight. For the same test day, 24 Feb., we set  $T_A = 37.0 + 16 e^{i\omega_0(t-8)}$ . For both  $S(t)$  and  $T_A(t)$ , the fit between real weather data and modelled weather data is excellent.

Our second experiment is performed on the test day of March 8. This day was chosen because solar gain data for the previous several days fits the idealization

$$S(t) = \begin{cases} (\bar{S} + \Delta S_w e^{i\omega_w t}) e^{i\omega_1 t} & \text{day} \\ 0 & \text{night} \end{cases}$$

where we use daily totals of solar gain to fit the curve.

The daily solar gain totals are shown in Table 1. If we normalize the solar gains to their value for 78/02/24 and Fourier-analyze the data for 78/02/21-78/03/06 using Eq. (4) with  $\omega_w = 2\pi/14$  days, we find that

$$S(t) = (.6403 + .3566 e^{i\omega_1(t-2.82 \text{ days})}) |S_1|$$

where  $t$  is measured in days, with  $t = 0$  at noon on the 21st of February and where all solar gain values are assumed to take place at noon on their respective days. Extending this expression to the 7th and 8th of March, we get excellent agreement as shown in Fig. 3, especially for the last few days. For the test of March 8, the (non-normalized) expression for solar gain leads to an estimate of 1702 Btu/day, compared with the observed value of 1753, or a 3% error.

To find  $\Delta T_{A_w}$ , we find best agreement for  $\omega_w' = 2\pi/10$  days; applying Eq. (4) to the data for  $\bar{T}_A$  for 78/02/27 to 78/03/08 we derive

$$T_A(t) = 37.5 \text{ }^\circ\text{F} + 4e^{i\omega_w'(t-5.5 \text{ days})}$$

where  $t = 0$  at noon on February 21, 1978. The predicted temperature for March 8 is thus 41.3  $^\circ\text{F}$  compared to the 41.2 $^\circ\text{F}$  observed. The overall agreement, shown in Fig. 3, is not as good as for  $S(t)$ , but is reasonably close. The predictions for  $T_R$  will not depend very sensitively on the precise modelling of long-term fluctuation in  $T_A$ . (Note that there is no reason to want the same value of  $\omega_w$  for the ambient temperature term as for the solar gain term).

We take  $\omega_1$  to be time-independent because seasonal changes in sunrise and sunset are not very large over the 3-week span of data. Thus we always take sunrise to be 7 a.m., sunset to be 6.52 p.m. and  $\omega_1$  to be 0.273 radians/hr.

This completes our parameterization of weather; these results will be used below and also in the Trombe wall modelling discussion.

3.3.3. Constant-Weather Experiment of 24 February 1978

We use the house and weather parameters described above to model the predicted response of the test cell. We first use the lumped parameter model and then the distributed parameter approach. Following the model predictions, we discuss the agreement with data.

Lumped Parameter Model of the Direct Gain Cell

For the lumped parameter model, we have only one heavy material - the concrete - rather than 2 as described in Sec. 2.3. We can therefore simplify the arithmetic somewhat by looking at one dynamic temperature  $T_c$  instead of two -  $T_w$  and  $T_f$ . Equation (2.10) therefore reads

$$T_R = \frac{N_C}{N_R} T_C + \frac{1}{N_R} T_A + \frac{N_S}{N_R} S \quad (6)$$

since the other terms drop out. The two differential equations (2.10a) simplify to one equation

$$\dot{T}_C + \Lambda_P T_C = a_2 S + a_3 T_A \quad (7)$$

where

$$\Lambda_P = \lambda_c \left( 1 - \frac{N_C}{N_R} \right) + \frac{\hat{U}_{co}}{C_C} = a_3$$

and 
$$a_2 = \lambda_c \left( \frac{\alpha_c}{\hat{h}_c} + \frac{N_S}{N_R} \right)$$

We set  $S = 255 \frac{\text{Btu}}{\text{ft}^2\text{-hr}} \times 0.7 \times 38.2 \text{ ft}^2 = 6819 \text{ Btu/hr e}^{i\omega_1(t-5.763 \text{ hours})}$

with  $\omega_1 = 0.273$  radians/hour. We then use the building parameters' values to find:

$$\begin{aligned} \Lambda_P &= .0312 \text{ hr}^{-1} \\ a_2 &= 8.513 \times 10^{-4} \text{ }^\circ\text{F}/(\text{Btu}/\text{hr}) \\ a_3 &= \Lambda_P \\ N_C &= 3.316 \\ N_R &= 4.316 \\ N_S &= .01103 \quad \text{ }^\circ\text{F}\text{-hr}/\text{Btu} \end{aligned}$$

We calculate  $T_w$  using the solutions to (7) and the boundary conditions  $T_w(0^+) = T_w(24 \text{ hrs}^-)$ ;  $T_w(t_d^+) = T_w(t_d^-)$ ; the result is (measured with respect to the average temperature of  $37 \text{ }^\circ\text{F}$ )

$$T_w = \begin{cases} 66.82 e^{-.0312t} + 1.89 e^{i\omega_0(t-13.55)} + 21.13 e^{i\omega_1(t-11.10)} & \text{day} \\ 67.63 e^{-.0312(t-t_d)} + 1.89 e^{i\omega_0(t-13.55)} & \text{night} \end{cases}$$

Then by (6), we can derive  $T_R$ :

$$T_R = \begin{cases} 51.34 e^{-.0312t} + 4.14 e^{i\omega_0(t-9.36)} + 25.13 e^{i\omega_1(t-8.316)} & \text{day} \\ 51.96 e^{-.0312(t-t_d)} + 4.14 e^{i\omega_0(t-9.36)} & \text{night} \end{cases}$$

This gives temperature elevation ( $T_R - T_A$ ) for 78/02/24; the result is plotted in Fig. 5 for comparison with the data. Room temperature is the label for the y-axis, although the zero of temperature is taken as  $\bar{T}_A$  to allow the reader to see relative error.

The LASL measurement of room temperature was performed by enclosing a thermocouple inside a plastic sphere, so their room temperature is really some average of room temperature and mean radiant

temperature. We derive a rough estimate of one model's mean radiant temperature below; the result is that mean radiant temperature (MRT) is only a few degrees F different from room air temperature, and is always larger than room temperature.

Mean radiant temperature of a point in a room is the temperature of the solid surfaces visible from that point, averaged over solid angle. Averaging over solid angle is complicated; as an approximation we average over surface area. We derive expressions for surface temperatures of the concrete, the styrofoam, and the glazing as follows.

For the concrete surface temperature Eq. (2.1) relates concrete surface temperature to concrete temperature, room temperature, and solar gain. Since all three quantities are known, we can easily solve for concrete surface temperature. The result is

$$T_{cs} = \begin{cases} 63.77 e^{-.0312t} + 2.02 e^{i\omega_0(t-12.15)} + 24.30 e^{i\omega_1(t-9.31)} & \text{day} \\ 64.55 e^{-.0312(t-t_d)} + 2.02 e^{i\omega_0(t-12.15)} & \text{night} \end{cases}$$

For the styrofoam surface temperature, we note that for any surface, Eq. (2.13) relates surface temperature to its driving forces as follows:

$$T_s = (h T_R + \bar{\alpha}S) R_1 + T_A R_2$$

Styrofoam is a quick-heat-transfer material in our model, so we take the limiting form of  $R_1$  for a pure conductance:  $R_1 = \frac{1}{h}$ . Also, the styrofoam is a good insulator, so  $R_2 \cong 0$ . Thus

$$T_{s_{\text{styro}}} = T_R + \frac{\bar{\alpha}_R S}{h} \quad \text{or since } h = 1 \text{ Btu/ft}^2\text{-degF-hr,}$$

$$T_{s_{\text{styro}}} = T_R + \bar{\alpha}_R S$$

Finally, the glass temperature is determined by looking at the glazing as consisting of two resistances in series - the outside resistance from the surface and the inside resistance. The inside resistance, accounting for radiant heat transfers to the other walls as well as convection to the air, should look like  $R_{\text{in}} \cong 1/h \cong 1/(1.5 \text{ Btu/hr-F-ft}^2)$ . The inside and outside resistances add to the inverse of the U-value, or  $1/0.55$ . Then the glass surface temperature is given by

$$\begin{aligned} T_{\text{gs}} &= \frac{R_{\text{total}} - R_{\text{in}}}{R_{\text{total}}} (T_R - T_A) + T_A \cong 0.633 (T_R - T_A) + T_A \\ &= 0.633 T_R + 0.367 T_A \end{aligned}$$

We can now evaluate mean radiant temperature as follows.

$$\text{MRT} = \frac{1}{A_{\text{styro}} + A_c + A_{\text{gl}}} (A_{\text{styro}} T_{s_{\text{styro}}} + A_c T_{\text{cs}} + A_{\text{gl}} T_{\text{gs}})$$

where the A's represent areas.

Using the previous numerical results, we find that

$$\text{MRT} = 0.509 T_R + 0.436 T_{\text{cs}} + 0.055 \Delta T_A + 4.447 e^{i\omega_1(t-5.763)},$$

or

$$\text{MRT} = \begin{cases} 53.94 e^{-.0312t} + 3.60 e^{i\omega_o(t-9.65)} + 26.40 e^{i\omega_1(t-8.31)} & \text{day} \\ 54.59 e^{-.0312(t-t_d)} + 3.60 e^{i\omega_o(t-9.65)} & \text{night} \end{cases}$$

These results are graphed in Fig. 5.

We note that MRT is 2° F warmer than room temperature at sunrise, less than 3° F warmer at its peak temperature, and 2-1/2° F warmer at midnight, or about 5% warmer on the average.

Looking at Fig. 5, we see generally excellent agreement between predicted room temperature and measurements; the agreement with mean radiant temperature is also reasonably good. The largest disagreement occurs during the early afternoon, when the model predicts temperatures 3-7° warmer than actually recorded. This error — still 10% or less — can be explained in two ways.

First, the wind speed increased during this period, increasing the U-value of the glazing and lowering room temperatures. Our model has a fixed U-value for the glass. Second, and perhaps more important, the weather was not precisely constant prior to the 24th of February; both solar gain and, to a larger extent ambient temperature, were slowly increasing. Including these effects would have produced lower predicted temperature, as shown by the next experiment.

Before we conclude the discussion of this experiment, we will briefly discuss the sensitivity to errors in assumptions. There are three assumptions we make that are not well-supported by data: net transmissivity of the glass of 70%; radiation balance parameters  $\alpha_c = 0.8$  and  $\alpha_R = 0.2$ ; and film coefficient  $h_c = 1 \text{ Btu/ft}^2\text{-deg F-hr}$ . We discuss next the sensitivity to varying the assumptions.

First, the sensitivity to solar transmission estimates is that, to good approximation, a 1% change in net transmissivity will produce a 1% change in temperature elevation at each hour. This occurs

because the response to ambient temperature fluctuations is relatively small.

To see the sensitivity to correct evaluation of the  $\alpha$ 's, we try another set of assumptions. One reasonable assumption is that even more of the light is absorbed on the concrete, since shaded concrete subtends most of the solid angle seen by the illuminated concrete. Suppose we set  $\alpha_c = 0.9$  and  $\alpha_R = 0.1$ . Then we can calculate  $T_R$  as we did before; the result is

$$\left\{ \begin{array}{l} 52.39 e^{-.0312t} + 4.14 e^{i\omega_0(t-9.36)} + 22.54 e^{i\omega_1(t-8.76)} \quad \text{day} \\ 53.02 e^{-.0312(t-t_d)} + 4.14 e^{i\omega_0(t-9.36)} \quad \text{night} \end{array} \right.$$

Neither this result nor the calculation for mean radiant temperature differs by more than a degree or two from the previous calculation; so we conclude that the result is insensitive to small errors in determining the  $\alpha$ 's.

We will later check the sensitivity to errors in  $h_c$ . We assume for this test that  $h_c = 1.5 \text{ Btu/ft}^2\text{-deg F-hr}$  instead of 1; the former being the usual combined film coefficient. This test also shows small sensitivity to the change. The calculation is performed later in conjunction with the distributed parameter model.

### 3.3.4 Distributed Parameter Model of the Direct Gain Cell

For the distributed parameter (continuum) model, the calculations are relatively straightforward applications of the results of section 2.4. Since the concrete walls are within the domain of the thin-wall

approximation, we expect excellent agreement between the lumped and distributed models; this is demonstrated below.

The distributed parameter solution is obtained from Eq. (2.15) with the building response functions A, B, and C given by (2.14) and (2.14a). We evaluate A, B, and C using  $\hat{U}_q = 32.4$  Btu/deg F-hr and using the materials properties  $\rho c_p = 18$  Btu/°F-ft<sup>3</sup> and  $K = .80$  Btu/ft-deg F-hr to derive response functions for the concrete.

The response functions  $R_1$  and  $R_2$  for the concrete are listed in Table 2. We anticipate the needs of our varying-weather experiment and evaluate the response functions for low frequencies as well as for multiples of  $\omega_0$ . We next Fourier-analyze  $S(t)$  in terms of the  $d_n$ :  $S(t) = |S_1| \sum_{n=0}^{\infty} d_n e^{i\omega_0 n t}$ . We find that

$$\begin{aligned} d_0 &= .3053 \\ d_1 &= .4769 e^{-1.508i} \\ d_2 &= .2261 e^{-3.016i} \\ d_3 &= .0157 e^{+1.7593i} \\ d_4 &= .0431 e^{-2.8903i} \\ d_5 &= .0086 e^{+1.885i} \end{aligned}$$

We next use (2.14) to calculate A, B, and C for all frequencies of interest. We will consider the frequencies  $0, \omega_w, \omega_w', \omega_0, 2\omega_0, 3\omega_0,$  and  $4\omega_0$  and truncate the series after that due to  $d_5$  being much smaller than the other coefficients. The results are given in Table 3.

We evaluate  $T_R(t)$  using Table 3 for A, B, and C and the weather parameterizations discussed previously, and find that

$$T_R(t) = 48.98 + 15.60 e^{i\omega_0(t-8.9 \text{ hrs})} + 4.188 e^{2i\omega_0(t-6.793 \text{ hrs})} + \\ 0.266 e^{3i\omega_0(t + 1.68 \text{ hrs})} + 0.694 e^{4i\omega_0(t-3.137 \text{ hrs})}$$

The first term is referred to ambient average temperature (37° F) for 78/02/24; so the Fahrenheit temperature would be 37° higher. This result is graphed in Fig. 5; it is seen to be almost identical to the lumped parameter result, but with slightly better agreement with the data during the early morning hours.

We next repeat the calculation for  $h_c = 1.5 \text{ Btu/ft}^2\text{-deg F-hr}$  to check the sensitivity to  $h_c$ . We find that

$$T_R = 49.55 + 14.88 e^{i\omega_0(t-9.23 \text{ hrs})} + 3.96 e^{2i\omega_0(t-6.96 \text{ hrs})} + \dots$$

We truncate after two terms because it is evident that there will be very little change in the results. The insensitivity to  $h_c$  probably is due to two competing effects cancelling. As  $h$  is increased, more of the heat absorbed on the concrete surface is conducted directly into the room, tending to increase diurnal fluctuations in temperature. But in addition, the (unheated) room is then more tightly coupled to the concrete walls, which damps fluctuations. Over this particular range of  $h_c$ , these effects cancel.

### 3.3.5 Varying Weather Experiment, 8 March 1978, Direct Gain Cell

We apply the results of our model to predict the response of the test cell on March 8, a day for which the previous two weeks of weather can be accurately modelled as a sinusoidal fluctuation added to a constant term, as shown in Fig. 3. This situation can most

conveniently be modelled using the distributed parameter approach.

The weather data are:

$$S = (.6403 + .3566 e^{i\omega_w (t-2.82 \text{ days})}) S_1$$

and  $T_A = 37.5 + 4 e^{i\omega_w' (t-5.5 \text{ days})}$

where  $t = 0$  corresponds to noon and 21 February 1978

$$S_1 = \begin{cases} 6819 e^{i\omega_1 (t-5.763 \text{ hrs})} & \text{day} \\ 0 & \text{night} \end{cases}$$

$$\omega_w = 2\pi/14 \text{ days}$$

$$\omega_w' = 2\pi/10 \text{ days}$$

We use (2.16) to derive  $T_R(t)$ ; in order to evaluate this expression we need to compute the building response functions  $A(\omega)$  and  $B(\omega)$  for  $\omega = \omega_w$  and  $A(\omega)$  and  $C(\omega)$  for  $\omega = \omega_w'$ . We find that

$$A(\omega_w) = 46.83 e^{+.3812i} \quad B(\omega_w) = .9396 e^{-.1112i}$$

$$A(\omega_w') = 51.93 e^{.4746i} \quad C(\omega_w') = 40.03 e^{-.0500i}$$

We evaluate (2.16) next; we first display the general equation and then derive the numerical results

$$T_R(t) = \bar{S} \frac{B(0)}{A(0)} d_o + \Delta S_w \frac{B(\omega_w)}{A(\omega_w)} d_o e^{i\omega_w t} + \left( \bar{S} + \Delta S_w e^{i\omega_w t} \right) \left( \sum_{n=1}^4 \frac{B(n\omega_o)}{A(n\omega_o)} d_n e^{i\omega_o n t} \right)$$

(8)

$$+ \bar{T}_A + \Delta T_{A_w} \frac{C(\omega_w')}{A(\omega_w')} e^{i\omega_w' t} + \Delta T_A e^{i\omega_o t}$$

The first term is just .6403 times the old steady-state term of 48.98°F. For the second term,  $\Delta S_w d_o$  is just .3566 times the old steady-state solar heat gain. The sum in the third term is the same sum as in the daily solution, but multiplied by a time-varying factor. This factor, evaluated at noon on March 8, when  $t = 15$  days, is equal to .8844. The rest of the terms are relatively straightforward to understand.

Numerically (8) is equivalent to:

$$T_R(t) = 30.88 + 14.90 e^{i\omega_w(t-3.92 \text{ days})} + \left( 10.35 e^{i\omega_o(t-8.72 \text{ hrs})} + 3.70 e^{2i\omega_o(t-6.793 \text{ hrs})} + .24 e^{3i\omega_o(t+1.68 \text{ hrs})} + .61 e^{4i\omega_o(t-3.14 \text{ hrs})} \right) + 37.5 + 3.08 e^{i\omega_w'(t-6.33 \text{ days})} + 3.336 e^{i\omega_o(t-9.65 \text{ hrs})}$$

(9)

Equation (9) follows the form of (8) term-for-term. A more compact version of (9) would combine the two terms at frequency  $\omega_o$  into one term. It would also evaluate the terms at frequencies  $\omega_w$  and  $\omega_w'$  numerically. Note that such an evaluation is not constant over the

course of a day. However, since  $\omega_w$  and  $\omega_w' \ll \omega_o$ , we can evaluate their terms at noon, midnight the night before, and midnight the night after and interpolate linearly for hours in between. So we can write

$$T_R(t) = \begin{Bmatrix} 70.2 \\ 74.3 \\ 78.0 \end{Bmatrix} + 13.61 e^{i\omega_o(t-8.95 \text{ hrs})} + 3.7 e^{2i\omega_o(t-6.79 \text{ hrs})} + .24 e^{3i\omega_o(t+1.68 \text{ hrs})} + .61 e^{4i\omega_o(t-3.14 \text{ hrs})}$$

for  $\begin{Bmatrix} \text{midnight} \\ \text{noon} \\ \text{midnight} \end{Bmatrix}$

This result is plotted in Fig. 6. For comparison, we plot the measured data and a calculation which ignored weather variations and assumed that all past history had the same weather as March 8. (That is, we used (2.15) for  $T_R(t)$  instead of (2.16)).

Several features are noteworthy in Fig. 6. First, the agreement between model and data is better than for Feb. 24. This is to be expected, since more detailed weather information was used for this prediction. Use of a mean-radiant temperature calculation would probably result in even better agreement, since measured room temperature would almost always lie between predicted room air temperature and predicted mean radiant temperature.

The difference between the curve labelled "no weather" in Fig. 6 and the model curve is the (calculated) response of the building to

long-term weather fluctuations. This response is fairly large: the test cell has a long time-constant and stores significant heat over two-week cycles. The model is apparently tracking the dynamic response to both daily and multi-week cycles. Response to long-term weather variations is an important feature of good passive solar performance; if a building can store heat from a week or more before a severely cloudy spell, it has a better chance of going through a design cold day without requiring artificial heat input.

### 3.3.6 2-1/2-week Historic Weather Experiment

In this experiment we attempt to solve for the lumped parameter model's response to historic weather. By historic weather, we mean the observed random day-to-day fluctuations in weather conditions as opposed to "typical" weather conditions. Historic weather is not periodic and so the Fourier transformation of the continuum model won't work; so we are limited to the lumped parameter model.

We treat this modelling exercise as an initial conditions problem. That is, we begin with the solution for 24 February 1978. We then solve the equations for the pre-dawn period of 25 February, using the weather conditions for that date (shown in Table 1) and using the initial condition that  $T_c$ , the concrete mass temperature, does not change discontinuously. We then proceed with solutions for each period of each successive day (pre-dawn, daylight, past-sunset), matching the initial value of  $T_c$  to the previous period's final value of  $T_c$ .

To simplify the algebra, we assume that ambient temperature can be modelled as an average temperature  $\bar{T}_A$  plus a sinusoidal term

$\Delta T_A e^{i\omega_0 t}$  for each day; their values are shown in Table 1. We assume that solar gain is sinusoidal and of the form

$$S = \begin{cases} S_2 e^{i\omega_1 t} & \text{day} \\ 0 & \text{night} \end{cases}$$

for each day. We derive  $S_2$  by scaling the old  $S_1$  (6819 Btu/hr) by the ratio of solar gain for that day (in Table 1) to solar gain for the 24th of February (1924 Btu/day-ft<sup>2</sup>).

Having derived  $T_c$  for each period of each day, we obtain the room temperature  $T_R$  from (6). The results are given in Tables 4ab and plotted in Fig. 7. As shown in the figure, agreement is generally good; the model is always within 8°F of the data except for some spikes during the day (when actual solar gain was, at times, much larger than the sinusoidal model). Furthermore, the largest errors occur on days in which data was missing for one or more daylight hours (indicated by dotted lines on the graph). When data is missing, we can't accurately sum the daily solar gain input. This always occurs on partly cloudy days, when the missing data could lie anywhere from full sunlight to deep overcast. Thus the solar gain is modelled inaccurately, perhaps accounting for the error.

Several things are noteworthy about Fig. 7. First, although  $T_c$  cannot change discontinuously by definition,  $T_R$  can and frequently does at midnight (when assumed weather conditions change discontinuously). But in Fig. 7, all the discontinuities are small and do not affect the general shape of the curves. Also, we

see in Fig. 7 that the model recovers from errors (perhaps caused by missing data) and tracks the measurements as well on the 18th day as on the eighth day. This stability is reassuring, particularly in light of the large amount of long-term heat storage demonstrated in Fig. 6.

This exercise demonstrates the flexibility of the lumped parameter model in describing conditions which would be impossible to model using the distributed parameter model. The two models are complementary in many ways; one may be more useful than another in solving any particular problem (or they may both work or both fail).

### 3.4 Experiments on the LASL Trombe Wall Cell

This section describes the comparisons between predicted room temperature for the Trombe wall cell and recorded temperatures. Its organization is similar to that of the previous section: we begin with a description of the test cell and then describe two experimental comparisons. Both are performed using the distributed parameter model; the lumped model breaks down for a non-thermocirculating Trombe wall.

Comparisons are made for the same days as in the direct gain cell experiments, so we use the weather formulations of Sec. 3.3.2. Results are summarized in Figs. 9 and 10 . As shown in the figures, we find excellent agreement between the model and the data.

#### 3.4.1 Trombe Wall Cell Description

The LASL Trombe wall cell is an insulated box about the same size as the direct gain cell. Immediately behind the glass collector window is a thick (15-5/8" or 39.7 cm) concrete wall painted black. As illustrated in Fig. 8, the air channel between the wall and the glazing is sealed to prevent air leakage between the channel and the room air.

The room behind the Trombe wall consists of styrofoam-and-wood-frame walls of similar construction to those in the direct gain cell. The room air can circulate into a small box-shaped space above the Trombe wall, as shown in the figure, but it can't easily exchange heat with the channel air.

The response of the Trombe cell is governed by Eq. (A2.4-39). Ordinarily, we would model the cell as consisting of one heavy element - the Trombe wall - and would lump the effects of the envelope walls into  $\hat{U}_q$ , the quick heat transfer coefficient. But for the LASL Trombe cell, the envelope walls are the only significant channel for heat loss from the cell, so we must model them as massive envelope walls and calculate response functions for them. The form of (A2.4-39) which we use in this section can therefore be written as:

$$\begin{aligned}
 T_R \left\{ \hat{U}_q + \hat{h}_e (1 - h_e R_{1e}) + \hat{U}_{cR} \left( 1 - \frac{1}{\Sigma} \left( U_{cR} + h_{Tc} \left[ R_{2T} + \frac{U_{cR} h_{Tc}}{\Sigma} R_{1T} \right] \right) \right) \right. \\
 \left. + \hat{U}_{TR} \left( 1 - U_{TR} \left( R'_{1T} + \frac{1}{U_{TR}^2} \frac{U_{cR} h_{Tc}}{\Sigma} R_{2T} \right) \right) \right\} \\
 = S \left( \alpha_T \left( \frac{U_{cR} h_{Tc}}{\Sigma} R_{1T} + R_{2T} \right) \right) \tag{10} \\
 + T_A \left( \hat{U}_q + \hat{h}_e R_{2e} + \frac{\hat{U}_{cR} \hat{U}_{cA}}{\hat{\Sigma}} + \frac{\hat{h}_{Tc} \hat{U}_{cA}}{\hat{\Sigma}} \left( R_{2T} + \frac{U_{cR} h_{Tc}}{\Sigma} R_{1T} \right) \right)
 \end{aligned}$$

where the subscript 'T' refers to Trombe wall, and where the parameters for the Trombe wall are defined in Fig. 2.7 and in Appendix 2.3. Note that since Trombe walls transmit solar heat gain through the wall, the  $R_2$  function enters into  $B(\omega)$  and  $A(\omega)$ .

We evaluate the parameters needed for Eq. (10) next. To begin with,  $\hat{U}_q$  consists only of infiltration losses. The volume of the cell consists of the volume of the main room (5.25' x 5.75' x 10.08' according to the author's measurements as displayed in Fig. 8) plus the volume of the small area over the Trombe wall (5.25' x 0.58' x 1.63')

floor:	$5.75' \times 5.25' = 30.19 \text{ ft}^2$
side wall:	$5.75' \times 10.08' = 57.96 \text{ ft}^2$
ceiling:	$7.39' \times 5.25' = 38.77 \text{ ft}^2$
back wall:	$5.25' \times 10.08' = 52.92 \text{ ft}^2$
walls above air channel:	$(1.63' + 5.25') \times 0.58' = 3.99 \text{ ft}^2$
TOTAL	<hr/> $183.8 \text{ ft}^2$

So  $A_e = 183.8 \text{ ft}^2$ . We assume  $h_e \cong 1 \text{ Btu/deg F-ft}^2\text{-hr}$  because the envelope walls see mostly other walls.

We next calculate solar transmission. The transparent area of the glazing is  $8.58' \times 4.58'$ . The transmissivity of the glass is assumed to be 75%; the amount of light reflected back out of the glass is apparently somewhat less than for the direct gain cell; we assume 72% for net transmissivity. Thus the solar gain is for 24 February when the peak solar gain is  $255 \text{ Btu/hr-ft}^2$  is  $7215 \text{ Btu/hr}$ . We take  $\alpha_T = 1.00$ .

Finally, we list some materials properties necessary in calculating response functions. For the Trombe wall,  $K = .80 \text{ Btu/hr-deg-ft}$ ,  $\rho c_p = 18 \text{ Btu/}^\circ\text{F-ft}^3$ , and  $d = 1.3021 \text{ ft}$ . For the envelope walls, we have two 2-layer walls in parallel. Both have styrofoam as an inside layer. Using ASHRAE handbook values, we find that for styrofoam,  $\rho = 2.2 \text{ lbs/ft}^3$ ,  $c_p = 0.29 \text{ Btu/lb}$ ,  $K = 0.01667 \text{ Btu/}^\circ\text{F-hr-ft}$ , and  $d = 1/12 \text{ ft}$ .

The second (outside) layer is fiberglass in one case ( $\rho c_p = 0.143 \text{ Btu/}^\circ\text{F-ft}^3$ ,  $K = 0.0238 \text{ Btu/}^\circ\text{F-ft-hr}$ ,  $d = 3.5/12 \text{ ft}$ ) and wood ( $\rho c_p = 9 \text{ Btu/}^\circ\text{F-ft}^3$ ,  $K = .068 \text{ Btu/}^\circ\text{F-ft-hr}$ ,  $d = 4.5/12 \text{ ft}$ ) in the

for a total of  $309.2 \text{ ft}^3$ . At 1/4 air change per hour, this represents a heat loss of  $1.08 \text{ Btu/deg F-hr}$  so  $\hat{U}_q = 1.08 \text{ Btu/}^\circ\text{F-hr}$ .

The Trombe wall itself has an area  $A_T = 46.83 \text{ ft}^2$ , based on dimensions of 8.92 ft height and 5.25 ft width. The film coefficient  $h_{TC}$  from the Trombe wall surface to the channel air is taken to be  $2.0 \text{ Btu/ft}^2\text{-deg F-hr}$ , slightly larger than usual due to the high surface temperatures ( $> 140^\circ\text{F}$ ) attained by the front Trombe wall surface, but not exceptionally large since free convection is impossible in the sealed air channel. The exact value of  $h_{TC}$  is not important for a non-circulating wall; what is important is that  $h_{TC}$  and  $U_{CA}$  (the heat transfer coefficient from channel to outside) add as series conductances to the U-value of  $0.55 \text{ Btu/ft}^2\text{-}^\circ\text{F-hr}$  for a double glazed window. This requires  $U_{CA} = 0.7586$ . Combining these heat transfer coefficients with the wall area, we get  $\hat{h}_{TC} = 93.66 \text{ Btu/}^\circ\text{F-hr}$  and  $\hat{U}_{CA} = 35.53 \text{ Btu/}^\circ\text{F-hr}$ .

The coupling between channel air and room air,  $\hat{U}_{CR}$ , while small, is not exactly zero, even for a noncirculating wall. Warm air can conduct through the 2" styrofoam atop the channel into the room; the magnitude of this conductance is given by the area:  $5.25 \text{ ft} \times .333 \text{ ft}$  multiplied by the U-value for styrofoam (R-10) plus two film coefficients (R-2/3 each). The U-value is  $.0882 \text{ Btu/ft}^2\text{-}^\circ\text{F-hr}$ , so  $\hat{U}_{CR} = .1544 \text{ Btu/}^\circ\text{F-hr}$ . Thus  $\hat{U}_a = 25.84 \text{ Btu/}^\circ\text{F-hr}$  and  $\hat{\Sigma} = 129.34 \text{ Btu/}^\circ\text{F-hr}$ . Finally the coupling between the back of the Trombe wall and the room,  $U_{TR}$ , is just a film coefficient of  $1.5 \text{ Btu/ft}^2\text{-}^\circ\text{F-hr}$ , thus  $\hat{U}_{TR} = 70.245 \text{ Btu/}^\circ\text{F-hr}$ .

The envelope walls consist of 1 inch styrofoam backed by insulated wood framing. The wall areas are:

other. We calculate the response functions for two-layer walls using (A2.4-50). The total response function is the stud area fraction (0.2) times the styrofoam-plus-studs response functions plus the insulated cavity fraction (0.8) times the styrofoam-plus-insulation response functions. The result for the total wall is given in Table 5.

We next calculate response functions for the Trombe wall, using the parameters given above. The response functions  $R_{1T}$ ,  $R_{2T}$ , and  $R'_{1T}$  are tabulated in Table 6.

This completes the computation of house parameters. The parameters, along with the weather description of Sec. 3.3.2, are used in the following two sections for simulation work.

#### 3.4.2. Experimental Results for 24 February 1978

The previous sections provide the background needed to model the Trombe wall for 24 February. As we have noted, this date was chosen for time-independence of daily weather patterns, as illustrated in Fig. 4. We thus model the cell using only a steady-state term and harmonics of one cycle per day. As we will show, the building response functions decrease very rapidly with increasing  $\omega$ , so only 3 terms are needed in the series.

We next calculate the building response functions  $A(\omega)$ ,  $B(\omega)$ , and  $C(\omega)$  using the weather parameters of Sec. 3.3.2 and the house parameters of the previous section to evaluate Eq. (10). The results are given in Table 7. Anticipating the needs of the next experiment, we also evaluate  $A$ ,  $B$ , and  $C$  for  $\omega_w$  and  $\omega_w'$ . Missing entries in the table are omitted because they are not needed in the calculation.

For example, we omit  $C(2\omega_0)$  because there is no input of temperature variation at frequency  $2\omega_0$ .

The room temperature response is given by (2.15), which is repeated below. Recall that  $|S_1| = 7215$  Btu/hr and the  $d$ 's are given in Sec. 3.3.3.

$$T_R = |S_1| \left\{ d_0 \frac{B(\omega_0)}{A(\omega_0)} + \sum_{n=1}^2 \frac{B(n\omega_0)}{A(n\omega_0)} d_n e^{in\omega_0 t} \right\} + \bar{T}_A + \frac{C(\omega_0)}{A(\omega_0)} \Delta T_A e^{i\omega_0 t} \quad (11)$$

We evaluate (11) term-by-term below, and point out some interesting effects:

$$T_R = 41.08^\circ \text{F} + 4.973 e^{-4.313i} e^{i\omega_0 t} + .695 e^{-.552i} e^{2i\omega_0 t} + 37^\circ \text{F} + 2.458 e^{-2.842i} e^{i\omega_0 t} \quad (12)$$

We first note that the response to sunlight is very heavily damped by passage through the Trombe wall; the daily fluctuations in temperature due to solar input are only  $\pm 5^\circ \text{F}$ . In addition, they are phase delayed by about  $0.9 \pi$ , or almost half a day. Thus even though the solar gain peaks at 12:30 p.m. and the ambient temperature peaks at 3 p.m., the effects of sunlight are felt six hours later than the effects of temperature.

This last effect illustrates why we had to model the envelope walls as massive objects. Comparing the last term  $\left( \frac{C(\omega_0)}{A(\omega_0)} \Delta T_A \right)$  to the second term  $\left( \frac{B(\omega_0)}{A(\omega_0)} d_1 S_1 \right)$ , we see that they are separated in phase by  $1/4$  cycle. This means that if the phase difference were to increase, these two terms would begin to interfere with each other. In other

words, if the envelope walls had really been sources of quick heat loss,  $C(\omega_0)$  would have been larger and would have had smaller phase lag, and the last term of (12) would have interfered destructively with the second term. So less insulation would lead to lower room temperature fluctuations, not higher, (at least until the last term dominated over the second (solar) term).

This discussion points up an interesting design possibility of Trombe wall buildings, which might not be apparent in a computer-based analysis. We can apparently design the Trombe wall and other elements to reduce temperature fluctuations by means of destructive interference between different waves at frequency  $\omega_0$ . We can produce not only interference between the Trombe-wall transmitted solar wave and the ambient-temperature-response wave, we can also add in a thermocirculation term to the Trombe wall. In (10) there are several terms of the form

$$\frac{U_{cR} h_{Tc}}{\Sigma} R_{1T} + R_{2T} . \text{ For this experiment, } R_{2T} \gg \frac{U_{cR} h_{Tc}}{\Sigma} R_{1T}, \text{ so the } R_{1T} \text{ term's}$$

effects are small; nevertheless the whole term is always smaller than  $R_{2T}$ , not larger, because  $R_{2T}$  is almost completely out of phase with  $R_{1T}$  at frequency  $\omega_0$ . Thus adding varying amounts of thermocirculation (increasing  $U_{cR}$ ) could decrease the fluctuations in room temperature for this cell. The results of Eq. (12) can be condensed and written as

$$T_R = 78.08^\circ \text{ F} + 5.76 e^{i\omega_0(t-14.8 \text{ hours})} + 0.7 e^{2i\omega_0(t-1.05 \text{ hours})} \quad (13)$$

This result is plotted in Fig. 9 for comparison with the data; as we can see, the agreement is excellent.

Note the very fast convergence of the series  $\sum_n^d \frac{B(n\omega_o)}{A(n\omega_o)}$  in Eqs. (12) and (13). This convergence is due to the fact that  $B(n\omega_o) \approx R_{2T}$ , which decreases very rapidly with  $\omega$ , coupled with the slower  $1/\omega^2$  dependence of the  $d_n$ . For this reason, we can completely ignore harmonics with  $n \geq 3$ ; even the 2nd harmonic is buried in the noise of the calculation.

Finally, we can check the conductivity measurement of LASL concrete in a very approximate way using the results derived above. We find that they are consistent with the LASL measurement of .80 Btu/°F-hr-ft. Our check consists of calculating the steady-state heat transfer from the Trombe wall into the room and comparing this with the steady-state heat losses from the room. The former is estimated by calculating  $U_T A_T (\bar{T}_{41} - \bar{T}_{45})$  where  $\bar{T}_{41}$  and  $\bar{T}_{45}$  are the front and back Trombe wall surface temperature at mid-height, averaged over the day (see Sec. 3.2 for values),  $U_T$  is the Trombe wall U-value of  $K_T/d_T = 0.6144$  Btu/ft<sup>2</sup>-deg F-hr. This should overestimate heat transfers, since the temperature of the wall is not uniform and the bottom is much colder than the middle or the top. (That is, the average back-surface temperatures for February 24 are: top: 88.79° F; middle: 86.94° F; bottom: 78.50° F. The middle temperature is thus somewhat hotter than the average temperature). The result is a heat transfer to the room of 615 Btu/hr.

The losses from the room are given by  $\left\{ \hat{U}_q + \hat{h}_e (1 - h_e R_{le}) \Big|_{\omega=0} \right\} \times (\bar{T}_R - \bar{T}_A)$ . This is numerically equal to 12.33 Btu/°F-hr  $\times$  41.08° F or

$$T_R(t) = \begin{cases} 62.7 \\ 66.2^\circ \text{F} \\ 69.6^\circ \text{F} \end{cases} + 5.14 e^{i\omega_o(t-14.92 \text{ hrs})} + .61 e^{2i\omega_o(t - 1.05 \text{ hrs})} \quad (15)$$

where the first term includes the effects of weather varying terms

evaluated at  $\left\{ \begin{array}{l} \text{previous midnight} \\ \text{noon March 8} \\ \text{following midnight} \end{array} \right\}$ . Values for intermediate

times can be approximated by linear interpolation. In comparing with (8), we are making the assumption that the second and fifth terms of (8) must be evaluated for each hour of each day (e.g.  $t = 15 \text{ days} + 2 \text{ hours}$ ) while the expression  $\Delta S_w e^{i\omega_w t}$  in the third term can be evaluated for  $t = \text{noon on March 8}$  and held constant throughout the day. The good agreement in Figs. 10 and 6 seems to validate this approximation.

506.5 Btu/hr. This estimate is about 20% different than the previous estimate, and the error is in the expected direction. So we see that the LASL conductivity estimate is self-consistent to better than 20% accuracy.

### 3.4.3. Weather Variations: Experimental Results for 8 March 1978

We next attempt to model the effects of long-term weather variations on the Trombe wall cell by looking at room temperature response on March 8. As we have described, March 8 was chosen because its weather patterns can be accurately described by a sinusoidally modulated solar gain amplitude with modulation frequency  $\omega_w = 2\pi/14$  days and a sinusoidally varying average temperature whose frequency  $\omega'_w = 2\pi/10$  days. This fit is illustrated in Fig. 3.

The mathematics are analogous to those derived for the direct gain cell in Sec. 3.3.5. The equations for S and  $T_A$  are identical, except that  $|S_1| = 7215$  Btu/hr for the Trombe cell instead of 6819 Btu/hr for the direct gain cell. The room temperature response is still described by (8), which is repeated below, only the building response functions  $A(\omega)$ ,  $B(\omega)$ , and  $C(\omega)$  are taken from Table 7 for the Trombe wall cell. Equation 8 says:

$$T_R(t) = \bar{S} \frac{B(0)}{A(0)} d_o + \Delta S_w \frac{B(\omega_w)}{A(\omega_w)} d_o e^{i\omega_w t} + \left( \bar{S} + \Delta S_w e^{i\omega_w t} \right) \sum_{n=1}^2 \frac{B(n\omega_o)}{A(n\omega_o)} d_n e^{in\omega_o t} \\ + \bar{T}_A + \Delta T_{A_w} \frac{C(\omega'_w)}{A(\omega'_w)} e^{i\omega'_w t} + \Delta T_A \frac{C(\omega_o)}{A(\omega_o)} e^{i\omega_o t}$$

We use Table 7 to evaluate this term-by-term, as follows:

$$\begin{aligned}
 T_R(t) = & 26.30^\circ\text{F} + 12.19 e^{i\omega_w(t-4.365 \text{ days})} + 4.398 e^{-i4.313 \omega_o t} \\
 + & 0.615 e^{2i\omega_o(t-1.05 \text{ hrs})} + 37.5^\circ\text{F} + 2.96 e^{i\omega_w'(t-6.52 \text{ days})} \\
 + & 2.072 e^{-i2.897 \omega_o t}
 \end{aligned} \tag{14}$$

As in the daily solution, the solar response term at frequency  $\omega_o$  is out of phase by 1/4 cycle with the ambient temperature response at that frequency.

We note that in (14), the time  $t$  is measured in days in the second and sixth terms; that at noon on March 8  $t = 15.0$  days (i.e.  $t = 0$  at noon on February 21).

What is the effect of long-term weather storage on the system? We note several effects. First, on the peak day of the cycle, the temperature elevation due to solar gain is  $26.30 + 12.19^\circ\text{F}$ , or  $38.49^\circ\text{F}$ . This is 2-1/2 degrees cooler than the steady-state result for 24 February, indicating that the storage of "coolth" is considerable. This is also evident in the reduced amplitude of the response to ambient temperature;  $\Delta T_{A_w}$  is  $4^\circ\text{F}$ , but the room temperature response to it is only  $3^\circ\text{F}$ .

Also, note the phase lag in the second term of (14). The response to weather-varying solar amplitude is delayed 1-1/2 days. This results in the second term contributing almost nothing to room temperature on March 8, but if there were no phase lag the contribution from a  $12^\circ\text{F}$  amplitude would have been  $8.3^\circ\text{F}$  (that is, the room would have been about  $8^\circ$  warmer).

To look at the effect of weather variations more precisely, we can model the cell's response as if all previous days had the same weather as March 8. This would involve using (11), evaluated with the values of  $|S_1|$  and  $\bar{T}_A$  for March 8. The results of this exercise are shown in Fig. 10 labelled as "no weather" and are contrasted to the results of (14) ("model") and the LASL measured data.

As seen in Fig. (10), the prediction including the effects of weather agrees very well with the data, while the no-weather curve is significantly different. The difference between the calculated curves with and without weather variation is a measure of the cell's response at low frequencies. It is larger than was the case for the direct gain cell, due to the greater thickness of the Trombe wall. This can be seen by looking at  $B(\omega_w)$  in Table 7 and comparing with  $R_{2T}$  in Table 6. The two functions are approximately equal. Half the phase delay in  $\frac{B(\omega_w)}{A(\omega_w)}$  is the lag present in  $R_{2T}$ .

One can also note from comparing  $B(\omega)$  in the direct gain and Trombe wall models that  $B(0)$  can be taken to represent the collection efficiency of the Trombe wall. Note from (2.14) that  $B$  is always less than 1, since each term  $h_j R_{1j} < 1$ . For the Trombe wall cell, this efficiency is 44%. It is low because of the large losses through the collector glazing from the hot front surface of the wall. For comparison, if the collector window had been triple-glazed, with U-value of  $0.35 \text{ Btu/ft}^2\text{-deg F-hr}$  for the glass, the collector efficiency  $B(0)$  would have been 55%.

Equation (14) can also be written in more condensed form as

### 3.5 The Sonoma House Model

In this section we discuss the comparison between the lumped parameter model and some rough measurements made on a small 1-room passive solar demonstration house built by Barbara Greene at Sonoma State College in Cotati, California in 1975, and since demolished. We model most of the building from architectural data and materials properties; however, one parameter is adjusted within a plausibility range to obtain the best fit.

The section of the house is shown in Fig. 11; it covered  $440 \text{ ft}^2$  ( $+115 \text{ ft}^2$  under the collector). Insulation was about R-11 on walls and floor, R-22 on ceiling; there were also  $2-15 \text{ ft}^2$  double-glazed windows on the west wall.

The thermal storage system consisted of 407 1-gallon milk bottles painted black and filled with water, mounted on a frame of  $2 \times 6$  studs backed by plywood. The assembly was facing  $10^\circ$  west of South and inclined with normal  $60^\circ$  from vertical. A few inches above the collector assembly was a single glazed window,  $220 \text{ ft}^2$  in gross area. At night it was covered by  $1\frac{1}{2}$ " of insulating polyurethane foam  $R \sim 10$ ; during the day, the back of the cover was reflective and increased the solar collection. Air could circulate through the narrow ( $\sim 1$ ") channel between the collector window and the storage assembly.

The equations of Sec. 2.3 describe the response of a house to sinusoidal solar gain and periodic weather, so to compare the predictions with experiment, one must find a day with weather patterns similar to those of preceding days. Unfortunately, the data collection

effort at Sonoma was spotty. Hourly values of  $T_R$  are generally available, but  $T_A$  was obtained from the campus weather station, which was frequently out of order. The calculations also require knowledge of when the collector window cover was opened and closed; this data was collected about half the time, and is sometimes incorrect (e.g. the data show that the cover was not opened on a given day, yet  $T_R$  increases as quickly as on sunny days when the collector was used).

The net result is that the only day for which all the data were available was December 13, 1975. Fortunately, the condition of time-independent weather was satisfied to good approximation on this date. Figure 12 graphs the results  $T_R - (\bar{T}_A)$  vs time; the solid line gives the data, the flatter dotted line gives the model predictions. The more curved dotted line gives the results of an extension of the model which accounts in an approximate way for the solar gain through the small west-facing windows. West window solar gain was assumed to be sinusoidal in time and centered at 2:30 p.m. To the extent that the real function was skewed towards later time, the house response should also be delayed further. The model also calculates the collector ("floor") temperature  $T_f$ , which was measured in a few spot checks. Measurements put the afternoon collector temperature  $T_f$  in the range of 125-140°F, which is consistent with the calculation.

The predictions agree reasonably well with the data, considering the amount of judgment required in evaluating the parameters of a house which was demolished before it could be seen by the authors, and considering the uncertainties in the weather data.

We next describe the details of the modelling.

This building might most properly be modelled using the Trombe wall equations. However, since we were unable to make any measurements on the building, it would have been difficult to evaluate all the conductances ( $\hat{h}_{wc}$ ,  $\hat{U}_{wo}$ ,  $\hat{U}_{ca}$ ,  $\hat{U}_{cr}$ ) used in the model. We further felt that the limited data accuracy did not warrant the extra algebraic complication, so we used the direct gain model. We thus assume that there is a direct path for heat loss from the receiver heat capacity to the ambient temperature reservoir through the glazing, which we call  $\hat{U}_o$ . We also assume a direct path from the receiver surface to the room, which is described by the "film coefficient"  $\hat{h}$ .

We use "floor" subscripts to describe the receiver. The most difficult parameter to evaluate will then be  $\hat{h}_f$ , the coupling between "floor" (receiver) surface and the room. Since the coupling is by natural convection through a narrow channel (between the bottles and the window glazing), the resistance (both mechanical resistance and thermal resistance) should be relatively high. The convective part of the usual  $h_f$  is about  $1/2$  Btu/hr-deg-ft<sup>2</sup>; for this case we expect a range of  $.1-1/2$ , corresponding to  $22 < \hat{h}_f < 110$ ; we will fit this empirically.

The other floor parameters,  $\hat{U}_{fi}$ ,  $\hat{U}_{fo}$ , and  $C_f$  are inherently lumped, and thus relatively easy to calculate. Since the heat transfer into the bottles involves free convection of water,  $U_{fi}$  is large; around  $50-60$  Btu/hr-ft<sup>2</sup>-deg. Thus  $\hat{U}_{fi} \sim 12,000$  for  $220$  ft<sup>2</sup>.

$\hat{U}_{fo}$  is the loss rate from the collector; it is the U value of the collector glazing. This ranges from about 1.1 for still air inside to about 2 for quickly circulating inside air, so  $\hat{U}_{fod} \cong 220 \text{ ft}^2 \times (1.1-2) = 230 - 440$ . Discussions with people at Cal State suggest the higher part of the range is more believable, since a jet of fast-moving air blew past the receiver and into the room when the sun was shining. So we take  $\hat{U}_{fod} = 400 \text{ Btu}/^\circ\text{F-hr}$ .

We estimate the collector heat capacity  $C_f$  as the sum of the contributions of the water and of the wood frame. The water has a heat capacity of  $407 \text{ gal} \times \frac{8.33 \text{ lbs}}{\text{gal}} \times \frac{1 \text{ Btu/deg}}{\text{lb}} = 3390 \text{ Btu/deg}$ .

The frame consists of  $2 \times 6$  studs 12" apart in a 240 gross square foot assembly. We use the entire heat capacity, since the lumped parameters for 1" half-thickness of interior wood are very nearly the steady-state parameters. Heat capacity of the frame is

$$240 \text{ ft}^2 \times \frac{6''}{12''} \times \frac{1-5/8'' \text{ of stud}}{12'' \text{ of space}} \times 9 \frac{\text{Btu}}{\text{ft}^3 \cdot ^\circ\text{F}} = 146 \frac{\text{Btu}}{^\circ\text{F}}$$

Thus,  $C_f = 3390 + 146 \cong 3535 \text{ Btu}/^\circ\text{F}$ .

To evaluate wall parameters, we use a thickness of 6" corresponding to an average wood thickness for ceiling and floor joints and wall studs. Thus for  $\rho c_p = 9 \text{ Btu/ft}^3 \cdot ^\circ\text{F}$  and  $K_w = 0.068 \text{ Btu/ft} \cdot ^\circ\text{F-hr}$ , we have  $U_{wi} = 0.564 \text{ Btu/ft}^2 \cdot ^\circ\text{F-hr}$ ,  $C_w = 2.164 \text{ Btu/ft}^2 \cdot ^\circ\text{F}$ .  $U_{wo}$  is normally chosen such that  $U_{wi}^{-1} + U_{wo}^{-1} = U_w^{-1}$  where  $U_w = K_w/d$  in order to assure the correct steady-state heat loss. However, in this problem, we use "wall" subscripts to describe both walls and some building contents, so that to get the correct steady state heat loss

we need  $\hat{U}_{wi}^{-1} + \hat{U}_{wo}^{-1} = (U_w A_w)^{-1}$ .  $\hat{U}_{wi}$  will involve some contributions from the house contents; so we hold off the evaluation of  $\hat{U}_{wo}$ .

We calculate square feet of wood as follows: The exterior framing was about 20% wood. (25% is typical but this building had few windows and doors, and used 24" centers for the framing). So wood area in walls is  $.20 \times 450 \text{ ft}^2 = 90 \text{ ft}^2$ . These were  $828 \text{ ft}^2$  of floor and ceiling, with about 13% of their area in wood, giving  $.13 \times 828 = 108 \text{ ft}^2$  of wood area in floor and ceiling.

Since the room was relatively uncluttered, and has no partition walls, heat transfer from the walls to the air is inhibited. Radiative heat transfer would be greatly reduced, since all the inside wall surfaces are roughly the same temperature, and since air is transparent to heat radiation. Therefore we take  $h \approx 1 \text{ Btu/ft}^2\text{-deg-hr}$ . The wall contributions to the lumped parameters are

$$\hat{h}_w = 1.0 \times 198 \text{ ft}^2 = 198 \text{ Btu/deg F-hr}$$

$$\hat{U}_{wi} = .566 \times 198 \text{ ft}^2 = 112 \text{ Btu/deg F-hr}$$

$$\hat{C}_w = 2.16 \times 198 \text{ ft}^2 = 428 \text{ Btu/deg F}$$

In addition, there was about 700 lbs of building materials, typically 2" thick wood, lying around the room. With  $\rho = 27 \text{ lbs/ft}^3$  this results in  $156 \text{ ft}^2$  of wood surface.

The lumped parameters for interior walls 2" thick (that is, assuming that the "wall" extends 2" below the surface and no heat flow occurs out the other side) are  $U_i = .910 \frac{\text{Btu}}{\text{ft}^2\text{-deg-hr}}$ ;  $U_o = 0$ ,

$C = 1.356 \text{ Btu/ft}^2\text{-deg}$ . Thus, adding the contributions for  $156 \text{ ft}^2$  of lumber to the wall stud contribution, we get

$$h_w = 198 + \left( 156 \text{ ft}^2 \times 1 \frac{\text{Btu}}{\text{hr-deg F-ft}^2} \right) = 354 \text{ Btu/deg F-hr}$$

$$U_{wi} = 112 + \left( 156 \text{ ft}^2 \times .91 \frac{\text{Btu}}{\text{hr-deg F-ft}^2} \right) = 254 \text{ Btu/deg F-hr}$$

$$C_w = 428 + \left( 156 \text{ ft}^2 \times 1.356 \frac{\text{Btu}}{\text{deg F-ft}^2} \right) = 637 \text{ Btu/deg F}$$

We take  $\hat{U}_{wo}$  such that  $\hat{U}_{wi}$  and  $\hat{U}_{wo}$  add in series to the steady-state U-value of  $198 \text{ ft}^2 \times U_w$ ; where  $U_w = \frac{K_w}{d} = .136 \text{ Btu/ft}^2\text{-deg F-hr}$ . Thus  $\hat{U}_{wo} = 30.1 \text{ Btu/deg F-hr}$ .

$\hat{U}_q$  is estimated using the steady-state U-values for the insulated spaces (cavities) in the envelope, the non-collector window, and air exchange.

The U-value for R-11 walls with no interior sheathing is  $.08 \text{ Btu/ft}^2\text{-deg F-hr}$ , for ceiling about  $.05$ , for floor about  $.06$  including the crawl space. Infiltration was not measured; we estimate it at 1 air exchange per hour (which is rather high for a 1-room, 1-story building) corresponding to the description of the house as "leaky".

We calculate  $\hat{U}_q$  as follows:

Floor cavity	$.87 \times 414 \text{ ft}^2 \times .06 \frac{\text{Btu}}{\text{ft}^2\text{-deg F-hr}}$	= 22 Btu/deg F-hr
Wall cavity	$.80 \times 450 \text{ ft}^2 \times .08$	= 29
Ceiling cavity	$.87 \times 414 \text{ ft}^2 \times .05$	= 18
Windows	$30 \text{ ft} \times .60$	= 18
Infiltration:	$8 \text{ ft} \times (414 \text{ ft}^2 + \frac{1}{2} 115 \text{ ft}^2) \times .018 \frac{\text{Btu}}{\text{ft}^3\text{°F}}$	= 68
		155 Btu/deg F-hr

Solar gain is estimated as follows: The ASHRAE solar heat gain factor<sup>3</sup> for a half-day in December is  $815 \frac{\text{Btu}}{\text{ft}^2}$  for a South-facing window at 40° latitude. A full day's solar gain is twice this or 1630 Btu/ft<sup>2</sup>. A sine-wave of half-period 9.2 hours, corresponding to the sunrise and sunset data for the house on December 13, 1975, would have an amplitude 278 Btu/ft<sup>2</sup>-hr to produce this solar gain, since

$$\int_{t=0}^{t=\pi/\omega_1} \sin \omega_1 t = \frac{2}{\omega_1} = \frac{2}{(\pi/9.2 \text{ hrs})} = 5.86 = \frac{1630}{278}$$

Solar collection is increased somewhat by the reflective backside of the collector window cover. If we assume a typical sun angle of 20° above the horizon, and an intensity of  $S_0$ , then the intensity on the reflector surface is  $S_0 \sin 20^\circ$ .

Not all of this reflected light will reach the receiver window; since the receiver is not infinitely wide, some of the early-morning or late-evening light will miss the window to the west or east. However, all specularly reflected light at noon will reach the receiver. The intensity of the reflected light should be about  $S_0 \times (\text{reflectivity}) \times \sin 20^\circ$  for a solar gain of  $S_0$ ; this equals about  $.2 S_0$  for a reflectivity of 60%.

Solar gain is thus approximately  $1.2 \times 278 \frac{\text{Btu}}{\text{ft}^2} \times 200$  (net  $\text{ft}^2$  of glazed area) = 66,700 Btu/hr.

This is rounded to 65,000 Btu/hr.

We have used solar gain data for a south facing vertical window, although the actual collector is tilted  $30^\circ$  upward. This should not make too much difference, since for the latitude of this house, maximum solar elevation angle is  $27\frac{1}{2}^\circ$ . Thus at noon, solar heat gain through a vertical window is reduced to approximately  $\cos 27\frac{1}{2}^\circ$  or .89 of its maximum value for the tilted window. For other hours, this ratio is larger, until in the early morning and late afternoon it exceeds 1. Weighting the cosine of the angle between solar flux and collector normal by ASHRAE solar heat gain factor for December 21 at  $40^\circ$  latitude, we find that a vertical collector receives 7% less solar gain than the tilted collector, this 7% is better than the accuracy of the calculation and is ignored.

Sunrise was at  $t = -1.7$  hrs, where  $t = 0$  is 9:30 a.m. when the collector cover was opened; sunset was at  $t = 7.5$  hrs =  $t_d + 1.0$ . Thus  $\omega_1 = \frac{\pi}{7.5 - (-1.7)} = .3415 \text{ hr}^{-1}$ . The phase of solar gain is such that it is centered between sunrise and sunset, thus  $S = 65,000 e^{i[\omega_1(t) - .9903]}$ .

Solar gain was also measured empirically; however, the measured quantity was solar gain on a horizontal surface rather than a vertical or tilted one. Converting to the tilted surface would require some assumptions about direct vs. scattered solar intensities and some lengthy calculations; for this reason we used handbook estimates. The data did, however, establish that solar gain varied approximately sinusoidally in time.

Ambient temperature was fit by eye to a sinusoidal form; the result was that  $T_A = 48^\circ\text{F} + 6.5^\circ e^{i\omega_0(t-3 \text{ p.m.})}$ . Since the collector-cover was opened at 9:30 a.m. and shut at 4 p.m. we set  $t = 0$  at 9:30 a.m. and  $t_d = 6.5 \text{ hrs}$ ; so  $\Delta T_A = 6.5^\circ e^{-i\omega_0(5.5 \text{ hrs})}$ .

We set  $\alpha_f = 1$  and  $\alpha_w = 0$  for the assumption that all the heat was absorbed in the milk bottles. Later, we checked the hypothesis that sunlight was also absorbed through the west windows; the results of that calculation are shown in the note below.

In summary, the inputs to the model are:

$$\hat{U}_q = 155 \text{ Btu/deg F-hr}$$

$$\hat{h}_w = 354 \frac{\text{Btu}}{\text{deg F-hr}} \quad \hat{U}_{wi} = 254 \text{ Btu/deg F-hr} \quad \hat{U}_{wo} = 30.1 \text{ Btu/deg F-hr} \quad C_w = 637 \text{ Btu/deg F}$$

$$\hat{h}_f = 75 \frac{\text{Btu}}{\text{deg F-hr}} \quad \hat{U}_{fi} = 12,000 \text{ Btu/deg F-hr} \quad \hat{U}_{fod} = 400$$

$$\hat{U}_{fon} = 30 \quad C_f = 3535 \text{ Btu/deg F}$$

$$S = 65,000 e^{-i(.9903)} \text{ Btu/hr}$$

$$\Delta T_A = 6.5 e^{-i\omega_0(5.5 \text{ hrs})} \quad \text{where } \omega_0 = \frac{2\pi}{24 \text{ hrs}}$$

$$\omega_1 = .3415 \text{ radians/hour}$$

Solving the lumped parameter model gives the temperature curves of Table 8 which are plotted for collector temperature and room temperature in Fig. 12.

NOTE: Modifications to the lumped parameter model for two sources of solar gain

This exercise is motivated by the desire to see the effect of explicitly modelling the solar gain through the west facing windows in the Sonoma house. This solar gain function has a different shape than the primary solar gain function, thus it generates new inhomogeneous solutions.

Assume that the secondary solar function has the form

$$S_2(t) = \begin{cases} S_2 e^{i\omega_2 t} & t_1 < t < t_2, \\ 0 & \text{otherwise.} \end{cases}$$

This is also a sinusoidal form, but  $\omega_2 \neq \omega_1$  and  $t_1$  and  $t_2$  have no relationship to the other times in the problem. In the Sonoma case,  $\omega_2$  would be faster than  $\omega_1$ , since the west windows collect sunlight for only about half the day. The time at which solar gain begins is  $t_1$ ; this would be about noon for a west window;  $t_2$  would correspond to sunset, at about 5:30 p.m. Note that for the example given  $t_2$  would occur at "night," while  $t_1$  would be during the "day."

The inhomogeneous solution produced by this new excitation is:

$$T_w = \chi_{S_{w2}} e^{i\omega_2 t}$$

$$T_f = \chi_{S_{f2}} e^{i\omega_2 t}$$

with the  $\chi$ 's being given by by the same equations as before (A2.3-11) except using  $\omega_2$  instead of  $\omega_1$ , and using  $\alpha$ 's appropriate to the secondary solar gain radiation balance in calculating the a's. To illustrate the last point, the primary solar gain is all absorbed in the milk bottle assembly, so that  $\alpha_f = 1$   $\alpha_w = 0$   $\alpha_R = 0$ . But the west-window solar gain is absorbed on the walls and floor of the structure. If it falls on studs or building materials, that heat is absorbed on the "wall" surface, and the heat gain is described by  $\alpha_w$ . If the sunlight falls on an area between the studs, the heat is transferred directly to the room, and this heat transfer is described by  $\alpha_R$ . Thus  $\alpha_f = 0$ ,

$$\alpha_w = 0.277 = \frac{198 \text{ ft}^2 + 156 \text{ ft}^2}{450 \text{ ft}^2 + 828 \text{ ft}^2}, \alpha_R = 0.723 = 1 - \alpha_w - \alpha_f.$$

Note that  $\chi_{Sf_2}$  and  $\chi_{Sf_2}$  may have two values, one for daytime and one for nighttime, since nighttime is defined as that time during which the main collector cover is closed.

We thus must solve the differential equations for 4 periods of the day, and match boundary conditions at 4 different times. The solutions are:

$$T_w = \begin{cases} A_1 e^{-\Lambda_{1d} t} + A_2 e^{-\Lambda_{2d} t} + \chi_{A_{wd}} \Delta T_A e^{i\omega_0 t} + \chi_{S_w} S_1 e^{i\omega_1 t} & 0 \leq t < t_1 \\ A_3 e^{-\Lambda_{1d} t} + A_4 e^{-\Lambda_{2d} t} + \chi_{A_{wd}} \Delta T_A e^{i\omega_0 t} + \chi_{S_{w2d}} S_2 e^{i\omega_2 t} & t_1 \leq t < t_d \\ A_5 e^{-\Lambda_{1n}(t-t_d)} + A_6 e^{-\Lambda_{2n}(t-t_d)} + \chi_{A_{wn}} \Delta T_A e^{i\omega_0 t} + \chi_{S_{w2n}} S_2 e^{i\omega_2 t} & t_d \leq t < t_2 \\ A_7 e^{-\Lambda_{1n}(t-t_d)} + A_8 e^{-\Lambda_{2n}(t-t_d)} + \chi_{A_{wn}} \Delta T_A e^{i\omega_0 t} & t_2 \leq t < 24 \end{cases}$$

(16a)

$$T_f = \begin{cases} A_1 K_{1d} e^{-\Lambda_{1d} t} + A_2 K_{2d} e^{-\Lambda_{2d} t} + \chi_{A_{fd}} \Delta T_A e^{i\omega_0 t} + \chi_{S_f} S_1 e^{i\omega_1 t} & 0 \leq t < t_1 \\ A_3 K_{1d} e^{-\Lambda_{1d} t} + A_4 K_{2d} e^{-\Lambda_{2d} t} + \chi_{A_{fd}} \Delta T_A e^{i\omega_0 t} + \chi_{S_f} S_1 e^{i\omega_1 t} + \chi_{f2d} S_2 e^{i\omega_2 t} & t_1 \leq t < t_d \\ A_5 K_{1n} e^{-\Lambda_{1n}(t-t_d)} + A_6 K_{2n} e^{-\Lambda_{2n}(t-t_d)} + \chi_{A_{fn}} \Delta T_A e^{i\omega_0 t} + \chi_{S_{f2n}} S_2 e^{i\omega_2 t} & t_d \leq t < t_2 \\ A_7 K_{1n} e^{-\Lambda_{1n}(t-t_d)} + A_8 K_{2n} e^{-\Lambda_{2n}(t-t_d)} + \chi_{A_{fn}} \Delta T_A e^{i\omega_0 t} & t_2 \leq t < 24 \text{ hrs} \end{cases} \quad (16b)$$

These solutions for  $T_w$  and  $T_f$  must be matched at each transition time: that is,  $T_w(t_1^-) = T_w(t_1^+)$   $T_f(t_1^-) = T_f(t_1^+)$ , etc. This procedure generates eight equations in the eight unknowns A. These are relatively easy to solve and can be expressed analogously to the ordinary lumped parameter case in terms of some nested definitions. The results are written in the form of a program below; see the final equations for the overall form.

$$F_1 = \frac{(K_{1n} - K_{1d}) e^{-\Lambda_{1n} t_n}}{K_{2d} - K_{1d}}$$

$$F_2 = \frac{(K_{2n} - K_{1d}) e^{-\Lambda_{2n} t_n}}{K_{2d} - K_{1d}}$$

$$F_3 = (K_{2d} - K_{1d})^{-1} \left\{ (\chi_{A_{fn}} - \chi_{A_{fd}}) \Delta T_A - \chi_{S_f} S_1 - K_{1d} \left( (\chi_{A_{wn}} - \chi_{A_{wd}}) \Delta T_A - \chi_{S_w} S_1 \right) \right\}$$

$$F_4 = e^{-\Lambda_{1n} t_n} - F_1$$

$$F_5 = e^{-\Lambda_{2n} t_n} - F_2$$

(17)

$$F_6 = (X_{Awn} - X_{Awd}) \Delta T_A - X_{Sw} S_1 - F_3$$

$$F_7 = \left\{ (K_{2d} - K_{1d}) e^{-\Lambda_{2d} t_1} \right\}^{-1} (X_{Sw2d} K_{1d} - X_{Sf2d}) S_2 e^{i\omega_2 t_1}$$

$$F_8 = -X_{Sw2d} S_2 e^{i\omega_2 t_1} + \Lambda_{1d} t_1 e^{(\Lambda_{1d} t_1 - \Lambda_{2d} t_1)} - F_7 e^{i\omega_2 t_1}$$

$$F_9 = (K_{2n} - K_{1n})^{-1} (K_{1d} - K_{1n}) e^{-\Lambda_{1d} t_d}$$

$$F_{10} = (K_{2n} - K_{1n})^{-1} (K_{2d} - K_{1n}) e^{-\Lambda_{2d} t_d}$$

$$F_{11} = (K_{2n} - K_{1n})^{-1} \left\{ (X_{Sf2d} - X_{Sf2n}) S_2 e^{i\omega_2 t_d} + (X_{Sf}) S_1 e^{i\omega_1 t_d} + (X_{Afd} - X_{Afn}) \Delta T_A e^{i\omega_0 t_d} \right\}$$

$$-K_{1n} \left[ (X_{Sw2d} - X_{Sw2n}) S_2 e^{i\omega_2 t_d} + X_{Sw} S_1 e^{i\omega_1 t_d} + (X_{Awd} - X_{Awn}) \Delta T_A e^{i\omega_0 t_d} \right]$$

(17 cont.)

$$F_{12} = e^{-\Lambda_1 t_d} - F_9$$

$$F_{13} = e^{-\Lambda_2 t_d} - F_{10}$$

$$F_{14} = (X_{Awd} - X_{Awn}) \Delta T_A e^{i\omega_0 t_d} + X_{Sw} S_1 e^{i\omega_1 t_d} + (X_{Sw_2d} - X_{Sw2n}) S_2 e^{i\omega_2 t_d} - F_{11}$$

$$F_{15} = \left\{ (K_{2n} - K_{1n}) e^{-\Lambda_{2n}(t_2 - t_d)} \right\}^{-1} (X_{sf2n} - K_{1n} X_{Sw2n}) S_2 e^{i\omega_2 t_2}$$

$$F_{16} = X_{Sw2n} S_2 e^{i\omega_2 t_2} + \Lambda_{1n}(t_2 - t_d) - F_{15} e^{(\Lambda_{1n} - \Lambda_{2n})(t_2 - t_d)}$$

$$Q_1 = F_9 F_4 + F_{10} F_1$$

$$Q_2 = F_9 F_5 + F_{10} F_2$$

$$Q_3 = F_{11} + F_9(F_6 + F_8) + F_{10}(F_3 + F_7)$$

$$Q_4 = F_{12} F_4 + F_{13} F_1$$

$$Q_5 = F_{12} F_5 + F_{13} F_2$$

$$Q_6 = F_{14} + F_{12}(F_6 + F_8) + F_{13}(F_3 + F_7)$$

Then

$$A_7 = \frac{(Q_6 + F_{16})(1 - Q_2) + Q_5(Q_3 + F_{15})}{(1-Q_4)(1-Q_2) - Q_5Q_1}$$

$$A_8 = \frac{Q_1}{1-Q_2} A_7 + \frac{Q_3 + F_{15}}{1-Q_2}$$

$$A_6 = Q_1 A_7 + Q_2 A_8 + Q_3$$

$$A_5 = Q_4 A_7 + Q_5 A_8 + Q_6$$

$$A_4 = F_1 A_7 + F_2 A_8 + F_3 + F_7$$

$$A_3 = F_4 A_7 + F_5 A_8 + F_6 + F_8$$

$$A_2 = F_1 A_7 + F_2 A_8 + F_3$$

$$A_1 = F_4 A_7 + F_5 A_8 + F_6$$

This completes the algebraic solutions; we use the results for the A's above in (A2.3-36). Room temperature is still derived from (A2.3-4). We next evaluate this solution for the Sonoma house. We use all the old parameters; in addition we need to calculate  $S_2$ ,  $\omega_2$ , and the  $\alpha$ 's for calculating the  $\chi_{S_2's}$ .

First we calculate the  $\alpha$ 's. The sunlight entering from the west window does not reach the collector bottles, so  $\alpha_f = 0$ . The light instead falls on the walls, and floor. Since the wall surface material in this building was very light (e.g. paper rather than gypsum board), all sunlight falling on the space between studs winds up heating the room air. Thus  $\alpha_R$  is given by the percentage of wall, building material

and floor area which is located between the studs, and  $\alpha_W = 1 - \alpha_R$ . Thus  $\alpha_R = 0.723$   $\alpha_W = 0.277$ . (Note that  $0.277 = \frac{198 \text{ ft}^2 + 156 \text{ ft}^2}{450 \text{ ft}^2 + 828 \text{ ft}^2}$ ).

Solar gain is derived from the ASHRAE solar heat gain values for west windows. We total the solar gain for the 6 hours 12 noon to 5 p.m. and find a sine wave whose integral gives this same value. We assume that the sine wave starts at 11:30 a.m. and ends at 5:30 p.m.

Since  $\int_0^{\omega x = \pi} \sin \omega x dx = \frac{2}{\omega}$ , we have that  $S_2 =$  (sum of solar gains)

$\times \frac{\omega_2}{2} \times 0.9$  (for double-pane glass transmission factor)  $\times 0.9$  (for net area of window)  $\times 30 \text{ ft}^2 = 2475 \text{ Btu/hr}$  for  $\omega_2 = \frac{\pi}{6} \text{ hrs} = 0.5236 \text{ hr}^{-1}$ . Solar gain peaks at 2:30 p.m. in this model; since  $t = 0$  occurs at 9:30 a.m.

second solar gain is given by  $S_2(t) = 2475 e^{i\omega_2(t-5 \text{ hrs})}$ . The times are then:  $t_1 = 2 \text{ hrs}$ ,  $t_d = 6.5 \text{ hrs}$ ,  $t_2 = 8 \text{ hrs}$ .

The algebra is then straightforward; we display the results below. The room temperature curve is plotted in Fig. 12.

Thus :

$$T_w = \left\{ \begin{array}{l} -39.1 e^{-.1943t} + 62.7 e^{-.1242t} + 3.06 e^{i(\omega_0(t-9.56))} + 6.13 e^{i\omega_1(t-9.120)} \\ -35.7 e^{-.1943t} + 63.6 e^{-.1242t} + 3.06 e^{i\omega_0(t-9.56)} + 6.13 e^{i\omega_1(t-9.12)} \\ - 3.8 e^{-.1907(t-t_d)} + 25.5 e^{-.02312(t-t_d)} + 2.87 e^{i\omega_0(t-9.21)} + 3.23 e^{i\omega_2(t-7.35)} \\ + 0.1 e^{-.1907(t-t_d)} + 25.6 e^{-.02312(t-t_d)} + 2.87 e^{i\omega_0(t-9.21)} + 3.22 e^{i\omega_2(t-7.35)} \end{array} \right.$$

$$T_f = \left\{ \begin{array}{l} 5.0 e^{-.1943t} + 87.9 e^{-.1242t} + 2.75 e^{i\omega_0(t-9.84)} + 49.99 e^{i\omega_1(t-6.44)} \\ 4.6 e^{-.1943t} + 89.1 e^{-.1242t} + 2.75 e^{i\omega_0(t-9.84)} + 49.99 e^{i\omega_1(t-6.44)} \\ 0.2 e^{-.1907(t-t_d)} + 92.0 e^{-.02312(t-t_d)} + 0.48 e^{i\omega_0(t-11.72)} + .88 e^{i\omega_2(t-9.41)} \\ + 92.4 e^{-.02312(t-t_d)} + 0.48 e^{i\omega_0(t-11.72)} + .32 e^{i\omega_2(t-8.81)} \end{array} \right.$$

$$T_R = \left\{ \begin{array}{l} -14.3 e^{-.1943t} + 41.9 e^{-.1242t} + 3.81 e^{i\omega_0(t-7.09)} + 11.65 e^{i\omega_1(t-6.69)} \\ -13.1 e^{-.1943t} + 42.5 e^{-.1242t} + 3.81 e^{i\omega_0(t-7.09)} + 11.65 e^{i\omega_1(t-6.69)} \\ - 1.4 e^{-.1907(t-t_d)} + 28.2 e^{-.02312(t-t_d)} + 3.45 e^{i\omega_0(t-6.65)} + 6.25 e^{i\omega_2(t-5.41)} \\ + 28.3 e^{-.02312(t-t_d)} + 3.45 e^{i\omega_0(t-6.65)} + 6.32 e^{i\omega_2(t-5.38)} \end{array} \right.$$

As seen in the figure, the solution differs from the 1-solar-gain-function solution only during the late afternoon, when it provides a closer fit to the data. Considering that the actual shape of the west-window solar gain function is skewed toward sunset from a sine wave, a solution using more Fourier terms for the west-window solar gain would be even closer to the data.

It is also evident from the A's that the 2-solar-gain solution could be obtained much more simply in this example as a perturbation onto the 1-solar-gain case.

### 3.6 Conclusions

We have shown that the analytic building models of Sec. 2 can successfully predict the performance of simple one-room passive solar buildings to within 10% accuracy, over a variety of weather conditions. Both the distributed and lumped parameter models show good patterns of agreement with the data, over their respective ranges of applicability.

We have also illustrated, by the detailed calculations in this section, how the theory of Sec. 2 can be used numerically for real buildings. In the process of describing these calculations, we have seen several interesting effects: the destructive interference of the responses to sunlight with the response to ambient temperature in a Trombe wall building, the long "memory" of both LASL test cells, and the possibility of thermally averaging over illuminated and shaded portions of a material surface.

We have derived a formula for the collector efficiency of a Trombe wall, and have seen several examples of how simple models can be used to describe building response to complex weather patterns.

These results show that the models give reasonable predictions for simple buildings. Comparison to more complex structures can be done both with multi-zone theoretical models or through larger-scale experiments. This will be the subject of future papers.

Section 3 Footnotes

1. The thermal properties of concrete are known to be dependent on the exact composition of the specimen, as well as on its moisture content and density. There are no canonical values for any of these parameters, and the building literature contains several inconsistencies with regard to concrete's heat capacity.

The Ashrae 1977 Handbook of Fundamentals (Ref. 15) lists concrete heat capacity as 0.21-0.22 Btu/°F-lb; depending on composition, in Chapter 22, Table 3A. However, the sources for data in this table are not listed, and the footnotes to the table warn the reader that the values it tabulates "are intended as design (not specification) values for materials in normal use. For properties of a particular product, use the value specified by the manufacturer or by unbiased tests."

As if to add emphasis to this cautionary statement, the same handbook gives a different estimate for concrete heat capacity in Table 3 of Chapter 37; in that table the heat capacity is listed as 0.156 Btu/°F-lb., and attributed to Perry's (Ref. 30).

Unfortunately, Perry's is also self-inconsistent on the heat capacity of concrete. Table 3-201 does indeed say that  $C_p = 0.156$  Btu/°F-lb. for concrete between 70°F and 312°F, but on the same line it also says that  $C_p = 0.219$  Btu/°F-lb. for concrete between 72°F and 1472 °F. No explanation is provided, nor is there a reference.

In addition, Perry's also discusses heat capacity of concrete on page 3-235, where it says that concrete components ("sand, crushed rock, cement mortars, etc.") all have heat capacity within

roughly 20% of 0.184 Btu/lb-°F (at 70°F). This is attributed to Cragoe, N.B.S. Misc. Publ. 97, 1929.

A third source of information on concrete, Neville (Ref. 16) says that its heat capacity is between 0.20 and 0.28 Btu/°F-lb. But this source also states that the diffusivity ( $K/\rho c_p$ ) of concrete ranges from 0.02 to 0.06 ft<sup>2</sup>/hr. Since Table 7.12 of Ref. 16 shows that K increases faster than linearly with  $\rho$ , the higher values of diffusivity must be associated with the heavier concretes. But for the densest type listed,  $\rho = 150 \text{ lbs/ft}^3$ , we would require  $c_p \leq 0.145$  to get the diffusivity as high as 0.06 ft<sup>2</sup>/hr.

We conclude that one cannot find a defensible single estimate for concrete heat capacity from tables, and that experimental observation is necessary to describe a specimen of concrete.

2. For example,  $\rho c_p = 18 \text{ Btu/°F-ft}^3$  gives  $c_p = 0.125 \text{ Btu/°F-lb}$ . if  $\rho = 144 \text{ lbs./ft}^3$ . The values from footnote 1 above average to .205 Btu/°F-lb. with standard deviation  $\sigma = 0.046 \text{ Btu/°F-lb}$ . So our measurement is only 1.75  $\sigma$  lower than the average of listed values, which is not unreasonable for  $n = 5$ . Furthermore, our measured diffusivity  $\frac{K}{\rho c_p} = 0.044 \text{ ft}^2/\text{hour}$  is within the range of 0.02-0.06 of Ref. 16.
3. Solar heat gain factors include the effects of light transmitted through glass into the room and light absorbed on the window and conducted back into the room. They are calculated for single pane glass, and tabulated for various window directions, times of year and latitudes, in Chapter 26 of the ASHRAE "Handbook of Fundamentals" for 1977 (Ref. 15).

Table 1 Los Alamos Weather Patterns

Date	$\bar{T}_A$ (°F)	$\Delta T_A$ (°F)	Solar Gain (Btu/ft <sup>2</sup> -day)
2/21	32.5		1923
/22	35.0		1915
/23	36.7		1909
/24	37.0	16 e <sup>iω<sub>0</sub></sup> (t-15:00)	1924
/25	40.2	14.3 e <sup>iω<sub>0</sub></sup> (t-14.71:00)	1851
/26	43.6	11.19 e <sup>iω<sub>0</sub></sup> (t-14.62:00)	1086
/27	42.4	3.96 e <sup>iω<sub>0</sub></sup> (t-12.46:00)	785*
/28	39.4	7.96 e <sup>iω<sub>0</sub></sup> (t-14.69:00)	775***
3/1	39.6	2.82 e <sup>iω<sub>0</sub></sup> (t-11.95:00)	144
/2	39.9	8.07 e <sup>iω<sub>0</sub></sup> (t-13.43:00)	950**
/3	25.0	4.11 e <sup>iω<sub>0</sub></sup> (t-18.61:00)	785**
/4	36.0	10.92 e <sup>iω<sub>0</sub></sup> (t-14.65:00)	1392*
/5	40.3	7.44 e <sup>iω<sub>0</sub></sup> (t-12.62:00)	710*
/6	36.3	9.36 e <sup>iω<sub>0</sub></sup> (t-14.57:00)	1107
/7	39.7	8.36 e <sup>iω<sub>0</sub></sup> (t-14.71:00)	1322
/8	41.2	13.49 e <sup>iω<sub>0</sub></sup> (t-15.21:00)	1753

Table 1 (cont.)

/9	43.5	$13.76 e^{i\omega_0(t-14.90:00)}$	1501 <sup>***</sup>
/10	37.2	$1.15 e^{i\omega_0(t-12.78:00)}$	404
/11	39.4	$8.75 e^{i\omega_0(t-13.83:00)}$	1029
/12	36.5	$6.49 e^{i\omega_0(t-12.07:00)}$	597 <sup>***</sup>
/13	35.1	$10.86 e^{i\omega_0(t-14.10:00)}$	1518

---

\* one hour of data missing

\*\* two hours of data missing

\*\*\* three hours of data missing

Table 2 Response Functions for Los Alamos Direct Gain Wall

$\omega$	$R_1$	$\left(\frac{\text{hr-ft}^2\text{-}^\circ\text{F}}{\text{Btu}}\right)$	$R_2$
0	.940		.0603
$2\pi/\text{month}$	.937	$e^{-.0665i}$	.0601 $e^{-.0875i}$
$2\pi/14$ days	.9265	$e^{-.1411i}$	.0594 $e^{-.1861i}$
$2\pi/10$ days	.9143	$e^{-.1953i}$	.05858 $e^{-.2584i}$
$2\pi/2$ days	.615	$e^{-.672i}$	.038 $e^{-.982i}$
$2\pi/\text{day}$	.3991	$e^{-.787i}$	.0228 $e^{-1.380i}$
$2\pi/12$ hours	.2645	$e^{-.726i}$	.0118 $e^{-1.764i}$
$2\pi/8$ hours	.2225	$e^{-.665i}$	.0077 $e^{-2.021i}$
$2\pi/6$ hours	.2017	$e^{-.639i}$	.0055 $e^{-2.238i}$

Table 3 Building Response Functions for the Direct Gain Cell

$\omega$	A (Btu/hr-°F)	B	C (Btu/hr-°F)
0	40.465	.952	40.465
$\omega_w$	46.83 e <sup>+.3812i</sup>	.9396 e <sup>-.1112i</sup>	_____ *
$\omega'_w$	51.93 e <sup>+.4746i</sup>	_____ *	40.03 e <sup>-.0500i</sup>
$\omega_o$	133.9 e <sup>+.286i</sup>	.4818 e <sup>-.4886i</sup>	33.11 e <sup>-.0905i</sup>
2 $\omega_o$	141.65 e <sup>+.167i</sup>	.3848 e <sup>-.374i</sup>	_____ *
3 $\omega_o$	143.91 e <sup>+.128i</sup>	.3574 e <sup>-.312i</sup>	_____ *
4 $\omega_o$	145.39 e <sup>+.111i</sup>	.3433 e <sup>-.284i</sup>	_____ *

\* not required for solution of the model

Table 4a Response of the Concrete Mass Temperature\*  
to Historic Weather, Direct Gain Cell

Date	Period	$T_c - \bar{T}_A$ (°F)
1978 02/24	day	$66.82e^{-.0312(t-7:00)} + 1.89e^{i\omega_o(t-20.55:00)} + 21.13e^{i\omega_1(t-18.10:00)}$
	night	$67.63e^{-.0312(t-18.52:00)} + 1.89e^{i\omega_o(t-20.55:00)}$
	/25 morning	$54.03e^{-.0312(t-0:00)} + 1.69e^{i\omega_o(t-20.26:00)}$
/25	day	$63.63e^{-.0312(t-7:00)} + 1.69e^{i\omega_o(t-20.26:00)} + 20.33e^{i\omega_1(t-18.1:00)}$
	evening	$64.62e^{-.0312(t-18.52:00)} + 1.69e^{i\omega_o(t-20.26:00)}$
	/26 morning	$51.29e^{-.0312(t-0:00)} + 1.32e^{i\omega_o(t-20.17:00)}$
/26	day	$53.08e^{-.0312(t-7:00)} + 1.32e^{i\omega_o(t-20.17:00)} + 11.93e^{i\omega_1(t-18.1:00)}$
	evening	$48.90e^{-.0312(t-18.52:00)} + 1.32e^{i\omega_o(t-20.17:00)}$
	/27 morning	$43.13e^{-.0312(t-0:00)} + 0.47e^{i\omega_o(t-18.01:00)}$
/27	day	$43.23e^{-.0312(t-7:00)} + 0.47e^{i\omega_o(t-18.01:00)} + 8.62e^{i\omega_1(t-18.1:00)}$
	evening	$38.74e^{-.0312(t-18.52:00)} + 0.47e^{i\omega_o(t-18.01:00)}$
	/28 morning	$35.13e^{-.0312(t-0:00)} + 0.94e^{i\omega_o(t-20.24:0)}$
/28	day	$36.70e^{-.0312(t-7:00)} + 0.94e^{i\omega_o(t-20.24:00)} + 8.51e^{i\omega_1(t-18.1:00)}$
	evening	$34.07e^{-.0312(t-18.52:00)} + 0.94e^{i\omega_o(t-20.24:00)}$
	03/1 morning	$29.08e^{-.0312(t-0:00)} + 0.33e^{i\omega_o(t-17.50:00)}$
03/1	day	$24.95e^{-.0312(t-7:00)} + 0.33e^{i\omega_o(t-17.50:00)} + 1.58e^{i\omega_1(t-18.1:00)}$
	evening	$18.98e^{-.0312(t-18.52:00)} + 0.33e^{i\omega_o(t-17.50:00)}$

\* Concrete temperature for each day is measured with respect to  $\bar{T}_A$  for that day. Since  $\bar{T}_A$  changes discontinuously at midnight, the definition and value of  $T_c - \bar{T}_A$  will also change, but the actual temperature will be constant.  $\bar{T}_A$  is given in Table 1.

Table 4a (cont.)

Date 1978	Period	$T_c - \bar{T}_A$ (°F)
03/02	morning	$15.41e^{-.0312(t-0:00)} + 0.95e^{i\omega_o(t-18.98:00)}$
	day	$22.76e^{-.0312(t-7:00)} + 0.95e^{i\omega_o(t-18.98:00)} + 10.43e^{i\omega_1(t-18.1:00)}$
	evening	$26.25e^{-.0312(t-18.52:00)} + 0.95e^{i\omega_o(t-18.98:00)}$
/03	morning	$36.79e^{-.0312(t-0:00)} + 0.48e^{i\omega_o(t-0.16:00)}$
	day	$38.14e^{-.0312(t-7:00)} + 0.48e^{i\omega_o(t-0.16:00)} + 8.62e^{i\omega_1(t-18.1:00)}$
	evening	$35.19e^{-.0312(t-18.52:00)} + 0.48e^{i\omega_o(t-0.16:00)}$
/04	morning	$18.44e^{-.0312(t-0:00)} + 1.29e^{i\omega_o(t-20.20:00)}$
	day	$30.01e^{-.0312(t-7:00)} + 1.29e^{i\omega_o(t-20.20:00)} + 15.29e^{i\omega_1(t-18.1:00)}$
	evening	$36.14e^{-.0312(t-18.52:00)} + 1.29e^{i\omega_o(t-20.20:00)}$
/05	morning	$26.82e^{-.0312(t-0:00)} + 0.88e^{i\omega_o(t-18.17:00)}$
	day	$29.31e^{-.0312(t-7:00)} + 0.88e^{i\omega_o(t-18.17:00)} + 7.80e^{i\omega_1(t-18.1:00)}$
	evening	$28.21e^{-.0312(t-18.52:00)} + 0.88e^{i\omega_o(t-18.17:00)}$
/06	morning	$27.24e^{-.0312(t-0:00)} + 1.10e^{i\omega_o(t-20.12:00)}$
	day	$33.98e^{-.0312(t-7:00)} + 1.10e^{i\omega_o(t-20.12:00)} + 12.16e^{i\omega_1(t-18.1:00)}$
	evening	$35.80e^{-.0312(t-18.52:00)} + 1.10e^{i\omega_o(t-20.12:00)}$
/07	morning	$26.80e^{-.0312(t-0:00)} + 0.99e^{i\omega_o(t-20.26:00)}$
	day	$35.98e^{-.0312(t-7:00)} + 0.99e^{i\omega_o(t-20.26:00)} + 14.52e^{i\omega_1(t-18.1:00)}$
	evening	$39.54e^{-.0312(t-18.52:00)} + 0.99e^{i\omega_o(t-20.26:00)}$

Table 4a (cont.)

Date 1978	Period	$T_c - \bar{T}_A$ (°F)
/08	morning	$31.33e^{-.0312(t-0:00)} + 1.59e^{i\omega_o(t-20.76:00)}$
	day	$44.32e^{-.0312(t-7:00)} + 1.59e^{i\omega_o(t-20.76:00)} + 19.25e^{i\omega_1(t-18.1:00)}$
	evening	$50.06e^{-.0312(t-18.52:00)} + 1.59e^{i\omega_o(t-20.76:00)}$
03/09	morning	$40.00e^{-.0312(t-0:00)} + 1.62e^{i\omega_o(t-20.40:00)}$
	day	$48.53e^{-.0312(t-7:00)} + 1.62e^{i\omega_o(t-20.40:00)} + 16.48e^{i\omega_1(t-18.1:00)}$
	evening	$50.25e^{-.0312(t-18.52:00)} + 1.62e^{i\omega_o(t-20.40:00)}$
03/10	morning	$49.60e^{-.0312(t-0:00)} + 0.14e^{i\omega_o(t-18.33:00)}$
	day	$44.28e^{-.0312(t-7:00)} + 0.14e^{i\omega_o(t-18.33:00)} + 4.44e^{i\omega_1(t-18.10:00)}$
	evening	$35.32e^{-.0312(t-18.52:00)} + 0.14e^{i\omega_o(t-18.33:00)}$
/11	morning	$27.22e^{-.0312(t-0:00)} + 1.03e^{i\omega_o(t-19.38:00)}$
	day	$33.11e^{-.0312(t-7:00)} + 1.03e^{i\omega_o(t-19.38:00)} + 11.30e^{i\omega_1(t-18.10:00)}$
	evening	$34.34e^{-.0312(t-18.52:00)} + 1.03e^{i\omega_o(t-19.38:00)}$
/12	morning	$32.29e^{-.0312(t-0:00)} + 0.77e^{i\omega_o(t-17.62:00)}$
	day	$32.47e^{-.0312(t-7:00)} + 0.77e^{i\omega_o(t-17.62:00)} + 6.56e^{i\omega_1(t-18.10:00)}$
	evening	$29.18e^{-.0312(t-18.52:00)} + 0.77e^{i\omega_o(t-17.62:00)}$
/13	morning	$25.38e^{-.0312(t-0:00)} + 1.28e^{i\omega_o(t-19.65:00)}$
	day	$36.97e^{-.0312(t-7:00)} + 1.28e^{i\omega_o(t-19.65:00)} + 16.67e^{i\omega_1(t-18.10:00)}$
	evening	$42.37e^{-.0312(t-18.52:00)} + 1.28e^{i\omega_o(t-19.65:00)}$

Table 4b. Response of Direct Gain Cell Room Temperature\* to Historic Weather

Date	Period	$T_R - \bar{T}_A$ (°F)
1978		
02/24	day	$51.34e^{-.0312(t-7:00)} + 4.14e^{i\omega_o(t-16.36:00)} + 25.13e^{i\omega_1(t-15.32:00)}$
	night	$51.96e^{-.0312(t-18.52:00)} + 4.14e^{i\omega_o(t-16.36:00)}$
/25	morning	$41.5e^{-.0312(t-0:00)} + 3.7e^{i\omega_o(t-16.07:00)}$
	day	$48.9e^{-.0312(t-7:00)} + 3.7e^{i\omega_o(t-16.07:00)} + 24.18e^{i\omega_1(t-15.32:00)}$
	evening	$49.6e^{-.0312(t-18.52:00)} + 3.7e^{i\omega_o(t-16.07:00)}$
/26	morning	$39.4e^{-.0312(t-0:00)} + 2.9e^{i\omega_o(t-15.96:00)}$
	day	$40.8e^{-.0312(t-7:00)} + 2.9e^{i\omega_o(t-15.96:00)} + 14.19e^{i\omega_1(t-15.32:00)}$
	evening	$37.6e^{-.0312(t-18.52:00)} + 2.9e^{i\omega_o(t-15.96:00)}$
/27	morning	$33.1e^{-.0312(t-0:00)} + 1.0e^{i\omega_o(t-13.82:00)}$
	day	$33.2e^{-.0312(t-7:00)} + 1.0e^{i\omega_o(t-13.82:00)} + 10.25e^{i\omega_1(t-15.32:00)}$
	evening	$29.7e^{-.0312(t-18.52:00)} + 1.0e^{i\omega_o(t-13.82:00)}$
/28	morning	$27.0e^{-.0312(t-0:00)} + 2.1e^{i\omega_o(t-16.05:00)}$
	day	$28.2e^{-.0312(t-7:00)} + 2.1e^{i\omega_o(t-16.05:00)} + 10.12e^{i\omega_1(t-15.32:00)}$
	evening	$26.2e^{-.0312(t-18.52:00)} + 2.1e^{i\omega_o(t-16.05:00)}$
03/01	morning	$22.3e^{-.0312(t-0:00)} + 0.7e^{i\omega_o(t-13.30:00)}$
	day	$19.2e^{-.0312(t-7:00)} + 0.7e^{i\omega_o(t-13.30:00)} + 1.88e^{i\omega_1(t-15.32:00)}$
	evening	$14.6e^{-.0312(t-18.52:00)} + 0.7e^{i\omega_o(t-13.30:00)}$

\*Temperature is measured with respect to  $\bar{T}_A$  on that day. Since  $\bar{T}_A$  changes discontinuously at midnight, the definition and value of  $(T_R - \bar{T}_A)$  will also change, even if the temperature  $T_R$  is constant. But usually, the actual temperature  $T_R$  also jumps a degree or so due to the approximation of this model.

Table 4b(cont.)

Date 1978	Period	$T_R - \bar{T}_A$ (°F)
03/02	morning	$11.8e^{-.0312(t-0:00)} + 2.1e^{i\omega_0(t-14.79:00)}$
	day	$17.5e^{-.0312(t-7:00)} + 2.1e^{i\omega_0(t-14.79:00)} + 12.41e^{i\omega_1(t-15.32:00)}$
	evening	$20.2e^{-.0312(t-18.52:00)} + 2.1e^{i\omega_0(t-14.79:00)}$
/03	morning	$28.3e^{-.0312(t-0:00)} + 1.1e^{i\omega_0(t-19.90:00)}$
	day	$29.3e^{-.0312(t-7:00)} + 1.1e^{i\omega_0(t-19.90:00)} + 10.25e^{i\omega_1(t-15.32:00)}$
	evening	$27.0e^{-.0312(t-18.52:00)} + 1.1e^{i\omega_0(t-19.90:00)}$
/04	morning	$14.2e^{-.0312(t-0:00)} + 2.8e^{i\omega_0(t-16.01:00)}$
	day	$23.1e^{-.0312(t-7:00)} + 2.8e^{i\omega_0(t-16.01:00)} + 18.18e^{i\omega_1(t-15.32:00)}$
	evening	$27.8e^{-.0312(t-18.52:00)} + 2.8e^{i\omega_0(t-16.01:00)}$
/05	morning	$20.6e^{-.0312(t-0:00)} + 1.9e^{i\omega_0(t-13.98:00)}$
	day	$22.5e^{-.0312(t-7:00)} + 1.9e^{i\omega_0(t-13.98:00)} + 9.28e^{i\omega_1(t-15.32:00)}$
	evening	$21.7e^{-.0312(t-18.52:00)} + 1.9e^{i\omega_0(t-13.98:00)}$
/06	morning	$20.9e^{-.0312(t-0:00)} + 2.4e^{i\omega_0(t-15.92:00)}$
	day	$26.1e^{-.0312(t-7:00)} + 2.4e^{i\omega_0(t-15.92:00)} + 14.46e^{i\omega_1(t-15.32:00)}$
	evening	$27.5e^{-.0312(t-18.52:00)} + 2.4e^{i\omega_0(t-15.92:00)}$
/07	morning	$20.6e^{-.0312(t-0:00)} + 2.2e^{i\omega_0(t-16.07:00)}$
	day	$27.6e^{-.0312(t-7:00)} + 2.2e^{i\omega_0(t-16.07:00)} + 17.27e^{i\omega_1(t-15.32:00)}$
	evening	$30.4e^{-.0312(t-18.52:00)} + 2.2e^{i\omega_0(t-16.07:00)}$

Table 4b (cont.)

Date 1978	Period	$T_c - \bar{T}_A$ (°F)
03/08	morning	$24.1e^{-.0312(t-0:00)} + 3.5e^{i\omega_o(t-16.57:00)}$
	day	$34.1e^{-.0312(t-7:00)} + 3.5e^{i\omega_o(t-16.57:00)} + 22.9e^{i\omega_1(t-15.32:00)}$
	evening	$38.5e^{-.0312(t-18.52:00)} + 3.5e^{i\omega_o(t-16.57:00)}$
03/09	morning	$30.7e^{-.0312(t-0:00)} + 3.6e^{i\omega_o(t-16.25:00)}$
	day	$37.3e^{-.0312(t-7:00)} + 3.6e^{i\omega_o(t-16.25:00)} + 19.6e^{i\omega_1(t-15.32:00)}$
	evening	$38.6e^{-.0312(t-18.52:00)} + 3.6e^{i\omega_o(t-16.25:00)}$
/10	morning	$38.1e^{-.0312(t-0:00)} + 0.3e^{i\omega_o(t-14.18:00)}$
	day	$34.0e^{-.0312(t-7:00)} + 0.3e^{i\omega_o(t-14.18:00)} + 5.28e^{i\omega_1(t-15.32:00)}$
	evening	$27.1e^{-.0312(t-18.52:00)} + 0.3e^{i\omega_o(t-14.18:00)}$
/11	morning	$20.9e^{-.0312(t-0:00)} + 2.3e^{i\omega_o(t-15.19:00)}$
	day	$25.4e^{-.0312(t-7:00)} + 2.3e^{i\omega_o(t-15.19:00)} + 13.44e^{i\omega_1(t-15.32:00)}$
	evening	$26.4e^{-.0312(t-18.52:00)} + 2.3e^{i\omega_o(t-15.19:00)}$
/12	morning	$24.8e^{-.0312(t-0:00)} + 1.7e^{i\omega_o(t-13.44:00)}$
	day	$24.9e^{-.0312(t-7:00)} + 1.7e^{i\omega_o(t-13.44:00)} + 7.8e^{i\omega_1(t-15.32:00)}$
	evening	$22.4e^{-.0312(t-18.52:00)} + 1.7e^{i\omega_o(t-13.44:00)}$
/13	morning	$19.5e^{-.0312(t-0:00)} + 2.8e^{i\omega_o(t-15.46:00)}$
	day	$28.4e^{-.0312(t-7:00)} + 2.8e^{i\omega_o(t-15.46:00)} + 19.83e^{i\omega_1(t-15.32:00)}$
	evening	$32.6e^{-.0312(t-18.52:00)} + 2.8e^{i\omega_o(t-15.46:00)}$

Table 5. Response Functions for Trombe Cell Envelope Wall

$\omega$	$R_{1e}$	$\left( \frac{\text{hr-ft}^2\text{-}^\circ\text{F}}{\text{Btu}} \right)$	$R_{2e}$
0	.9388		.06119
$2\pi/14$ days $\equiv \omega_w$	$.9387e^{-.002i}$		$.06104e^{-.0379i}$
$2\pi/10$ days $\equiv \omega'_w$	$.93864e^{-.0025i}$		$.06090e^{-.0528i}$
$2\pi/\text{day}$	$.9319e^{-.0165i}$		$.04803e^{-.2892i}$
$2\pi/12$ hrs	$.9279e^{-.0255i}$		$.04175e^{-.2593i}$

Table 6. Response Functions for the LASL Trombe Wall

$\omega$	$R_{1T} \left( \frac{\text{hr-ft}^2\text{-}^\circ\text{F}}{\text{Btu}} \right)$	$R_{2T}$	$R'_{1T} \left( \frac{\text{hr-ft}^2\text{-}^\circ\text{F}}{\text{Btu}} \right)$
0	1.0125	.4413	.5584
$2\pi/14$ days	$.97633e^{-.1953i}$	$.42197e^{-.3826i}$	$.54278e^{-.1404i}$
$2\pi/10$ days	$.9458e^{-.2638i}$	$.4055e^{-.5251i}$	$.52966e^{-.1884i}$
$2\pi/\text{day}$	$.4195e^{-.620i}$	$.08256e^{-2.516i}$	$.3116e^{-.441i}$
$2\pi/12$ hrs	$.3167e^{-.660i}$	$.02799e^{+2.734i}$	$.2535e^{-.513i}$
$2\pi/8$ hrs	$.265e^{-.682i}$	$.01225e^{+1.966i}$	$.220e^{-.551i}$

Table 7. Building Response Functions for the LASL Trombe Wall Cell

$\omega$	A ( $\frac{\text{Btu}}{\text{°F-hr}}$ )	B	C ( $\frac{\text{Btu}}{\text{°F-hr}}$ )
0	23.79	.4437	23.79
$2\pi/14$ days	$27.35e^{.3116i}$	$.4243e^{-.3816i}$	_____*
$2\pi/10$ days	$29.92e^{.3739i}$	_____*	$22.17e^{-.2664i}$
$2\pi/\text{day}$	$56.90 e^{+.3007i}$	$.08224e^{-2.504i}$	$8.741e^{-.447i}$
$2\pi/12$ hours	$63.95 e^{+.2765i}$	$.02726e^{+2.741i}$	_____*

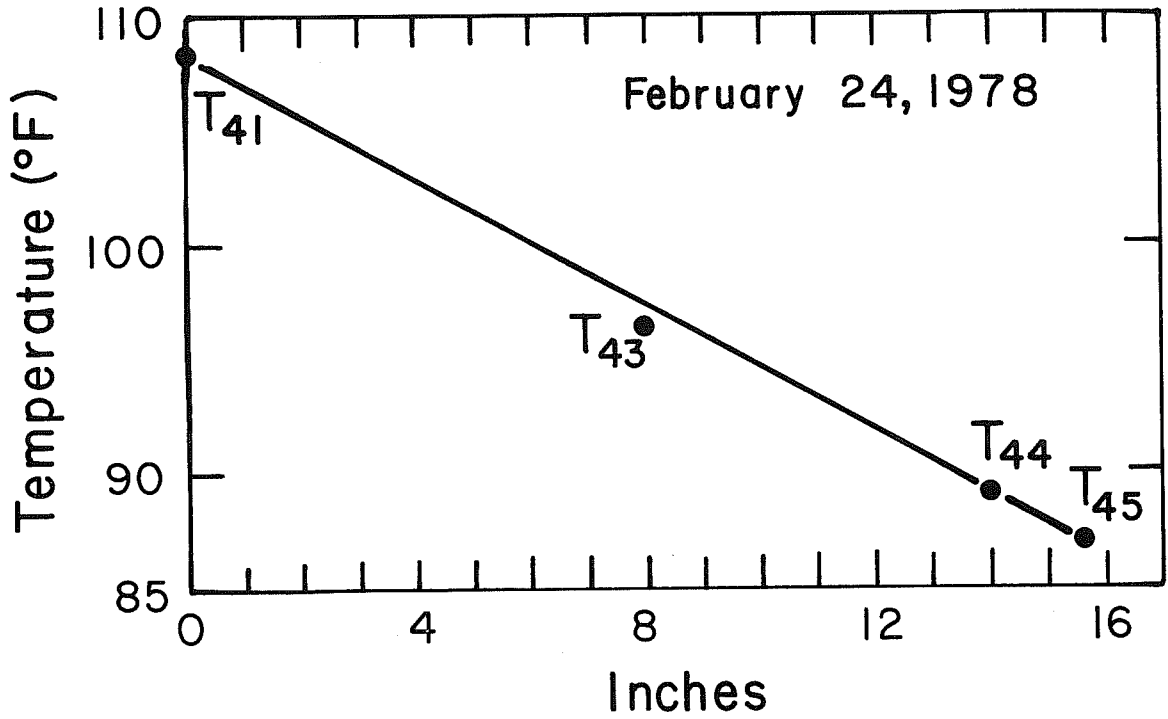
\*not required for solution of the model

Table 8

Sonoma House Model Predictions, 13 December 1975.

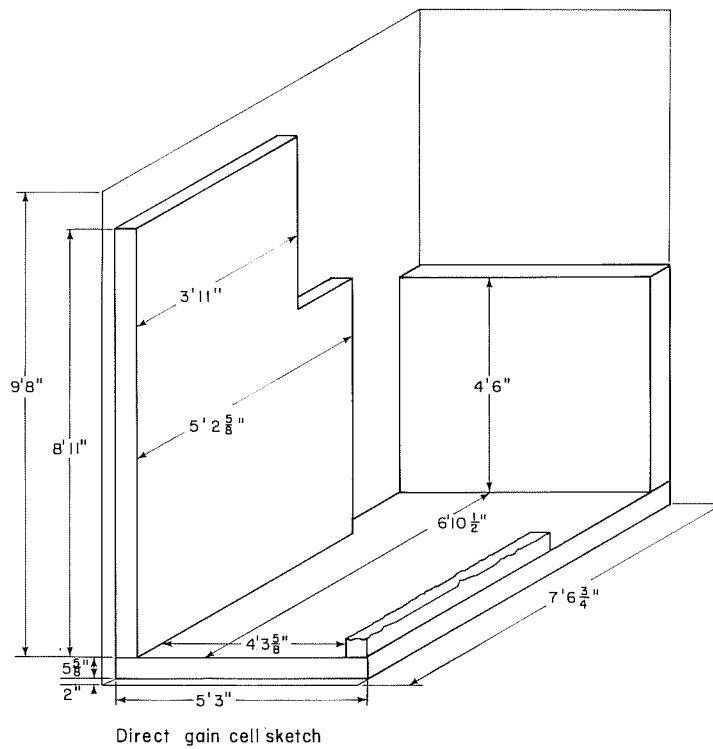
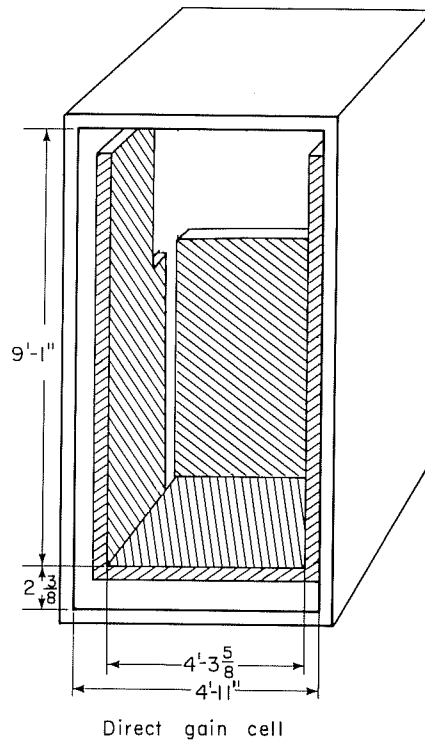
$T_W(t) = \begin{cases} -39.2 e^{-.1943t} + 62.4 e^{-.1242t} + 3.06 e^{i\omega_0(t-9.56 \text{ hrs})} + 6.13 e^{i\omega_1(t-9.12 \text{ hrs})} & 0 \leq t < t_d \\ -5.2 e^{-.1907(t-t_d)} + 25.5 e^{-.02312(t-t_d)} + 2.87 e^{i\omega_0(t-9.21)} & t_d \leq t < 24 \text{ hrs} \end{cases}$
$T_f = \begin{cases} 5.0 e^{-.1943t} + 87.5 e^{-.1242t} + 2.75 e^{i\omega_0(t-9.84)} + 49.99 e^{i\omega_1(t-6.44)} & 0 \leq t < t_d \\ .3 e^{-.1907(t-t_d)} + 91.8 e^{-.02312(t-t_d)} + .48 e^{i\omega_0(t-11.72)} & t_d \leq t < 24 \text{ hrs} \end{cases}$
$T_R = \begin{cases} -14.4 e^{-.1943t} + 41.7 e^{-.1242t} + 3.81 e^{i\omega_0(t-7.09)} + 11.65 e^{i\omega_1(t-6.69)} & 0 \leq t < t_d \\ -2.0 e^{-.1907(t-t_d)} + 28.1 e^{-.02312(t-t_d)} + 3.45 e^{i\omega_0(t-6.65)} & t_d \leq t < 24 \text{ hrs} \end{cases}$

### Trombe wall average temperature vs. Depth into wall



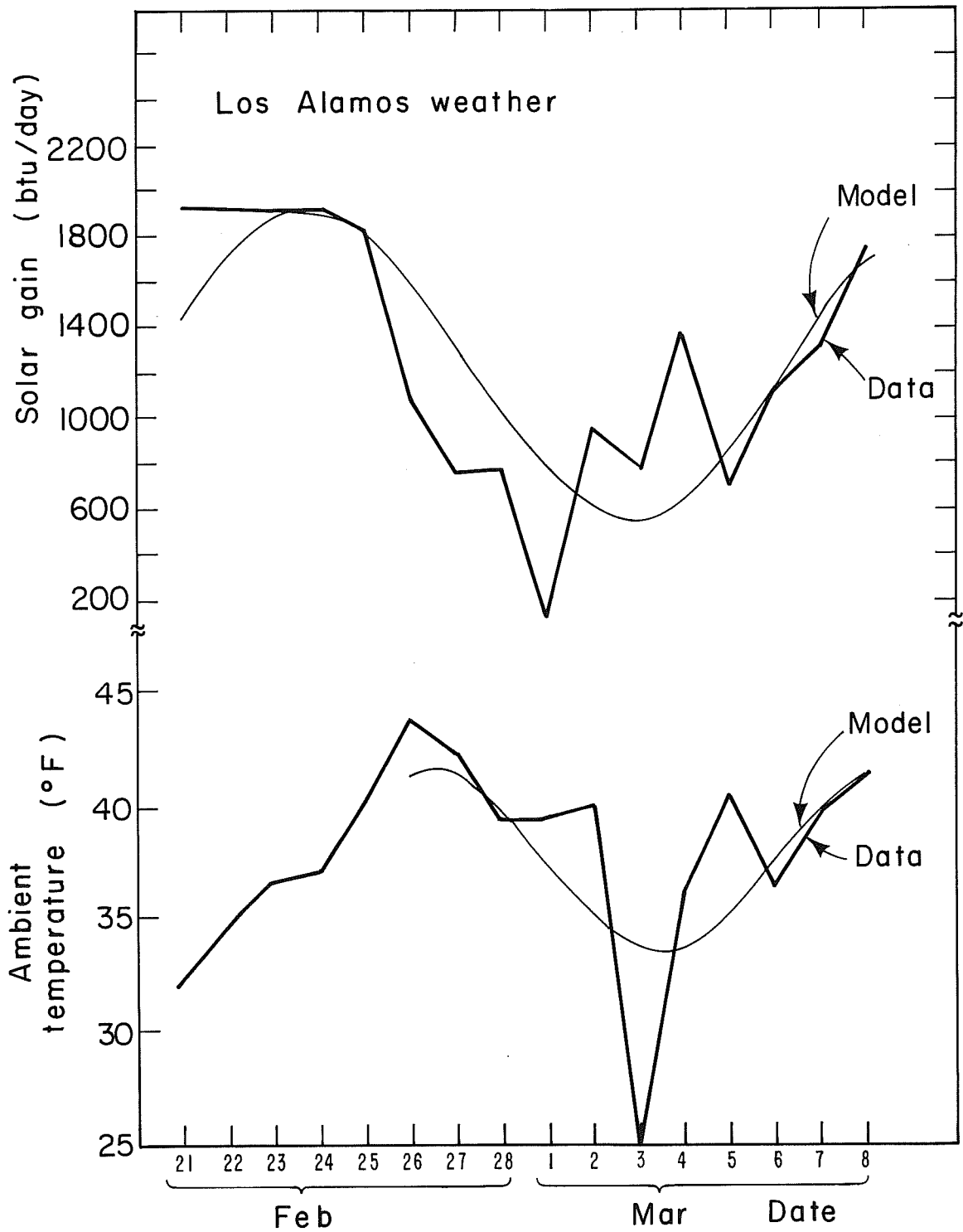
XBL 789-1765

Fig. 1. Trombe wall steady-state temperature as a function of thickness into the wall. The temperatures are averages for the day of 24 February 1978.



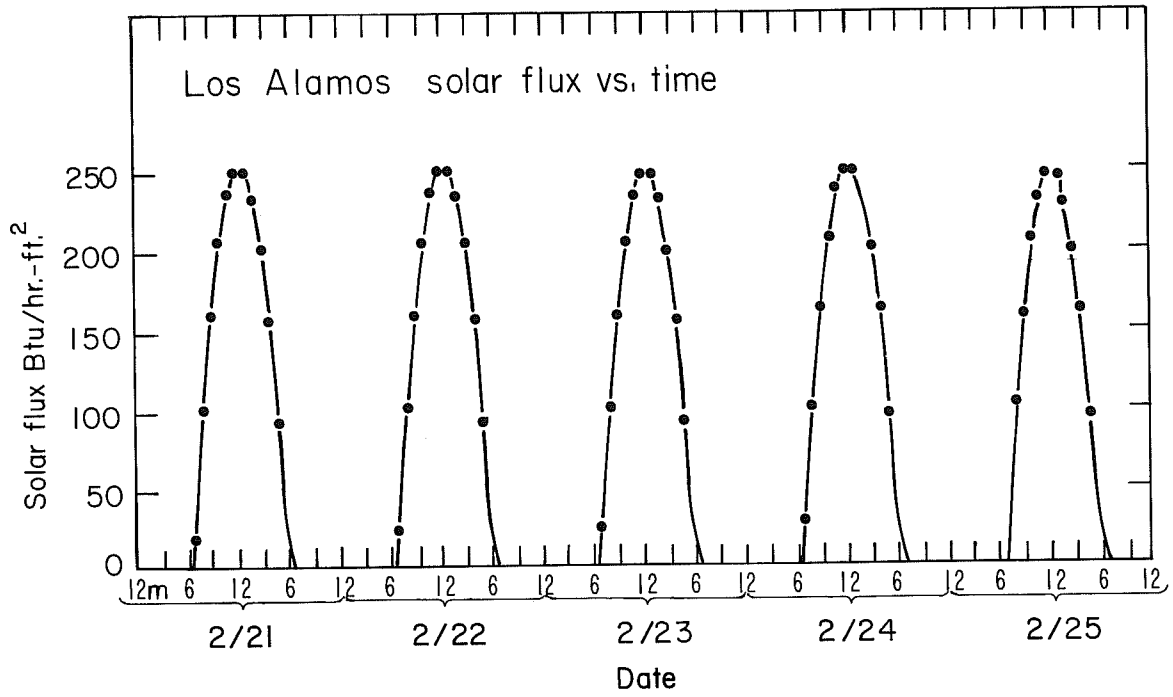
XBL 789-2201A

Fig. 2. The Los Alamos direct gain cell. Dimensions are based on measurements by the author.



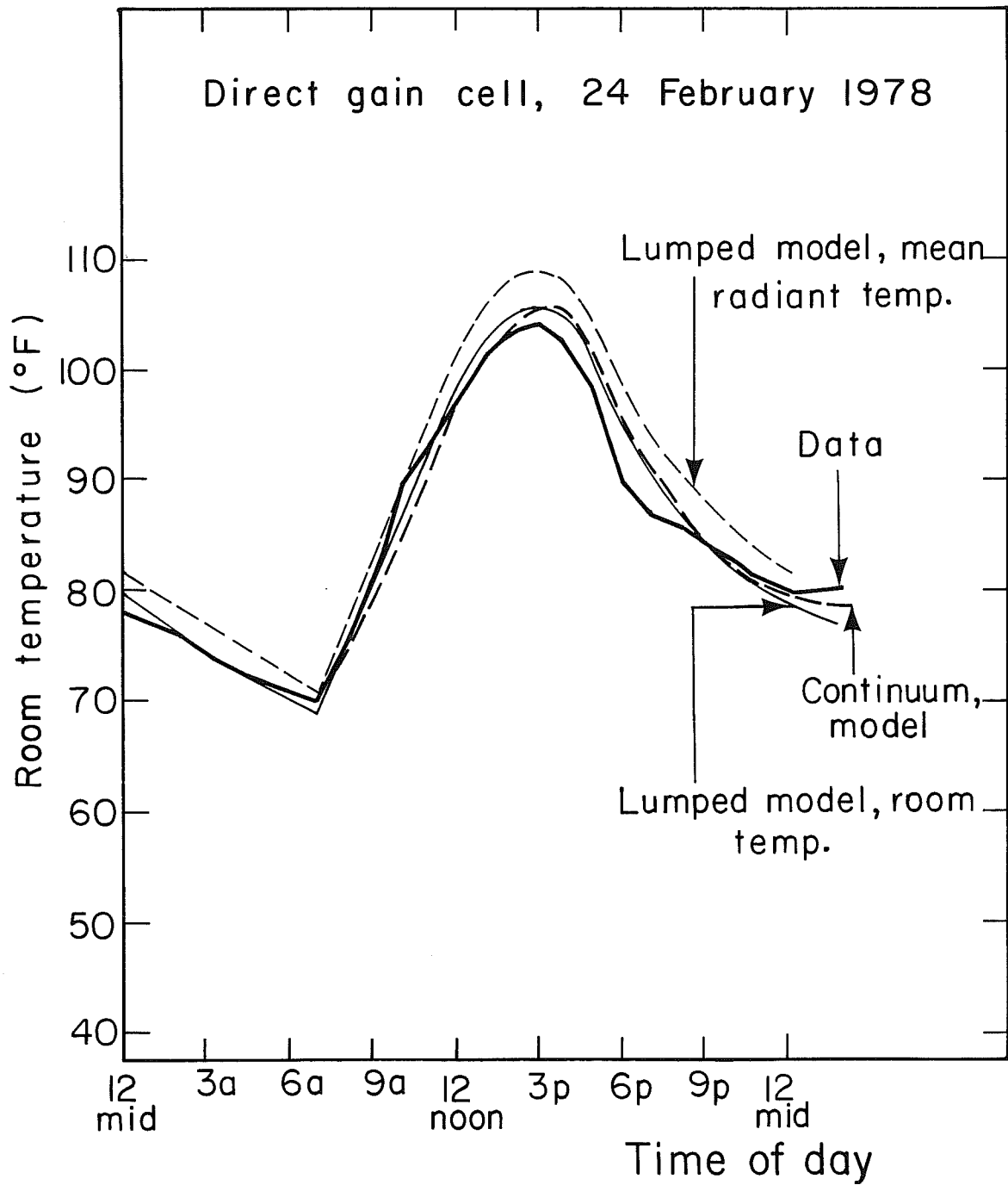
XBL788-1467

Fig. 3. Los Alamos weather as a function of date. This figure shows total solar gain (the sum of hourly solar flux for the whole day), and average ambient temperature. We model the variations in weather using a constant term plus one sinusoidally-varying term; the result is labelled "model." This idealized weather is used to predict building response for March 8.



XBL 789-1764

Fig. 4. Los Alamos solar flux as a function of time for the days preceding February 24. Note the constancy of solar patterns from day to day.



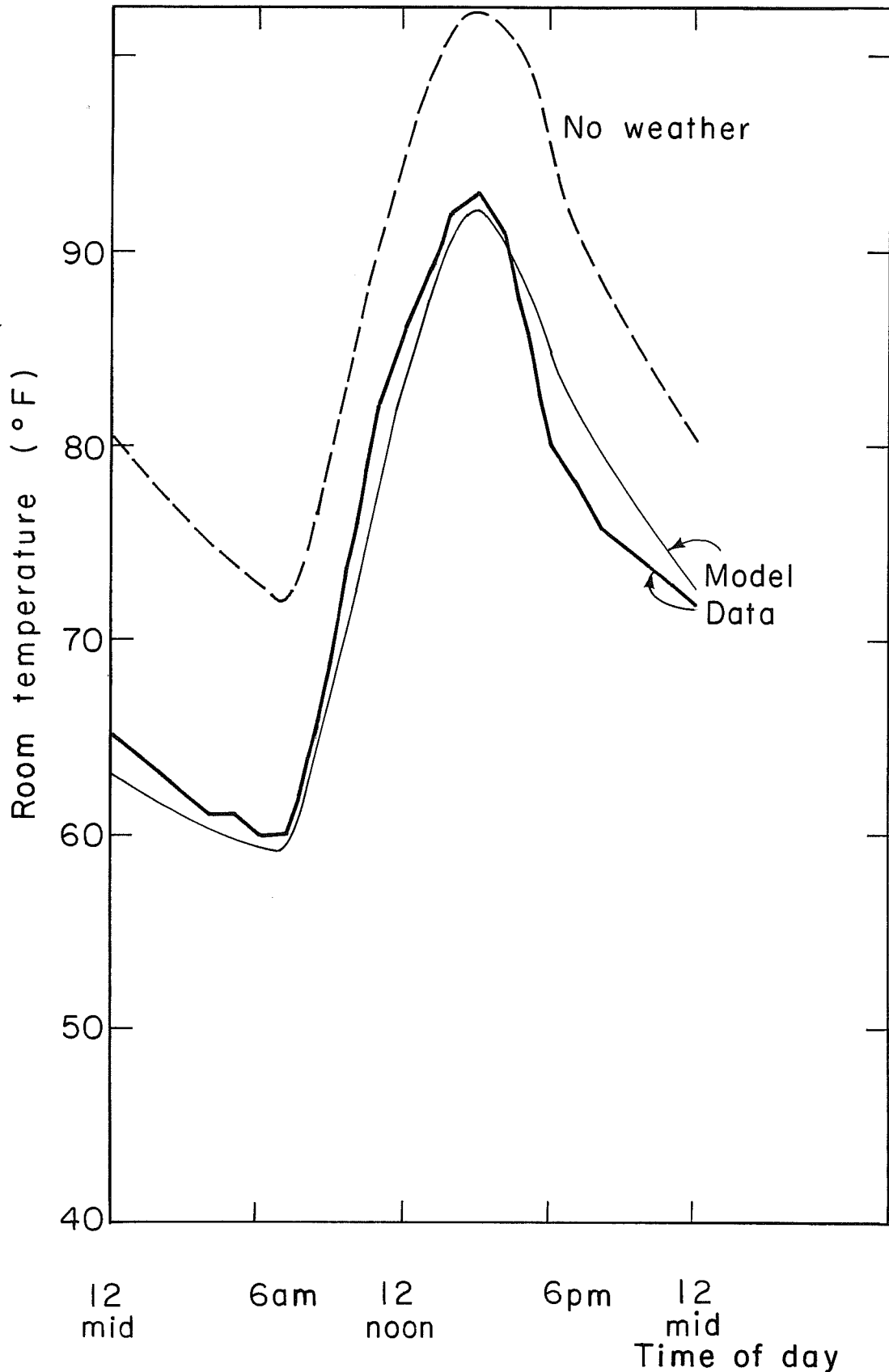
XBL 789-1470

Fig. 5. Predicted room temperature and observed data as a function of time of day for the direct gain cell for 24 February 1978.

Section 3

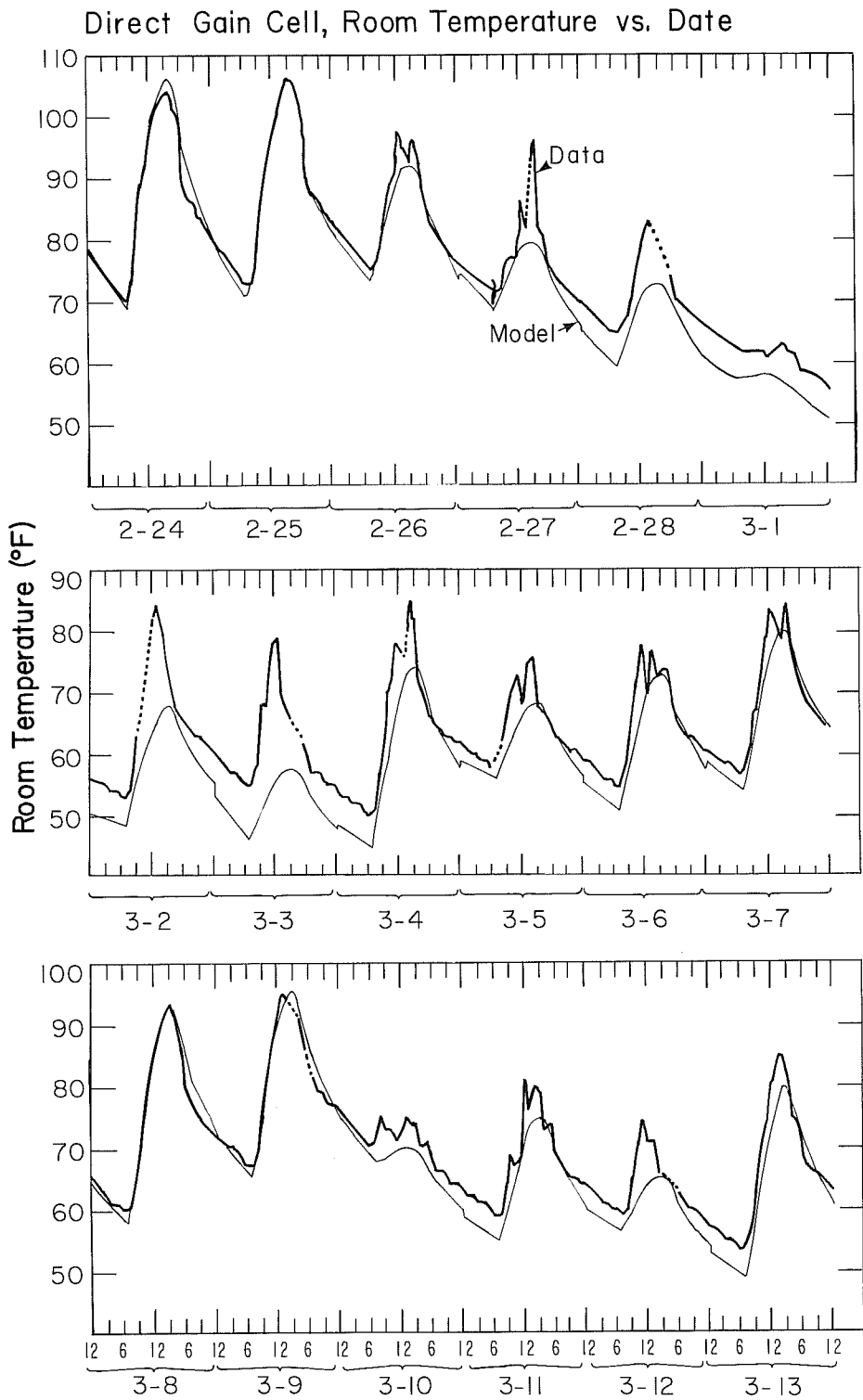
Fig. 6 Predicted room temperature and observed data for the direct gain cell as a function of time of day on March 8, 1978. The curve labelled "model" was calculated taking into account the weather variations for the previous two weeks. The curve labelled "no weather" shows the predictions of the model for the case where all days before March 8 were assumed to have the same weather.

Direct gain cell, 8 March 1978



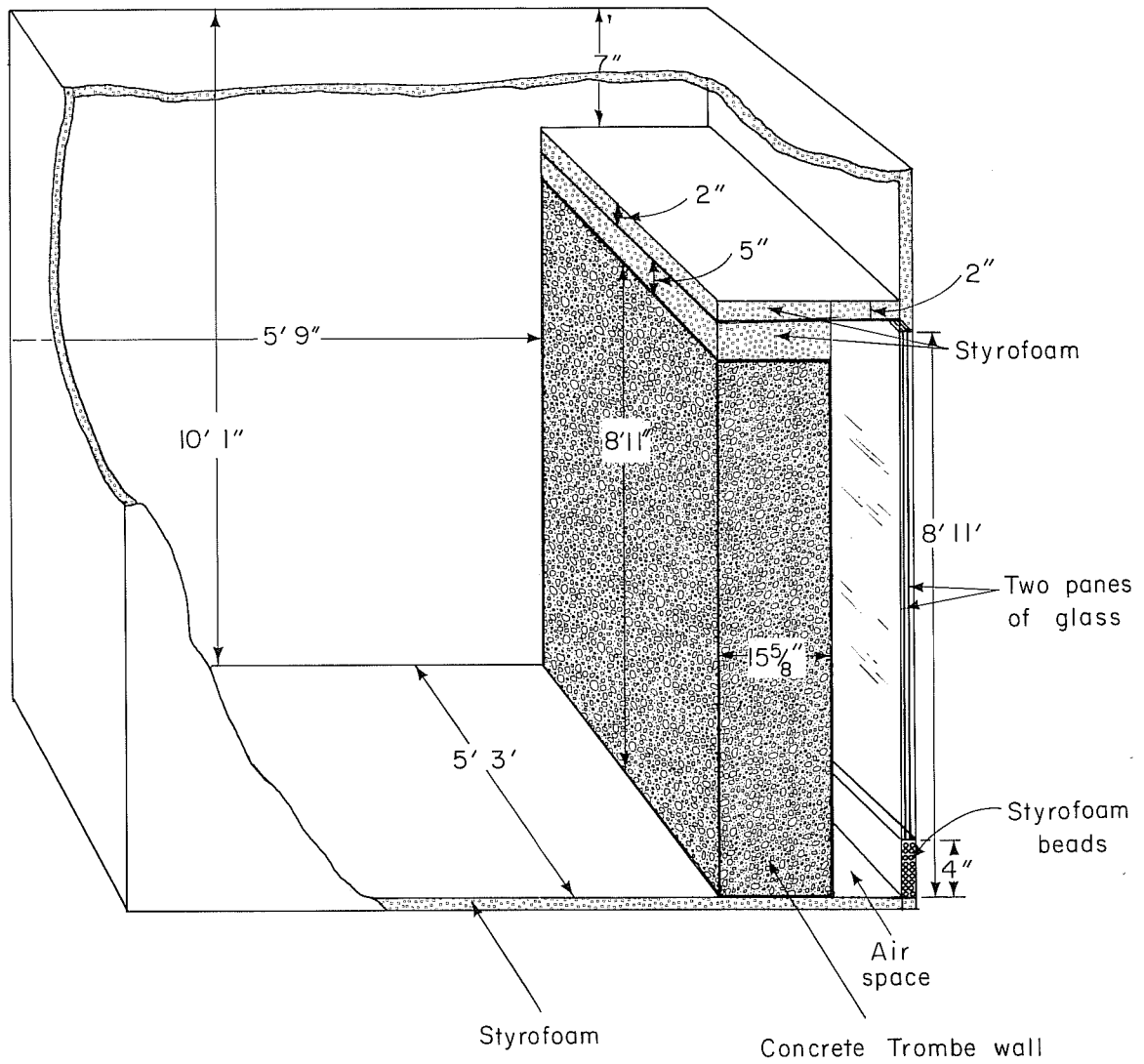
XBL788-1466

Fig. 6.



XBL 789-1766

Fig. 7. Comparison between room temperature observations and predictions of the lumped parameter model for the direct gain cell. Dotted portions of the "data" curve indicate where data is missing. Model input data, such as solar flux, is also missing at these times; interpolations were used for the calculations.



XBL 789-11086

Fig. 8. The Los Alamos Trombe wall cell. Dimensions are based on measurements by the author.

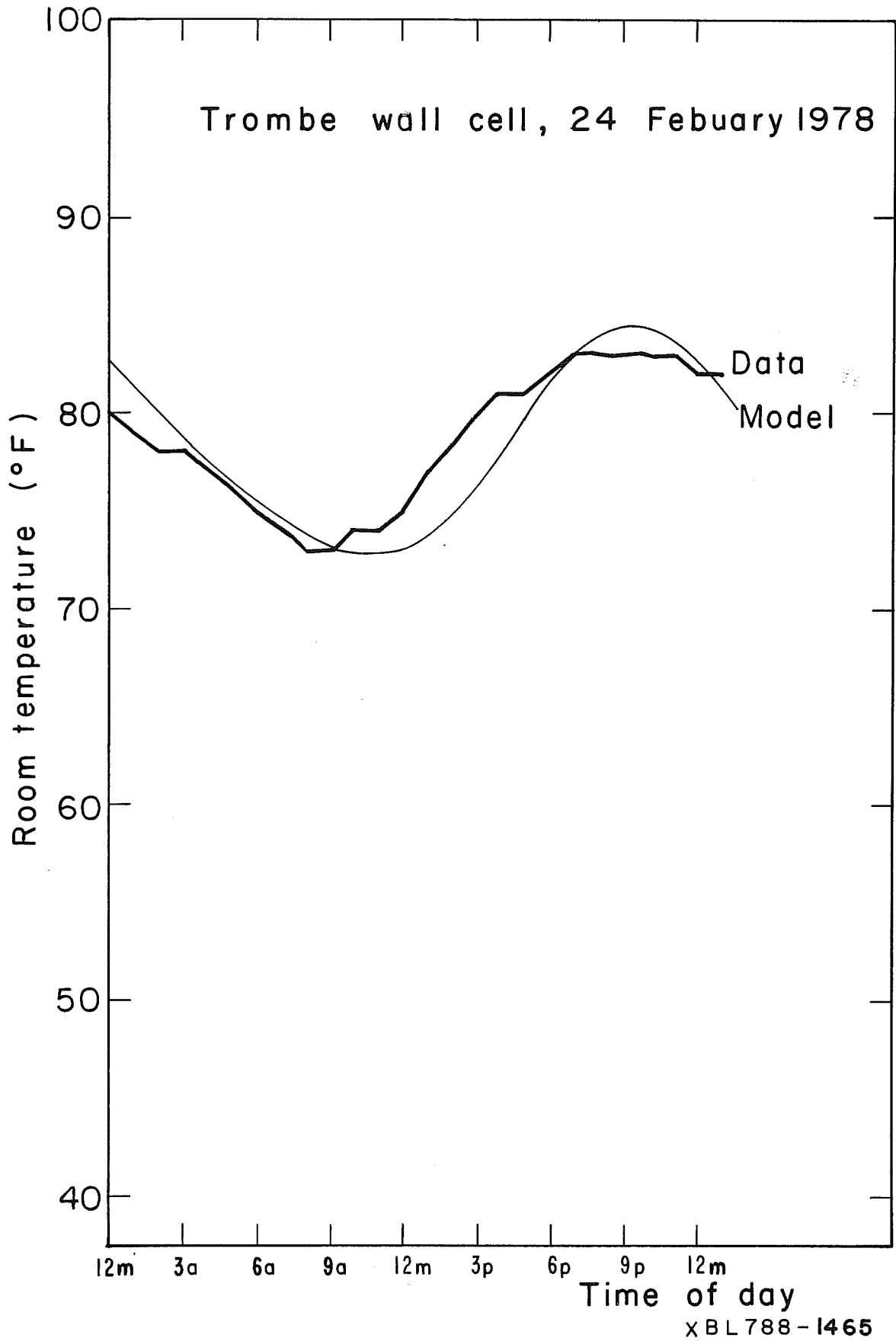
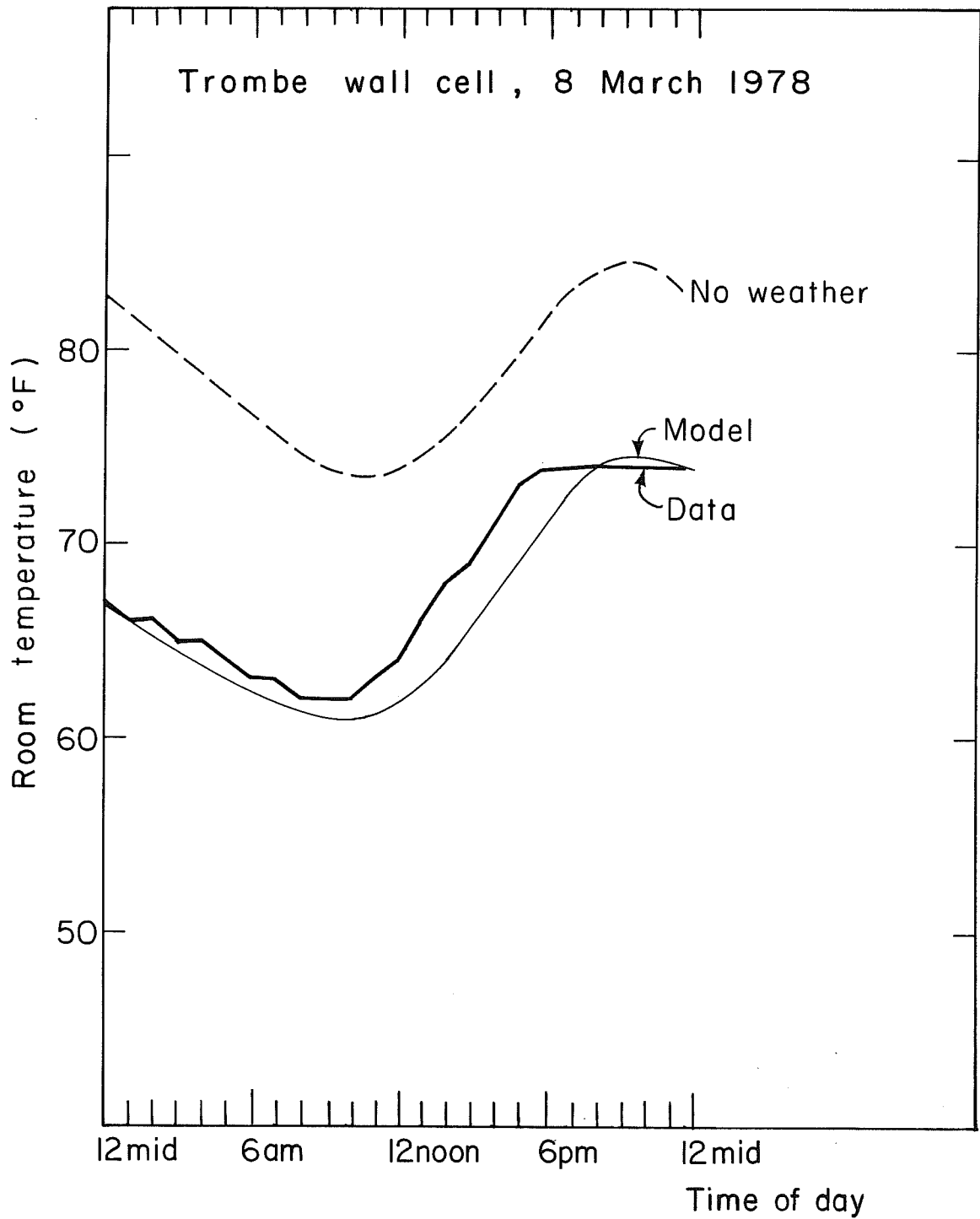
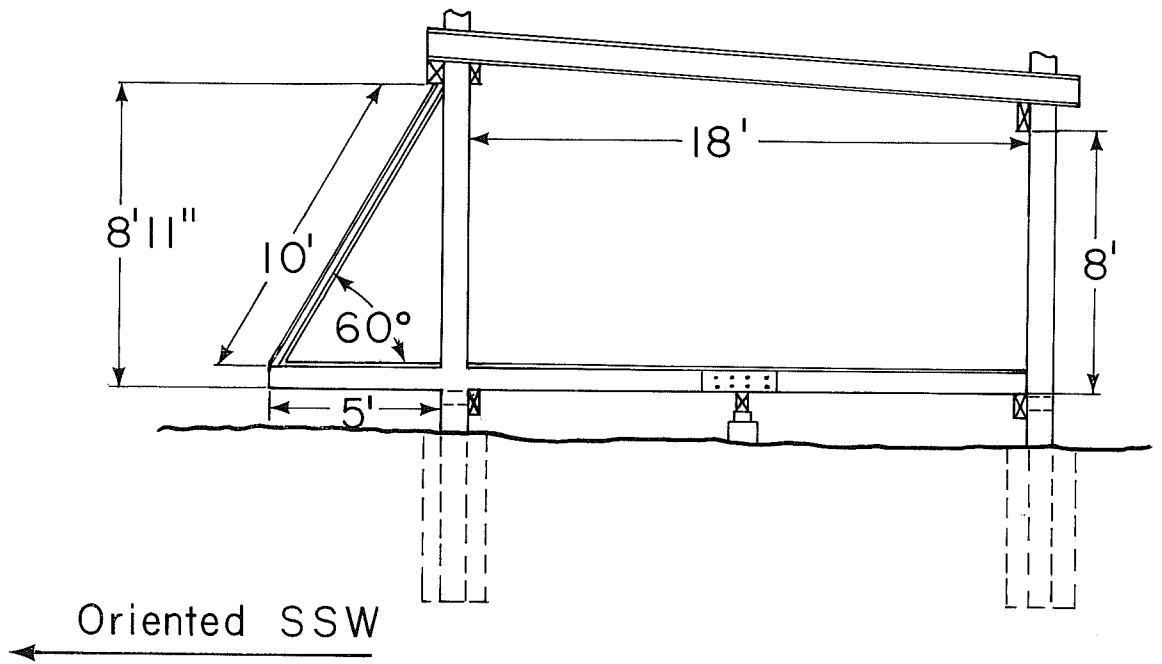


Fig. 9. Predicted room temperature and observed data as a function of time of day for the LASL Trombe wall cell, 24 February 1978.



XBL788-1469

Fig. 10. Predicted room temperature and observed data as a function of time of day for the LASL Trombe wall cell, 8 March 1978. The curve labelled "no weather" was calculated by assuming that all days before March 8 had the same weather; the curve labelled "model" accounts for weather using the idealization illustrated in Fig. 3.



EAST SIDE SECTION  
SONOMA HOUSE

XBL 786 - 1108

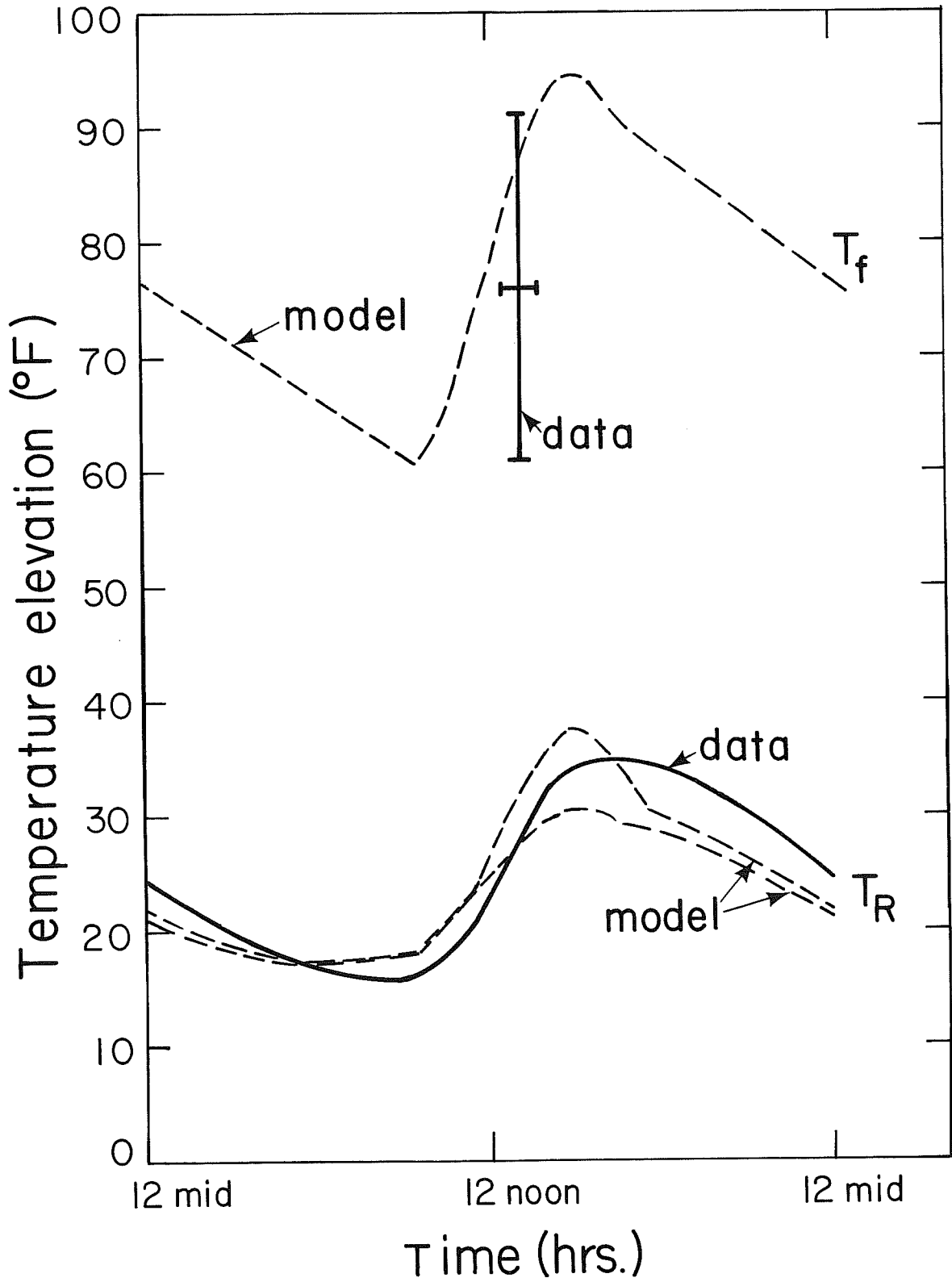
Fig. 11. Section view of the Sonoma house. The 60° surface at left is the collector window; the heat storage assembly is directly behind (to the right of) the window.

Section 3

Fig. 12. Comparison of temperature data and model calculations for the Sonoma house described in Section 3.5. The lower curves ( $T_R$ ) graph temperature elevation ((room temperature)-(average ambient temperature)) as a function of time. The solid curve is the data for the day of 13 December 1975; the two dotted curves describe model simulations. The flatter dotted curve is calculated assuming that the solar gains through the small west-facing windows are unimportant, while the more peaked dotted curve includes a term approximating the effects of solar transmission through the west window.

The upper curve plots collector ("floor") temperature elevation ( $T_f$ ) and compares to one data point measured on a similar day in February. The vertical error bars refer to the range in temperatures from the bottom to the top of the collector. The average temperature, " $T_f$ ", is probably closer to the top of the range (~80 - 85°F of elevation with respect to ambient average of 48°F).

### Sonoma house comparison



XBL 786-1112

Fig. 12.

#### 4. OVERALL SUMMARY

Passive solar design is one of several promising conservation strategies which can, taken as a whole, reduce space heating needs to insignificance. Current efforts at solar building construction are impeded by a lack of theoretical understanding of the performance of passive solar buildings, and the concomitant inability to predict the results of various designs.

Existing public-domain building models do not yet handle solar gains correctly — they fail to consider where sunlight is absorbed within the building — and so are inaccurate for passive solar modeling. Even when they are revised to treat solar buildings precisely, they will still provide no insight into the thermally important features of the building. To address these problems, we derive an analytic model of passive solar building performance.

Of central importance in describing the heat transfers in passive solar buildings is the distribution of solar energy gains within the building. Our building models are therefore based on surface heat balance equations for the surfaces on which the sunshine is absorbed. In the distributed parameter model, we use the diffusion equation and the surface heat balance to derive response functions for surface temperatures as a response to sunlight and ambient temperature. These surface response functions are combined to form building response functions, which give the room temperature response to these weather variables or to heater output.

Using the building response functions, and simple sinusoidal representations of the input functions for a typical design day:

$$\text{solar gain } S(t) = \begin{cases} S_1 e^{i\omega_1 t} & \text{day} \\ 0 & \text{night} \end{cases}$$

$$\text{ambient temperature } T_A(t) = \bar{T}_A + \Delta T_A e^{i\omega_0 t}$$

$$\text{heater output} = H_O, \quad \text{a constant}$$

we can compute an analytic expression for room temperature as a function of time. We can generalize the results somewhat by allowing the solar amplitude  $S$ , and the ambient temperature  $T_A$  to vary slowly over time, simulating the response of the building to weather variations.

We also develop a lumped parameter model, in which the response of an element of the building is simulated by assigning it a lumped thermal mass at a single temperature coupled to the inside and outside air. This model is less intuitively transparent than the distributed parameter model, but it can be applied to some problems where the distributed model is unusable.

Both lumped and distributed models have been applied to predict the performance of three one-room buildings. The predictions track the observed temperature to better than 10% accuracy at all hours of the day. More precise comparisons are not possible because of uncertainties in some of the input data (e.g. U-values and transmissivities of the windows). This accuracy is comparable to that achieved by computerized building models as applied to non-solar buildings.

We expect that this model can be used as a design tool for passive solar architects, and also as a guide for adding passive solar modifications to existing building simulation programs. We will address the question of application of our model to the needs of building designers in a future paper.

Analytic models are more limited in scope of application than computer models. They can easily be used to predict floating (that is, non-thermostated) behavior of internal temperatures, and to predict response to design conditions of weather, but they cannot easily model thermostat behavior in response to historic weather. These are tasks best left to computer models. But insights gained from the analytic models can be used to improve the accuracy of computer models in their treatment of passive solar buildings. We will use the results of the analytic models in a later paper to modify the program TWOZONE so that it simulates solar absorption in a manner parallel to that used in the analytic models.

REFERENCES

1. "Efficient Use of Energy: A Physics Perspective". American Physical Society, 1974.
2. S. Berman and S. Silverstein, "Energy Conservation and Window Systems", American Physical Society, 1973.
- 3a. J. Douglas Balcomb, "Simulation Analysis of Passive Solar Heated Buildings - Preliminary Results" Los Alamos Scientific Laboratory LA-UR-76-89, 1976.
- 3b. "Passive Solar Heating and Cooling, Conference and Workshop Proceedings", May 18-19, 1977; Albuquerque, New Mexico.
- 3c. J. D. Balcomb, James C. Hedstrom, Robert D. McFarland, "Passive Solar Heating of Buildings", Los Alamos Scientific Laboratory LA-UR-77-1162, 1977.
4. City of Davis, Calif., Building Code; Ordinance #784 (1975) and Resolution #1833 Series 1975.
5. John I. Yellott, "Early Tests of the 'Skytherm' System", in Ref. 3b.
6. W. A. Shurcliff, Solar Heated Buildings, A Brief Survey, 12th Edition (Shurcliff, Cambridge, Mass., 1976).
7. R. P. Stromberg and S. O. Woodall, "Passive Solar Buildings: A Compilation of Data and Results", Sandia Laboratories, SAND77-1204, Albuquerque, New Mexico.
8. Leonard W. Wall, T. Dey, A. J. Gadgil, A. B. Lilly, A. Rosenfeld, "Conservation Options in Residential Energy Use: Studies Using the Computer Program TWOZONE", Lawrence Berkeley Laboratory LBL-5271, 1977.

9. Robert C. Sonderegger, "Dynamic Models of House Heating Based on Equivalent Thermal Parameters", Princeton University Center for Environmental Studies, 1977.
10. Philip W.B. Niles, "Modeling the Atascadero House" in Ref. 3b.
11. T. Kusuda, "NBSLD, Computer Program for Heating and Cooling Loads in Buildings", Center for Building Technology, National Bureau of Standards, NBS Building Science Series 69, 1976.
12. R. H. Henninger, "NECAP-NASA's Energy-Cost Analysis Program", U.S. Department of Commerce, National Technical Information Service N76-10751, 1975.
13. California Administrative Code Title 20 Chapter 1.
14. Robert H. Socolow and Robert C. Sonderegger, "The Twin Rivers Program on Energy Conservation in Housing: Four Year Summary Report. Princeton University, Center for Environmental Studies, Report #32 August 1976.
15. American Society of Heating, Refrigeration, and Air Conditioning Engineers, "Ashrae Handbook".
16. A. M. Neville, Properties of Concrete, (New York: John Wiley & Sons.)
17. C. W. Rose, Agricultural Physics, (Oxford, Pergamon Press, 1966), Ch. 2.1.
18. M. Lokmanhekim, F. C. Winkelmann, A. H. Rosenfeld, Z. Cumali, G. Leighton, "Cal-ERDA, A New State of the Art Computer Program for the Energy Utilization of Buildings", Presented at the Third International Symposium on the Use of Computers for Environmental Engineering Related to Buildings, Banff, Alberta, Canada, May 1978.

19. R. E. Goodson, "Distributed System Simulation Using Infinite Product Expansions", in Simulation, Dec. 1970, pps. 255-263.
20. F. Trombe et al., "Some Performance Characteristics of the CNRS Solar House Collectors" in Ref. 3b.
21. A.H.C. Van Paassen and A. G. de Jong, "The Synthetical Reference Outdoor Climate", Delft University of Technology, The Netherlands WTHD-106 May 1978.
22. P. P. Craig, D. B. Goldstein, R. W. Kukulka, A. H. Rosenfeld, "Energy Extension in California, Context and Potential Impact." Lawrence Berkeley Laboratory UCID-3911, in LBL-5236, 1977.
23. S. M. Berman, C. J. Blumstein, D. B. Goldstein, et al. "Electrical Energy Consumption in California: Data Collection and Analysis", Lawrence Berkeley Laboratory, UCID-3847, 1976.
24. A. H. Rosenfeld, D. B. Goldstein, A. J. Lichtenberg, P. P. Craig, "Saving Half of California's Energy and Peak Power Through Long-Range Standards and Other Legislation". To be published by the California Policy Seminar, Institute of Governmental Studies, University of California, 1978.
25. Frank Sinden, "A Two-Thirds Reduction in Energy Consumption of a Princeton Townhouse." PU-CES 56, 1977. Center for Environmental Studies, Princeton University.
26. "Study of Energy-Saving Options for Refrigerators and Water Heaters. Volume 1: Refrigerators" Arthur D. Little, Inc., Cambridge, Mass., 1977.
27. "Building Construction Cost Data, 1971(77)" R. S. Means, Inc. Doxbury, Mass., 02332.

28. G. P. Mitalas and D. G. Stephenson, "Fortran IV Programs to Calculate Radiant Energy Interchange Factors." Computer Program No. 25 of the Division of Building Research, National Research Council of Canada, Ottawa, Canada, 1966.
29. D. G. Stephenson and G. P. Mitalas, "Calculation of Heat Conduction Transfer Functions for Multi-Layer Slabs." Ashrae Transactions 77 Part II, pp. 117-126, 1971.
30. J. H. Perry, Chemical Engineers Handbook, 5th Edition, 1973.
31. M. S. Ghausi and J. J. Kelly, Introduction to Distributed Parameter Networks (San Francisco: Holt, Rinehart, and Winston, 1968).
32. S. M. Berman, D. B. Goldstein, R. W. Richardson, "Lumped Parameters in Analytic Building Models", Lawrence Berkeley Laboratory, in process.
33. N. O. Milbank and J. Harrington-Lynn, "Thermal Response and the Admittance Procedure," British Building Research Establishment, Current Paper CP-61/74 (1974).

### APPENDIX 2.3 The Lumped Parameter Model

In this section we derive the solution of the lumped parameter model. This model describes a heavy material as a sandwich of two thermal resistances  $1/\hat{U}_i$  and  $1/\hat{U}_o$  surrounding a heat capacity C. It is relatively simple to solve the equations for 1 or 2 heavy materials, but the solution for 3 or more materials becomes clumsy, as it involves inverting several  $3 \times 3$  matrices.

Below we solve the model for a direct gain house with two heavy materials, called "floor" and "walls", for free-floating temperature. Next, we discuss modifications needed to model a Trombe wall system. We then discuss the solution of the model for a house with fixed thermostat and continuous heater output.

We assume that we have already evaluated the lumped parameters for the floor and walls in accordance with the formulae derived in Appendix 2.5A.

#### Free Floating House

The solution begins with the two surface heat balance equations

$$\alpha_f S + \hat{h}_f (T_R - T_{fs}) + \hat{U}_{fi} (T_f - T_{fs}) = 0 \quad (\text{A2.3-1a})$$

for the floor surface, and

$$\alpha_w S + \hat{h}_w (T_R - T_{ws}) + \hat{U}_{wi} (T_w - T_{ws}) = 0 \quad (\text{A2.3-1b})$$

for the wall surface, where the symbols are those used in Sec. 2.3

We solve these equations for the surface temperatures  $T_{fs}$ , and  $T_{ws}$ :

$$T_{fs} = \frac{1}{\hat{U}_{fi} + \hat{h}_f} (\alpha_f S + \hat{h}_f T_R + \hat{U}_{fi} T_f) \quad (\text{A2.3-2a})$$

$$T_{ws} = \frac{1}{\hat{U}_{wi} + \hat{h}_w} (\alpha_w S + \hat{h}_w T_R + \hat{U}_{wi} T_w) \quad (\text{A2.3-2b})$$

and use the results in the room heat balance, Eq. (2.2)

$$\hat{U}_q (T_R - T_A) + \hat{h}_f (T_R - T_{fs}) + \hat{h}_w (T_R - T_{ws}) = H + \alpha_R S$$

to derive the result

$$T_R N_R = T_w N_w + T_f N_f + \frac{H}{\hat{U}_q} + S N_s + T_A \quad (\text{A2.3-3})$$

where

$$N_w = \frac{1}{\hat{U}_q} \frac{\hat{h}_w \hat{U}_{wi}}{\hat{h}_w + \hat{U}_{wi}}$$

$$N_f = \frac{1}{\hat{U}_q} \frac{\hat{h}_f \hat{U}_{fi}}{\hat{h}_f + \hat{U}_{fi}}$$

$$N_R = 1 + N_w + N_f$$

$$N_s = \frac{N_w \alpha_w}{\hat{U}_{wi}} + \frac{N_f \alpha_f}{\hat{U}_{fi}} + \frac{\alpha_R}{\hat{U}_q}$$

All the N's except  $N_s$  are dimensionless;  $N_s$  has dimensions of  $\frac{1}{\hat{U}}$  or  $\frac{1}{UA}$ . Note that  $N_w$  is the ratio of the conductance from wall-to-room to the quick heat loss coefficient and  $N_f$  is the same ratio for the floor.  $N_s$  involves terms with the ratios of material-to-room conductances to material-to-surface conductances; these terms are large for good insulators or high film coefficients (e.g. forced convection) and small for good conductors or low film coefficients (e.g. glazed walls).

Thus we can express room temperature in terms of the materials temperatures  $T_w$  and  $T_f$  and the driving forces  $T_A$ , S and H, as

$$T_R = \frac{N_w}{N_R} T_w + \frac{N_f}{N_R} T_f + \frac{1}{N_R \hat{U}_q} H + \frac{N_s}{N_R} S + \frac{1}{N_R} T_A \quad (\text{A2.3-4})$$

The S term says that for good conductors or low film coefficients, the direct response of room temperature to sunlight will be small; the response will be primarily through solar heating of walls and floor. Equation (A2.3-4) is repeated as (10) in the text of Sec. 2.3.

The dynamic response of the building is given by two differential equations, which are Eq. (7) applied to the two materials, wall and floor:

$$C_w \dot{T}_w + \hat{U}_{wi}(T_w - T_{ws}) + \hat{U}_{wo}(T_w - T_A) = 0 \quad (\text{A2.3-5a})$$

$$C_f \dot{T}_f + \hat{U}_{fi}(T_f - T_{fs}) + \hat{U}_{fo}(T_f - T_A) = 0 \quad (\text{A2.3-5b})$$

We use (A2.3-2a and b) to eliminate the surface temperatures from these equations. This brings in terms containing  $T_R$ , which is eliminated by (A2.3-4). The resulting differential equations are:

$$\begin{aligned} \dot{T}_w + \left[ \lambda_w \left( 1 - \frac{N_w}{N_R} \right) + \frac{\hat{U}_{w0}}{C_w} \right] T_w - \frac{\lambda_w N_f}{N_R} T_f & \quad (A2.3-6a) \\ = \frac{\lambda_w}{N_R \hat{U}_q} H + \left[ \frac{\lambda_w}{N_R} + \frac{U_{w0}}{C_w} \right] T_A + \lambda_w \left[ \frac{\alpha_w}{\hat{h}_w} + \frac{N_S}{N_R} \right] S \end{aligned}$$

$$\begin{aligned} \dot{T}_f + \left[ \lambda_f \left( 1 - \frac{N_f}{N_R} \right) + \frac{\hat{U}_{f0}}{C_f} \right] T_f - \frac{\lambda_f N_w}{N_R} T_w & \quad (A2.3-6b) \\ = \frac{\lambda_f}{N_R \hat{U}_q} H + \left[ \frac{\lambda_f}{N_R} + \frac{\hat{U}_{f0}}{C_f} \right] T_A + \lambda_f \left[ \frac{\alpha_f}{\hat{h}_f} + \frac{N_S}{N_R} \right] S \end{aligned}$$

where

$$\lambda_w = \frac{\hat{U}_q}{C_w} N_w$$

$$\lambda_f = \frac{\hat{U}_q}{C_f} N_f$$

To simplify the algebra, we rewrite these as

$$\dot{T}_w + \Lambda_P T_w - \Lambda_F T_f = a_1 H + a_2 S + a_3 T_A \quad (A2.3-7a)$$

$$\dot{T}_f + \Lambda_G T_f - \Lambda_Q T_w = a_4 H + a_5 S + a_6 T_A \quad (A2.3-7b)$$

where the  $\Lambda$ 's and  $a$ 's are defined by (A2.3-6 and 7) and have no special significance except to simplify the algebraic expressions. Their definitions are repeated in Table 2.1.

These are two linear first-order coupled differential equations. Their solution is simple, but some of the algebra becomes complicated. We first obtain the homogeneous solution, then a particular solution for

some assumed forms of solar gain  $S(t)$  and ambient temperature  $T_A(t)$ . For the free-floating house, we let the heater output be a constant  $H_0$  which may be zero.

### Homogeneous Solution

We differentiate the left-hand side of (A2.3-7a) and then use (A2.3-7b) to eliminate  $T_f$ . This yields an expression relating  $\ddot{T}_w$ ,  $\dot{T}_w$ ,  $T_w$ , and  $T_f$ . We then use (A2.3-7a) again to eliminate  $T_f$  in favor of  $T_w$  and  $\dot{T}_w$ ; the resulting equation is

$$\ddot{T}_w + (\Lambda_P + \Lambda_G) \dot{T}_w + \Lambda_X T_w = 0 \quad (\text{A2.3-8})$$

where  $\Lambda_X = \Lambda_P \Lambda_G - \Lambda_F \Lambda_Q$

The solution is:

$$T_w = B_1 e^{-\Lambda_1 t} + B_2 e^{-\Lambda_2 t} \quad (\text{A2.3-9a})$$

where  $\Lambda_1 = \frac{1}{2}(\Lambda_P + \Lambda_G) \mp \frac{1}{2} \sqrt{(\Lambda_P + \Lambda_G)^2 - 4\Lambda_X}$

Using this result in (A2.3-7a) we find that

$$T_f = B_1 K_1 e^{-\Lambda_1 t} + B_2 K_2 e^{-\Lambda_2 t} \quad (\text{A2.3-9b})$$

where  $K_1 = \frac{-\Lambda_1 + \Lambda_P}{\Lambda_F}$

These two equations are the homogeneous solution.  $B_1$  and  $B_2$  are arbitrary constants, which will be determined by the boundary conditions.  $\Lambda_1$  and  $\Lambda_2$  are the two relaxation constants of the house; we choose  $\Lambda_1$  to

be the slower decay ( $\Lambda_1 < \Lambda_2$ ). For a typical passive solar house  $\Lambda_1 \sim \frac{1}{2 \text{ days}}$  while  $\Lambda_2 \sim \frac{1}{5 \text{ hours}}$ .

### Inhomogeneous Solution

The inhomogeneous solution depends on the driving forces. We illustrate its solution with simplified driving forces which are sinusoidal in form. We approximate ambient temperature  $T_A$  by a single term  $T_A = \Delta T_A e^{i\omega_0 t}$  where  $\Delta T_A$  is complex. We have set average ambient air temperature equal to zero (that is, we measure all temperatures with respect to the average ambient temperature) and  $\omega_0 = 2\pi/\text{day}$ . Solar gain is approximated by a sine wave of frequency  $\omega_1$ . This sine wave repeats every 24 hours, and is set equal to zero at night.

Thus we take

$$S(t) = \begin{cases} S_1 e^{i\omega_1 t} & \text{day} \\ 0 & \text{night} \end{cases}$$

We take sunrise to be  $t = 0$ , and sunset at  $t = t_d$ . Heater output is taken as a constant,  $H_0$ . We further assume that the house parameters may change at night, producing two inhomogeneous solutions, one for day and one for night.

### Ambient Temperature Response

The form of the solution for ambient temperature response is  $T_w = \chi_{A_w} \Delta T_A e^{i\omega_0 t}$  and  $T_f = \chi_{A_f} \Delta T_A e^{i\omega_0 t}$  where  $\chi_{A_w}$  and  $\chi_{A_f}$  have the values  $\chi_{A_{wd}}$  and  $\chi_{A_{fd}}$  for daytime parameters and  $\chi_{A_{wn}}$  and  $\chi_{A_{fn}}$  for the night. Substituting these expressions into (A2.3-7) we

$$(i\omega_0 + \Lambda_P) \chi_{A_w} \Delta T_A - \Lambda_F \chi_{A_f} \Delta T_A = a_3 \Delta T_A$$

$$(i\omega_0 + \Lambda_G) \chi_{A_f} \Delta T_A - \Lambda_Q \chi_{A_w} \Delta T_A = a_6 \Delta T_A$$

Solving these we find that

$$\chi_{A_w} = \frac{a_3(\Lambda_G + i\omega_0) + a_6 \Lambda_F}{(\Lambda_G + i\omega_0)(\Lambda_P + i\omega_0) - \Lambda_F \Lambda_Q} \quad (A2.3-10)$$

$$\chi_{A_f} = \frac{a_6(\Lambda_P + i\omega_0) + a_3 \Lambda_Q}{(\Lambda_G + i\omega_0)(\Lambda_P + i\omega_0) - \Lambda_F \Lambda_Q}$$

### Solar gain

The solution for solar gain is analogous to that for ambient temperature; we set  $T_w = \chi_{S_w} S_1 e^{i\omega_1 t}$  and  $T_f = \chi_{S_f} S_1 e^{i\omega_1 t}$  and use (A2.3-7) to show that

$$\chi_{S_w} = \frac{a_2(\Lambda_G + i\omega_1) + a_5 \Lambda_F}{(\Lambda_G + i\omega_1)(\Lambda_P + i\omega_1) - \Lambda_F \Lambda_Q} \quad (A2.3-11)$$

$$\chi_{S_f} = \frac{a_5(\Lambda_P + i\omega_1) + a_2 \Lambda_Q}{(\Lambda_G + i\omega_1)(\Lambda_P + i\omega_1) - \Lambda_F \Lambda_Q}$$

### Heater output

The response to a constant heater output  $H_0$  is a constant temperature increase  $T_{H_w}$  for the walls and  $T_{H_f}$  for the floor. Using (A2.3-7), we get

$$\Lambda_P T_{H_w} - \Lambda_F T_{H_f} = a_1 H_0$$

$$\Lambda_G T_{H_f} - \Lambda_Q T_{H_w} = a_4 H_0$$

so that

$$T_{H_w} = \frac{a_1 \Lambda_G + a_4 \Lambda_F}{\Lambda_x} H_0 \quad T_{H_f} = \frac{a_4 \Lambda_P + a_1 \Lambda_Q}{\Lambda_x} H_0 \quad (A2.3-12)$$

### Complete Solution

The complete solution for a given problem is the sum of the homogeneous and inhomogeneous solutions. For a house whose temperature floats freely (e.g. no thermostatically controlled heater), and with the driving forces given above, we solve the equations (A2.3-7) separately for the day and night conditions. The solutions are joined smoothly using the assumption that the floor and wall temperatures do not change discontinuously. Note that this form of solution is for static weather: the same temperature and cloudiness conditions every day.

The boundary conditions are thus

$$T_w(t = 0^+) = T_w(t = 24 \text{ hrs}^-) \quad (\text{A2.3-13})$$

$$T_w(t = t_d^-) = T_w(t = t_d^+)$$

$$T_f(t = 0^+) = T_f(t = 24 \text{ hrs}^-)$$

$$T_f(t = t_d^-) = T_f(t = t_d^+)$$

These four equations determine the four unknowns  $B_{1d}$   $B_{1n}$   $B_{2d}$  and  $B_{2n}$ . (Recall that the 'd' and 'n' subscripts refer to day and night solutions). These expressions are:

$$\begin{aligned}
 & B_{1d} + B_{2d} + (\chi_{A_{wd}} - \chi_{A_{wn}}) \Delta T_A + \chi_{S_w} S_1 + (T_{H_{wd}} - T_{H_{wn}}) \\
 & = B_{1n} e^{-\Lambda_{1n} t_n} + B_{2n} e^{-\Lambda_{2n} t_n}
 \end{aligned} \tag{A2.3-14a}$$

$$\begin{aligned}
 & B_{1d} e^{-\Lambda_{1d} t_d} + B_{2d} e^{-\Lambda_{2d} t_d} + (\chi_{A_{wd}} - \chi_{A_{wn}}) \Delta T_A e^{i\omega_0 t_d} \\
 & + \chi_{S_w} S_1 e^{i\omega_1 t_d} + (T_{H_{wd}} - T_{H_{wn}}) = B_{1n} + B_{2n}
 \end{aligned} \tag{A2.3-14b}$$

$$\begin{aligned}
 & B_{1d} K_{1d} + B_{2d} K_{2d} + (\chi_{A_{fd}} - \chi_{A_{fn}}) \Delta T_A + \chi_{S_f} S_1 + (T_{H_{fd}} - T_{H_{fn}}) \\
 & = B_{1n} K_{1n} e^{-\Lambda_{1n} t_n} + B_{2n} K_{2n} e^{-\Lambda_{2n} t_n}
 \end{aligned} \tag{A2.3-14c}$$

$$\begin{aligned}
 & B_{1d} K_{1d} e^{-\Lambda_{1d} t_d} + B_{2d} K_{2d} e^{-\Lambda_{2d} t_d} + (\chi_{A_{fd}} - \chi_{A_{fn}}) \Delta T_A e^{i\omega_0 t_d} \\
 & + \chi_{S_f} S_1 e^{i\omega_1 t_d} + (T_{H_{fd}} - T_{H_{fn}}) = B_{1n} K_{1n} + B_{2n} K_{2n}
 \end{aligned} \tag{A2.3-14d}$$

where  $t_d + t_n = 24$  hours

These four equations can be solved by first using (b) to find  $B_{1n}$  and then using the result in (a). This produces an equation for  $B_{2n}$  which can also be used in the  $B_{1n}$  equation to express  $B_{1n}$  and  $B_{2n}$  in terms of  $B_{1d}$  and  $B_{2d}$ . The results are

$$B_{1n} = Y_1 B_{1d} + Y_2 B_{2d} + Y_3$$

$$B_{2n} = Y_4 B_{1d} + Y_5 B_{2d} + Y_6$$

where the Y's are given explicitly in Table 2.1 .

Using these expressions above in (A2.3-14b) produces an equation of the form  $B_{1d} Q_6 + B_{2d} Q_5 + Q_4 = 0$ .

with the Q's given in Table 2.1.

Analogously using the  $B_{1n}$  and  $B_{2n}$  expressions on (A2.3-14d) we get

$$B_{1d} Q_2 + B_{2d} Q_3 - Q_1 = 0$$

Thus

$$B_{1d} = \frac{Q_3 Q_4 + Q_1 Q_5}{Q_2 Q_5 - Q_3 Q_6} \tag{A2.3-15}$$

$$B_{2d} = \frac{Q_1 - Q_2 B_{1d}}{Q_3}$$

$$B_{1n} = Y_1 B_{1d} + Y_2 B_{2d} + Y_3$$

$$B_{2n} = Y_4 B_{1d} + Y_5 B_{2d} + Y_6$$

where the Q's and Y's are summarized in Table 2.1 . This determines the B's ; the complete solution for this problem can be written as

$$T_w = \begin{cases} B_{1d} e^{-\Lambda_{1d} t} + B_{2d} e^{-\Lambda_{2d} t} + \chi_{A_{wd}} \Delta T_A e^{i\omega_0 t} + \chi_{S_w} S_1 e^{i\omega_1 t} + T_{H_{wd}} & \text{(day)} \\ B_{1n} e^{-\Lambda_{1n}(t-t_d)} + B_{2n} e^{-\Lambda_{2n}(t-t_d)} + \chi_{A_{wn}} \Delta T_A e^{i\omega_0 t} + T_{H_{wn}} & \text{(night)} \end{cases}$$

$$T_f = \begin{cases} B_{1d} K_{1d} e^{-\Lambda_{1d} t} + B_{2d} K_{2d} e^{-\Lambda_{2d} t} + \chi_{A_{fd}} \Delta T_A e^{i\omega_0 t} + \chi_{S_f} S_1 e^{i\omega_1 t} + T_{H_{fd}} & \text{(day)} \\ B_{1n} K_{1n} e^{-\Lambda_{1n}(t-t_d)} + B_{2n} K_{2n} e^{-\Lambda_{2n}(t-t_d)} + \chi_{A_{fn}} \Delta T_A e^{i\omega_0 t} + T_{H_{fn}} & \text{(night)} \end{cases}$$

$$T_R(t) = \frac{N_w}{N_R} T_w(t) + \frac{N_f}{N_R} T_f(t) + \frac{1}{N_R} (\Delta T_A e^{i\omega_0 t}) + \frac{N_s}{N_R} S(t) + \frac{1}{N_R} \hat{U}_q H_o \quad (\text{A2.3-16})$$

Note that the solution for  $T_R$  can change discontinuously, since it includes terms proportional to  $S$  and  $H_o$ , both of which can change discontinuously.

### Discussion

The solution derived in this section applies to either a managed or an unmanaged passive solar house subjected to constant weather conditions day after day. Several variations are possible. For example, if one wanted to find the response of the house to a day of clouds following a succession of sunny days, one could solve for  $B_1$  and  $B_2$  as an initial value problem using the new lower value for  $S_1$ . That is, one would set  $T_w(0) = T_w(24 \text{ hrs}^-)$  and  $T_f(0) = T_f(24 \text{ hrs}^-)$ , where '0' refers to the beginning of the cloudy day, and derive new values of  $B_1$  and  $B_2$  based on the new value of  $S_1$ . One would then find  $B_{1n}$  and  $B_{2n}$  for the "cloudy-day" night by solving the equations

for night conditions and setting the initial values of  $T_w$  and  $T_f$  equal to their new calculated values at  $t = t_d$ . This process is illustrated in Sec. 3.3.5.

Further changes would include turning on the heater at some time before sunrise to simulate morning warm-up of the building (but this would involve matching boundary conditions at 3 times and finding 3 sets of B's), or adding the effects of a non-south facing window (discussed in Sec. 3.5).

One should note that the coefficients  $\chi$  are actually linear response functions giving the response of wall or floor temperatures to solar or other excitations at a given frequency. They are similar to the response functions derived in Sec. 2.4 for the continuum model except that they describe the response of bulk material temperature rather than surface temperature.

The  $\chi$  coefficients are shown here for walls and floor only; one can also derive response functions for room temperature as influenced by ambient temperature or sunlight using (A2.3-16). These response functions  $\chi_{AR}$  and  $\chi_{SR}$  can also be derived from the continuum model Eq. (A2.4-22), using lumped-parameter response functions in place of the distributed-parameter functions implied in that section. Lumped response functions are discussed in Appendix 2.5A.

Trombe Wall/Waterwall

The Trombe wall or waterwall solar collector can be modelled using lumped parameters in a way analogous to the direct gain system solution just derived. Some of the variables ( $\Lambda_p, \Lambda_G$ , etc.) change definitions in order to accommodate the Trombe wall solution.

A Trombe wall collector consists of a massive wall located directly behind the solar collector window. Sun streaming in the window strikes the Trombe wall surface and is either absorbed or reflected; - the absorbed heat can either conduct into the wall material or conduct into the air in front of the wall. This air in the channel between the wall and the window is coupled to the room by natural convection. Often this coupling can be altered by movable louvers at the top or bottom of the channel. The heat flows in the Trombe wall are illustrated in Fig. 2.7.

We model the surface heat balance slightly differently for the Trombe wall than for other cases; the surface is now coupled to the air in the channel rather than the room air. We assume this coupling is linear. Thus the surface heat balance becomes

$$\hat{h}_{wc}(T_{ws} - T_c) - \alpha_w S + \hat{U}_{wi}(T_{ws} - T_w) = 0 \quad (A2.3-17)$$

where  $\hat{h}_{wc}$  is the heat transfer coefficient from the wall surface to the channel air (Btu/hr-deg-F or W/°C),

$T_c$  is the channel air temperature,

$\hat{U}_{wi}$  is the lumped conductance into the Trombe wall, (Btu/hr-deg-F or W/°C),

$T_w$  is the lumped wall temperature.

This equation replaces (A2.3-1b); it says that the losses from the surface to the channel air plus the losses from sunlight (the minus sign indicates that these are really heat gains) plus the losses from the surface to the wall interior add to zero. Note that  $\alpha_w \cong 1.0$  since almost all the sunlight passing through the window is absorbed on the wall.

We assume a constant channel temperature and constant wall temperature as a function of height; actually there will be a distribution of temperature. The channel air can then exchange heat with the outdoor air by conduction through the window or with room air through natural convection. Natural convection is a very complicated process; for this model we use a linear approximation and say that heat transfer from the channel air to the room is given by  $\hat{U}_{CR}(T_c - T_R)$ .

The heat balance for the channel air can then be expressed as

$$\hat{h}_{wc}(T_c - T_{ws}) + \hat{U}_{CA}(T_c - T_A) + \hat{U}_{CR}(T_c - T_R) = 0 \quad (\text{A2.3-18})$$

where  $\hat{U}_{CA}$  is the heat transfer coefficient through the collector glazing (Btu/deg F-hr).

This simply says that the sum of the heat losses from the channel air is zero.

The room heat balance is altered in the Trombe model in two ways: the heat loss from the room to the wall surface occurs indirectly through the term  $\hat{U}_{CR}(T_R - T_c)$  rather than directly through

the term  $\hat{h}_w (T_R - T_{ws})$  and the heat flow through the back of the wall affects the room and not the outside air. Thus the room heat balance is

$$\hat{U}_q (T_R - T_A) + \hat{h}_f (T_R - T_{fs}) + \hat{U}_{CR} (T_R - T_C) + \hat{U}_{wo} (T_R - T_w) = H + \alpha_R S \quad (A2.3-19)$$

where  $\hat{U}_{wo}$  is the lumped conductance out the back of the wall from the wall interior to the room (Btu/deg F-hr or W/°C).

We remind the reader that the heat leaving the back of the wall goes to the room and not to the outside. It should be noted that the back surface temperature of the Trombe wall is not equal to room temperature; the back surface is coupled to the room using  $\hat{U}_{WR}$ . Thus in evaluating the lumped parameters for the wall, one should model a wall insulated on the outside with a resistance of  $(\hat{U}_{WR})^{-1}$ . Typically  $\hat{U}_{WR} = \text{area of wall} \times 1.5 \text{ Btu/deg F-ft}^2\text{-hr}$ . The value of the wall's lumped parameter  $\hat{U}_{wo}$  includes the effects of  $\hat{U}_{WR}$  as well as the effects of the wall materials.

The second material surface to be modelled with lumped parameters (as opposed to being incorporated into  $\hat{U}_q$  and  $\alpha_R$ ) can be either the floor or the non-Trombe walls; we will consider the floor to be the second surface for notational convenience. The floor heat balance is still given by (A2.3-1a).

To solve the model, we use (A2.3-18) to express  $T_C$  in terms of the other temperatures:

$$T_C = \frac{\hat{h}_{wc} T_{ws} + \hat{U}_{CA} T_A + \hat{U}_{CR} T_R}{\hat{\Sigma}} \quad (A2.3-20)$$

where

$$\hat{\Sigma} = \hat{h}_{wc} + \hat{U}_{CA} + \hat{U}_{CR}$$

We can use this to get an expression for wall surface temperature:

$$T_{ws} = \frac{1}{(\hat{U}_{wi} + \hat{U}_a)} \left( \alpha_w S + \hat{U}_{wi} T_w + \frac{\hat{h}_{wc} \hat{U}_{cA}}{\hat{\Sigma}} T_A + \frac{\hat{h}_{wc} \hat{U}_{cR}}{\hat{\Sigma}} T_R \right)$$

where

$$\hat{U}_a = \frac{\hat{h}_{wc} (\hat{U}_{cA} + \hat{U}_{cR})}{\hat{\Sigma}} \quad (A2.3-21)$$

We use these expressions along with (A2.3-2a) for floor surface temperature to derive a new room heat balance analogous to (A2.3-3); the expression has almost the same form as (A2.3-3) but the N's are different:

$$T_R N_R = T_w N_w + T_f N_f + \frac{H}{\hat{U}_q} + S N_S + T_A N_A$$

where

$$N_w = \frac{\hat{h}_{wc} \hat{U}_{cR} \hat{U}_{wi}}{\hat{U}_q \hat{\Sigma} (\hat{U}_{wi} + \hat{U}_a)} + \frac{\hat{U}_{wo}}{\hat{U}_q} \quad (A2.3-22)$$

$$N_f = \frac{1}{\hat{U}_q} \frac{\hat{h}_f \hat{U}_{fi}}{\hat{h}_f + \hat{U}_{fi}}$$

$$N_R = \left( 1 + N_f + \frac{\hat{U}_{wo}}{\hat{U}_q} + \frac{\hat{U}_{cR}}{\hat{\Sigma} \hat{U}_q} \left( \hat{h}_{wc} + \hat{U}_{cA} - \frac{\hat{h}_{wc}^2 \hat{U}_{cR}}{\hat{\Sigma} (\hat{U}_{wi} + \hat{U}_a)} \right) \right)$$

$$N_S = \left( \frac{\alpha_w \hat{h}_{wc} \hat{U}_{cR}}{\hat{U}_q (\hat{U}_{wi} + \hat{U}_a) \hat{\Sigma}} + \frac{\alpha_f N_f}{\hat{U}_{fi}} + \frac{\alpha_R}{\hat{U}_q} \right)$$

$$N_A = \left( 1 + \frac{\hat{U}_{cA} \hat{U}_{cR}}{\hat{U}_q \hat{\Sigma}} + \frac{\hat{h}_{wc}^2 \hat{U}_{cA} \hat{U}_{cR}}{\hat{\Sigma}^2 (\hat{U}_{wi} + \hat{U}_a)} \right)$$

To derive the equations of motion, we keep (A2.3-5b) intact and change (A2.3-5a) to

$$C_w \dot{T}_w + \hat{U}_{wi} (T_w - T_{ws}) + \hat{U}_{wo} (T_w - T_R) = 0$$

We use (A2.3-21 and 22b) to eliminate  $T_{ws}$  and  $T_R$ ; the resulting differential equations are:

$$\dot{T}_w + \left[ \frac{1}{C_w} \left( \left( \frac{\hat{U}_{wi} \hat{U}_a}{\hat{U}_{wi} + \hat{U}_a} \right) \hat{U}_{wo} \right) - \lambda_R \frac{N_w}{N_R} \right] T_w - \lambda_R \frac{N_f}{N_R} T_f \quad (A2.3-23a)$$

$$= \left( \frac{\alpha_w \hat{U}_{wi}}{C_w \hat{U}_{wi} + \hat{U}_a} + \lambda_R \frac{N_s}{N_R} \right) S + \left( \frac{\hat{h}_{wc} \hat{U}_{ca}}{C_w \hat{\Sigma}(\hat{U}_{wi} + \hat{U}_a)} + \lambda_R \frac{N_A}{N_R} \right) T_A + \frac{\lambda_R}{N_R} \frac{H}{\hat{U}_q}$$

$$\dot{T}_f + \left[ \lambda_f \left( 1 - \frac{N_f}{N_R} \right) + \frac{\hat{U}_{fo}}{C_f} \right] T_f - \frac{\lambda_f N_w}{N_R} T_w = \frac{\lambda_f}{N_R} \frac{H}{\hat{U}_q} + \left( \frac{\lambda_f N_A}{N_R} + \frac{\hat{U}_{fo}}{C_f} \right) T_A + \lambda_f \left( \frac{\alpha_f}{\hat{h}_f} + \frac{N_s}{N_R} \right)$$

where 
$$\lambda_R = \frac{1}{C_w} \left( \hat{U}_{wo} + \frac{\hat{h}_{wc} \hat{U}_{cr} \hat{U}_{wi}}{\hat{\Sigma}(\hat{U}_{wi} + \hat{U}_q)} \right) \quad (A2.3-23b)$$

and 
$$\lambda_f = \frac{1}{C_w} \frac{\hat{U}_{fi} \hat{h}_f}{\hat{U}_{fi} + \hat{h}_f}$$

Note that these can be expressed in the same form as (A2.3-7ab) with suitable redefinitions of the  $\Lambda$ 's and  $a$ 's; these redefinitions are summarized in Table 2.1a.

The rest of the solution proceeds exactly as before; the parameters defined above have new values but the functional relationships are the same.

To check this, consider a limiting case. Assume a perfectly insulated collector ( $\hat{U}_{cA} \rightarrow 0$ ) and look at (A2.3- 23a). In this limit,

$$\hat{U}_a \rightarrow \frac{\hat{h}_{wc} \hat{U}_{cR}}{\hat{h}_{wc} + \hat{U}_{cR}}, \quad \lambda_R \rightarrow \frac{\hat{U}_{wo}}{C_w} + \lambda_w, \quad \text{and the equation simplifies to:}$$

$$\begin{aligned} \dot{T}_w + \left[ \left( \lambda_w + \frac{\hat{U}_{wo}}{C_w} \right) \left( 1 - \frac{N_w}{N_R} \right) \right] T_w - \frac{N_f}{N_R} \left( \lambda_w + \frac{\hat{U}_{wo}}{C_w} \right) T_f \\ = \left( \lambda_w + \frac{\hat{U}_{wo}}{C_w} \right) \frac{1}{N_R \hat{U}_q} H + \left( \frac{\alpha_w \lambda_w}{\hat{h}_w} + \left( \lambda_w + \frac{\hat{U}_{wo}}{C_w} \right) \frac{N_s}{N_R} \right) S + \left( \lambda_w + \frac{\hat{U}_{wo}}{C_w} \right) \frac{1}{N_R} T_A \end{aligned} \quad (A2.3-24)$$

Next consider solving the same problem with the earlier set of equations.

We use (A2.3-5a) with (A2.3-2b) for  $T_{ws}$  and use  $\hat{U}_{wo}(T_w - T_R)$  in place of  $\hat{U}_{wo}(T_w - T_A)$ . This produces the identical differential equation; in addition, the expressions for  $N_R$ ,  $N_w$ , etc. agree.

This shows that much of the algebraic complication in the Trombe wall solution comes from the use of channel temperature  $T_c$  instead of pure series or parallel heat transfer paths in the direct gain model.

Thus the Trombe wall solution proceeds similarly to the direct gain building solution with the insertion of the definitions in Table 2.1a for those in Table 2.1 .

The lumped parameters for the Trombe wall are evaluated as in the case of an envelope wall with insulation outside, with  $\hat{U}_a$  substituted for  $\hat{h}_w$  ; and  $\hat{U}_{wr}$ , the coupling between rear Trombe-wall surface and the room, substituted for  $\hat{U}_r$ , the conductance of the insulation. As shown in Appendix 2.5A, the error in using lumped parameters to describe

a Trombe wall is larger than in the case of an envelope wall, particularly for weak convective coupling between the air channel and the room ( $\hat{U}_{cR}$  small). For relatively thick walls (Eq. 1-2 feet of concrete) and very weak convective coupling ( $\hat{U}_{cR} \ll \hat{U}_{wo}$ ), the lumped parameter approximation is unusable. However, for waterwalls, the lumped parameter approach should be an excellent approximation.

Continuously heated house

In this part we discuss the solution to the lumped parameter model for a house kept at a fixed thermostat setting in which the heater output varies with time. This solution applies only in a very cold climate, when the heater is needed 24 hours a day. As we will show, "very cold" will turn out to be unreasonable for a typical passive solar design, rendering this solution of little practical interest.

We use the notation for the direct gain system described at the beginning of this appendix. The equations of motion are the room heat balance (A2.3-3)

$$N_R T_R = N_W T_W + N_f T_f + \frac{1}{\hat{U}_q} H = N_S S + T_R \quad (\text{A2.3-25})$$

and the differential equations (A2.3-5a and b)

$$C_W \dot{T}_W + \hat{U}_{wi} (T_W - T_{ws}) + \hat{U}_{wo} (T_W - T_A) = 0 \quad (\text{A2.3-26a})$$

$$C_f \dot{T}_f + \hat{U}_{fi} (T_f - T_{fs}) + \hat{U}_{fo} (T_f - T_A) = 0 \quad (\text{A2.3-26b})$$

In this case  $T_R$  is fixed at the thermostat level  $T_t$ , so we solve these differential equations differently than before. Rather

than using (A2.3-25) to eliminate  $T_R$  in the differential equations, we set  $T_R = T_t$  and use only the surface temperature equations (A2.3-2) to produce:

$$\dot{T}_w + \left( \lambda_w + \frac{\hat{U}_{wo}}{C_w} \right) T_w - \lambda_w T_t = \frac{\lambda_w \alpha_w}{\hat{h}_w} S + \frac{\hat{U}_{wo}}{C_w} T_A \quad (\text{A2.3-27a})$$

$$\dot{T}_f + \left( \lambda_f + \frac{\hat{U}_{fo}}{C_f} \right) T_f - \lambda_f T_t = \frac{\lambda_f \alpha_f}{\hat{h}_f} S + \frac{\hat{U}_{fo}}{C_f} T_A \quad (\text{A2.3-27b})$$

We next solve (A2.3-25) for H and then use the differential equations for  $T_w$  and  $T_f$  to derive a single differential equation for H:

$$H = \hat{U}_q N_R T_t - \hat{U}_q N_w T_w - \hat{U}_q N_f T_f - \hat{U}_q N_s S - U_q T_A \quad (\text{A2.3-28})$$

Differentiate this equation and multiply by  $(\lambda_w + \frac{\hat{U}_{wo}}{C_w})$ ; adding the result to the equation itself, we see that

$$\begin{aligned} \dot{H} + \left( \lambda_w + \frac{\hat{U}_{wo}}{C_w} \right) H = & \hat{U}_q T_t \left( \left( \lambda_w + \frac{\hat{U}_{wo}}{C_w} \right) N_R - \lambda_w N_w \right) - \hat{U}_q \left( N_s \dot{S} + \left[ \frac{N_w \lambda_w \alpha_w}{\hat{h}_w} + \left( \lambda_w + \frac{\hat{U}_{wo}}{C_w} \right) \right] \right) \\ & - \hat{U}_q \left( \dot{T}_A + \left( \lambda_w + \frac{\hat{U}_{wo}}{C_w} \right) (1 + N_w) \right) T_A - \hat{U}_q N_f \left( \dot{T}_f + \left( \lambda_w + \frac{\hat{U}_{wo}}{C_w} \right) T_f \right) \end{aligned} \quad (\text{A2.3-29})$$

We use (A2.3-27b) to replace  $\dot{T}_f$  in the last term above, and then differentiate the result:

$$\ddot{H} + \Lambda_w \dot{H} = -\hat{U}_q \left( N_s \ddot{S} + \left( \frac{N_w \lambda_w \alpha_w}{\hat{h}_w} + \frac{N_f \alpha_f \lambda_f}{\hat{h}_f} + N_s \Lambda_w \right) \dot{S} \right) - \hat{U}_q \left( \ddot{T}_A + \left( \Lambda_w + \frac{N_w \hat{U}_{wo}}{C_w} + \frac{N_f \hat{U}_{fo}}{C_f} \right) \dot{T}_A \right) - \hat{U}_q N_f (\Lambda_w - \Lambda_f) \dot{T}_f \quad (A2.3-30)$$

where

$$\Lambda_w = \lambda_w + \frac{\hat{U}_{wo}}{C_w}$$

$$\Lambda_f = \lambda_f + \frac{\hat{U}_{fo}}{C_f}$$

We then add  $\Lambda_f$  times (A2.3-30) to itself to get the equation of motion

for H:

$$\ddot{H} + (\Lambda_w + \Lambda_f) \dot{H} + \Lambda_w \Lambda_f H = -\hat{U}_q \left( N_s \ddot{S} + \left[ (\Lambda_w + \Lambda_f) N_s + \frac{N_w \lambda_w \alpha_w}{\hat{h}_w} + \frac{N_f \lambda_f \alpha_f}{\hat{h}_f} \right] \dot{S} + \left[ N_s \Lambda_f \Lambda_w + \frac{N_w \lambda_w \Lambda_f \alpha_w}{\hat{h}_w} + \frac{N_f \Lambda_w \lambda_f \alpha_f}{\hat{h}_f} \right] S \right) - \hat{U}_q \left( \ddot{T}_A + \left( (\Lambda_w + \Lambda_f) + \frac{N_w \hat{U}_{wo}}{C_w} + \frac{N_f \hat{U}_{fo}}{C_f} \right) \dot{T}_A + \left( \Lambda_f \Lambda_w + \frac{N_w \hat{U}_{wo} \Lambda_f}{C_w} + \frac{N_f \hat{U}_{fo} \Lambda_w}{C_f} \right) T_A \right) + \hat{U}_q \left( \Lambda_w \Lambda_f N_R - \lambda_w \Lambda_f N_w - \lambda_f \Lambda_w N_f \right) T_t \quad (A2.3-31)$$

The homogeneous solution of this equation is

$$A_1 e^{-\Lambda_w t} + A_2 e^{-\Lambda_f t}$$

Note that the decay constants are substantially different from the free-floating temperature time constants. In general, they are faster decays for example, for house #1 described later in this appendix, the free-floating temperature decay times are 1/(41 hrs) and 1/(2.35 hrs) whereas the heater decay constants are 1/(10 hrs) and 1/(8 hrs). However, the heater decay constants are still inversely proportional to the heat capacities.

The inhomogeneous solution can be expressed as  $H_o + H_A e^{i\omega_o t} + H_s e^{i\omega_1 t}$  for ambient temperature given by  $T_A = \Delta T_A e^{i\omega_o t}$  and solar

$$\text{gain by } S(t) = \begin{cases} S_1 e^{i\omega_1 t} & \text{day} \\ 0 & \text{night} \end{cases}$$

However, this solution is only meaningful if it is positive definite.

This is because a negative solution for  $H(t)$  means that artificial cooling is being provided to maintain a constant temperature, and rational operation of a passive solar building would require allowing the temperature  $T_R$  to rise instead. So the solution derived here is useful only if  $H_o > \text{Re} (H_s e^{i\omega_1 t})$  for all times.

We calculate  $H_o$ ,  $H_A$ , and  $H_s$  from (A2.3-31), the result is

$$H_o = \hat{U}_q \left( 1 + \frac{N_f \hat{U}_{fo}}{\Lambda_f C_f} + \frac{N_w \hat{U}_{wo}}{\Lambda_w C_w} \right) (T_t - T_A) \quad (\text{A2.3-32})$$

This is a reasonable result, since  $\frac{N_f \hat{U}_{fo}}{\Lambda_f C_f} = \frac{C_f}{\hat{U}_q} \frac{\lambda_f \hat{U}_{fo}}{\lambda_f C_f + \hat{U}_{fo}}$  which for

$\lambda_f C_f \gg \hat{U}_{fo}$  is just  $\hat{U}_f / \hat{U}_q$ ; and analogously for the wall term,

so that  $H_o \cong (\hat{U} + \hat{U}_f + \hat{U}_w)(T_t - T_A)$  which is the degree-day or steady-state result.

We next compute  $H_A$  and  $H_s$ :

$$H_A = \Delta T_A \hat{U}_q \frac{\left[ \omega_o^2 - \left( \Lambda_w \Lambda_f + \frac{N_w \hat{U}_{wo} \Lambda_f}{C_w} + \frac{N_f \hat{U}_{fo} \Lambda_w}{C_f} \right) \right] - i\omega_o \left( \Lambda_w + \Lambda_f + \frac{N_w \hat{U}_{wo}}{C_w} + \frac{N_f \hat{U}_{fo}}{C_f} \right)}{(\Lambda_w \Lambda_f - \omega_o^2) + i\omega_o (\Lambda_w + \Lambda_f)} \quad (\text{A2.3-33})$$

$$H_s = S_1 \hat{U}_q \frac{\left[ N_s \omega_1^2 - \left( N_s \Lambda_w \Lambda_f + \frac{N_w \lambda_w \Lambda_f \alpha_w}{\hat{h}_w} + \frac{N_f \lambda_f \Lambda_w \alpha_f}{\hat{h}_f} \right) \right] - i\omega_1 \left( (\Lambda_w + \Lambda_f) N_s + \frac{N_w \lambda_w \alpha_w}{\hat{h}_w} + \frac{N_f \lambda_f \alpha_f}{\hat{h}_f} \right)}{(\Lambda_w \Lambda_f - \omega_1^2) + i\omega_1 (\Lambda_w + \Lambda_f)} \quad (\text{A2.3-34})$$

For house #1, we see the following departure from steady-state results:

$$\begin{aligned}
 H_o &= 0.998 (\hat{U}_q + \hat{U}_f + U_w) (T_t - T_A) \\
 H_A &= 0.946 (\hat{U}_q + \hat{U}_f + \hat{U}_w) \Delta T_A e^{-i(\omega_o(0.16 \text{ hrs}))} \\
 H_s &= 0.581 S_1 e^{-i\omega_1(0.72 \text{ hrs})}
 \end{aligned}$$

Thus the steady-state heater output agrees to within 1/4% with simple methods, while the response to ambient temperature is damped by 5% and phase-lagged by a trivial amount (10 minutes). The response to sunlight is greatly damped, but only phase-delayed by 45 minutes. The greater damping is to be expected; the sunlight falls on surfaces and some fraction of it is used to heat the materials under the surfaces; this portion is unavailable (at that time) for reducing furnace output.

However, the magnitude of these expressions shows that this constant-thermostate solution is unrealistic for a passive solar house. For the reference house described below with 250 ft<sup>2</sup> of solar collector window (1/6 of floor area) H<sub>s</sub> gets as large as 28,800 Btu/hr. Since H<sub>o</sub> ≈ 539 Btu/°F-hr (ΔT) and H<sub>1</sub>/ΔT ≈ H<sub>o</sub>/ΔT we would require an ambient temperature of 52° below thermostat for the solution to work. For a typical indoor temperature of 70°F, ambient temperatures would have to remain below 18°F. This is unlikely enough in any North American climate, but even if it occurred, the optimum passive house would likely have triple glazing rather than double and extra caulking and insulation, reducing  $\hat{U}_q$  from 450 Btu/°F-hr

to about 300, thus lowering the acceptable ambient to below  $-1^{\circ}$  F. Thus the constant thermostat solution only is useful for cloudy days or relatively small collector-window areas.

#### Reference House Description

We describe in this section a reference house which is used in the text to illustrate some points numerically. The house is a direct-gain passive-solar version of a conventional wood-frame concrete-floor California single-story house. We describe it below and evaluate its parameters for use in the lumped-parameter model.

We assume that the house is 50'  $\times$  30' with its short axis oriented north-south. It has 250 ft<sup>2</sup> of south-facing double glazing, and 125 ft<sup>2</sup> of glass facing the other three directions. The walls are constructed of 2  $\times$  6" studs on 24" centers to allow the use of R-19 insulation; the ceiling is also insulated to R-19. We assume that 20% of the wall area is studs (typical for 2  $\times$  6  $\times$  24 construction); also 10% of the ceiling area and 15% of partition wall area. There are 1920 ft<sup>2</sup> of partition walls; corresponding to 150% of the envelope wall area, as measured for one typical house by the author. The building is sealed in normally tight fashion against air infiltration (not as well as the Princeton retrofit of Ref. 25), and loses about 1/2 air change per hour.

We model the windows, air leakage, and insulation cavities as quick heat transfers, along with the doors. The wall area is 1280 ft<sup>2</sup> gross minus 375 ft<sup>2</sup> for windows minus about 40 ft<sup>2</sup> for doors, or 865 ft<sup>2</sup>. Thus  $\hat{U}_q =$

walls	80% × 865 ft <sup>2</sup> × 0.05 Btu/°F-ft <sup>2</sup> -hr	= 35 Btu/°F-hr
ceiling	90% × 1500 ft <sup>2</sup> × 0.05 Btu/°F-ft <sup>2</sup> -hr	= 67
windows	375 ft <sup>2</sup> × 0.60 Btu/°F-ft <sup>2</sup> -hr	= 225
infiltration	$\frac{1}{2}$ hr <sup>-1</sup> × 8 ft × 1500 ft <sup>2</sup> × 0.018 Btu/ft <sup>3</sup> -°F	= 108
doors	2 × 6 $\frac{2}{3}$ ft × 3 ft × 0.37 Btu/ft <sup>2</sup> -°F	= 15
TOTAL $\hat{U}_q$ =		450 Btu/°F-hr

For the lumped parameter model, we divide the heavy materials into two surfaces, floor and walls. The floor parameters' evaluation is straightforward; we set  $U_{fi} = 2.52$  Btu/°F-ft<sup>2</sup>-hr and  $\bar{C}_f = 9.64$  Btu/°F-ft<sup>2</sup> for concrete. Thus  $\hat{U}_{fi} = 3780$  Btu/°F-hr,  $C_f = 14,460$  Btu/°F.

The walls are a little more complicated, since we are combining the effects of two materials. We evaluate lumped parameters for wood (studs) and then for (non-wood-stud-backed) gypsum board, and then combine them.

Consider first the wood studs. The area in studs is  $0.20 \times 865$  ft<sup>2</sup> +  $0.15 \times 1920$  ft<sup>2</sup> +  $0.10 \times 1500$  ft<sup>2</sup> = 611 ft<sup>2</sup>. We evaluate the lumped parameters  $U_i$  and  $\bar{C}$  for 6" wood, except that we hold off in evaluating  $U_o$  until we have added the effects of the gypsum board. Note that some of the walls are partition walls.) When only part of the wall area communicates with outside, we want  $(\hat{U}_i^{-1} + \hat{U}_o^{-1})^{-1}$  to equal the steady state heat loss, and we determine  $\hat{U}_o$  accordingly. For the 6" wood,  $U_i = 0.564$  Btu/°F-ft<sup>2</sup>-hr and  $\bar{C} = 2.16$  Btu/°F-ft<sup>2</sup>. Next, the gypsum board has  $\rho c_p = 13$  Btu/°F-ft<sup>3</sup> and  $K = 0.0936$  Btu/hr-deg F-ft. If the thickness is 5/8", the lumped parameters (for partition walls) are  $U_i = 4.23$  Btu/°F-ft<sup>2</sup>-hr and  $\bar{C} = 0.646$  Btu/°F-ft<sup>2</sup>. The areas (excluding

stud areas already counted) are  $865 \text{ ft}^2 \times 0.80 + 1920 \text{ ft}^2 \times 0.85 + 1500 \text{ ft}^2 \times 0.90 = 3674 \text{ ft}^2$ .

Thus the wall lumped parameters are:

$$U_{wi} = 0.564 \text{ Btu/}^\circ\text{F-ft}^2\text{-hr} \times 611 \text{ ft}^2 + 4.23 \text{ Btu/}^\circ\text{F-ft}^2\text{-hr} \times 3674 \text{ ft}^2 \\ = 15,890 \text{ Btu/}^\circ\text{F-hr}$$

$$C_w = 2.16 \text{ Btu/}^\circ\text{F-ft}^2 \times 611 \text{ ft}^2 + 0.646 \text{ Btu/}^\circ\text{F-ft}^2 \times 3674 \text{ ft}^2 \\ = 3690 \text{ Btu/}^\circ\text{F}$$

To calculate  $\hat{U}_{wo}$ , we need the steady-state heat losses for  $173 \text{ ft}^2$  of exterior wall studs. The U-value is  $K/d = (0.068 \text{ Btu/}^\circ\text{F-ft-hr})$ ,  $0.5 \text{ ft} = 0.136 \text{ Btu/}^\circ\text{F-ft}^2\text{-hr}$ ; thus total losses are  $23.52 \text{ Btu/}^\circ\text{F-hr}$ . So we take  $\hat{U}_{wo} = 23.56 \text{ Btu/}^\circ\text{F-hr}$ .

Finally, for a typical day, we assume that sunrise and sunset are four hours before (after) solar noon, and that solar gain amplitude  $S_1$  is  $250 \text{ Btu/ft}^2\text{-deg F} \times 0.75 \text{ transmissivity} \times 250 \text{ ft}^2 = 46,875 \text{ Btu/hr}$ . Ambient temperature amplitude  $\Delta T_A$  is taken to be  $10^\circ\text{F}$  e  $i\omega_o(t-7 \text{ hrs})$  so that temperature peaks at 3 p.m. Usual assumptions for the  $\alpha$ 's are that  $\alpha_f = 0.70$ ,  $\alpha_w = 0.20$ ,  $\alpha_R = 0.10$ , although these assumptions are often varied parametrically.

APPENDIX 2.4: The Distributed Parameter Model

The distributed parameter model is an exact solution of the diffusion equations (2.3) for each of the heavy materials and the heat balance equations (2.1) and (2.2). The solution is computed in Fourier transform space; that is, we calculate response functions for room temperature (at a given frequency) as a function of the driving forces (sunlight, ambient temperature) at that frequency.

In this section, we solve the model for a case with three different material surfaces, floor ("f"), envelope walls ("e") and partition walls ("p"). We derive response functions relating material surface temperatures to sunlight, heater output, and ambient temperature. We then use these response functions to set up a simple approximate solution for room temperature as a function of time.

Note that our choice of three surfaces is arbitrary; extension to more surfaces is trivial.

We first write the equations of heat transfer for the model. For the floor, we have the diffusion equation (2.3) and the surface heat balance: (2.1):

$$\frac{K_f}{(\rho c_p)_f} \frac{\partial^2 T_f(z,t)}{\partial z^2} = \frac{\partial T_f(z,t)}{\partial t} \quad (A2.4-1)$$

$$\hat{h}_f(T_f(0,t) - T_R) - \alpha_f S - A_f K_f \left. \frac{\partial T_f(z,t)}{\partial z} \right|_{z=0} = 0 \quad (A2.4-2)$$

where  $T_f(0,t)$  is the floor surface temperature and  $-A_f K_f \left. \frac{\partial T_f}{\partial z} \right|_{z=0}$

is the surface heat flux into the floor.

Treating the partition walls and envelope walls analogously, we have

$$\frac{K_p}{(\rho C_p)_p} \frac{\partial^2 T_p(x,t)}{\partial x^2} = \frac{\partial T_p(x,t)}{\partial t} \quad (\text{A2.4-3})$$

$$\hat{h}_p(T_p(0,t) - T_R) - \alpha_p S - A_p K_p \left. \frac{\partial T_p(x,t)}{\partial x} \right|_{x=0} = 0 \quad (\text{A2.4-4})$$

$$\frac{K_e}{(\rho C_p)_e} \frac{\partial^2 T_e(y,t)}{\partial y^2} = \frac{\partial T_e(y,t)}{\partial t} \quad (\text{A2.4-5})$$

$$\hat{h}_e(T_e(0,t) - T_R) - \alpha_e S - A_e K_e \left. \frac{\partial T_e(y,t)}{\partial y} \right|_{y=0} = 0 \quad (\text{A2.4-6})$$

In addition we have the room heat balance

$$\hat{h}_e(T_R - T_e(0,t)) + \hat{h}_p(T_R - T_p(0,t)) + \hat{h}_f(T_R - T_f(0,t)) + \hat{U}_q(T_R - T_A) = H + \alpha_R S \quad (\text{A2.4-7})$$

We look for solutions to the partial differential equation (A2.4-1)

of the form (2.5).

$$T_f(z,t) = \left( T_f^{(+)} e^{k_f z} + T_f^{(-)} e^{-k_f z} \right) e^{i\omega t}$$

or 
$$T_f(z,t) = \left[ A_f \cosh k_f d_f (1-\xi) + B_f \sinh k_f d_f (1-\xi) \right] e^{i\omega t}$$

where 
$$k_f = \sqrt{\frac{i\omega(\rho C)_f}{K_f}} = \sqrt{\frac{\omega(\rho C)_f}{2K_f}} (1+i)$$

$$\xi = \frac{z}{d_f}, \quad d_f = \text{the floor thickness}$$

These forms suggest that we look at a Fourier transform solution

$$\tilde{T}_f(z,\omega) = T_f^{(+)} e^{k_f z} + T_f^{(-)} e^{-k_f z}$$

or 
$$\tilde{T}_f(z,\omega) = A_f \cosh k_f d_f (1-\xi) + B_f \sinh k_f d_f (1-\xi)$$

So we will solve the Eqs. (A2.4-(1-7)) in Fourier transform space and drop the "~" notation.

Equations (A2.4(1-7)) provide 3 differential equations and 3 inside-surface boundary conditions. We also require boundary conditions on the outside surfaces. These will vary from case to case; we pick some representative cases below and present the appropriate boundary conditions.

Knowing the boundary conditions lets us represent a temperature distribution (e.g.  $T_f(z,\omega)$ ) with one coefficient. That is, we can represent  $B_f$  or  $T_f^{(-)}$  in terms of  $A_f$  or  $T_f^{(+)}$ .

For the floor, we assume a slab of masonry on top of the ground. (If instead we wish to treat a suspended floor, the boundary conditions are the same as for an envelope wall. Envelope walls are discussed below.)

The properties of concrete are not that different from those of dry soil, so for simplicity we will approximate the floor as a semi-infinite 1-dimensional slab of concrete. This approximation should be reasonable for most frequencies since the penetration depth for a daily cycle in concrete is only 4-6", or comparable to the actual slab thickness. Perimeter insulation of the slab will minimize edge effects.

This approximation breaks down for zero frequency; at this frequency we must assume some finite depth. However, the resulting room temperature will be very insensitive to the thickness chosen.

The boundary condition for a semi-infinite floor is that  $T_f(z,t)$  remains finite for large  $z$ . This requires  $T_f^{(+)} = 0$ , so that

$$T_f(z,\omega) = T_{f\omega} e^{-k_f z} \quad (\text{A2.4-8})$$

For envelope walls, the outside boundary condition can be approximated by assuming perfect thermal contact with the ambient air. For a single-layer wall this means that  $T_e(d_e,\omega) = T_A(\omega)$  where  $d_e$  is the thickness of the envelope wall.

We next look at a slightly more complicated case: an envelope wall covered by a pure resistance of value  $R_e$ . The interface between the wall material and the insulation has a temperature  $T_{int}$ , and the heat flow through the insulation is given by

$$Q = A_e/R_e (T_{int} - T_A) \quad (\text{A2.4-9})$$

The boundary condition for envelope wall temperature is then

$$T_e(d_e,\omega) = T_{int} \quad (\text{A2.4-10})$$

where  $d_e$  is the thickness of the envelope wall. We also require conservation of energy at the wall/resistance interface, so

$$Q = -A_e K_e \left. \frac{\partial T_e(\omega, y)}{\partial y} \right|_{y=d_e} \quad (\text{A2.4-11})$$

We look for a solution of the form  $T_e = A \cosh k_e d_e (1-\xi) + B \sinh k_e d_e (1-\xi)$ . Equation (A2.4-10) requires that  $T_{int} = A$ . Equating the right-hand sides of (A2.4-9 and 11), we see that  $A = (R_e K_e k_e) B + T_A$  so that

$$T_e(\omega, y) = (R_e K_e k_e T_{e\omega} + T_A) \cosh k_e d_e (1-\xi) + T_{e\omega} \sinh k_e d_e (1-\xi) \quad (\text{A2.4-12})$$

where we have set  $T_{e\omega} \equiv B$ .

For the partition walls, the boundary condition embodies the fact that partition walls are two-sided. If they are driven by equal solar absorption on both sides, then the heat flux through the middle must be identically zero. Thus for a half-thickness  $d_p$ , we have

$$\left. \frac{\partial T_p}{\partial x} \right|_{x=d_p} = 0$$

We can then write  $T_p$  as

$$T_p = T_{p\omega} \cosh k_p d_p (1-\xi) \quad (\text{A2.4-13})$$

where  $d_p$  = the half-thickness of the wall.

This completes the discussion of boundary conditions; we use the results (A2.4-(8,12, and 13)) to derive the solution to the model. We first obtain expressions for the surface temperatures from the surface heat balance equations, then use these results in (A2.4-7).

For the floor, we use (A2.4 - (2 and 8)) to show that

$$T_{f\omega} = \frac{\hat{h}_f T_R + \alpha_f S}{\hat{h}_f + A_f K_f k_f} = \frac{h_f T_R + \bar{\alpha}_f S}{h_f + K_f k_f} \quad (\text{A2.4-14})$$

where  $\bar{\alpha}_f = \frac{\alpha_f}{A_f}$

Also (A2.4-8) says that

$$T_f(\omega, z = 0) = T_{f\omega} = (h_f T_R + \bar{\alpha}_f S) \frac{1}{h_f + K_f k_f} \quad (\text{A2.4-15})$$

For the envelope walls, (A2.4- (12 and 6)) imply that

$$T_{ew} = \frac{h_e T_R + \bar{\alpha}_e S}{D_e} + \frac{T_A}{D_e} (-h_e \cosh k_e d_e - K_e k_e \sinh k_e d_e) \quad (\text{A2.4-16})$$

where  $D_e = (h_e R_e K_e k_e + K_e k_e) \cosh k_e d_e +$   
 $(h_e + R_e K_e^2 k_e^2) \sinh k_e d_e$

and  $\bar{\alpha}_e = \frac{\alpha_e}{A_e}$

Then we can use (A2.4-12) to find  $T_e(\omega, y=0)$ ; this equation says that

$T_e(\omega, y=0) = (R_e K_e k_e T_{ew} + T_A) \cosh k_e d_e + T_{ew} \sinh k_e d_e$ . Using the previous expression for  $T_{ew}$ , we can show after some manipulation that

$$T_e(\omega, y=0) = (h_e T_R + \bar{\alpha}_e S) \frac{R_e K_e k_e \cosh k_e d_e + \sinh k_e d_e}{D_e} + T_A \frac{K_e k_e}{D_e} \quad (\text{A2.4-17})$$

For the partition walls, (A2.4-4 and 13) say that

$$T_{p\omega} = \frac{h_p T_R + \bar{\alpha}_p S}{h_p \cosh k_p d_p + K_p k_p \sinh k_p d_p} \quad (\text{A2.4-18})$$

Since by (A2.4-13),  $T_p(\omega, x=0) = T_{p\omega} \cosh k_p d_p$ ,

$$T_p(\omega, x=0) = (h_p T_R + \bar{\alpha}_p S) \frac{\cosh k_p d_p}{h_p \cosh k_p d_p + K_p k_p \sinh k_p d_p} \quad (\text{A2.4-19})$$

Before substituting the surface temperature equations (A2.4-15,17, and 19) into the room heat balance (A2.4-7), we note the similarity in form of the three equations. Each computes the response of the surface temperature of the  $i^{\text{th}}$  material to  $T_R$ ,  $S$ , and  $T_A$ ; in each there is a term of the form  $R_{1_i} (h_i T_R + \bar{\alpha}_i S)$  where  $R_{1_i}$  is a frequency-dependent linear response function. For the envelope walls, there is also a term  $R_{2_i} T_A$  where  $R_{2_i}$  is another linear response function. Examination of the equations leading to this term ( $R_{2_e} T_A$ ) shows that any material surface whose outside is coupled to the ambient air will produce a similar term.

These response functions turn up again in Appendix 2.5A on optimal evaluation of the lumped parameters. They characterize the response of the continuum materials for this model; in other words, as we shall see below, the entire effect of distributed materials on room temperature can be expressed in terms of these materials response functions.  $R_1$  has the dimensions of  $1/U$ , while  $R_2$  is dimensionless.

We thus abbreviate (A2.4-15, 17 and 19) as follows:

$$T_f(\omega, z = 0) = R_{1f}(h_f T_R + \bar{\alpha}_f S) + R_{2f} T_A \quad (\text{A2.4-20a})$$

$$T_e(\omega, y = 0) = R_{1e}(h_e T_R + \bar{\alpha}_e S) + R_{2e} T_A \quad (\text{A2.4-20b})$$

$$T_p(\omega, x = 0) = R_{1p}(h_p T_R + \bar{\alpha}_p S) + R_{2p} T_A \quad (\text{A2.4-20c})$$

where 
$$R_{1f} = \frac{1}{h_f + K_f k_f}, \quad R_{2f} = 0 \quad (\text{A2.4-21})$$

$$R_{1e} = \frac{\cosh k_e d_e + \frac{1}{R_e K_e k_e} \sinh k_e d_e}{\left(h_e + \frac{1}{R_e}\right) \cosh k_e d_e + \left(K_e k_e + \frac{h_e}{R_e K_e k_e}\right) \sinh k_e d_e} \quad (\text{A2.4-21})$$

$$R_{2e} = \frac{\frac{1}{R_e}}{\left(h_e + \frac{1}{R_e}\right) \cosh k_e d_e + \left(K_e k_e + \frac{h_e}{R_e K_e k_e}\right) \sinh k_e d_e}$$

$$R_{1p} = \frac{\cosh k_p d_p}{h_p \cosh k_p d_p + K_p k_p \sinh k_p d_p}, \quad R_{2p} = 0$$

Note that  $R_1$  and  $R_2$  for partition walls are equal to the limit of the expressions for envelope walls as  $R_e \rightarrow \infty$ , and that  $R_1$  and  $R_2$  for the floor are also equal to the limit of the envelope wall expressions for  $d \rightarrow \infty$ . We finally substitute (A2.4-20) into (A2.4-7) to obtain

$$\begin{aligned} T_R \left( \hat{U}_q + \hat{h}_e (1 - h_e R_{1e}) + \hat{h}_p (1 - h_p R_{1p}) + \hat{h}_f (1 - h_f R_{1f}) \right) \\ = S(\alpha_R + \alpha_e h_e R_{1e} + \alpha_p h_p R_{1p} + \alpha_f h_f R_{1f}) + T_A (\hat{U}_q + \hat{h}_e R_{2e}) + H \end{aligned} \quad (\text{A2.4-22})$$

We can express this as  $T_R \cdot A(\omega) = S \cdot B(\omega) + T_A \cdot C(\omega) + H$  (A2.4-22a)

where A, B, and C are frequency-dependent building response functions given by (A2.4-22).

We note several things about (A2.4-22). First, all the frequency-dependence is contained in the materials response functions; the coefficients in the equation ( $\hat{U}_q$ ,  $\hat{h}_e$ , etc.) are all time-dependent. Second, the response of the room to sunlight ( $\frac{B}{A}$ ) differs substantially in form from its response to ambient temperature ( $\frac{C}{A}$ ) or heater output ( $\frac{1}{A}$ ). However, the responses to temperature and heater output are usually about the same, since  $\hat{h}_e R_{2e} \ll \hat{U}_q$  for most buildings.

Third, the form of (A2.4-22) shows all materials entering into the A, B and C coefficients in identical fashion. Thus adding another material 'x' to the system simply adds a term  $\hat{h}_x(1-h_x R_{1x})$  to A, adds  $\alpha_x h_x R_{1x}$  to B, and adds  $\hat{h}_x R_{2x}$  to C. Extension of (A2.4-22) to any number of materials is thus trivial to do; we can write the equation for N materials as:

$$T_R \left[ \hat{U}_q + \sum_{j=1}^N \hat{h}_j (1-h_j R_{1j}) \right] = S \left[ \alpha_R + \sum_{j=1}^N \alpha_j h_j R_{1j} \right] + T_A \left[ \hat{U}_q + \sum_{j=1}^N \hat{h}_j R_{2j} \right] + H$$

(A2.4-22b)

The form of (A2.4-22) also demonstrates an important linearity in the building response: linearity with respect to illuminated area. Suppose we have a surface, call it surface K, which receives an amount

of sunlight  $\alpha_K S$ . Then it makes no difference to the building response how this sunlight is distributed over the surface.

For example, suppose all the illumination falls over a part of surface K. Then divide the material K into two subsections  $K_1$  and  $K_2$  with the former receiving all the illumination. Then  $\hat{h}_K = \hat{h}_{K_1} + \hat{h}_{K_2}$  and  $\alpha_K = \alpha_{K_1}$  while  $\alpha_{K_2} = 0$ . The response functions  $R_1$  and  $R_2$  are the same for K,  $K_1$  or  $K_2$ . The  $T_R$  coefficient ( $A(\omega)$ ) then contains the terms  $\hat{h}_{K_1}(1 - h_{K_1} R_{1K_1}) + \hat{h}_{K_2}(1 - h_{K_2} R_{2K_2})$  which equal  $(\hat{h}_{K_1} + \hat{h}_{K_2})(1 - h_K R_{1K})$ ; this is the same as the term for the whole material K.

The S coefficient contains the terms  $h_{K_1} \alpha_{K_1} R_{1K_1} + h_{K_2} \alpha_{K_2} R_{1K_2}$  which equals  $h_K \alpha_K R_{1K}$ , the old term for the whole material K. Thus dividing the material K into illuminated and non-illuminated sections has no effect on the response of the building.

This linearity can be understood intuitively as follows: exciting temperature oscillations in material K at a certain frequency will produce a given temperature profile  $T_K(x)$ . This profile has the same shape regardless of the magnitude of the oscillations. Thus illuminating a part of the surface K with more sunlight will simply produce a higher amplitude for the function  $T_K(x)$  at that point, and proportionally higher surface temperatures. Since heat transfer from surface K to the room is linear in temperature, we can average over brightly illuminated and dimly illuminated parts of the material K without changing the results.

Linear response to illumination simplifies the task of modelling the building: it means we can consider all materials with equal thermal properties ( $\rho C_p$ , K, thickness, and film coefficient h) to be part of

the same material. That is, for a building with 8" concrete floor and walls, we can lump the floor and walls into a single heavy material, and not worry about the distribution of sunlight between walls and floor, or between the south part of the floor and the north part. (This may, however, introduce an error if the film coefficients  $h$  are different for walls and floor, or if the  $h$ 's differ between the illuminated part of the floor and the shaded part.)

We note further that in the derivation of (A2.4-22), all the information about the heavy materials and their surface boundary conditions is contained in the response functions. Thus this equation is valid for the lumped parameter model as well as the distributed parameter model, provided we interpret the  $R_1$  and  $R_2$  functions as lumped-parameter response functions: Lumped parameter response functions are discussed extensively in Appendix 2.5A: they are of the form:

$$R_1 = \frac{U_i + U_o + i\omega\bar{C}}{(U_i + U_o + i\omega\bar{C})(h + U_i) - U_i^2} \tag{A2.4-21a}$$

$$R_2 = \frac{U_o U_i}{(U_i + U_o + i\omega\bar{C})(h + U_i) - U_i^2}$$

(Alternately, a physically lumped-parameter material, such as a water wall, would be modelled using these response functions.)

To show some of the information contained in (A2.4-22), we look at its low frequency limit, noting that the semi-infinite floor approximation may produce an error in the floor term. The  $\omega \rightarrow 0$  limit of this equation depends on the limits of the response functions. As  $\omega$  becomes small,  $k$  becomes small, so  $\cosh kd \rightarrow 1$  and  $\sinh kd \rightarrow kd$ .

$$\text{Thus } R_{1f} \rightarrow \frac{1}{h_f}, \quad R_{1e} \rightarrow \frac{U_e + 1/R_e}{U_e/R_e + U_e h_e + h_e/R_e}, \quad \text{where } U_e = \frac{K_e}{d_e}$$

$$R_{1p} \rightarrow \frac{1}{h_p}, \quad R_{2e} \rightarrow \frac{U_e/R_e}{U_e/R_e + U_e h_e + h_e/R_e}, \quad \text{and } R_{2f} = R_{2p} = 0$$

Then (A2.4-22) becomes:

$$T_R(\hat{U}_q + A_e U_{\text{tot},e}) = S \left( \alpha_R + \alpha_e \frac{U_{\text{tot},e}}{U_{\text{solid},e}} + \alpha_p + \alpha_f \right) + H$$

$$+ T_A(\hat{U}_q + A_e U_{\text{tot},e}) \quad (\text{A2.4-23})$$

where  $U_{\text{solid},e}$  is the U-value of the envelope material-plus-insulation

$$U_{\text{solid},e} = (U_e^{-1} + R_e)^{-1}$$

$U_{\text{tot},e}$  is the U-value of the envelope including the inside air

$$\text{film, so } U_{\text{tot},e} = (U_{\text{solid},e}^{-1} + h_e^{-1})^{-1}$$

Note that  $A(\omega = 0) = C(\omega = 0)$  which is required by thermodynamics:

the building cannot be at a higher temperature than the air unless it is caused by the driving forces (eg. S). Also the coefficient of  $T_R: (A(\omega))$  is the steady-state heat transfer coefficient: the sum of the products of U-values times areas. It is clear that if we modelled the floor correctly we would get another term  $A_f U_{\text{tot},f}$  in A and C and an analogous change in B; however, these changes would be small in magnitude.

We can see from the form of Eq. (2.4-22) a justification for our approximation of using single-layer walls to derive the response functions. Since for insulated envelope walls,  $\hat{h}_e R_{2e} \ll \hat{U}_q$  while  $\hat{h}_j (1 - h_j R_{1j}) \sim \hat{U}_q$ , it is much more crucial to evaluate  $R_1$  correctly than  $R_2$ .  $R_1$  describes the response of the surface temperature of a material to heat flow inputs on the same side of the material. Thus it is most sensitive to the correct description of the thermal properties of those parts of the wall near

the inside surface. Details of elements near the outside surface will be relatively unimportant, since they have little influence on the inside surface, except at very low frequencies. But at zero frequency,  $R_1$  is simply related to the U-value of the wall, as shown in (A2.4-23), so if we get the correct U-value with a 1-layer-wall model, the  $R_1$  function should be very closely approximated at all frequencies.

We expect that A, B, and C should have the property that  $A(\omega) = A^*(-\omega)$ ; this is confirmed by looking at the form of (A2.4-22 and 21).

These equations show that  $\omega$  appears only in the k's with  $k = \sqrt{i\omega\rho C_p/K}$ . If we change the sign of  $\omega$ , we change k to  $k^*$ , which changes  $R_1$  to  $R_1^*$  and this changes A, B, and C to  $A^*$ ,  $B^*$ , and  $C^*$ .

The thermal performance of the building is governed by Eq. (A2.4-22). When transformed back into the time domain, this says that

$$T_R = \int d\omega \quad \text{or} \quad \sum_n \left( \frac{B(\omega)}{A(\omega)} S(n\omega_f) + \frac{C(\omega)}{A(\omega)} T_A(n\omega_f) + \frac{1}{A(\omega)} H(n\omega_f) \right) \quad (\text{A2.4-24})$$

where the sum is taken over integral multiples of the fundamental frequency  $\omega_f$  or else the integral over all  $\omega$  is used. Note that the sum or integral is over all frequencies, both positive and negative.

We can convert to a sum or integral over positive frequencies by noting that since S,  $T_A$ , and H are real-valued  $S(\omega) = S^*(-\omega)$ ,  $T_A(\omega) = T_A^*(-\omega)$ , etc. Thus for  $\omega_p > 0$ , the sum includes the terms  $\frac{B}{A}(\omega_p) S(\omega_p) + \left(\frac{B}{A}\right)^*(\omega_p) S^*(\omega_p)$ . These terms add to  $2\text{Re}\left(\frac{B}{A}(\omega_p) S(\omega_p)\right)$ . Thus the sum or integral over only positive frequencies (not including zero frequency) will be exactly half the sum or integral over positive and negative frequencies (also not including  $\omega = 0$ ). So we will take the Fourier transforms of S,  $T_A$ , and H to be twice their normal values for  $\omega \neq 0$  and sum over positive frequencies only.

The sum of Eq. (A2.4-24) can usually be truncated with only a few terms. Ambient temperature can be described relatively well as a daily sinusoidal oscillation on top of a steady-state value or a weather-varying term. Higher harmonics of  $\omega_o = 2\pi/\text{day}$ , besides being relatively small, will be fairly unimportant in determining  $T_R$ , since the  $T_A$  coefficient  $C(\omega)$  depends on  $R_2$ , which decays rapidly with  $\omega$ .

Solar gain can, as shown in Ref. 21, be modelled adequately as a sine wave during the day and zero at night. If we set

$$S = \begin{cases} |S_1| \sin \omega_1 t & 0 \leq t < t_d \\ 0 & t_d \leq t < 24 \text{ hrs} \end{cases}$$

with  $\omega_1 t_d = \pi$  and Fourier-analyze  $S$  in harmonics of  $2\pi/\text{day}$ , we find that  $S = |S_1| \sum_{-\infty}^{\infty} c_n e^{in\omega_o t}$  implies that

$$c_n = \begin{cases} \frac{\omega_o}{2\pi} \frac{\omega_1}{\omega_1^2 - (n\omega_o)^2} (1 + e^{-in\omega_o t_d}) & n \omega_o \neq \omega_1 \\ \frac{\omega_o}{4\pi} \frac{t_d}{i} & n \omega_o = \omega_1 \end{cases}$$

$$c_o = \frac{\omega_o}{\pi\omega_1}$$

So to write a sum over non-negative frequencies  $S = |S_1| \sum_{n=0}^{\infty} d_n e^{in\omega_o t}$  we have

$$d_n = \begin{cases} \frac{\omega_o}{2\pi} \frac{2\omega_1}{\omega_1^2 - (n\omega_o)^2} (1 + e^{-in\omega_o t_d}) & n \omega_o \neq \omega_1 \\ \frac{\omega_o}{2\pi} \frac{t_d}{i} & n \omega_o = \omega_1 \end{cases} \quad (\text{A2.4-25})$$

$$d_o = \frac{\omega_o}{\pi\omega_1}$$

To show that the  $d_n$ 's converge quickly, we calculate the first five for  $t_d = 7$  hrs and  $t_d = 8$  hrs.

$\frac{n}{t_d}$	0	1	2	3	4	5
7	.186	$.343e^{-.916i}$	$.266e^{-1.833i}$	$.167e^{-2.748i}$	$.0724e^{2.618i}$	$.0065e^{1.702i}$
8	.212	$.382e^{-1.047i}$	$.272e^{-2.094i}$	$.141e^{-i\pi}$	$.0347e^{2.094i}$	$.0210e^{-2.094i}$

As shown in (A2.4-25) for large  $n$ ,  $d_n \propto \frac{1}{n^2}$ . Thus we see that truncating the Fourier series at  $n = 3$  will not lead to serious (~10%) error.

The response of the building to the simple diurnal cycle described above is given by

$$T_R(t) = |S_1| \sum_{n=1}^3 \frac{B(n\omega_0)}{A(n\omega_0)} d_n e^{in\omega_0 t} + |S_1| \frac{B(0)}{A(0)} d_0 + \frac{C(\omega_0)}{A(\omega_0)} \Delta T_A e^{i\omega_0 t} + \bar{T}_A + \frac{H}{A(0)} \quad (\text{A2.4-26})$$

where the real part of complex quantities is taken after multiplication. Note again that  $A(0)$  is just the steady-state heat loss coefficient for the building.

We have derived the response of the distributed-parameter house to diurnal weather cycles; we next discuss the response to longer-duration weather.

Weather patterns can be Fourier-analyzed into a number of frequencies slower than  $\omega_0 = 2\pi/\text{day}$ . We choose one such frequency and call it  $\omega_w$  and discuss the response of the building to a design weather

cycle at frequency  $\omega_w$ . Typically  $\omega_w \sim 2\pi/\text{week}$  or  $2\pi/2$  weeks. For mathematical simplicity, we require that  $\omega_o = m\omega_w$  where  $m$  is an integer.

Temperature oscillations at frequency  $\omega_w$  are straightforward to handle; the Fourier series for  $T_A$  has the additional term  $\Delta T_{A_w} e^{i\omega_w t}$ , so the series for  $T_R$  has the additional term

$$\Delta T_{A_w} \frac{C(\omega_w)}{A(\omega_w)} e^{i\omega_w t},$$

where  $C$  and  $A$  are from (A2.4-22).

Weather varying solar gain can be described by a sinusoidally modulated form of the daily solar gain function. We assume an average amplitude of solar gain  $\bar{S}$  and oscillations at frequency  $\omega_w$  between amplitudes of  $\bar{S} + \Delta S_w$  and  $\bar{S} - \Delta S_w$ . Thus we express  $S(t)$  as

$$S(t) = \begin{cases} (\bar{S} + \Delta S_w \cos \omega_w t) \sin \omega_1 (t - t_{sr}) & \text{day} \\ 0 & \text{night} \end{cases} \quad (\text{A2.4-27})$$

where  $t_{sr}$  is the time of the most recent sunrise.

We next show that  $S(t)$  can be Fourier-analyzed into a small number of terms which are related to  $d_n$ , the Fourier coefficients of the daily solar gain function. The results are that the steady-state amplitude is  $d_o \bar{S}$  while the amplitude at  $\omega_w$  is  $d_o \Delta S_w$ . For frequencies  $n\omega_o$ , the amplitudes are  $d_n \bar{S}$ , while for frequencies  $n\omega_o \pm \omega_w$ , the amplitudes are  $\frac{d_n}{2} \Delta S_w$ .

This is derived as follows:  $S(t)$  is the product of two functions: an envelope function  $F(t) = \bar{S} + \Delta S_w \cos \omega_w t$  and a daily solar gain function  $G(t) = \begin{cases} \sin \omega_1 t & \text{day} \\ 0 & \text{night} \end{cases}$ . Each of these functions can be written as a Fourier integral:  $S(t) = \int_{-\infty}^{\infty} d\omega s(\omega) e^{i\omega t}$ ,  $F(t) = \int_{-\infty}^{\infty} d\omega f(\omega) e^{i\omega t}$ ,  $G(t) = \int_{-\infty}^{\infty} d\omega g(\omega) e^{i\omega t}$ , with  $s$ ,  $f$ , and  $g$  given by  $s(\omega) = \frac{1}{2\pi} \int_{-\infty}^{\infty} dt S(t) e^{-i\omega t}$  and  $f$  and  $g$  given by analogous expressions. We also know that  $g(\omega) = |S| c_n \delta(\omega_0 n)$  from the daily cycle analysis and that  $f(\omega) = \bar{S} \delta(0) + \frac{\Delta S_w}{2} (\delta(\omega_w) + \delta(-\omega_w))$  from inspection, where  $\delta$  is the Dirac delta function.

We are interested in finding  $s(\omega)$ ; we write an expression for it as follows:

$$s(\omega) = \frac{1}{2\pi} \int_{-\infty}^{\infty} S(t) e^{-i\omega t} dt = \frac{1}{2\pi} \int_{-\infty}^{\infty} F(t) G(t) e^{-i\omega t} dt \quad (\text{A2.4-28})$$

We replace  $F(t)$  and  $G(t)$  by their Fourier expansions:

$$\begin{aligned} s(\omega) &= \frac{1}{2\pi} \int_{-\infty}^{\infty} dt e^{-i\omega t} \int_{-\infty}^{\infty} d\omega' e^{i\omega' t} f(\omega') \int_{-\infty}^{\infty} d\omega'' e^{i\omega'' t} g(\omega'') \\ &= \frac{1}{2\pi} \int_{-\infty}^{\infty} d\omega' f(\omega') \int_{-\infty}^{\infty} d\omega'' g(\omega'') \int_{-\infty}^{\infty} dt e^{i(\omega' + \omega'' - \omega)t} \\ &= \frac{1}{2\pi} \int_{-\infty}^{\infty} d\omega' f(\omega') \int_{-\infty}^{\infty} d\omega'' g(\omega'') \times 2\pi \delta(\omega' + \omega'' - \omega) \end{aligned}$$

We use the  $\delta$ -function in the  $f(\omega')$  integral to get

$$s(\omega) = \int_{-\infty}^{\infty} d(\omega'') f(\omega - \omega'') g(\omega'')$$

Using the explicit form of  $f$ , this says

$$s(\omega) = \int_{-\infty}^{\infty} d(\omega'') g(\omega'') \left( \bar{S} \delta(\omega - \omega'') + \frac{\Delta S_w}{2} \left( \delta(\omega - \omega'' + \omega_w) + \delta(\omega - \omega'' - \omega_w) \right) \right)$$

Integrating the  $\delta$ -functions over  $\omega''$  we find that

$$s(\omega) = \bar{S} g(\omega) + \frac{\Delta S_w}{2} g(\omega + \omega_w) + \frac{\Delta S_w}{2} g(\omega - \omega_w) \quad (\text{A2.4-29})$$

Since  $g(\omega)$  is a Fourier sum,  $s(\omega)$  can be expressed as a sum.

Equation (A2.4-29) says that we replace each term

$|S_1| c_n e^{i\omega_n t}$  in the sum for  $S(t)$  with the triplet  $\bar{S} c_n e^{i\omega_n t} +$

$$\Delta S_w \frac{c_n}{2} e^{i(\omega_n - \omega_w)t} + \Delta S_w \frac{c_n}{2} e^{i(\omega_n + \omega_w)t} . \text{ Note that this sum adds}$$

to  $(\bar{S} + \Delta S_w \cos \omega_w t) c_n e^{i\omega_n t}$ . For positive  $\omega_n$ , we can replace

$|S_1| d_n e^{i\omega_n t}$  in the sum of positive frequencies for  $S(t)$  with the same triplet (using  $d_n$  in place of  $c_n$ ). But for  $\omega_n = 0$ , the triplet contains one term at negative frequency (the term  $\Delta S_w \frac{c_0}{2} e^{-i\omega_w t}$ ), so we must

first add all three terms. They sum to  $(\bar{S} + \Delta S_w \cos \omega_w t) c_0$  which is equal to

$$\text{Re} \left( c_0 (\bar{S} + \Delta S_w e^{i\omega_w t}) \right) = \text{Re} \left( d_0 (\bar{S} + \Delta S_w e^{i\omega_w t}) \right)$$

Thus the steady-state amplitude is  $d_0 \bar{S}$  and the amplitude at  $\omega_w$  is  $d_0 \Delta S_w$ , while the amplitudes at frequencies  $n\omega_0$  and  $n\omega_0 \pm \omega_w$  are given

by  $\bar{S} d_n$  and  $\frac{\Delta S_w}{2} d_n$  respectively.

We have now derived a Fourier-expansion for the weather-varying solar gain function; we next look at how this expansion can be used to calculate  $T_R$ . We have shown that adding a weather-varying component to

$T_A$  simply adds the terms  $\Delta T_{A_w} \frac{B(\omega_w)}{A(\omega_w)} e^{i\omega_w t}$  to (A2.4-27). Adding a weather-varying effect onto  $S(t)$  will replace the steady-state term

$|S_1| \frac{B(0)}{A(0)} d_o$  with the analogous term  $\bar{S} \frac{B(0)}{A(0)} d_o$ . It will also add a

term at frequency  $\omega_w$  :

$$\Delta S_w \frac{B(\omega_w)}{A(\omega_w)} d_o e^{i\omega_w t}$$

In addition, it will replace each of the terms

$$|S_1| \frac{B(n\omega_o)}{A(n\omega_o)} d_n e^{in\omega_o t} \text{ with a triplet } \bar{S} \frac{B(n\omega_o)}{A(n\omega_o)} d_n e^{in\omega_o t} \\ + \Delta S_w \frac{d_n}{2} \left( \frac{B(n\omega_o + \omega_w)}{A(n\omega_o + \omega_w)} e^{i(n\omega_o + \omega_w)t} + \frac{B(n\omega_o - \omega_w)}{A(n\omega_o - \omega_w)} e^{i(n\omega_o - \omega_w)t} \right)$$

Since  $\frac{B}{A}$  will generally not vary too much with small changes in  $\omega$  (note that  $\omega_w$  will be about 10% of  $n\omega_o$  or less), we can approximate

the triplet by  $(\bar{S} + \Delta S_w \cos \omega_w t) \frac{B(n\omega_o)}{A(n\omega_o)} d_n e^{in\omega_o t}$ , as shown below.

Suppose  $\frac{B}{A}$  varies only slowly with  $\omega$ ; so let

$$\frac{B}{A} (\omega_n \pm \omega_w) = \frac{B}{A} (\omega_n) (1 \pm \epsilon_n) \left( \text{ignoring terms of order } \frac{\partial^2 (B/A)}{\partial \omega^2} \omega_w^2 \right)$$

Then the triplet is equal to

$$\left\{ \frac{B(n\omega_o)}{S A(n\omega_o)} + \frac{\Delta S_w}{2} \left[ \left( \frac{B(n\omega_o)}{A(n\omega_o)} (1+\epsilon_n) e^{i\omega_w t} \right) + \left( \frac{B(n\omega_o)}{A(n\omega_o)} (1-\epsilon_n) e^{-i\omega_w t} \right) \right] \right\} \\ \times d_n e^{in\omega_o t}$$

or

$$\frac{B(n\omega_o)}{A(n\omega_o)} d_n e^{in\omega_o t} \left( \bar{S} + \frac{\Delta S_w}{2} \left( e^{i\omega_w t} + e^{-i\omega_w t} + \epsilon_n \left[ e^{i\omega_w t} - e^{-i\omega_w t} \right] \right) \right) \\ = \frac{B(n\omega_o)}{A(n\omega_o)} d_n e^{in\omega_o t} \left( \bar{S} + \Delta S_w (\cos \omega_w t + i \epsilon_n \sin \omega_w t) \right)$$

For  $\epsilon$  small, this is just the amplitude of  $S(t)$  for the day in question  $(\bar{S} + \Delta S_w \cos \omega_w t)$  times the daily response of  $T_R$  to  $S$ . To summarize for weather cycles with  $T_A = \Delta T_{A_w} e^{i\omega_w t} + \Delta T_A e^{i\omega_o t} + \bar{T}_A$  and

$$S(t) = \begin{cases} (\bar{S} + \Delta S_w \cos \omega_w t) \sin \omega_1(t - t_{sr}) & \text{day} \\ 0 & \text{night} \end{cases}$$

and with  $d_n$  the Fourier expansion coefficients for the daily part of  $S(t)$  (for non-negative frequencies only), then

$$T_R(t) \cong (\bar{S} + \Delta S_w \cos \omega_w t) \left\{ \sum_{n=1}^3 \frac{B(n\omega_o)}{A(n\omega_o)} d_n e^{in\omega_o t} \right\} + \bar{S} \frac{B(0)}{A(0)} d_o + \\ + \Delta S_w \frac{B(\omega_w)}{A(\omega_w)} d_o e^{i\omega_w t} \\ + \bar{T}_A + \Delta T_{A_w} \frac{C(\omega_w)}{A(\omega_w)} e^{i\omega_w t} + \Delta T_A \frac{C(\omega_o)}{A(\omega_o)} e^{i\omega_o t} + \frac{H}{A(0)} \quad (A2.4-30)$$

This equation is useful in evaluating the response of the building to design weather conditions. The design conditions for checking whether the house overheats might be that for  $\Delta S_w \cos \omega_w t$  in phase with  $\Delta T_{AW}$ , we calculate the response of  $T_R$  on the hottest day of the cycle. We then determine the response on the coldest day, for the same weather conditions. These two daily-temperature calculations then bracket the range of performance of the building under all expected weather conditions.

Design weather conditions could be determined in principle from Fourier analysis of real weather data; but such analysis has not been done to present.

The preceding analysis has been done for a "direct gain" building. Extension to include Trombe wall structures is relatively straightforward and is shown below.

#### Trombe Wall Solution

In this section we show how to include the effects of a Trombe wall. Because of the constraints of the Fourier solution, the Trombe wall must be completely unmanaged in this solution; that is, the degree of thermocirculation from wall surface to room cannot change from day to night, nor can the glazing on the Trombe wall be insulated at night.

We use the same parameters to describe the wall's coupling to the room and to the outside as are used in the lumped parameter model, Appendix 2.3. The Trombe wall surface is coupled to the channel air through the film heat transfer coefficient  $\hat{h}_{TC}$ . The channel air is then coupled to the ambient air by  $\hat{U}_{CA}$ , which describes heat loss through the collector glazing; it is also coupled convectively to the

room air through the heat transfer coefficient  $\hat{U}_{CR}$ , which is chosen to be a linear approximation for the natural convection heat transfers. The back surface of the Trombe wall is then coupled to the room by heat transfer coefficient  $\hat{U}_{TR}$ , which is typically just a film coefficient.

The temperature profile in the Trombe wall solves the diffusion equation

$$(\rho C_p)_T \frac{\partial T_T(x,t)}{\partial t} = K_T \frac{\partial^2 T_T(x,t)}{\partial x^2} \quad (A2.4-31)$$

It is subject to heat balances on its front and back surfaces, which are analogous to (A2.3-17) and (A2.5A-21) :

$$\hat{h}_{Tc} (T_T(x=0,t) - T_c) - \alpha_T S - A_T K_T \left. \frac{\partial T_T(x,t)}{\partial x} \right|_{x=0} \quad (A2.4-32)$$

and

$$-A_T K_T \left. \frac{\partial T_T(x,t)}{\partial x} \right|_{x=d_T} = \hat{U}_{TR} (T_{int} - T_R) \quad (A2.4-33)$$

where  $T_c$  is the temperature of the channel air ,

$d_T$  is the thickness of the Trombe wall ,

$T_{int}$  is the temperature of the interface between

the Trombe wall and the resistance  $1/\hat{U}_{TR}$  .

(For an uninsulated wall  $T_{int}$  is just the back surface temperature).

Note that we have made the approximation of one-dimensional heat flow — that there is no temperature variation from bottom to top in the Trombe wall or air channel. In fact, temperature gradients will exist; however, they will not be important unless they affect the heat transfer coefficients  $\hat{h}_{Tc}$ ,  $\hat{U}_{TR}$ , etc. If these heat transfers are really linear, then by the arguments of the previous section we can take  $T_c$ ,  $T_T$ , and  $T_{int}$  to be averages over all heights and the solution will not be affected.

The diffusion equation is solved by

$$T_T(x,t) = A_T \cosh k_T d_T (1-\xi) + B_T \sinh k_T d_T (1-\xi) \quad (A2.4-34)$$

where  $\xi = x/d_T$ .

Since  $T_{int}$  is the rear surface temperature of the Trombe wall,  $T_T(x = d_T, t) = T_{int}$ . Then by (A2.4-33),  $B_T = \frac{\hat{U}_{TR}}{A_T K_T k_T} (A_T - T_R)$  so that

$$T_T(x,t) = T_{T\omega} \left( \cosh k_T d_T (1-\xi) + \frac{(T_{T\omega} - T_R) \hat{U}_{TR}}{A_T K_T k_T} \sinh k_T d_T (1-\xi) \right) \quad (A2.4-35)$$

where  $T_{T\omega} \equiv A_T$ .

Before we substitute this into (A2.4-32), we eliminate  $T_c$  using the channel heat balance (A2.3-20); then using (A2.4-35) for  $T_T$  and its derivatives; we find that

$$T_{T\omega} = \frac{\hat{U}_{cA} \hat{h}_{Tc}}{\hat{\Sigma}} \frac{1}{D_T} T_A + \frac{\alpha_T}{D_T} S + \frac{T_R}{D_T} \left( \hat{U}_{TR} \cosh k_T d_T + \frac{\hat{U}_{TR} \hat{U}_a}{A_T K_T k_T} \sinh k_T d_T + \frac{\hat{U}_{cR} \hat{h}_{Tc}}{\hat{\Sigma}} \right) \quad (A2.4-36)$$

where  $D_T = (\hat{U}_a + \hat{U}_{TR}) \cosh k_T d_T + \left( A_T K_T k_T + \frac{\hat{U}_a \hat{U}_{TR}}{A_T K_T k_T} \right) \sinh k_T d_T$

and  $\hat{\Sigma} = \hat{h}_{Tc} + \hat{U}_{cA} + \hat{U}_{cR}$

$$\hat{U}_a = \frac{\hat{h}_{Tc} (\hat{U}_{cA} + \hat{U}_{cR})}{\hat{\Sigma}}$$

We use these last two equations to show that

$$T_T(x=0) = \frac{\hat{U}_{cA} \hat{h}_{Tc}}{\hat{\Sigma}} R_{1T} T_A + \alpha_T S R_{1T} + \left( R_{2T} + \frac{\hat{U}_{cR} \hat{h}_{Tc}}{\hat{\Sigma}} R_{1T} \right) T_R \quad (A2.4-37)$$

where  $R_{1T} = \frac{\cosh k_T d_T + \frac{U_{TR}}{K_T k_T} \sinh k_T d_T}{(U_a + U_{TR}) \cosh k_T d_T + \left( K_T k_T + \frac{U_a U_{TR}}{K_T k_T} \right) \sinh k_T d_T}$

$$R_{2T} = \frac{U_{TR}}{(U_a + U_{TR}) \cosh k_T d_T + \left( K_T k_T + \frac{U_a U_{TR}}{K_T k_T} \right) \sinh k_T d_T}$$

Note that  $R_{1T}$  and  $R_{2T}$  have exactly the same form as (A2.4-21) for  $R_{1e}$  and  $R_{2e}$  except that  $U_{TR}$  replaces  $1/R_e$  and  $U_a$  replaces  $h_e$ . The first replacement is a matter of definition only; both  $U_{TR}$  and  $1/R_e$  are the conductances away from the back wall surface.

This completes the derivation of Trombe wall surface temperature as a function of materials properties; we use the result in the room heat balance to obtain the solution for room temperature. The room heat balance is slightly altered to take into account the Trombe wall; instead of A2.4-7, we have:

$$\begin{aligned} \hat{h}_e(T_R - T_e(0,t)) + \hat{h}_p(T_R - T_p(0,t)) + \hat{h}_f(T_R - T_f(0,t)) + \hat{U}_q(T_R - T_A) \\ + \hat{U}_{cR}(T_R - T_c) + \hat{U}_{TR}(T_R - T_{int}) = \alpha_R S + H \end{aligned} \quad (2.4-38)$$

This equation is the same as (A2.4-7) except for the addition of the last two terms on the left-hand side. We can write these terms as

$$\begin{aligned} (\hat{U}_{cR} + \hat{U}_{TR})T_R - \hat{U}_{cR} \left( \frac{\hat{U}_{cA}}{\hat{\Sigma}} T_A + \frac{\hat{U}_{cR}}{\hat{\Sigma}} T_R + \frac{\hat{h}_{Tc}}{\hat{\Sigma}} T_T(x=0) \right) \\ - \hat{U}_{TR} \left( \frac{\hat{U}_{cA}\hat{h}_{Tc}}{\hat{\Sigma}} \frac{1}{D_T} T_A + \frac{\alpha_T}{D_T} S + T_R \frac{1}{D_T} \left( \hat{U}_{TR} \cosh k_T d_T + \frac{\hat{U}_{TR}\hat{U}_a}{A_T K_T k_T} \sinh k_T d_T + \frac{\hat{U}_{cR}\hat{h}_{Tc}}{\hat{\Sigma}} \right) \right) \end{aligned}$$

using (A2.3-20) for  $T_c$  and (A2.4-36) for  $T_{int} = T_{Tw}$ . Then with (A2.4-37) for  $T_T(x=0)$ , we can derive the relationship between  $T_R$ ,  $T_A$ ,  $S$ , and  $H$  as:

$$\begin{aligned}
 & T_R \left\{ \hat{U}_q + \hat{h}_e (1 - R_{1e} h_e) + \hat{h}_p (1 - R_{1p} h_p) + \hat{h}_f (1 - R_{1f} h_f) \right. \\
 & + \hat{U}_{cR} \left( 1 - \frac{1}{\Sigma} \left( U_{cR} + h_{Tc} \left[ R_{2T} + \frac{U_{cR} h_{Tc}}{\Sigma} R_{1T} \right] \right) \right) \\
 & \left. + \hat{U}_{TR} \left( 1 - U_{TR} \left( R'_{1T} + \frac{1}{U_{TR}} \frac{U_{cR} h_{Tc}}{\Sigma} R_{2T} \right) \right) \right\} \\
 & = S \left\{ \alpha_R + h_e \alpha_e R_{1e} + h_p \alpha_p R_{1p} + h_f \alpha_f R_{1f} + \alpha_T \left( \frac{U_{cR} h_{Tc}}{\Sigma} R_{1T} + R_{2T} \right) \right\} \\
 & + T_A \left\{ \hat{U}_q + \hat{h}_e R_{2e} + \frac{\hat{U}_{cR} \hat{U}_{cA}}{\hat{\Sigma}} + \frac{\hat{h}_{Tc} \hat{U}_{cA}}{\hat{\Sigma}} \left[ R_{2T} + \frac{U_{cR} h_{Tc}}{\Sigma} R_{1T} \right] \right\} + H
 \end{aligned} \tag{A2.4-39}$$

where  $R'_{1T}$  is  $R_{1T}$  with  $U_{TR}$  and  $U_a$  reversed. We note that for nonlinear convection ( $\hat{U}_{cR}$  dependent on  $T_c - T_R$ ) we can solve for the steady-state part of (A2.4-39) using an exact expression for convective heat transfer and use the linear approximation for  $\omega \neq 0$  terms only.

The form of this equation is slightly messier than (A2.4-22); instead of just  $R_{1T}$  or  $R_{2T}$ , it contains terms like  $\left( R_{2T} + \frac{U_{cR} h_{Tc}}{\Sigma} R_{1T} \right)$ . It also contains the new function  $R'_{1T}$ . The response of the surface temperature of a material to heat flux on the same side of the material is described by  $R_1$ ; the function  $R'_1$  describes the same thing for the surface on the opposite side of the wall. Since the room is coupled to the back side of the Trombe wall, the use of the  $R'_{1T}$  function is not surprising.

So for a Trombe wall building, we use (A2.4-39) above in place of (A2.4-22) to derive  $A(\omega)$ ,  $B(\omega)$ , and  $C(\omega)$ ; the  $T_R(t)$  equations (A2.4-26 and 30) still are valid with these new A, B, and C functions.

For a non-convecting Trombe wall ( $\hat{U}_{cR} = 0$ ), these expressions simplify considerably, and the A, B, and C functions of (A2.4-39) compare to the earlier form (A2.4-22) as follows:

$$\begin{aligned}
 A(\omega) &= (\dots \text{ old terms } \dots + \hat{U}_{TR} (1 - U_{TR} R'_{1T})) \\
 B(\omega) &= (\dots \text{ old terms } \dots + \alpha_T R_{2T}) \\
 C(\omega) &= \left( \dots \text{ old terms } \dots + \frac{\hat{h}_{Tc} \hat{U}_{cA}}{\hat{h}_{Tc} + \hat{U}_{cA}} R_{2T} \right)
 \end{aligned}
 \tag{A2.4-40}$$

These are not quite analogous to the forms for interior walls, due to the appearance of  $R'_{1T}$  in  $A(\omega)$  instead of  $R_{1T}$ , and due to the use of  $R_{2T}$  in  $B(\omega)$  rather than  $R_{1T}$ . However, the new term in  $C(\omega)$  is analogous to that for an envelope wall.

All the material derived above for Trombe walls works equally well for water walls, with the lumped response functions (A2.4-21a) replacing the continuum functions (A2.4-37).

Two Layer Wall Response Functions

In this section we derive expressions for the response functions  $R_1$  and  $R_2$  for a two-layer wall in which both layers have large heat capacity. An example of such a two-layer material is a concrete floor with wood surface. As shown below, the form of these response functions is not dissimilar to the form of the single-layer-plus-resistance functions.

Consider a two layer wall characterized by  $K_1$ ,  $k_1$ , and  $d_1$ , for the inside layer and  $K_2$ ,  $k_2$ , and  $d_2$  for the outside layer. The solution to the diffusion equation for each layer is given by

$$\begin{aligned} T_1(\omega, x_1) &= A \cosh k_1 d_1 (1-\xi) + B \sinh k_1 d_1 (1-\xi) \\ T_2(\omega, x_2) &= C \cosh k_2 d_2 (1-\zeta) + D \sinh k_2 d_2 (1-\zeta) \end{aligned} \tag{A2.4-41}$$

where  $\xi = \frac{x_1}{d}$                        $\zeta = \frac{x_2}{d}$

The boundary conditions are, for the inside surface, the surface heat balance (1) :

$$K_1 \left. \frac{\partial T_1}{\partial x_1} \right|_{x_1=0} + S' - h T_1(0) = 0 \tag{A2.4-42}$$

where  $S' \equiv h T_R + \alpha S$

For the interface, we have continuity of heat flux:

$$K_1 \left. \frac{\partial T_1}{\partial x_1} \right|_{x_1=d_1} = K_2 \left. \frac{\partial T_2}{\partial x_2} \right|_{x_2=0} \tag{A2.4-43}$$

We also have continuity of temperature at the interface (e.g. perfect thermal contact) or

$$T_1(d_1) = T_2(0) \quad (\text{A2.4-44})$$

Finally, we have perfect thermal contact between the outside surface of layer 2 and the outside air.

$$T_2(d_2) = T_A \quad (\text{A2.4-45})$$

Using (A2.4-41) in (A2.4-45) we see that  $C = T_A$ . Then (A2.4-42) requires that

$$S' = A(h \cosh k_1 d_1 + K_1 k_1 \sinh k_1 d_1) + B(h \sinh k_1 d_1 + K_1 k_1 \cosh k_1 d_1) \quad (\text{A2.4-46})$$

while (A2.4-42) says that

$$K_1 k_1 B = K_2 k_2 T_A \sinh k_2 d_2 + K_2 k_2 D \cosh k_2 d_2 \quad (\text{A2.4-47})$$

Finally, from (A2.4-44), we get

$$A = T_A \cosh k_2 d_2 + D \sinh k_2 d_2 \quad (\text{A2.4-48})$$

We solve the last of these equations for D and use the result in (A2.4-47) to express B in terms of A and  $T_A$ . This result is then used in (A2.4-46) to obtain the following expressions for A and B:

$$A = \frac{S}{D_{en}} + \frac{T_A}{D_{en}} \left( K_2 k_2 \frac{\cosh k_2 d_2}{\sinh k_2 d_2} + \frac{K_2 k_2 h \sinh k_1 d_1}{K_1 k_1 \sinh k_2 d_2} \right) \quad (\text{A2.4-49})$$

$$B = \frac{S}{D_{en}} \frac{K_2 k_2}{K_1 k_1} \coth k_2 d_2 - \frac{T_A}{D_{en}} K_2 k_2 \frac{h \cosh k_1 d_1}{K_1 k_1 \sinh k_2 d_2} + \frac{\sinh k_1 d_1}{\sinh k_2 d_2}$$

where  $D_{en} = (h + K_2 k_2 \coth k_2 d_2) \cosh k_1 d_1 + \left( K_1 k_1 + \frac{K_2 k_2 h}{K_1 k_1} \coth k_2 d_2 \right) \sinh k_1 d_1$ .

Then the surface temperature  $T_s = A \cosh k_1 d_1 + B \sinh k_1 d_1$  from (A2.4-41). Using the expressions (A2.4-49) for A and B we find the response functions  $R_1$  and  $R_2$ ; they are:

$$R_1 = \frac{\cosh k_1 d_1 + \frac{K_2 k_2}{K_1 k_1} \coth k_2 d_2 \sinh k_1 d_1}{(h + K_2 k_2 \coth k_2 d_2) \cosh k_1 d_1 + \left( K_1 k_1 + \frac{K_2 k_2 h}{K_1 k_1} \coth k_2 d_2 \right) \sinh k_1 d_1}$$

$$R_2 = \frac{\frac{K_2 k_2}{\sinh k_2 d_2}}{(h + K_2 k_2 \coth k_2 d_2) \cosh k_1 d_1 + \left( K_1 k_1 + \frac{K_2 k_2 h}{K_1 k_1} \coth k_2 d_2 \right) \sinh k_1 d_1}$$

(A2.4-50)

Radiative Coupling Solution

In this section we derive the modifications necessary to precisely calculate convection and radiation exchanges within a building. Previously, we assumed that each material surface was in thermal contact with the room air through a coupling coefficient  $\hat{h}$  which combined the effects of convection and radiation.

In this section, we model the more realistic case where the surface  $j$  is coupled to the air through the convective coefficient  $\hat{h}'_j$ , and is also coupled to each other surface  $i$  through the coefficient  $\hat{h}_{ij}$ . This radiation coefficient includes a geometric form factor.

The surface heat balance for the  $j^{\text{th}}$  surface is then modified to read:

$$\hat{h}'_j T_R + \alpha_j S + \sum_{\substack{i=1 \\ i \neq j}}^N \hat{h}_{ij} T_{si} - \hat{h}'_j T_{sj} - \sum_{\substack{i=1 \\ i \neq j}}^N \hat{h}_{ij} T_{sj} - A_j K_j \left. \frac{\partial T_j}{\partial x} \right|_{x=0} = 0 \quad (\text{A2.4-51})$$

where  $T_{sj}$  is the temperature of the  $j^{\text{th}}$  surface and  $N$  is the number of material surfaces in the building.

We can simplify the notation somewhat if we define  $\hat{h}'_j \equiv \hat{h}_{jj}$  and

$$\sum_{i=1}^N \hat{h}_{ij} \equiv \hat{h}_{j,\text{tot}}$$

Then we have

$$\hat{h}_{jj} T_R + \alpha_j S + \sum_{\substack{i=1 \\ i \neq j}}^N \hat{h}_{ij} T_{si} - \hat{h}_{j,\text{tot}} T_{sj} - A_j K_j \left. \frac{\partial T_j}{\partial x} \right|_{x=0} = 0 \quad (\text{A2.4-52})$$

We see that (A2.4-52) is exactly the same as previous heat balances except that we have the term  $\hat{h}_{jj} T_R + \alpha_j S + \sum_{i=1}^N \hat{h}_{ij} T_{si}$  in place of  $\hat{h}_j T_R + \alpha_j S$ . (We also have  $\hat{h}_{j,tot} T_{sj}$  instead of  $\hat{h}_j T_{sj}$ , but these expressions should be numerically equal). Therefore the response function equations come out analogously, and

$$T_{sj} = R_{1j} (h_{jj} T_R + \bar{\alpha}_j S + \sum_{\substack{i=1 \\ i \neq j}}^N h_{ij} T_{si}) + R_{2j} T_A \quad (\text{A2.4-53})$$

where  $R_{1j}$  and  $R_{2j}$  have the same form as before, except that we replace  $\hat{h}_j$  with  $\hat{h}_{j,tot}$ .

The room heat balance for this model is

$$\sum_{j=1}^N \hat{h}_{jj} (T_R - T_{sj}) + \hat{U}_q (T_R - T_A) = H \quad (\text{A2.4-54})$$

where the term  $\alpha_R S$  is missing from the right-hand side because we can no longer assume that sunlight falling on a light surface is absorbed directly into the room air. (Some of it is radiated to other surfaces instead). We now have to model light surfaces explicitly.

Previously we used the surface temperature result analogous to (A2.4-53) to replace  $T_{sj}$  in (A2.4-54). However, in this case, (A2.4-53) is not an expression for  $T_{sj}$  in closed form. It is actually a system of  $N$  equations for the  $N$  surface temperatures, which must be solved before substitution into (A2.4-54). We solve the system (A2.4-53) formally in the following manner:

Represent  $T_{sj}$  as a column vector  $\underline{T}_s$ . We can then write (A2.4-53) as a matrix equation

$$\tilde{T}_s = \tilde{T}_{eq} + \tilde{M} \tilde{T}_s \quad (A2.4-55)$$

where  $\tilde{T}_{eq}$  is a column vector whose  $j^{\text{th}}$  component is

$$R_{1j} (h_{jj} T_R + \bar{\alpha}_j S) + R_{2j} T_A$$

and  $\tilde{M}$  is an  $N \times N$  matrix whose  $ij^{\text{th}}$  component is

$$R_{1j} h_{ij} \text{ and whose diagonal elements are all zero.}$$

Solving (A2.4-55) formally, we have

$$\tilde{T}_s = (\tilde{1} - \tilde{M})^{-1} \tilde{T}_{eq} \quad (A2.4-56a)$$

where  $\tilde{1}$  is the  $N \times N$  identity matrix; or

$$T_{sj} = \sum_{i=1}^N \left\{ (\tilde{1} - \tilde{M})^{-1} \right\}_{ji} \left\{ R_{1i} (h_{ii} T_R + \bar{\alpha}_i S) + R_{2i} T_A \right\} \quad (A2.4-56b)$$

Let  $L \equiv (\tilde{1} - \tilde{M})^{-1}$ ; then we can write (A2.4-54) as

$$\begin{aligned} T_R \left\{ \hat{U}_q + \sum_{j=1}^N \hat{h}_{jj} \left( 1 - \sum_{i=1}^N L_{ji} h_{ii} R_{1i} \right) \right\} \\ S \left\{ \sum_{j=1}^N \sum_{i=1}^N h_{jj} L_{ji} \alpha_i R_{1i} \right\} \\ + T_A \left\{ \hat{U}_q + \sum_{j=1}^N \hat{h}_{jj} \sum_{i=1}^N L_{ji} R_{2i} \right\} \end{aligned}$$

+ H

(A2.4-57)

This solution replaces (A2.4-22) for the relationship between  $T_R$  and the driving forces. It is apparent from examining (A2.4-57) that the amount of computation needed to evaluate it is orders of magnitude larger than the simpler equation. For our simple example of a building with envelope walls, partition walls, and floor, we would have to add a fourth surface — light furniture — and set  $N = 4$ . We would then have to calculate radiation exchange form factors ( $\hat{h}_{ij}$ ) between these four surfaces, and then invert  $4 \times 4$  matrices for each frequency of interest (say,  $\omega = 0, \omega_w, \omega_o, 2\omega_o, 3\omega_o$ ) or 5 matrices. The sums to produce  $A(\omega), B(\omega),$  and  $C(\omega)$  would be double sums of 16 terms compared to 3 in the simple case.

In addition to the extra computation, the intuitive clarity is compromised in (A2.4-57). There is no obvious way to see how a change in a response function will affect the building performance, since we cannot intuitively invert  $\frac{1}{\approx} - \frac{M}{\approx}$ . For these reasons, we do not compute solutions using the precise thermal radiation balances.

APPENDIX 2.5A: Simulating Distributed Walls  
with Lumped Parameters

Fourier transform techniques allow the exact solution of the passive solar house model for distributed walls. However, these techniques are practical only in those cases where the parameters of the house are not time-dependent. For time-dependent parameters, such as night insulation of the windows, it is much simpler to solve the model using lumped parameters. This section discusses the derivation of lumped parameters which approximate the behavior of a distributed wall.

The most important elements of the house to model are those which receive and store solar energy (e.g. a slab floor). At the surface of the massive solar receiver, the temperature  $T_S$  will be determined by a heat balance between solar gain, convection/radiation to the room, and diffusion into the receiver. Call the receiver a "floor" although the analysis would be the same if it were a wall. The heat balance of the surface is given by

$$A_f K_f \left. \frac{\partial T_f(z,t)}{\partial z} \right|_{z=0} + \alpha_f S + \hat{h}_f (T_R - T_S) = 0 \quad (A2.5A-1)$$

where  $A_f$  is the area of the floor  
 $K_f$  is the conductivity of the floor  
 $\hat{h}_f$  is the floor surface film coefficient times the floor area  
 $T_R$  is the room temperature  
 $T_S$  is the floor surface temperature  
 $\alpha_f S$  is the solar gain on the floor (in  $\text{Btu h}^{-1}$  or W)  
 $z$  is the distance into the floor material

In a lumped model, this heat balance is given by

$$\hat{U}_i(T_f - T_S) + \alpha_f S + \hat{h}_f(T_R - T_S) = 0 \quad (\text{A2.5A-2})$$

where  $\hat{U}_i$  is the heat transfer coefficient into the floor  
 $T_f$  is the floor thermal mass temperature.

The lumped-model floor will exchange the same amount of heat with the house as the distributed-model floor provided that the surface temperature is the same in both cases. This also implies that the amount of heat stored is the same in both models.

The heat balance equations (A2.5A-1) and (2), together with equations describing the details of the walls or floor, will give the floating surface temperature  $T_S$  as a function of the driving forces of solar gain ( $S$ ) and ambient temperature ( $T_A$ ). We can expect to find different response functions for  $T_S$  in terms of  $T_A$  and  $S$  for the distributed model and for the lumped model. If we can find values of the lumped parameters ( $\hat{U}_i$ , the heat transfer coefficient between the floor surface and the floor heat capacity;  $\hat{U}_o$ , the heat transfer coefficient between the floor heat capacity and the outside; and  $C$ , the floor heat capacity) which allow the lumped-parameter response functions to approximate the distributed model response functions, then we can use these parameter values to simulate the heat transfer of the distributed floor or wall.

Since  $S$  and  $T_A$  are independent excitations, we expect that in Fourier transform space, the equation for  $\tilde{T}_S$  will be

$$\tilde{T}_S = R_1(\omega)\tilde{S} + R_2(\omega)\tilde{T}_A \quad (\text{A2.5A-3})$$

where  $\sim$  indicates Fourier transform, and  $R_1$  and  $R_2$  are the response functions of Section 2.4; so the simulation process will involve calculating  $R_1(\omega)$  and  $R_2(\omega)$  for lumped and continuum cases, and choosing

lumped parameters which allow  $R_1$  and  $R_2$  to be approximately the same over the relevant range of frequencies.

"The relevant range of frequencies" is from  $\omega = 0$  to  $\omega \approx 2\pi/1 \text{ day} \times 3$ . The lower limit is important because there is a fairly large DC component (or at least yearly component) to the response of the house. The fundamental frequency for solar gain and ambient temperature is usually one day, while the first few harmonics are necessary to describe day and night solar gain conditions.

We will discuss several cases of walls to be modeled. The simplest case is the single-layer wall of finite thickness. We then model a semi-infinite wall. The results for the semi-infinite wall are extended to cover moderately thick walls. The moderately thick wall solution will be compared to the thin-wall solution.

We next discuss insulated walls: that is, walls of a homogeneous material with nonzero heat capacity covered by a pure insulator. There are two cases of interest: insulation outside (e.g. concrete block with exterior foam insulation) and insulation inside (e.g. carpeted slab floors). In addition, we look at simulations for interior walls. To avoid complication we model each element (floor, walls, etc.) separately; that is, we do not consider the properties of the walls in choosing the lumped parameters for the floor. The validity of this approach is demonstrated by the form in which the response functions  $R_1$  and  $R_2$  appear in (A2.4-22); each element enters independently.

Thin Single-Layer Walls

Calculating continuum and lumped response functions.

We first look at envelope walls or floors, and calculate  $R_1$  and  $R_2$  for the continuum and lumped models. Sunlight is absorbed on the inside surface of the material and heat is lost to ambient from the outside surface.

For the continuum model, the diffusion equation for the temperature distribution  $T_f(z,t)$  is

$$\rho c_p \frac{\partial T_f(z,t)}{\partial t} = K_f \frac{\partial^2 T_f(z,t)}{\partial z^2} .$$

We assume perfect thermal contact at the outside, so for a floor of thickness  $d$ ,

$$T_f(z = d, t) = T_A(t) . \quad (A2.5A-4)$$

Solving the diffusion equation in Fourier transform space, we get

$$T_f = A \cosh k_f d \left(1 - \frac{z}{d}\right) + B \sinh k_f d \left(1 - \frac{z}{d}\right)$$

with

$$k_f = \sqrt{\frac{i\omega\rho c_p}{K_f}} \quad (A2.5A-5a)$$

Equation (A2.5A-4) requires  $A$  to be equal to  $T_A$ , while (A2.5A-1) requires that

$$B = -\tilde{T}_A \frac{K_f k_f \sinh k_f d + h_f \cosh k_f d}{h_f \sinh k_f d + K_f k_f \cosh k_f d} + \frac{\bar{\alpha}_f \tilde{S} + h_f \tilde{T}_R}{h_f \sinh k_f d + K_f k_f \cosh k_f d} \quad (A2.5 -5b)$$

where

$$\bar{\alpha}_f = \alpha_f / A_f$$

We note that surface temperature is given by  $T_S = T_f(z = 0, t)$ , so that

$$T_S = T_A \cosh k_f d + B \sinh k_f d .$$

Using expression (A2.5A-5b) for B, we obtain the result that

$$T_S = R_1 \bar{\alpha}_f S + R_2 T_A + R_1 (h_f T_R) \quad (\text{A2.5A-6a})$$

where  $R_1$  and  $R_2$  are given by (A2.5-6b) below.

The last term in this expression comes about because when we look at only one heavy material, the room temperature is indeterminate and must be considered as a separate independent excitation. This is not a problem since the response of  $T_S$  to  $T_R$  is given by the function  $h_f R_1$  which is proportional to  $R_1$ ; thus if we match  $R_1$  correctly in the lumped and distributed models, we have automatically modeled the response to  $T_R$  correctly.

It should be noted that  $R_1$  is not the response of the surface temperature  $T_S$  to solar gain, since solar gain affects  $T_S$  indirectly through  $T_R$  as well as directly.  $R_1$  is the response of  $T_S$  to a unit heat flux input on the inside. For this particular case, the heat flux is given by  $h_f T_R + \bar{\alpha}_f S$ , but  $R_1$  characterizes the surface temperature's response to any heat flux on the surface, just as  $R_2$  characterizes the response to temperature input on the opposite surface.

In obtaining (A2.5A-6a) we find that

$$R_{1c} = \frac{\sinh k_f d}{K_f k_f \cosh k_f d + h_f \sinh k_f d}$$

(A2.5A-6b)

$$R_{2c} = \frac{K_f k_f}{K_f k_f \cosh k_f d + h_f \sinh k_f d}$$

Note that the subscript  $c$  refers to the continuum model. Note also that the  $R_{1c}$  response function has dimensions of  $\text{hr-ft}^2\text{-}^\circ\text{F/Btu}$  or  $\text{m}^2\text{-}^\circ\text{C/W}$ , while  $R_2$  is dimensionless.

Next we look at the lumped parameter wall. The inside boundary condition is (A2.5A-2); the outside boundary condition is contained in the differential equation for  $T_f$ :

$$C_f \dot{T}_f + \hat{U}_i (T_f - T_S) + \hat{U}_o (T_f - T_A) = 0 \quad (\text{A2.5A-7})$$

Note that  $T_f$  is an "artificial" temperature; it is the lumped temperature which simulates the continuum temperature  $T_f(z,t)$ . It is not a spatial

average of  $T_f(z,t)$ ; thus it cannot be measured or compared to anything in the continuum model or in the real world. It should, however, lead to the correct values of  $T_S$  and other measurable quantities.

Solving (A2.5A-7) and (A2.5A-2) in Fourier transform space, we get

$$\tilde{T}_f(i\omega C_f + \hat{U}_i + \hat{U}_o) = \hat{U}_i \tilde{T}_S + \hat{U}_o \tilde{T}_A \quad (\text{A2.5A-8a})$$

$$-\hat{U}_i \tilde{T}_f + (\hat{h}_f + \hat{U}_i) \tilde{T}_S = \bar{\alpha}_f \tilde{S} + \hat{h}_f \tilde{T}_R \quad (\text{A2.5A-8b})$$

Solving this gives

$$\tilde{T}_S = \frac{\hat{U}_o + \hat{U}_i + i\omega C_f}{(\hat{U}_o + \hat{U}_i + i\omega C_f)(\hat{h}_f + \hat{U}_i) - \hat{U}_i^2} (\hat{h}_f \tilde{T}_R + \alpha_f \tilde{S}) + \frac{\hat{U}_i \hat{U}_o}{(\hat{U}_o + \hat{U}_i + i\omega C_f)(\hat{h}_f + \hat{U}_i) - \hat{U}_i^2} \tilde{T}_A \quad (\text{A2.5A-9a})$$

We can identify the first coefficient as the lumped version of  $R_1$  and the second as the lumped version of  $R_2$ . That is, writing (A2.5A-9a) for a unit area of floor,

$$R_{1\ell} = \frac{U_i + U_o + i\omega \bar{C}_f}{(U_i + U_o + i\omega \bar{C}_f)(h_f + U_i) - U_i^2} \quad (\text{A2.5A-9b})$$

$$R_{2\ell} = \frac{U_i U_o}{(U_i + U_o + i\omega \bar{C}_f)(h_f + U_i) - U_i^2} \quad (\text{A2.5A-9c})$$

where  $\bar{C}_f = C_f/A_f$ .

To sum up, we have derived an expression for the Fourier transform of the inside receiver surface temperature  $\tilde{T}_S$  in terms of the driving functions  $\tilde{T}_A$  and  $\tilde{S}$ . We have done this for both the continuum and the lumped models. We next attempt to find values of  $\hat{U}_o$ ,  $\hat{U}_i$ , and  $C_f$  which

allow the lumped  $R_1$  and  $R_2$  to most closely approximate the continuum functions over the appropriate frequency range.

Matching the response functions.

We illustrate two methods of matching lumped to continuum response functions, one of which is applicable to thin walls, and the other to thick walls (which is discussed in the next section).

The first method is the one used by Robert Sonderegger in his models of Twin Rivers, New Jersey houses; <sup>(1)</sup> it is also a standard approach in system dynamics. <sup>(2)</sup> We look at the two functions  $R_1$  and  $R_2$  as (complex)-frequency-dependent functions and locate their poles and zeroes in the complex plane. The lumped function  $R_{1\ell}$  evidently has its only zero at

$$i\omega = - \frac{U_o + U_i}{\bar{C}_f}$$

and its only pole at

$$i\omega = \frac{1}{\bar{C}_f} \left[ \frac{U_i^2}{h_f + U_i} - (U_o + U_i) \right].$$

$R_{2\ell}$  has no zeroes and the same pole as  $R_{1\ell}$ .

In contrast, the continuum functions have an infinite number of poles and zeroes. We can see these by expanding the numerator and denominator of  $R_{1c}$  and  $R_{2c}$  as infinite products: <sup>(3)</sup>

$$R_1 = \frac{\frac{1}{k_f d} \sinh k_f d}{\frac{K_f}{d} \cosh k_f d + \frac{h_f}{k_f d} \sinh k_f d} = \frac{\prod_{n=1}^{\infty} \left[ 1 + \frac{(k_f d)^2}{n^2 \pi^2} \right]}{\frac{K_f}{d} \left( 1 + \frac{dh_f}{K_f} \right) \prod_{n=1}^{\infty} \left[ 1 + \frac{(k_f d)^2}{p_n^2} \right]}$$

where  $p_n$  is the  $n^{\text{th}}$  solution of  $\tan p_n = -p_n K_f / dh_f$ .

The numerator of  $R_{2c}$  is a constant, while the denominator of  $R_{2c}$  is the same as the denominator of  $R_{1c}$ : thus we get no new poles or zeros from looking at  $R_{2c}$ .

To make use of (A2.5A-10) in choosing  $U_i U_o$  and  $C_f$ , we approximate the exact function  $R_1$  by following three rules:

- 1) The steady-state conductance  $\left( (U_i)^{-1} + (U_o)^{-1} \right)^{-1}$  is equal to the steady-state conductance in the continuum model ( $K_f/d$ ). This ensures that the limit of  $R_1$  and  $R_2$  as  $\omega \rightarrow 0$  is the same in both models.
- 2) The first pole of the continuum  $R_1$  occurs at the same frequency as the only pole of the lumped  $R_1$ .
- 3) The first zero of the continuum  $R_1$  occurs at the same frequency as the only zero of the lumped  $R_1$ .

These conditions say that the truncated product for  $R_1$  will approximate the exact function for  $R_1$ , if they agree for  $\omega = 0$  and if the interesting range of  $\omega$  ( $0 \leq \omega \lesssim 3 \times 2\pi/\text{day}$ ) is smaller than the second pole or zero of the expansion. If  $\omega \ll p_2$  and  $z_2$  we say the wall is "thin." If  $\omega \gtrsim p_2$  and  $z_2$  then the approximation breaks down and we treat the wall as "thick" (see the section on thick walls for numerical definitions of thick and thin).

This can be understood intuitively in the following way: If a function  $F$  of a complex  $\omega$  has an isolated pole at  $\omega = \omega_p$  on the positive imaginary  $\omega$  axis, then a graph  $\log F$  vs.  $\log \omega$  will be approximately constant for  $\omega \ll \omega_p$  and will have a derivative of  $-1$  for  $\omega \gg \omega_p$ . If it has an isolated zero at  $\omega = \omega_z$ , it will be constant for  $\omega \ll \omega_z$  and have a

derivative of +1 for  $\omega \gg \omega_z$ .

If the zero occurs at  $\omega_z$  slightly larger than  $\omega_p$ , the function  $\log F$  will start to decline with the derivative tending to -1 for  $\omega > \omega_p$  but will flatten out again as  $\omega > \omega_z$ . Thus knowing the location of the poles and zeroes of  $F$  will show where  $F(\omega)$  changes from constant behavior. The three conditions above require that  $R_{1\ell}$  and  $R_{1c}$  approach the same constant at  $\omega = 0$  and that they have the same shape for  $\omega$  smaller than the zero of  $R_{1c}$ . For larger  $\omega$ , the additional poles and zeroes of  $R_{1c}$  will allow it to decrease with  $\omega$  while  $R_{1\ell}$  tends to a finite constant.

These three conditions lead to three equations for the lumped parameters:

$$\frac{1}{U_o} + \frac{1}{U_i} = \frac{d}{K_f} \quad (\text{A2.5A-11a})$$

$$-\frac{p_1^2 K_f}{\rho c_p d^2} = \frac{1}{C_f} \left( \frac{U_i^2}{h_f + U_i} - [U_o + U_i] \right) \quad (\text{A2.5A-11b})$$

$$-\frac{\pi^2 K_f}{\rho c_p d^2} = -\frac{1}{C_f} (U_o + U_i) \quad (\text{A2.5A-11c})$$

It should be noted that all poles and zeroes in both the lumped and continuum models fall on the positive imaginary  $\omega$ -axis, and provide that  $\hat{U}_i, \hat{U}_o$  and  $C$  are real. Thus this method gives real-valued lumped parameters.

Solving (A2.5A-11a,b,c) gives the following rather messy expressions for the lumped parameters

$$\hat{U}_i = \frac{\pi^2}{p_1^2} \frac{A_f K_f}{d} + \left( \frac{\pi^2}{p_1^2} - 1 \right) \hat{h}_f \quad (\text{A2.5-12a})$$

$$\hat{U}_o = \frac{\frac{A_f^2 K_f^2}{d} + \left( 1 - \frac{p_1^2}{\pi^2} \right) (K_f A_f) \hat{h}_f}{\left( 1 - \frac{p_1^2}{\pi^2} \right) (K_f A_f + d \hat{h}_f)} \quad (\text{A2.5-12b})$$

$$C_f = \frac{d^2 \rho c_p (\hat{U}_i + \hat{U}_o)}{\pi^2 K_f} = \frac{(U_i + U_o)}{U_f} \frac{1}{\pi^2} C_{fo} \quad (\text{A2.5-12c})$$

where  $C_{fo}$  is the bulk heat capacity  $\rho c_p d A_f$ . Note that these are expressed in terms of the extensive parameters  $\hat{h}_f$  and  $A_f K_f$ , and are proportional to area.

We look at the limiting behavior of these quantities as  $d \rightarrow 0$  (thin wall/floor), and find that

$$U_i \rightarrow 4 \frac{K_f}{d} = 4U_f$$

where  $U_f$  is the steady-state "U"-value of the floor, while

$$U_o \rightarrow 4/3 U_f$$

Thus the wall has the correct static U-value, but 3/4 the resistance is on the outside and only 1/4 on the inside.

$$C_f \rightarrow \frac{16 A_f d \rho c_p}{3\pi^2} = \frac{16}{3\pi^2} C_{fo} \cong 0.540 C_{fo}$$

where  $C_{fo}$  is the static heat capacity of the floor ( $= (d A_f) (\rho c_p)$ ).

For thick walls,  $d \rightarrow \infty$  and  $p_1 \rightarrow \pi$ ,

$$\hat{U}_i \rightarrow \frac{A_f K_f}{d} = U_f A_f \rightarrow 0$$

$$U_i \rightarrow 0$$

$$C_f \rightarrow C_{f0}/\pi^2 \rightarrow \infty$$

Here all the resistance is on the outside and  $C_f$  becomes infinite. This is not realistic behavior, and as we will see, this method breaks down for "large"  $d$ .

How do the "simulated" lumped response functions  $R_{1\ell}$  and  $R_{2\ell}$  compare to the exact continuum functions?  $R_{1c}$  has alternating poles and zeroes along the positive imaginary  $\omega$  axis, while  $R_{1\ell}$  has only one set of poles and zeroes along that axis.  $R_{2c}$  has only poles along the positive imaginary  $\omega$  axis, while  $R_{2\ell}$  has one pole. Thus all four functions start out at  $\omega=0$  with zero slope, and of course,  $R_{1c} = R_{1\ell}$  and  $R_{2c} = R_{2\ell}$  for  $\omega=0$ . As  $\omega$  gets larger, the slope of  $|R|$  vs.  $\omega$  becomes negative.

The continuum  $R_1$  declines steadily with  $\omega$ ; the lumped function, while also monotone decreasing starts to level out for  $\omega$  larger than the zero, and tends to a finite constant and zero slope as  $\omega \rightarrow \infty$ . So the continuum  $R_1$  looks like "" while the lumped function is S-shaped, "". The agreement will be good if the lumped  $R_1$  flattens out at  $\omega \gg 3\omega_0$ .

Both the lumped and continuum  $R_2$ 's begin to decline as  $\omega$  increases, but the slope  $\partial \ln R / \partial \ln \omega$  tends to  $-1$  for the lumped  $R_2$  and continues to become more negative for the continuum  $R_2$ . This occurs because each additional pole of  $R_2$  makes the slope more negative, and  $R_{2c}$  has an infinity of poles where  $R_{2\ell}$  has one. Good agreement will be obtained when the second pole of  $R_2$  occurs for  $|\omega| > 3\omega_0$ .

The agreement between the exact  $R_1$  and  $R_2$  and the simulated functions for 4-inch wood is shown in Fig. 2.8 and Table 2.5. As seen, the agreement is good, despite the fact that 4 inches of wood is not especially thin.

For 2-inch concrete the agreement is even better, as shown in Table 2.4

For thicker walls, the method starts to break down. Tables 2.6 and 2.8 show  $R_1$  and  $R_2$  for two simulation techniques. In the pole-and-zero method  $|R_1|$  is 20% off for  $\omega = 2\pi/\text{day}$  and 50% off for  $\omega = 2\pi/8 \text{ hrs.}$   $|R_2|$  is even less accurate. Finally, for a 20-foot concrete wall (or 20 feet of concrete slab floor plus dry soil) the agreement is very poor (Table A2.5-1).

#### Semi-Infinite and Thick Walls

As we approach the limit of the semi-infinite wall, a large number of poles and zeroes occur at low frequencies, so the pole-and-zero approach is useless. Instead we choose  $\hat{U}_i$  and  $C_f$  ( $\hat{U}_o$  is now zero) in such a way that  $R_1$  is exactly the same in lumped and continuum models at a particular frequency. The frequency at which the match occurs is arbitrary; we choose  $\omega = 2\pi/\text{day}$  for the match frequency because most of the spectrum of the driving functions (sunlight and ambient temperatures) occur at or near this frequency.

We now calculate  $R_1$  for the continuum and lumped models. For the continuum model, the diffusion equation is solved by  $\tilde{T}(\omega, z) = \tilde{T}_s e^{-k_f z}$  for a semi-infinite wall. Then the heat balance equation (A2.5-1) says

$$-A_f K_f k_f \tilde{T}_s + \hat{h}_f \tilde{T}_R + \alpha_f \tilde{S} - \hat{h}_f \tilde{T}_s = 0$$

or

$$\tilde{T}_s = \frac{1}{\hat{h}_f + K_f k_f A_f} (\hat{h}_f \tilde{T}_R + \alpha_f \tilde{S})$$

so

$$R_{1c} = \frac{1}{h_f + K_f k_f}$$

For the lumped model we simply set  $\hat{U}_0 = 0$  in (A2.5A-9) to get

$$R_{1l} = \frac{U_i + i\omega\bar{C}_f}{(U_i + h_f)(U_i + i\omega\bar{C}_f) - U_i^2}$$

Equating these two expressions for  $R_1$ , we get

$$\rho c_p (U_i + i\omega\bar{C}_f) = k_f \bar{C}_f U_i \quad (\text{A2.5A-18})$$

which can also be written as

$$\left(\bar{C}_f - \frac{\rho c_p}{k_f}\right) (U_i - K_f k_f) = \frac{\rho c_p K_f (1-i)}{k_f} \quad (\text{A2.5A-19})$$

This illustrates that with one (complex) equation in two (complex) unknowns we get an indeterminate result. Note that for one specific choice of  $U_i$ , namely,  $U_i = K_f k_f$ , we get  $\bar{C}_f = \infty$  or for one choice of  $\bar{C}_f$  we can get  $U_i = \infty$ .

We note though, that complex  $U_i$  and  $C_f$  values produce poles with nonzero real part, whereas real  $U_i$  and  $C_f$  will require the poles and zeroes to be in the right place. Poles and zeroes off the imaginary axis will produce peaks in  $R_1$  and  $R_2$  which would violate the second law of thermodynamics. Therefore we add two more real equations to get a determinate solution:  $\text{Im}(C_f) = 0$  and  $\text{Im}(U_i) = 0$ . These yield

$$\hat{U}_i = \sqrt{2} A_f K_f |k_f| \quad (\text{A2.5A-20a})$$

$$C_f = \frac{\sqrt{2} \rho c_p A_f}{|k_f|} \quad (\text{A2.5A-20b})$$

This models the semi-infinite slab as being equivalent to a finite-thickness penetration depth. The heat capacity is equal to that of one penetration depth of material (penetration depth =  $\sqrt{2}/k_f$ ), while  $\hat{U}_i$  is equal to the heat transfer coefficient for one-half a penetration depth. (The penetration depth is for a frequency  $\omega = 2\pi/\text{day}$ .)

The semi-infinite model is not useful by itself, since real walls have finite thickness. However, it can be extended to finite walls by letting  $\hat{U}_o$  have nonzero value.

We know in the limit of  $\omega \rightarrow 0$  that the heat transfer coefficient of a thick slab of homogeneous material is  $K_f/d$ . We also know that  $R_1$  and  $R_2$  should have the same steady-state behavior in the simulation as in the exact solution since a significant part of the driving forces occur at zero frequency. Therefore we set the value of  $U_o$  such that  $\left( (\hat{U}_o)^{-1} + (\hat{U}_i)^{-1} \right)^{-1} = A_f K_f / d$  where  $\hat{U}_i$  is obtained from the semi-infinite model.

To reiterate, for thick walls, we set

$$\hat{U}_i = \sqrt{2} A_f K_f |k_f| \quad (\text{A2.5A-20a})$$

$$C_f = \frac{\sqrt{2} \rho c_p A_f}{|k_f|} \quad (\text{A2.5A-20b})$$

$$\hat{U}_o = \left( \left( \frac{A_f K_f}{d} \right)^{-1} - (\hat{U}_i)^{-1} \right)^{-1} \quad (\text{A2.5A-20c})$$

This assures that  $R_{1 \text{ lumped}}$  and  $R_{2 \text{ lumped}}$  have the same limit as  $\omega \rightarrow 0$  as the continuum response functions.

Table 2.9 and Fig. 2.9 for 20-ft (or semi-infinite) concrete walls, and Table 2.8 and Fig. 2.9 for 1½-ft concrete walls illustrate how well the

semi-infinite model simulates the exact model for thick walls. Figure A2.5-1 also illustrates the effect of changing the match frequency from  $2\pi/\text{day} \equiv \omega_0$  to  $3/2 \omega_0$  and  $2\omega_0$ . As shown, the  $R_1$  function does not change drastically. Raising the match frequency improves the fit for  $\omega \sim 2\pi/4$  days but worsens it for higher frequencies ( $> 2\pi/2$  day).

In looking at the response functions one should note that a good fit for  $R_1$  is more important than for  $R_2$ .  $R_1$  describes the wall's reaction to sunlight, while  $R_2$  describes the reaction to ambient temperature. The walls are the primary place where solar heat is collected and stored, thus a 1% error in  $R_1$  for the wall will cause about a 1% error in the room's thermal response to solar gain (look at the form of the coefficient of  $S$  in A2.4-22). In contrast, the walls are in parallel with other channels for heat exchange between the room and outdoors. The other channels (infiltration, conduction through windows) are larger, thus a 1% error in  $R_2$  results in a much-less-than 1% error in room response to ambient temperature (compare the  $T_A$  coefficient in (A2.4-22)).

We have now modeled homogeneous walls in the approximation of thick walls and thin walls. We next show that these two models are sufficient for all thicknesses of walls and present a decision rule for when a wall is thick and when it is thin.

Tables 2.10 and 2.11 compare the lumped parameter values for various thicknesses of wall for wood and concrete. These results are also displayed for concrete in Fig. 2.10. The tables list values of  $U_i$ ,  $U_o$ , and  $\bar{C}_f$  for both pole-and-zero and thick-wall models. It is seen that the two techniques are consistent; that if they yield equal values for one of the parameters ( $\bar{C}_f$ , for example) they produce nearly equal values for

the others. Thus we can divide the range of material thickness into two regions:

- 1) Walls thinner than the thickness at which the two techniques produce equal parameter values,
- 2) Walls thicker than this.

From the tables we see that the dividing point between thick and thin wall is 5 to 6 inches for wood and 10 inches for concrete. This dividing point is logical for another reason. The semi-infinite model shows that only a finite amount of heat capacity is effective no matter how thick the material is. It is unreasonable to simulate a finite-thickness wall using a larger value of  $C_f$  than for a semi-infinite wall.

Thus, a reasonable decision-rule seems to be to use the pole-and-zero approach when it produces a heat capacity less than  $\sqrt{2} \rho c_p A_f / |k_f|$  and to use the thick-wall method otherwise. At the dividing point it should make little difference which method is used since they apparently produce approximately the same results for  $\hat{U}_i$  and  $\hat{U}_o$ .

To show that the two methods should describe all walls, we note that the semi-infinite approximation should work well when the wall is thicker than the penetration depth: when

$$d \geq \sqrt{\frac{2K_f}{\omega_0 \rho c_p}}$$

where  $\omega_0 = 2\pi/\text{day}$ . Sonderegger<sup>1</sup> says that the pole-and-zero approach is within 10% for  $\omega RC < 10$ , where  $C = \rho c_p d$  and  $R = d/K_f$ . This condition says

$$d < \sqrt{\frac{10K_f}{\rho c_p \omega}} .$$

In this case  $\omega$  represents the highest frequency of interest, thus  $\omega \sim 3\omega_0$ . So the pole-and-zero approach works for  $\omega \lesssim \sqrt{3K_f / \rho c_p \omega_0}$ . We conclude that all values of  $d$  can be modeled.

### Insulated Walls

Insulated walls can also be modeled by both the pole-and-zero approach and by the semi-infinite approach. Again, the ranges of validity for these approaches seem to overlap, and the same decision rule (use the pole-and-zero approach whenever it gives a lower value of  $C_f$ ) appears to apply.

### Insulation on the Outside

We next attempt to model two layer walls composed of a continuous material inside (e.g. masonry) and insulation (with  $\rho c_p \rightarrow 0$ ) outside. This exercise is necessary because, as we will show, adding a resistance  $R_o$  to the outside does not simply increase the outside resistance  $1/U_o$  by  $R_o$ .

Suppose that the wall/floor we are modeling has two layers, one a continuum and one a pure resistance. We first assume that the resistance is on the outside, as this is a reasonable design for a passive solar house. In this case the continuum model response functions change while the lumped functions look the same, but have different values for the parameters. The solution to the diffusion equation is given by

$$T_f = A_1 \cosh k_f d(1 - z/d) + B_1 \sinh k_f d(1 - z/d) .$$

But the boundary conditions are

$$-A_f K_f \left. \frac{\partial T_f}{\partial z} \right|_{z=d} = \hat{U}_r (T_{int} - T_A) \quad (A2.5A-21a)$$

$$T_f(z=d) = T_{int} \quad (A2.5A-21b)$$

and

$$A_f K_f \left. \frac{\partial T_f}{\partial z} \right|_{z=0} + \alpha_f S + \hat{h}_f (T_R - T_S) = 0 \quad (A2.5A-1)$$

where  $T_{int}$  is the temperature of the resistance/continuum interface

$\hat{U}_r$  is the heat transfer coefficient of the resistance.

Using the equation for  $T_f$  in these three boundary conditions, and recalling that  $T_S = T_f(z=0)$ , we get

$$A_1 = T_A \frac{U_r \cosh k_f d + \frac{U_r h_f}{K_f k_f} \sinh k_f d}{D} + (h_f T_R + \bar{\alpha}_f S) \frac{1}{D} \quad (A2.5A-22a)$$

$$B_1 = T_A \times \left( - \frac{\frac{U_r h_f}{K_f k_f} \cosh k_f d + U_r \sinh k_f d}{D} \right) + (h_f T_R + \bar{\alpha}_f S) \frac{U_r}{K_f k_f} \frac{1}{D} \quad (A2.5A-22b)$$

where  $D = (U_r + h_f) \cosh k_f d + \left( K_f k_f + \frac{U_r h_f}{K_f k_f} \right) \sinh k_f d$ .

We set  $T_S = T_f(z=0)$  and solve for  $R_1$  and  $R_2$ . The result is

$$R_1 = \frac{\cosh k_f d + \frac{U_r}{K_f k_f} \sinh k_f d}{(U_r + h_f) \cosh k_f d + \left( K_f k_f + \frac{U_r h_f}{K_f k_f} \right) \sinh k_f d} \quad (A2.5A-23a)$$

$$R_2 = \frac{U_r}{(U_r + h_f) \cosh k_f d + K_f k_f \frac{U_r h_f}{K_f K_f} \sinh k_f d} \quad (\text{A2.5A-23b})$$

Note that these reduce to (A2.5A-6a,b) in the limit of  $U_r \rightarrow \infty$  or no insulation. We rewrite these expressions as infinite products

$$\begin{aligned} R_1 &= \frac{\cosh k_f d + \frac{U_r d}{K_f} \left( \frac{1}{k_f d} \sinh k_f d \right)}{(U_r + h_f) \left( \cosh k_f d + \frac{1}{(U_r + h_f)} \left( \frac{K_f}{d} (k_f d) + \frac{U_r h_f d}{K_f} \left( \frac{1}{k_f d} \right) \right) \sinh k_f d \right)} \\ &= \frac{\left( 1 + \frac{U_r d}{K_f} \right) \prod_{n=1}^{\infty} \left( 1 + \frac{(k_f d)^2}{z_n^2} \right)}{(U_r + h_f) \left( 1 + \frac{U_r h_f d}{(U_r + h_f) K_f} \right) \prod_{n=1}^{\infty} \left( 1 + \frac{(k_f d)^2}{p_n^2} \right)} \end{aligned} \quad (\text{A2.5A-24})$$

where  $p_n$  and  $z_n$  are the solutions of

$$\tan z_n = \frac{-z_n K_f}{U_r d} \quad (\text{A2.5A-25a})$$

$$\tan p_n = \frac{p_n (U_r + h_f)}{\frac{K_f}{d} p_n^2 - \frac{U_r h_f d}{K_f}} \quad (\text{A2.5A-25b})$$

As before,  $R_2$  is just a constant divided by the same denominator as  $R_1$ , so it contributes no new poles or zeroes.

Also as before, we require the steady-state conductances to be the same in lumped and continuum models, and that the first pole and zero

be the same. This requires

$$\frac{1}{\hat{U}_o} + \frac{1}{\hat{U}_i} = \frac{d}{A_f K_f} + \frac{1}{\hat{U}_r} \quad (\text{A2.5A-26a})$$

$$-\frac{p_1^2 K_f}{\rho c_p d^2} = \frac{1}{C_f} \left( \frac{\hat{U}_i}{\hat{h}_f + \hat{U}_i} - [\hat{U}_o + \hat{U}_i] \right) \quad (\text{A2.5A-26b})$$

$$-\frac{z_1^2 K_f}{\rho c_p d^2} = -\frac{1}{C_f} (\hat{U}_o + \hat{U}_i) \quad (\text{A2.5A-26c})$$

These are similar in form to (A2.5A-11a,b,c), and have similar solutions:

$$\hat{U}_i = \frac{z_1^2}{p_1^2} \frac{A_f K_f}{d \hat{U}_r + A_f K_f} \hat{U}_r + \left( \frac{z_1^2}{p_1^2} - 1 \right) \hat{h}_f \quad (\text{A2.5A-27a})$$

$$\hat{U}_o = \left( \frac{d}{A_f K_f} + \hat{U}_r^{-1} + \hat{U}_i^{-1} \right)^{-1} \quad (\text{A2.5A-27b})$$

$$C_f = \frac{d^2 \rho c_p (\hat{U}_i + \hat{U}_o)}{z_n^2 K_f} \quad (\text{A2.5A-27c})$$

For the thick wall case, we use the same values (A2.5A-20a,b) for  $\hat{U}_i$  and  $C_f$  and use (A2.5A-26a) to solve for  $\hat{U}_o$ :

$$\hat{U}_o = \left\{ \left( \frac{A_f K_f}{d} \right)^{-1} + \hat{U}_r^{-1} - \hat{U}_i^{-1} \right\}^{-1}$$

For  $d \rightarrow 0$ ,  $p_1 \rightarrow ((\hat{h}_f + \hat{U}_r)/\hat{U}_f)^{1/2}$ , and  $z_1 \rightarrow \pi/2$ , so  $\hat{U}_i \rightarrow \pi^2/4 \hat{U}_f \cong 2.467 \hat{U}_f$ , and  $C_f \rightarrow C_{f0}$ . We note that for the example of thin concrete walls with 1-inch of polyurethane foam insulation board (R-8), that  $C_f \rightarrow 0.95 C_o$  or 95% of the heat capacity of the walls is effective -- in contrast to about 50% for an uninsulated wall. Even for a 6-inch wall, 90% of the heat capacity is effective. (For thicker than 6 inches, the thick-wall model gives larger  $C_f$ .)

We plot the comparison between the continuum  $|R_1|$  and the thick-wall and thin-wall approximations for  $|R_1|$  in Fig. A2.5-2. This figure gives response functions for 8-inch concrete and 4-inch wood, both insulated with R-8 insulation. As seen in the figure, both the thin and thick wall models give reasonable agreement, but the fit is better in both cases with the thick wall model, as expected from the discussion above. The response functions for insulated concrete are also tabulated in Table A2.5-2, and for comparison, response functions for bare concrete are in Table A2.5-3.

### Insulation on the Inside

The purpose of this section is to simulate the adverse effects of carpeting a massive floor. We model a diffusive material with a pure insulator ( $\rho c_p \rightarrow 0$ ) on the inside. Solar absorption takes place at the top surface of the insulator, so the surface heat balance is given by

$$\hat{U}_c(T_{int} - T_S) + \alpha_f S + \hat{h}_f(T_R - T_S) = 0 \quad (A2.5A-28)$$

instead of (A2.5A-1), where  $T_{int}$  is the temperature of the interface between the insulator, and the slab, and  $\hat{U}_c$  is the heat transfer coefficient at the insulator ("carpet").

Then conservation of energy at the interface gives us

$$\hat{U}_c(T_S - T_{int}) = -A_f K_f \left. \frac{\partial T_f}{\partial z} \right|_{z=0} \quad (A2.5A-29)$$

also

$$T_{int} = T_f(z=0) \quad (A2.5A-30a)$$

$$T_A = T_f(z=d) \quad (A2.5A-30b)$$

$T_f$  solves the diffusion equation, and is given by

$$T_f(z) = A_2 \cosh k_f d \left(1 - \frac{z}{d}\right) + B_2 \sinh k_f d \left(1 - \frac{z}{d}\right)$$

Equation (A2.5A-30b) requires that  $A_2 = T_A$ . Using this expression for  $T_f$  in (A2.5A-29) and (30a) gives two equations in two unknowns ( $B_2$  and  $T_S$ ). These are solved by

$$B_2 = T_A \left( \frac{\left( \frac{U_c}{h_f + U_c} - 1 \right) \cosh k_f d - \frac{K_f k_f}{U_c} \sinh k_f d}{D} \right) + (h_f T_R + \bar{\alpha}_f S) \frac{1}{(h_f + U_c) D} \quad (A2.5A-31)$$

where

$$D = \frac{K_f k_f}{U_c} \cosh k_f d + \frac{h_f}{h_f + U_c} \sinh k_f d$$

$$T_S = \frac{K_f k_f}{(h_f + U_c) D} T_A + \frac{\frac{K_f k_f}{U_c} \cosh k_f d + \sinh k_f d}{(h_f + U_c) D} (h_f T_R + \bar{\alpha}_f S) \quad (A2.5A-32)$$

So we conclude that the continuum version of  $R_1$  is given by

$$R_1 = \frac{\cosh k_f d + \frac{U_c d}{K_f} \frac{1}{k_f d} \sinh k_f d}{(h_f + U_c) \left( \cosh k_f d + \frac{h_f U_c d}{K_f (h_f + U_c)} \frac{1}{k_f d} \sinh k_f d \right)}$$

(A2.5A-32)

$$= \frac{\left( 1 + \frac{U_c d}{K_f} \right) \prod_{n=1}^{\infty} \left( 1 + \frac{(k_f d)^2}{z_n^2} \right)}{1 + \frac{h_f U_c d}{(h_f + U_c) K_f} \prod_{n=1}^{\infty} (h_f + U_c) \left( 1 + \frac{(k_f d)^2}{p_n^2} \right)}$$

where  $p_n$  and  $z_n$  are the  $n^{\text{th}}$  solutions to

$$\tan z_n = \frac{-z_n K_f}{U_c d} \tag{A2.5A-32a}$$

$$\tan p_n = \frac{-p_n K_f (h_f + U_c)}{h_f U_c d} \tag{A2.5A-32b}$$

Then the three conditions: 1)  $R_1(\omega = 0)$  is equal for both models,

2) first pole and 3) first zero are at the same  $\omega$  in both models require

$$\hat{U}_o^{-1} + \hat{U}_i^{-1} = \frac{d}{A_f K_f} + \hat{U}_c^{-1} \tag{A2.5A-33a}$$

and (A2.5A-26b,c).

Note that the definitions of  $p_1$  and  $z_1$  have changed from what they were in (A2.5A - 25b,c). Note also that (A2.5A-25 b,c) are the same here as for external insulation because the lumped response functions have

the same form irrespective of whether the real wall is insulated; only the values of  $\hat{U}_i$  and  $\hat{U}_o$  and  $C_f$  change. The results are

$$\hat{U}_i = \frac{z_1^2}{p_1^2} \frac{A_f K_f}{A_f K_f + d \hat{U}_c} \hat{U}_c + \left( \frac{z_1^2}{p_1^2} - 1 \right) \hat{h}_f \quad (\text{A2.5A-34a})$$

$$\hat{U}_o = \frac{\hat{U}_i^2}{\left(1 - \frac{p_1^2}{z_1^2}\right) (\hat{h}_f + \hat{U}_i)} - \hat{U}_i \quad (\text{A2.5A-34b})$$

$$C_f = \frac{d^2 \rho_c p (\hat{U}_i + \hat{U}_o)}{z_1^2 K_f} \quad (\text{A2.5A-34c})$$

These are the same as (A2.5A-26abc) with different values of  $z_1$  and  $p_1$  and with  $\hat{U}_c$  replacing  $\hat{U}_r$ .

A thick-wall model would set  $\hat{U}_i = \left\{ \left( \sqrt{2} A_f K_f |k_f| \right)^{-1} + (\hat{U}_c^{-1}) \right\}^{-1}$

and 
$$\hat{U}_o = \left( \frac{d}{A_f K_f} + \hat{U}_i^{-1} \right)^{-1}. \quad (\text{A2.5A-35})$$

Again, the switch between pole-zero and semi-infinite models is done whenever  $d$  is so large that  $C_{p.z.} > C_{s.i.}$ . Table A2.5-3 shows the response functions for a carpeted concrete floor, compared to a bare floor. Note the drastic difference in shape between the response function for bare concrete, which drops with frequency as  $\omega \gtrsim 2\pi/2$  days, while the carpeted response function is nearly frequency-independent. Results are tabulated in Table A2.5-4.

Interior Walls

Interior walls are modeled similarly to insulated walls. For a partition wall, the diffusion equation is solved by

$T_p = A_3 \cosh k_f d(1-z/d) + B_3 \sinh k_f d(1-z/d)$ . In this case, the wall has two interior surfaces, so the heat flux halfway through the wall is identically zero. Thus  $d$  = the half-thickness of the wall.

For centerline flux =  $-K_f \frac{dT}{dx} \Big|_{x=d}$  to be zero,  $B_3 = 0$ .

Then Eq. (A2.5A-1), the heat balance at the surface, says

$$-A_f K_f k_f A_3 \sinh k_f d + \alpha_f S + \hat{h}_f T_R - \hat{h}_f A_3 \cosh k_f d = 0 \quad (\text{A2.5A-36})$$

so 
$$A_3 = (h_f T_R + \bar{\alpha}_f S) \frac{1}{h_f \cosh k_f d + K_f k_f \sinh k_f d}$$

Then  $T_s = A_2 \cosh k_f d$  so

$$R_1 = \frac{\cosh k_f d}{h_f \cosh k_f d + K_f k_f \sinh k_f d} = \frac{\prod_{n=0}^{\infty} \left( 1 + \frac{(k_f d)^2}{\left(\frac{2n+1}{2}\right)^2 \pi^2} \right)}{h_f \prod_{n=1}^{\infty} \left( 1 + \frac{(k_f d)^2}{p_n^2} \right)} \quad (\text{A2.5A-37})$$

$R_2 = 0$  ,

where  $\tan p_n = \frac{h_f d}{K_f p_n}$  .

For the lumped case,  $R_1 = \frac{U_i + i\omega\bar{C}_f}{(h_f + U_i)(U_i + i\omega\bar{C}_f) - U_i^2}$  as before.

In this case there are only two match conditions, first pole and first zero, since the steady-state conduction is zero. The conditions are:

$$\frac{-p_1^2 K_p}{\rho c_p d^2} = -\frac{1}{C_f} \frac{\hat{h}_f \hat{U}_i}{\hat{h}_f + \hat{U}_i} \quad (\text{A2.5A-38a})$$

$$-\frac{\pi^2 K_f}{4\rho c_p d^2} = -\frac{\hat{U}_i}{C_f} \quad (\text{A2.5A-38b})$$

The solution is:

$$\hat{U}_i = \hat{h}_f \left( \frac{\pi^2}{4p_1^2} - 1 \right) \quad (\text{A2.5A-39a})$$

$$C_f = \frac{4\hat{U}_i \rho c_p d^2}{\pi^2 K_f} \quad (\text{A2.5A-39b})$$

Note that this solution is the same as that for an outside-insulated envelope wall in the limit that  $\hat{U}_r \rightarrow 0$  (perfect insulation).

Example: For 5/8" gypsum board, use ASHRAE values of

$$\begin{aligned}K &= 0.0936 \text{ Btu/hr-ft-}^\circ\text{F} \text{ ,} \\C_p &= 0.26 \text{ Btu/lb-}^\circ\text{F} \text{ (for gypsum);} \\ \rho &= 50 \text{ lbs/ft}^3 \text{ (for gypsum board).}\end{aligned}$$

Then,

$$\begin{aligned}p_1 &= 0.804 \\U_i &= 4.226 \text{ Btu/}^\circ\text{F-hr-ft}^2 = 2.35 U_o \text{ , } (U_o = K/d) \\C &= 0.646 \text{ Btu/}^\circ\text{F-ft}^2 = 0.953 C_o \text{ , } (C_o = \rho c_p d)\end{aligned}$$

Thus 95% of the heat capacity is effective, and  $U_i$  is greater than the conductance of half the thickness of board.

2nd Example: 8" concrete block partitions ( $d = 4"$ );  $K = 0.54 \text{ Btu/hr-ft-}^\circ\text{F}$ ,

$$\begin{aligned}\rho &= 144. \text{ lbs/ft}^2; \quad C_p = 0.156 \text{ Btu/lb-}^\circ\text{F} \\p_1 &= 0.836 \\U_i &= 3.796 \text{ Btu/ft}^2\text{-}^\circ\text{F-hr} = 2.343 U_o \\C &= 7.11 \text{ Btu/ft}^2\text{-}^\circ\text{F} = 0.950 C_o\end{aligned}$$

Again, if  $C > C_{\text{semi-infinite}}$ , we use the thick-wall approximation with  $\hat{U}_o = 0$ . Similar expressions could be derived for a wall/floor insulated on both sides; this is omitted here because we can see no immediate application for the results.

The preceding lumped parameter approximations are more accurate for envelope walls, but can also be used for Trombe walls, as discussed below.

Trombe wall lumped parameters

Modelling a Trombe wall differs from the previous models for envelope walls in three ways. First, the surface heat balance involves the channel air temperature instead of the room temperature. That is, Eq. (A2.3-17) is used as the surface heat balance in place of (A2.3-16) or (2.1). Second, the back-side-of-material boundary condition involves room temperature rather than ambient temperature. Third, the back-side boundary condition is not perfect thermal contact but rather coupling through a film coefficient.

We discuss next how these changes affect the process of evaluating lumped parameters, and how the accuracy of the lumped model is impaired. We focus the discussion on the thick wall model, since most distributed Trombe walls are "thick".

Since the basic equations differ, we must rederive the lumped and distributed response functions from scratch. We first consider the continuum case.

The solution to the diffusion equation is

$$T_w(x,\omega) = A_4 \cosh k_w d(1 - \frac{x}{d}) + B_4 \sinh k_w d(1 - \frac{x}{d}) \quad (A2.5A-39)$$

The outside boundary condition is similar to that given in the "insulation outside" case (A2.5A-21):

$$-A_w K_w \frac{\partial T_w}{\partial x} \Big|_{x=d} = \hat{U}_{wR} (T_{int} - T_R)$$

where  $\hat{U}_{wR}$  is the film coefficient coupling the back of the Trombe wall to the room air (Btu/deg-h)

and  $T_{int}$  is the back surface temperature of the wall

Combining these two equations, and noting that  $T_{int} = T_w(x=d)$ ,  
 we get that  $A_w K_w k_w B_4 = U_{wR} (A_4 - T_R)$  (A2.5A-40)

$$-A_w K_w \left. \frac{\partial T_w}{\partial x} \right|_{x=0} - \alpha_w S + \hat{h}_{wc} (T_{ws} - T_c) = 0 \quad (A2.5A-41)$$

where  $T_{ws}$  is the wall (front) surface temperature  $T_w(x=0)$   
 $\hat{h}_{wc}$  is the heat transfer coefficient between the Trombe  
 wall surface and the air in the channel between that  
 surface and the collector window (See Appendix 2.3  
 $T_c$  is the channel air temperature

The channel air temperature is obtained from (A2.3-20);  
 substituting this and (A2.5A-39) into (A2.5A-41) produces the following  
 equation.

$$\begin{aligned} & A_4 (A_w K_w k_w \sinh k_w d + \hat{U}_a \cosh k_w d) \\ & + B_4 (A_w K_w k_w \cosh k_w d + \hat{U}_a \sinh k_w d) \\ & = \alpha_w S + \frac{\hat{h}_{wc} \hat{U}_{cA}}{\hat{\Sigma}} T_A = \frac{\hat{h}_{wc} \hat{U}_{cR}}{\hat{\Sigma}} T_R \end{aligned}$$

where

$$\begin{aligned} \hat{\Sigma} &= \hat{h}_{wc} + \hat{U}_{cA} + \hat{U}_{cR} \\ \hat{U}_a &= \frac{\hat{h}_{wc} (\hat{U}_{cA} + \hat{U}_{cR})}{\hat{\Sigma}} \end{aligned}$$

and  $\hat{U}_{cA}$  and  $\hat{U}_{cR}$  are described in Appendix 2.3.

Using (A2.5A-40) on this equation, and rearranging terms we find that

$$A_4 = T_R \frac{U_{wR} \cosh k_w d + \frac{U_a U_{wR}}{K_w k_w} \sinh k_w d + \frac{h_{wc} U_{cR}}{\Sigma}}{D} + \bar{\alpha}_w S \frac{1}{D} + T_A \frac{h_{wc} U_{cA}}{\Sigma} \frac{1}{D} \quad (A2.5A-43a)$$

$$B_4 = -T_R \left( \frac{\frac{U_a U_{wR}}{K_w k_w} \cosh k_w d + U_{wR} \sinh k_w d - \frac{h_{wc} U_{cR}}{\Sigma} \frac{U_{wR}}{K_w k_w}}{D} \right) \quad (A2.5A-43b)$$

$$+ \bar{\alpha}_w S + \frac{h_{wc} U_{cA}}{\Sigma} T_A \frac{U_{wR}}{K_w k_w} \frac{1}{D}$$

where  $D = (U_a + U_{wR}) \cosh k_w d + \left( K_w k_w + \frac{U_a U_{wR}}{K_w k_w} \right) \sinh k_w d$ .

We note that  $T_{ws} = A_4 \cosh k_w d + B_4 \sinh k_w d$ ; thus the previous equation shows that

$$T_{ws} = T_R \left( \frac{U_{wR} + \frac{h_{wc} U_{cR}}{\Sigma} \left( \cosh k_w d + \frac{U_{wR}}{K_w k_w} \sinh k_w d \right)}{D} \right) + \left( \bar{\alpha}_w S + \frac{h_{wc} U_{cA}}{\Sigma} T_A \right) \left( \frac{\cosh k_w d + \frac{U_{wR}}{K_w k_w} \sinh k_w d}{D} \right) \quad (A2.5A-44)$$

This can be expressed as linear sums of the response functions  $R_1$  and  $R_2$  for insulated walls given in (A2.5A-23) with  $U_{wR}$  replacing  $U_r$ ,  $U_a$  replacing  $h_f$  and wall subscripts replacing floor subscripts. Written in this fashion, we have

$$T_{ws} = \left( \frac{h_{wc} U_{cR}}{\Sigma} R_1 + R_2 \right) T_R + \left( \bar{\alpha}_w S + \frac{h_{wc} U_{cA}}{\Sigma} T_A \right) R_1 \quad (A2.5A-45)$$

Comparing this with the previous expression

$$T_s = R_1 (hT_R + \bar{\alpha}S) + R_2 T_A$$

we see that the important solar term is still  $R_1 \bar{\alpha}S$  but that the  $T_A$  term now involves  $R_1$  instead of  $R_2$  and the  $T_R$  term involves both.

For the lumped model, we use the differential equation (A2.3-23) for the bulk wall temperature and (A2.3-21) for the surface heat balance to give the following two equations:

$$(i\omega C_w + \hat{U}_{wo} + \hat{U}_{wi}) T_w - \hat{U}_{wi} T_{ws} - \hat{U}_{wo} T_R = 0 \quad (A2.5-46a)$$

$$(\hat{U}_{wi} + \hat{U}_a) T_{ws} = \alpha_w S + \hat{U}_{wi} T_w + \frac{\hat{h}_{wc} \hat{U}_{cA}}{\hat{\Sigma}} T_A + \frac{\hat{h}_{wc} \hat{U}_{cR}}{\hat{\Sigma}} T_R = 0 \quad (A2.5-46b)$$

where  $\hat{U}_{wi}$  and  $\hat{U}_{wo}$  are the inside (absorber surface) and outside (room side) lumped conductances, respectively. Solving for  $T_{ws}$ , we get

$$T_{ws} = \frac{U_{wi} + U_{wo} + i\omega \bar{C}_w}{D} \left( \bar{\alpha}_w S + \frac{h_{wc} U_{cA}}{\Sigma} T_A \right) + \frac{\frac{h_{wc} U_{cR}}{\Sigma} \left( U_{wi} + U_{wo} + i\omega \bar{C}_w \right) + U_{wi} U_{wo}}{D} T_R \quad (A2.5-47)$$

where  $D = \left( U_{wi} + U_{wo} + i\omega \bar{C}_w \right) \left( U_a + U_{wi} \right) - U_{wi}^2$

Using (A2.5A-9) for the lumped response functions, we find that we can express the surface temperature as

$$T_{ws} = R_1 \left( \frac{1}{\alpha_w} S + \frac{h_{wc} U_{cA}}{\Sigma} T_A \right) + \left( \frac{h_{wc} U_{cR}}{\Sigma} R_1 + R_2 \right) T_R \quad (\text{A2.5A-48})$$

in the lumped model; note that this is precisely the same form as that given in (A2.5A-45) for the distributed parameter model. Thus the Trombe wall response functions are just linear combinations of the envelope wall response functions, and the same matching procedures should work, (again using  $U_{wR}$  instead of  $U_r$  and  $U_a$  instead of  $h_f$ ).

However, one new problem crops up. While the response function coupling  $T_{ws}$  with  $T_A$  was relatively unimportant for an envelope wall (being relatively small in magnitude and in parallel with much larger couplings) the Trombe response function coupling  $T_{ws}$  and  $T_R$  is important. This is because the coupling works in both directions; we are concerned with how  $T_{ws}$  affects  $T_R$  as well as how  $T_R$  affects  $T_{ws}$ . (The analogous statement was not true for the envelope wall. We are not concerned with how  $T_R$  affects  $T_A$ ; we know that the influence is infinitesimal).

Thus while for the envelope wall, we were only concerned with the accuracy of  $R_1$ , we are now concerned with the accuracy of  $h_{wc} U_{cR} / \Sigma \times R_1 + R_2$ . Consider the following typical values of the U's for a Trombe wall:  $h_{wc}$ , the coupling from receiver surface to channel air is about 4 Btu/ft<sup>2</sup>-deg F-hr;  $U_{cA}$  linking the channel air to the outside is about 0.75 for double glazing, and  $U_{cR}$ , the convective heat flow to the room, is about 0.35. Then  $h_{wc} U_{cR} / \Sigma \cong 0.275$ , so we look at the comparison between lumped and continuum versions of  $R_2 + 0.275 R_1$ .

Tables A2.5-5 and 6 give  $R_1$  and  $R_2$  in both the continuum and lumped models (both thin wall and thick wall) for 18"-thick concrete with  $U_a = 0.86 \text{ Btu/ft}^2\text{-degF-hr}$  and  $U_{wr} = 1.5$ . The thick-wall lumped parameters are  $U_{wi} = 2.52 \text{ Btu/ft}^2\text{-deg-hr}$   $C = 9.64 \text{ Btu/ft}^2\text{-deg}$  and  $U_{wo} = 0.3281 \text{ Btu/ft}^2\text{-deg-hr}$ . As shown in the table, the lumped  $R_1$  is correct for  $\omega = 2\pi/\text{yr}$ , too large for  $\omega \cong 2\pi/4$  days, correct for  $\omega = 2\pi/\text{day}$  to about  $2\pi/12$  hours, and too large thereafter. Maximum errors are on the order of 20%.  $R_2$  is 1/3 the magnitude of  $R_1$  or less. The lumped  $R_2$  starts off at  $\omega = 0$  equal to the continuum  $R_2$ , but it declines more slowly with  $\omega$ , differing by more than a factor of 2 for  $\omega = 2\pi/2$  days and a factor of 4 for  $\omega = 2\pi/\text{day}$ . The absolute magnitude of error is smaller; about 45% of  $R_2$  ( $\omega = 0$ ) at most and 25% at  $\omega = 2\pi/\text{day}$ . Thus the lumped model will overpredict the amount of energy entering the room via conduction through the Trombe wall at finite frequencies. This overprediction is most important in the range of  $\omega \sim 2\pi/3$  days.

Error in the function " $(R_2 + 0.275 R_1)$ " (compared to its value at  $\omega = 0$ ) is zero for  $\omega = 0$ , 15% for  $\omega = 2\pi/\text{week}$ , rising to 22% for  $\omega = 2\pi/2$  days, then declining to 15% for  $\omega = 2\pi/\text{day}$ , and 9% for  $\omega = 2\pi/8$  hrs and  $2\pi/3$  hrs. This is relatively larger than the error for envelope walls, but still not overwhelmingly large.

It is of interest to compare the thin-wall lumped parameter model with the thick wall model. Using the thin wall model produces  $U_{wi}$  considerably lower than before:  $1.068 \text{ Btu/ft}^2\text{-deg-hr}$  instead of 2.52.  $U_{wo}$  increases to 0.3987, and  $C$  is  $20.53 \text{ Btu/ft}^2\text{-deg}$  instead of 9.64. These lumped parameters produce the values of  $R_1$  and  $R_2$

listed in Table A2.5-6. As seen, the form of these response functions differs greatly from the thick-wall model. The thin  $R_2$  is more accurate, although still twice as large as the continuum  $R_2$  at  $\omega = 2\pi/\text{day}$ . The thin  $R_1$  is slightly more accurate for  $\omega$  small, but reaches its high frequency limit near  $\omega = 2\pi/\text{day}$ , and starts disagreeing with the continuum  $R_1$  by a large factor for  $\omega \sim 2\pi/8$  hrs. Error in the thin-wall function ( $R_2 + 275 R_1$ ) is only 1% for  $\omega = 2\pi/\text{week}$ , 6% for  $\omega = 2\pi/2$  days, 11% for  $\omega = 2\pi/\text{day}$ , but rises to 17% for  $\omega = 2\pi/8$  hrs and 30% for  $\omega = 2\pi/3$  hrs.

All three functions,  $R_1$ ,  $R_2$  and  $R_2 + 275 R_1$  are plotted in Fig. 2.5-4 for both the thin and the thick models. This graph is done on semi-log paper to provide with reader with a better estimate of error magnitudes.

What is happening is that the thick-wall model is calculating the collector surface temperature better, and estimating surface-to-room and surface-to-outdoors heat transfers more accurately, but the thin wall model is doing a better job of calculating heat diffusion through the wall.

It is not surprising that the  $R_2$  function is simulated most poorly, since that function describes heat transfers through the wall. For a very thick wall, the continuum nature of the wall is very important in describing heat flow from one side to the other; no choice of lumped parameters would provide an adequate simulation. To see this, note in Table A2.5-5 that the daily heat transmission is phase delayed by more than  $\pi$ , while the maximum phase delay for any

lumped representation with only one heat capacity is  $\pi/2$ . This phase error can be important, since delaying the daily transmitted sine wave by more than  $\pi$  puts it completely out of phase with the direct solar gain and ambient temperature fluctuations, and allows one to design the response of the building to provide for their cancellation. For the parameters given above, the thick-wall model is preferable, since the two response functions to be simulated are  $R_1$  and  $(R_2 + 0.275 R_1)$ . The thick model simulates  $R_1$  better, and does about equally well on  $(R_2 + 0.275 R_1)$ . However, if the convective coupling from the Trombe wall surface to the room is very weak, the thin-wall model would be preferable (although neither would be especially good: the response of the Trombe wall to ambient temperature - which is large because the solar glazing is a good conductor - would be badly modeled through the inaccuracy of the thin-wall  $R_1$ ).

### Conclusions

We have shown that the thermal performance of continuum walls (or floors) can be approximated (over the range of frequencies from 0 to about  $3 \times 2\pi/\text{day}$ ) by the performance of a sandwich wall composed of a heat capacity  $C_f$  coupled to inside and outside by two heat transfer coefficients  $\hat{U}_i$  and  $\hat{U}_o$ . The equations for the lumped parameters depend on whether the wall/floor is bare or insulated.

In each case, the wall is modeled by one of two methods. If the wall is thin [roughly, if  $d < \sqrt{2}/|k|$ , ( $k = \sqrt{i\omega\rho c_p/K}$ )] the method involves matching the poles and zeros of a response function. If the wall is thick, the method involves setting the lumped response function equal to the continuum function at one frequency, typically  $\omega_o = 2\pi/d$ .

The equations for the lumped parameter are summarized in Table 2.3.

Appendix 2.5A Footnotes

- 1) See Ref. 9, Chapter IV.
- 2) See, for example, Ref. 31, Chapter 3.
- 3) See Ref. 19.

TABLE A2.5-1  
 Response Functions for 20-foot-thick Concrete  
 ( $R_1$  only,  $R_2 \sim 0$ )

$\omega$	Continuum model $R_1$ (hr-ft <sup>2</sup> -°F/Btu)	Thin-wall lumped model $R_1$ (hr-ft <sup>2</sup> -°F/Btu)
0	0.655	0.655
$2\pi/\text{year}$	$0.638 e^{-0.943i}$	$0.641 e^{-0.018i}$
$2\pi/\text{month}$	$0.573 e^{-0.132i}$	$0.632 e^{-0.002i}$
$2\pi/\text{week}$	$0.492 e^{-0.237i}$	$0.632 e^{-0.001i}$
$2\pi/\text{day}$	$0.329 e^{-0.428i}$	0.632
$2\pi/8 \text{ hrs}$	$0.234 e^{-0.535i}$	0.632

TABLE A2.5-2  
 Response Functions for Insulated\* 8-inch Concrete† Block.

$\omega$	Continuum Model		Lumped Model (Thick Wall)	
	$R_1$ (hr-ft <sup>2</sup> -°F/Btu)	$R_2$	$R_1$ (hr-ft <sup>2</sup> -°F/Btu)	$R_2$
0	0.622	0.067	0.622	0.067
2 $\pi$ /month	0.618 e <sup>-0.070i</sup>	0.067 e <sup>-0.144i</sup>	0.620 e <sup>-0.048i</sup>	0.067 e <sup>-0.080i</sup>
2 $\pi$ /week	0.567 e <sup>-0.268i</sup>	0.060 e <sup>-0.578i</sup>	0.594 e <sup>-0.194i</sup>	0.064 e <sup>-0.330i</sup>
2 $\pi$ /2 days	0.391 e <sup>-0.456i</sup>	0.032 e <sup>-1.403i</sup>	0.442 e <sup>-0.428i</sup>	0.043 e <sup>-0.875i</sup>
2 $\pi$ /day	0.316 e <sup>-0.451i</sup>	0.016 e <sup>-1.955i</sup>	0.332 e <sup>-0.411i</sup>	0.026 e <sup>-1.175i</sup>
2 $\pi$ /8 hrs	0.234 e <sup>-0.529i</sup>	0.004 e <sup>+3.082i</sup>	0.261 e <sup>-0.196i</sup>	0.009 e <sup>-1.433i</sup>
2 $\pi$ /3 hrs	0.161 e <sup>-0.614i</sup>	5 × 10 <sup>-4</sup> e <sup>+1.284i</sup>	0.251 e <sup>-0.078i</sup>	0.004 e <sup>-1.519i</sup>

\* Insulation is R-8:  $\frac{1}{U_T} = 8 \frac{\text{ft}^2\text{-hr-}^\circ\text{F}}{\text{Btu}}$

† Assumes  $\rho = 144 \text{ lb/ft}^3$ ,  $c_p = 0.156 \text{ Btu/lb}$ ,  $K = 0.54 \frac{\text{Btu}}{^\circ\text{F-hr-ft}}$ ,  $h = 1.5 \frac{\text{Btu}}{^\circ\text{F-hr-ft}^2}$

TABLE A2.5-3

Response Functions for 8-inch-thick Concrete\* Block.

$\omega$	Continuum Model		Lumped Model (Thin Wall)	
	$R_1$ (hr-ft <sup>2</sup> -°F/Btu)	$R_2$	$R_1$ (hr-ft <sup>2</sup> -°F/Btu)	$R_2$
0	0.433	0.351	0.433	0.351
2 $\pi$ /month	0.433 e <sup>-0.019i</sup>	0.350 e <sup>-0.046i</sup>	0.433 e <sup>-0.015i</sup>	0.351 e <sup>-0.052i</sup>
2 $\pi$ /week	0.430 e <sup>-0.080i</sup>	0.346 e <sup>-0.195i</sup>	0.430 e <sup>-0.065i</sup>	0.348 e <sup>-0.135i</sup>
2 $\pi$ /2 days	0.401 e <sup>-0.256i</sup>	0.315 e <sup>-0.655i</sup>	0.403 e <sup>-0.203i</sup>	0.317 e <sup>-0.443i</sup>
2 $\pi$ /day	0.345 e <sup>-0.407i</sup>	0.249 e <sup>-1.181i</sup>	0.350 e <sup>-0.303i</sup>	0.254 e <sup>-0.759i</sup>
2 $\pi$ /8 hrs	0.233 e <sup>-0.541i</sup>	0.097 e <sup>+3.835i</sup>	0.255 e <sup>-0.259i</sup>	0.116 e <sup>-1.233i</sup>
2 $\pi$ /3 hrs	0.161 e <sup>-0.613i</sup>	0.020 e <sup>+2.052i</sup>	0.229 e <sup>-0.119i</sup>	0.046 e <sup>-1.440i</sup>

\* Assumes ASHRAE materials properties of  $\rho = 144$  lbs/ft<sup>3</sup>,  $c_p = 0.156$  Btu/lb-°F,  
 $K = 0.54$  Btu/°F-hr-ft,  $h = 1.5$  Btu/ft<sup>2</sup>-°F-hr.

TABLE A2.5-4  
 Response Functions for Carpeted\* Concrete<sup>†</sup> Floor, 8-inch-thick.

$\omega$	Continuum Model		Lumped Model (Thin Wall)	
	$R_1$ (hr-ft <sup>2</sup> -°F/Btu)	$R_2$	$R_1$ (hr-ft <sup>2</sup> -°F/Btu)	$R_2$
0	0.525	0.213	0.525	0.213
2 $\pi$ /month	0.525 e <sup>-0.006i</sup>	0.212 e <sup>-0.060i</sup>	0.525 e <sup>-0.005i</sup>	0.212 e <sup>-0.045i</sup>
2 $\pi$ /week	0.523 e <sup>-0.024i</sup>	0.209 e <sup>-0.253i</sup>	0.523 e <sup>-0.023i</sup>	0.209 e <sup>-0.189i</sup>
2 $\pi$ /2 days	0.506 e <sup>-0.062i</sup>	0.175 e <sup>-0.813i</sup>	0.506 e <sup>-0.059i</sup>	0.177 e <sup>-0.591i</sup>
2 $\pi$ /day	0.484 e <sup>-0.070i</sup>	0.124 e <sup>-1.372i</sup>	0.484 e <sup>-0.064i</sup>	0.127 e <sup>-0.930i</sup>
2 $\pi$ /8 hrs	0.461 e <sup>-0.048i</sup>	0.042 e <sup>-2.592i</sup>	0.464 e <sup>-0.033i</sup>	0.051 e <sup>-1.327i</sup>
2 $\pi$ /3 hrs	0.450 e <sup>-0.037i</sup>	0.008 e <sup>+1.949i</sup>	0.461 e <sup>-0.013i</sup>	0.020 e <sup>-1.478i</sup>
$\infty$	0.433	0	0.460	0

\*Assumes carpet is a pure resistance with  $U_c = 0.81$  Btu/ft<sup>2</sup>-°F-hr.  
 (ASHRAE value for carpet with foam pad)

<sup>†</sup>Assumes  $\rho = 144$  lb/ft<sup>3</sup>,  $c_p = 0.156$  Btu/lb-°F,  $K = 0.54$  Btu/°F-hr-ft,  $h = 1.5$  Btu/°F-hr-ft<sup>2</sup>

Table A2.5-5 Response Functions for 1½-Foot-Thick Trombe Wall, Concrete\*

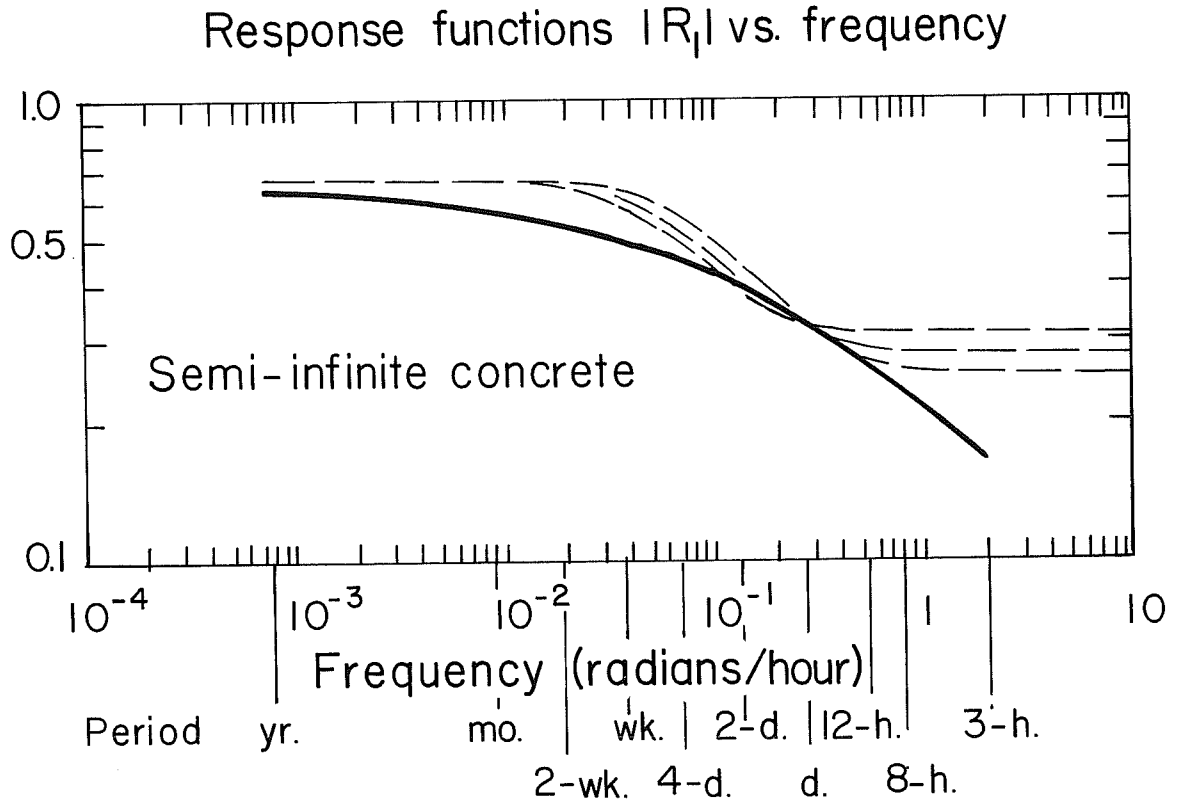
$\omega$	Continuum Model		Lumped Model (Thick Wall)	
	$R_1 \left( \frac{\text{hr-ft}^2-\text{°F}}{\text{Btu}} \right) R_2$	$R_2 + \frac{h_{wc} U}{\Sigma} R_1$	$R_1 \left( \frac{\text{hr-ft}^2-\text{°F}}{\text{Btu}} \right) R_2$	$R_2 + \frac{h_{wc} U}{\Sigma} R_1$
0	.877	.255	.877	.255
2 $\pi$ /month	.865 e <sup>-1.104i</sup>	.249e <sup>-2.292i</sup>	.874e <sup>-0.058i</sup>	.254e <sup>-0.087i</sup>
2 $\pi$ /week	.735e <sup>-0.335i</sup>	.187e <sup>-1.102i</sup>	.828e <sup>-0.232i</sup>	.238e <sup>-0.358i</sup>
2 $\pi$ /4 days	.628e <sup>-0.415i</sup>	.131e <sup>-1.653i</sup>	.751e <sup>-0.362i</sup>	.213e <sup>-0.580i</sup>
2 $\pi$ /2 days	.509e <sup>-0.474i</sup>	.0637e <sup>-2.520i</sup>	.582e <sup>-0.502i</sup>	.155e <sup>-0.919i</sup>
2 $\pi$ /day	.407e <sup>-0.578i</sup>	.022e <sup>+2.603i</sup>	.418e <sup>-0.481i</sup>	.091e <sup>-1.206i</sup>
2 $\pi$ /8 hrs	.268e <sup>-0.624i</sup>	.001e <sup>-0.152i</sup>	.314e <sup>-0.233i</sup>	.032e <sup>-1.444i</sup>
2 $\pi$ /3 hrs	.176e <sup>-0.679i</sup>	~ 0	.299e <sup>-0.092i</sup>	.012e <sup>-1.523i</sup>

\* Assumes Ashrae materials properties and  $U_a = .85 \frac{\text{Btu}}{\text{F-hr-ft}^2}$ ,  $U_r = 1.5 \frac{\text{Btu}}{\text{F-hr-ft}^2}$ .

Table A2.5-6 A Comparison of Two Alternate Lumped Parameter Approaches to the Trombe Wall Response Functions of Table A2.5-5

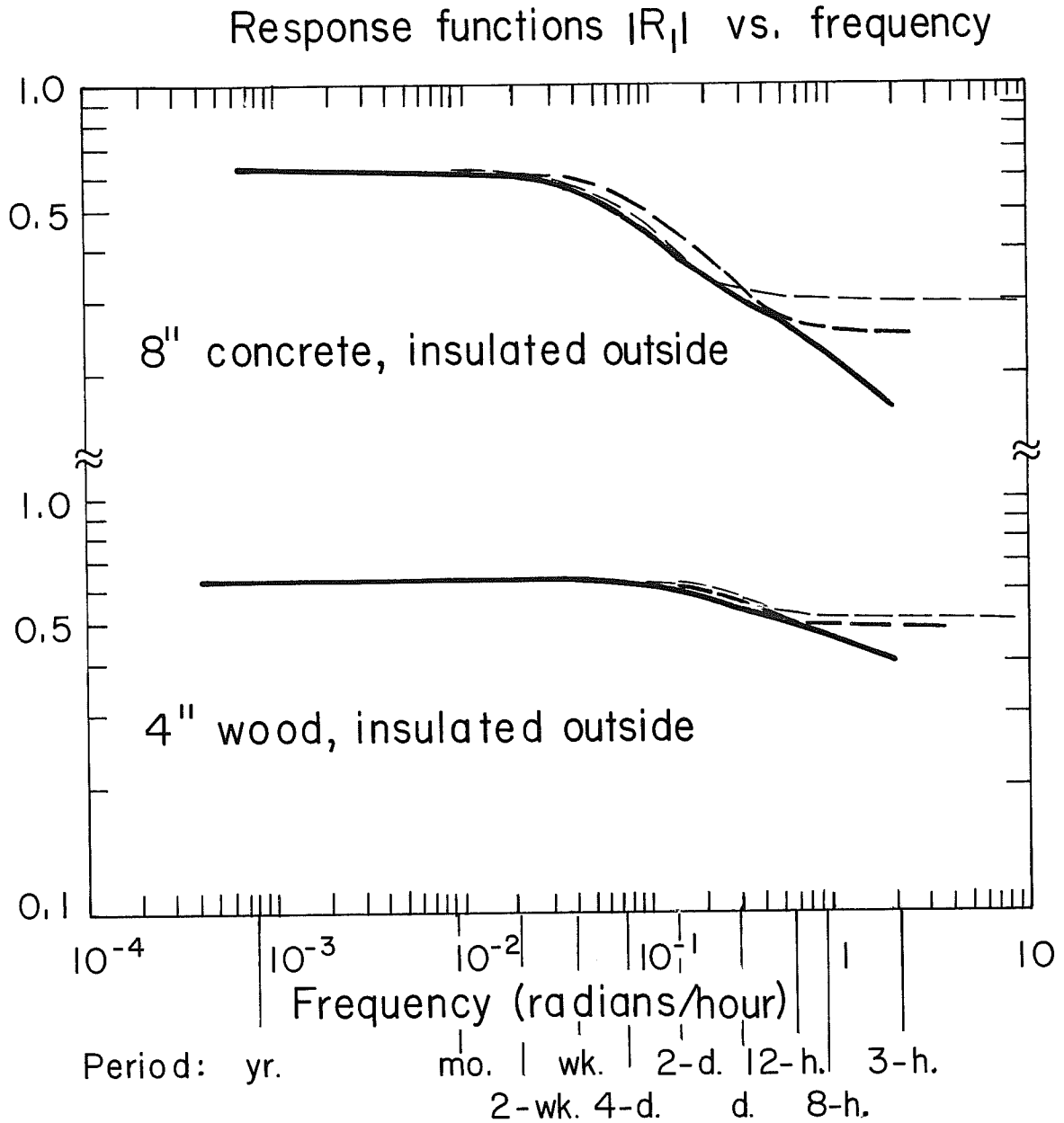
$\omega$	Thin-Wall Model			Naive* Lumped Parameters		
	$R_1 \left( \frac{\text{hr-ft}^2 - ^\circ\text{F}}{\text{Btu}} \right)$	$R_2$	$R_2 + \frac{h_{wc} U_{cR}}{\Sigma} R_1$	$R_1 \left( \frac{\text{hr-ft}^2 - ^\circ\text{F}}{\text{Btu}} \right)$	$R_2$	$R_2 + \frac{h_{wc} U_{cR}}{\Sigma} R_1$
0	.877	.255	.496	.877	.255	.496
2 $\pi$ /month	.865e <sup>-081i</sup>	.249e <sup>-203i</sup>	.486e <sup>-143i</sup>	.856e <sup>-085i</sup>	.241e <sup>-324i</sup>	.473e <sup>-206i</sup>
2 $\pi$ /week	.743e <sup>-240i</sup>	.191e <sup>-722i</sup>	.384e <sup>-473i</sup>	.724e <sup>-156i</sup>	.145e <sup>-963i</sup>	.317e <sup>-492i</sup>
2 $\pi$ /4 days	.647e <sup>-253i</sup>	.139e <sup>-945i</sup>	.298e <sup>-555i</sup>	.675e <sup>-122i</sup>	.094e <sup>-1193i</sup>	.245e <sup>-465i</sup>
2 $\pi$ /2 days	.565e <sup>-186i</sup>	.079e <sup>-1257i</sup>	.205e <sup>-531i</sup>	.648e <sup>-071i</sup>	.050e <sup>-1375i</sup>	.197e <sup>-318i</sup>
2 $\pi$ /day	.533e <sup>-106i</sup>	.041e <sup>-1410i</sup>	.162e <sup>-352i</sup>	.640e <sup>-037i</sup>	.025e <sup>-1472i</sup>	.181e <sup>-174i</sup>
2 $\pi$ /8 hrs	.523e <sup>-037i</sup>	.014e <sup>-1517i</sup>	.146e <sup>-133i</sup>	.637e <sup>-012i</sup>	.008e <sup>-1538i</sup>	.176e <sup>-057i</sup>
2 $\pi$ /3 hrs	.522e <sup>-014i</sup>	.005e <sup>-1531i</sup>	.144e <sup>-049i</sup>	.637e <sup>-005i</sup>	.003e <sup>-1558i</sup>	.175e <sup>-022i</sup>

\* Sets  $U_i = U_o = 2K/d$  and  $\bar{C} = \rho c_p d$



XBL 786 - 1104

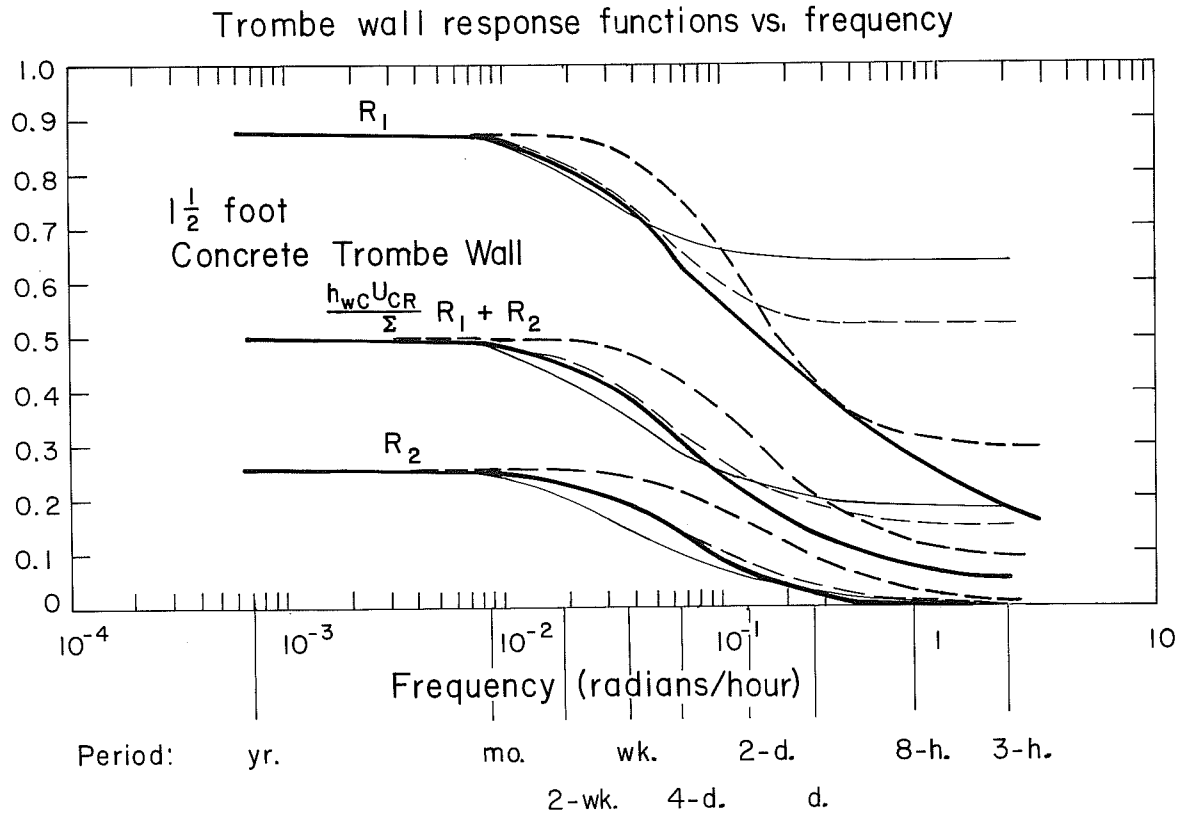
Fig. A2.5-1. Response functions for semi-infinite concrete for three choices of match frequency. The solid line gives the continuum  $|R_1|$  as a function of frequency. The dotted line with the lowest limit for  $\omega \rightarrow \infty$  is derived for a match frequency of  $\omega_0 = 2\pi/\text{day}$ . The other dotted curves give  $|R_1|$  for match frequencies of  $3/2 \omega_0$  and  $2\omega_0$ .



XBL 786-1106A

Fig. A2.5-2. Response functions for insulated materials as a function of frequency.  $\log|R_1|$  is plotted vs  $\log \omega$  for two materials with insulation of  $R-8$  ( $8 \text{ ft}^2\text{-hr-}^\circ\text{F/Btu}$ ) on the outside. The solid lines represent the continuum response functions. The heavy dashed lines describe the thick-wall lumped model response functions, while the light dashed lines represent the thin-wall functions.





XBL 786-1114

Fig. A2.5-4. Response functions for a 1.5-ft-thick Trombe wall. The most important function is  $(h_{wc} U_{CR} / \Sigma) R_1 + R_2$ . In this figure the y-axis is  $|R|$  rather than  $\log|R|$  to better display the magnitude of errors. The heavy solid lines represent the continuum response functions. The heavy dashed lines describe the thick-wall lumped model response functions, while the light dashed lines represent the thin-wall functions. The light solid line describes the naive lumped parameter case where  $U_i = U_o = 2U_w$  and  $C_w = (\rho c_p)_w A_w d$ .

APPENDIX 2.5B: A Comparison Between an Exact Solution and Its  
Lumped Parameter Representation

In this section we develop an exact general solution to the differential equations of Sec. 2.4 which comprise the distributed parameter solution to the passive solar house model. This solution is an extension of the methods described in Ref. 32; it is used here to check the validity of the lumped parameter approach. We find that for the numerical values we tried, there is excellent agreement between the two approaches.

The Fourier solution of Sec. 2.4 is actually the inhomogeneous solution to the differential equations (2.1)(2.2)(2.3) and (2.4) presented in that section. If the boundary conditions of the differential equations change, (for example, the windows are shuttered at night), one must also consider the homogeneous solution of these equations. The complete solution is the sum of the homogeneous solution and the inhomogeneous solution. It is extremely tedious to compute; however, for a few "typical" cases it can be used to check the validity of the lumped parameter approximations.

In this section we consider a simplified passive solar house, similar to the Sonoma house described in Sec. 3.5. The "floor" of this house consists of water-filled bottles, and is an inherently lumped component. Thus we need consider only one diffusion equation for the continuum walls, simplifying the calculations.

The results of the calculation are plotted in Figs. 2.11 and A2.5B-1. Figure 2.11 displays room temperature as a function of time, with the exact solution plotted as a solid line and the lumped-parameter

solution plotted as a dotted line. Figure A2.5B-1 is a similar representation of wall surface temperature.

Both figures show the same pattern of agreement. Except for the first hour or two after the windows are shuttered, both solutions are identical to within 5% or less. During the transition periods, the lumped parameter model shows discontinuous changes in temperature, which occur because the room and wall surface have no heat capacity. The distributed model requires continuous temperatures as a function of time, because the surface layer has finite heat capacity (per unit thickness). However, the sudden difference between the two models decreases quickly as the faster exponential decays in the continuum model go to zero.

The equations for the house to be modelled are presented next. The "floor" subscripts are used to describe the solar collector. The heat balance for the floor surface is (from (2.1) and (2.6))

$$\hat{h}_f (T_{f_s} - T_R) - \alpha_f S(t) + \hat{U}_{fi} (T_{f_s} - T_f) = 0$$

where  $\hat{h}_f$  is heat transfer coefficient from floor surface to room air (Btu/°F-hr, or W/°C)

$T_{f_s}$  is the floor surface temperature (°F or °C)

$\hat{U}_{fi}$  is the heat transfer coefficient from floor surface to floor interior (Btu/°F-hr, or W/°C),

and the other symbols are defined in Sec. 2.2.

The floor is modeled using lumped parameters because the heat capacity of the floor consists of water, which mixes readily.

The floor heat balance, from (2.7) is

$$C_f \dot{T}_f - \hat{U}_{fi} (T_{fs} - T_f) + \hat{U}_{fo} (T_f - T_A) = 0$$

where  $\hat{U}_{fo}$  is the heat transfer coefficient from floor heat storage to the outside (Btu/°F-hr, or W/°C)

$C_f$  is the floor heat capacity.

Since  $\hat{U}_{fi}$  is very large, we simplify the equations by taking their limit as  $\hat{U}_{fi} \rightarrow \infty$ .

We do this by eliminating  $T_f$  between these two equations and then taking the limit; we get a simplified floor heat balance

$$C_f \dot{T}_f = \hat{h}_f (T_R - T_f) + \hat{U}_{fo} (T_A - T_f) + \alpha_f S(t) \quad (A2.5B-1)$$

The wall heat balance is (also from 2.1)

$$\alpha_w S + \hat{h}_w (T_R - T_{ws}) - A_w K_w \left. \frac{\partial T_w}{\partial x} \right|_0 = 0 \quad (A2.5B-2)$$

where  $\hat{h}_w$  is the heat transfer coefficient from room air to the wall surface (Btu/°F-hr, or W/°C)

$T_{ws}$  is the wall surface temperature (°F or °C)

$A_w$  is the wall surface area (ft<sup>2</sup> or m<sup>2</sup>)

$K_w$  is the wall bulk conductivity (Btu/°F-hr-ft, or W/°C-m)

$T_w$  is the wall temperature as a function of  $x$ , the distance into the wall from the interior surface.

Heat flows within the wall are described by the diffusion equation (2.3)

$$\frac{\partial T_w}{\partial t} = \frac{K_w}{(\rho c_p)_w} \frac{\partial^2 T_w}{\partial x^2} \quad (\text{A2.5B-3})$$

The boundary conditions are

$$T_w(0,t) = T_{ws} \quad (\text{A2.5B-4})$$

which is true by definition and

$$T_w(d,t) = T_A \quad (\text{A2.5B-5})$$

where  $d$  is the wall thickness. This equation assumes perfect thermal contact between the outside wall surface and the outside air.

Finally, the room heat balance from (2.2) is (in the limit of  $\hat{U}_{fi} \rightarrow \infty$ )

$$\hat{h}_f(T_R - T_f) + \hat{h}_w(T_R - T_{ws}) + \hat{U}_q(T_R - T_A) = 0 \quad (\text{A2.5B-6})$$

where  $\hat{U}_q$  is the quick heat transfer coefficient for all heat losses except those through the floor and walls (e.g. infiltration, windows) (Btu/°F-hr, or W/°C).

These six equations will be solved under the assumption that  $\hat{U}_{fo}$  changes values between day and night (corresponding to the fact that the window covering the collector is shut at night). Thus the equations will be solved for the day period using the daytime value of  $\hat{U}_{fo}$  and then solved again for the night period, and the two solutions will be joined continuously at sunrise and sunset, as was done in the lumped parameter case (see Section 2.3).

To begin the solution, we note that the two independent variables or driving forces are  $T_A$  and  $S$ , while the two dependent variables are

$T_w(x,t)$  and  $T_f(t)$ .  $T_R$  is an intermediate variable; we eliminate it by solving (A2.5B-6) and (A2.5B-2) for  $T_R$  and  $T_{ws}$ . We first write these two equations as:

$$\hat{h}_w T_R - \hat{h}_w T_{ws} = -\alpha_w S - A_w K_w \left. \frac{\partial T_w}{\partial x} \right|_0$$

$$(\hat{h}_f + \hat{h}_w + \hat{U}_q) T_R - \hat{h}_w T_{ws} = \hat{h}_f T_f + \hat{U}_q T_A$$

We then solve them for  $T_R$  and  $T_w$  as follows:

$$T_R = \frac{1}{(\hat{h}_f + \hat{U}_q)} \left[ \left( \alpha_w S + A_w K_w \left. \frac{\partial T_w}{\partial x} \right|_0 \right) + (\hat{h}_f T_f + \hat{U}_q T_A) \right]$$

$$T_{ws} = \frac{1}{\hat{h}_w (\hat{h}_f + \hat{U}_q)} \left[ \hat{h}_w (\hat{h}_f T_f + \hat{U}_q T_A) + (\hat{h}_f + \hat{h}_w + \hat{U}_q) \left( \alpha_w S + A_w K_w \left. \frac{\partial T_w}{\partial x} \right|_0 \right) \right]$$

Using these results in (A2.5B-1), we get:

$$\dot{T}_f + \Lambda_1 T_f - \Lambda_3 \left. \frac{\partial T_w}{\partial \xi} \right|_0 = \Lambda_2 T_A + AS \quad (A2.5B-7)$$

where we have defined

$$\Lambda_1 = \frac{1}{C_f} \left( \frac{\hat{h}_f \hat{U}_q}{\hat{h}_f + \hat{U}_q} + \hat{U}_{fo} \right)$$

$$\Lambda_2 = \frac{1}{C_f} \left( \hat{U}_{fo} + \frac{\hat{h}_f \hat{U}_q}{\hat{h}_f + \hat{U}_q} \right) = \Lambda_1$$

$$\Lambda_3 = \frac{1}{C_f} \frac{\hat{h}_f A_w K_w}{(\hat{h}_f d + A_w K_w)}$$

$$A_3 = \alpha_f + \frac{\alpha_w \hat{h}_f}{\hat{h}_f + \hat{U}_q}$$

$$\xi = \frac{x}{d}$$

The above solutions for  $T_R$  and  $T_{ws}$  also transform (A2.5B-2) into

$$T_w|_0 - D_1 \frac{\partial T_w}{\partial \xi} - D_2 T_f = D_3 T_A + D_4 S \quad (\text{A2.5B-8})$$

where  $\xi = x/d$  (so  $\xi$  goes from 0 to 1).

and where

$$D_1 = \frac{(\hat{h}_f + \hat{h}_w + \hat{U}_q) A_w K_w}{d \hat{h}_w (\hat{h}_f + \hat{U}_q)}$$

$$D_2 = \frac{\hat{h}_f}{\hat{h}_f + \hat{U}_q}$$

$$D_3 = \frac{\hat{U}_q}{\hat{h}_f + \hat{U}_q}$$

$$D_4 = \frac{(\hat{h}_f + \hat{h}_w + \hat{U}_q) \alpha_w C_f}{(\hat{h}_f + \hat{U}_q) \hat{h}_w}$$

The last two equations (2.5B-7) and (A2.5B-8) will yield the solution. We have already obtained the inhomogeneous solution in Section 2.4 and Appendix 2.4; it was expressed in the form

$$T_R(\omega) = \chi_S(\omega) S(\omega) + \chi_A(\omega) T_A(\omega)$$

where we use the notation  $\chi_S$  and  $\chi_A$  to represent the ratios of building response functions  $B(\omega)/A(\omega)$  and  $C(\omega)/A(\omega)$ . Since we are trying to compare an exact solution to a lumped parameter approximation, we can take only one Fourier component to represent  $S$  and one other (plus a steady-state term) to represent  $T_A$ , as was done in the lumped model solution (Sec. 2.3). As in the lumped model, we set

$$S(t) = \begin{cases} S_1 e^{i\omega_1 t} & 0 \leq t < t_d \\ 0 & t_d \leq t < 24 \text{ hrs} \end{cases}$$

We let  $T_A = \Delta T_A e^{i\omega_0 t}$  where  $\omega_0 = 2\pi/\text{day}$ .

We measure all temperatures with respect to daily average  $T_A$  so that the steady-state part of  $T_A$  is zero.

Thus the inhomogeneous solution is

$$T_R(t) = \begin{cases} \chi_S(\omega_1) S(t) + \chi_A(\omega_0) T_A(t) & 0 \leq t < t_d \\ \chi'_A(\omega_0) T_A(t) & t_d \leq t < 24 \text{ hrs} \end{cases}$$

where  $\chi'_A$  is calculated using nighttime values of the parameters.

We also will need to calculate the inhomogeneous solution for  $T_f$  and  $T_w$ ; these can be obtained from the  $T_R$  solution by calculating the response of each to stimulation by either  $S$  or  $T_A$ . We expect solutions of the form

$$T_f = \chi_{S_f} S(t) + \chi_{A_f} T_A(t)$$

and

$$T_w(x,t) = \chi_{S_w}(x) S(t) + \chi_{A_w} T_A(t)$$

Equations (A2.4-20) and (A2.5-9bc) imply that

$$T_{f\omega} = \left( \frac{\hat{h}_f}{\hat{U}_{fo} + \hat{h}_f + i\omega C_f} \right) T_{R\omega} + \frac{\alpha_f}{\hat{U}_{fo} + \hat{h}_f + i\omega C_f} S + \frac{\hat{U}_{fo}}{\hat{U}_{fo} + \hat{h}_f + i\omega C_f} T_A \quad (\text{A2.5B-9})$$

while (A2.4-12 and 16) (with  $R_e = 0$ ) require that

$$T_{w\omega} = T_{A\omega} \left( - \frac{\hat{h}_w \cosh k_w d + A_w K_w k_w \sinh k_w d}{D} \right) + \frac{\hat{h}_w}{D} T_{R\omega} + \frac{\alpha_w}{D} S_\omega$$

where  $k_w = \sqrt{\frac{i\omega(\rho C_p)_w}{K_w}}$  (A2.5B-10)

and  $D = (A_w K_w k_w \cosh k_w d + \hat{h}_w \sinh k_w d)$

and  $T_w(x) = T_{w\omega} \sinh k_w d (1-\xi) + T_A \cosh k_w d (1-\xi)$  (A2.5B-11)

For response to sunlight, we set  $\omega = \omega_1$  and  $T_A = 0$ ; we note that

$T_{R\omega} = \chi_S S_\omega$  and write

$$T_f = \frac{h_f \chi_S + \alpha_f}{\hat{U}_{fo} + \hat{h}_f + i\omega_1 C_f} S(t) \quad \text{where } \omega \text{ is set to } \omega_1$$

(A2.5B-12a)

$$T_w = \frac{h_w \chi_S + \alpha_w}{D} (\sinh k_w d (1 - \xi)) S(t)$$

For response to ambient temperature, we set  $\omega = \omega_0$ , and re-evaluate  $\chi_A$  and  $k_w$  and get

$$T_f = \frac{\hat{h}_f \chi_A + \hat{U}_{fo}}{\hat{U}_{fo} + \hat{h}_f + i\omega_0 C_f} T_A(t)$$

$$T_w = \left\{ \cosh k_w d (1-\xi) + \frac{h_w \chi_A - (\hat{h}_w \cosh k_w d + A_w K_w k_w \sinh k_w d)}{D} \sinh kd(1-\xi) \right\}$$

(A2.5B-13a)

Thus

$$\chi_{S_f} = \frac{\hat{h}_f \chi_S + \alpha_f}{\hat{U}_{fo} + \hat{h}_f + i\omega_1 C_f} \quad (A2.5B-12b)$$

$$\chi_{S_w} = \frac{h_w \chi_S + \alpha_w}{D} \left( \sinh k_w d (1-\xi) \right)$$

$$\chi_{A_f} = \frac{\hat{h}_f \chi_A + \hat{U}_{fo}}{\hat{U}_{fo} + \hat{h}_f + i\omega_0 C_f} \quad (A2.5B-13b)$$

$$\chi_{A_w} = \cosh k_w d (1-\xi) + \frac{\hat{h}_w \chi_A - \left( \hat{h}_w \cosh k_w d + A_w K_w k_w \sinh k_w d \right)}{D} \sinh k_w d (1-\xi) \quad (A2.5B-13b)$$

### Homogeneous Solution

We look for solutions of the form

$$T_f = T_{fo} e^{-\lambda t}$$

$$T_w(x,t) = T_{wo}(x) e^{-\lambda t}$$

since we are solving a diffusion equation and a lumped parameter heat balance, both of which are solved by a series of (one or infinitely many) decaying exponentials.

The diffusion equation (A2.5B-3) tells us that for this form of solution

$$-\lambda T_{wo} = \frac{K_w}{\rho c_p} \frac{\partial^2 T_w}{\partial x^2} = \Lambda_w \frac{\partial^2 T_w}{\partial \xi^2}$$

where  $\xi = \frac{x}{d}$  and  $\Lambda_w = \frac{\hat{U}_w}{C_w} = \frac{K_w/d}{\rho c_p d}$

Let  $\frac{\lambda}{\Lambda_w} \equiv \ell^2$ ,

then  $T_{w_0}(x) = A_1 e^{i\ell\xi} + A_2 e^{-i\ell\xi}$

The boundary condition (A2.5B-4) that  $T_w(d,t) = T_A = 0$  for the homogeneous solution allows us to write this solution as

$$T_{w_0}(x) = B \sin \ell(1 - \xi)$$

Then the homogeneous solution to (A2.5B-7) and (A2.5B-8) is

$$(-\Lambda_w^2 \ell^2 + \Lambda_1) T_{f_0} + \ell \Lambda_3 B \cos \ell = 0$$

and  $B(\sin \ell + D_1 \ell \cos \ell) - D_2 T_{f_0} = 0$

These two equations can only be true if the determinant of the coefficients  $B$  and  $T_{f_0}$  is zero, so we require

$$(\Lambda_1 - \Lambda_w \ell^2)(\sin \ell + D_1 \ell \cos \ell) + \ell \Lambda_3 D_2 \cos \ell = 0$$

or

$$\ell \cot \ell = \frac{-(\Lambda_1 - \Lambda_w \ell^2)}{(\Lambda_1 - \Lambda_w \ell^2) D_1 + \Lambda_3 D_2} \tag{A2.5B-14}$$

This is the condition under which the exponentially decaying solutions solve the problem. We can therefore look at a series of exponentially decaying functions

$$T_f = T_{f_0} e^{-\Lambda_w \ell_n^2 t} \quad \text{and} \quad T_w(x,t) = B \sin \ell_n (1-\xi) e^{-\Lambda_w \ell_n^2 t}$$

only for those values of  $\ell_n$  which solve (A2.5B-14). There will clearly be an infinite number of such  $\ell$ 's, as shown in Fig. A2.5B-2 where we plot the left-hand side of (2.5-14) as solid lines and the right as a dotted line.

Orthogonality

We next show that we can arrange the homogeneous solutions to this set of equations in a vector format, with one vector for each decay constant  $\lambda_n$ . We will show that the vectors can be chosen in such a way that the solutions at each  $\lambda_n$  are orthogonal to each other.

First, consider the relationship between  $T_f$  and  $T_{ws}$ . We showed that

$$T_{wo}^{(n)}(\xi) = B \sin \lambda_n (1 - \xi)$$

then (A2.5B-8) requires that

$$B = \frac{D_2}{\sin \lambda_n + D_1 \lambda_n \cos \lambda_n} T_{fo} \quad (A2.5B-15a)$$

Thus it is reasonable to look at basis vectors of the form:

$$T_n \left( \begin{pmatrix} 1 \\ \frac{D_2 \sin \lambda_n (1 - \xi)}{\sin \lambda_n + D_1 \lambda_n \cos \lambda_n} \end{pmatrix} \right) \quad (A2.5B-15b)$$

We show next that such basis vectors are orthogonal to each other, and in the process calculate the form of scalar product between two vectors.

Consider two vectors

$$\begin{pmatrix} T_f^{(n)} \\ T_w^{(n)} \end{pmatrix} \quad \text{and} \quad \begin{pmatrix} T_f^{(m)} \\ T_w^{(m)} \end{pmatrix}$$

Then by (A2.5B-3),

$$\frac{\partial^2 T_w^{(n)}}{\partial \xi^2} + \lambda_n^2 T_w^{(n)} = 0 \quad (A2.5B-16)$$

and

$$\frac{\partial^2 T_w^{(m)}}{\partial \xi^2} + \lambda_m^2 T_w^{(m)} = 0$$

Multiply the first of these equations by  $T_w^{(m)}$  and the second by  $T_m^{(n)}$  and subtract:

$$T_w^{(m)} \frac{\partial^2 T_w^{(n)}}{\partial \xi^2} - T_w^{(n)} \frac{\partial^2 T_w^{(m)}}{\partial \xi^2} = 0 \quad (\text{A2.5B-17})$$

The lefthand side of this equation is equal to

$$\frac{\partial}{\partial \xi} \left( T_w^{(m)} \frac{\partial T_w^{(n)}}{\partial \xi} \right) - \frac{\partial}{\partial \xi} \left( T_w^{(n)} \frac{\partial T_w^{(m)}}{\partial \xi} \right)$$

Then (A2.5B-17) can be integrated (by parts) from  $\xi=0$  to  $\xi=1$ ; the result is:

$$\left[ T_w^{(n)}(0) \left( T_w^{(m)} \right)'(0) - T_w^{(m)}(0) \left( T_w^{(n)} \right)'(0) \right] + (\ell_n^2 - \ell_m^2) \int_0^1 d\xi T_w^{(m)} T_w^{(n)} = 0 \quad (\text{A2.5B-18})$$

where we have used the fact that  $T_w(1) = 0$  for any  $m$  or  $n$ , and where ('') signifies  $\frac{\partial}{\partial \xi}$

We next eliminate the term in brackets by using the homogeneous part of equation (A2.5 B-7). We write the equation as

$$(\Lambda_1 - \Lambda_w \ell_m^2) T_f^{(m)} = \Lambda_3 T_w^{(n)'}(0) \quad \text{for the } m^{\text{th}} \text{ vector}$$

and

$$(\Lambda_1 - \Lambda_w \ell_n^2) T_f^{(n)} = \Lambda_3 T_w^{(m)'}(0) \quad \text{for the } n^{\text{th}} \text{ .}$$

Multiply the first by  $T_f^{(n)}$  and the second by  $T_f^{(m)}$  and subtract, to get

$$\Lambda_w (\ell_n^2 - \ell_m^2) T_f^{(n)} T_f^{(m)} = \Lambda_3 (T_f^{(n)} T_w^{(m)'}(0) - T_f^{(m)} T_w^{(n)'}(0)) \quad (\text{A2.5B-19})$$

Then we use (A2.5B-8) in homogeneous form to eliminate  $T_f$  from the righthand side of (A2.5B-19); the result is

$$\Lambda_w (\ell_n^2 - \ell_m^2) T_f^{(n)} T_f^{(m)} = \frac{\Lambda_3}{D_2} \left( T_w^{(n)}(0) T_w^{(m)'}(0) - T_w^{(m)}(0) T_w^{(n)'}(0) \right)$$

This result is used to replace the bracketed term in (A2.5B-18), to yield the final result

$$(\ell_n^2 - \ell_m^2) \left\{ \frac{D_2 \Lambda_w}{\Lambda_3} T_f^{(n)} T_f^{(m)} + \int_0^1 d\xi T_w^{(m)}(\xi) T_w^{(n)}(\xi) \right\} = 0$$

or

$$(\ell_n^2 - \ell_m^2) \left( C_f T_f^{(n)} T_f^{(m)} + C_w \int_0^1 d\xi T_w^{(m)}(\xi) T_w^{(n)}(\xi) \right) = 0 \tag{A2.5B-20}$$

where  $C_w = (\rho c_p)_w d A_w$

This equation gives the form of the scalar product between two basis vectors and proves their orthogonality. The scalar product is in an intuitively appealing form, it is the sum of the product of the  $T_f$  components of each sector, weighted by the floor heat capacity, and the integral of the  $T_w$  components, weighted by the wall heat capacity. This form is analogous to the scalar product derived in Ref. 32.

Orthogonality comes about because (A2.5B-20) requires the product of  $\ell_m^2 - \ell_n^2$  and the scalar product of basic vectors  $m$  and  $n$  to be zero; if  $m \neq n$ , then  $\ell_m^2 - \ell_n^2 \neq 0$  and the scalar product must be zero. This equation also allows us to normalize the vectors, such that the scalar

product of any basis vector with itself is one.

Using the form (A2.5B-15b) for the basis vectors, we find by (A2.5B-20) that the square of basis vector  $n$  is

$$T_n^2 \left( C_f + C_w \frac{D_2^2}{(\sin \ell_n + \ell_n D_1 \cos \ell_n)^2} \left( \frac{1}{2} - \frac{1}{4\ell_n} \sin 2\ell_n \right) \right) \quad (\text{A2.5B-21})$$

Thus the normalization condition requires  $T_n$  to be given by

$$T_n = N_n = \left( C_f + C_w \frac{D_2^2}{(\sin \ell_n + D_1 \ell_n \cos \ell_n)^2} \left( \frac{1}{2} - \frac{1}{4\ell_n} \sin 2\ell_n \right) \right)^{-\frac{1}{2}} \quad (\text{A2.5B-22})$$

where we have renamed  $T_n$  as  $N_n$  as a reminder that it is a normalization factor. Note that in practice, the form of (A2.5B-22) is unsuitable for numerical calculations, since the values of  $\ell_n$  are determined approximately from solving the transcendental equation (A2.5B-14). Since  $(\sin \ell_n + D_1 \ell_n \cos \ell_n) \ll 1$ , the value of  $N_n$  is very sensitive to the computational accuracy in deriving  $\ell_n$ . So in practice, we use (A2.5B-14) to rearrange (A2.5B-22) into the following form:

$$N_n = \left\{ C_f + C_w \frac{1}{2\Lambda_3^2} \left[ E_1^2 + \frac{E_1 E_2}{\ell_n^2} + \left( \frac{E_2}{\ell_n} \right)^2 \right] \right\}^{-\frac{1}{2}} \quad (\text{A2.5B-23})$$

where

$$E_1 = (\Lambda_1 - \Lambda_w \ell_n^2) D_1 + \Lambda_3 D_2$$

$$E_2 = \Lambda_1 - \Lambda_w \ell_n^2$$

This completes the solution to the homogeneous equations. The solution can be written as

$$\sum_{n=1}^{\infty} A_n e^{-\Lambda_w \ell_n^2} \mathcal{J}_n \quad (\text{A2.5B-24})$$

where  $A_n$  are arbitrary constants determined by the boundary conditions, and  $\mathcal{J}_n$  are basis vectors, given by

$$\mathcal{J}_n = N_n \begin{pmatrix} 1 \\ \left( \frac{D_2 \sin \ell_n (1 - \xi)}{\sin \ell_n + D_1 \ell_n \cos \ell_n} \right) \end{pmatrix}$$

Complete Solution

For a house which changes the parameter  $\hat{U}_{fo}$  from day to night, we can write the complete solution for each period as the sum of the homogeneous and inhomogeneous solutions. This solution is

$$\mathcal{J}(t) = \begin{cases} \sum_{n=1}^{\infty} A_n \mathcal{J}_n e^{-\Lambda_w \ell_n^2} + \chi_{\sim S} S(t) + \chi_{\sim A} T_A(t) & 0 \leq t < t_d \\ \sum B_n \mathcal{J}'_n e^{-\Lambda_w \ell_n'^2} + \chi'_{\sim A} T_A(t) & t \leq t_d < 24 \text{ hr} \end{cases} \quad (\text{A2.5B-25})$$

where a primed variable is evaluated using nighttime parameter values and where the  $\chi$ 's are vectors  $\begin{pmatrix} \chi_f \\ \chi_n \end{pmatrix}$  whose form is given by (A2.5B-12 and 13).

To derive a numerical solution, we must solve for the  $A_n$ 's and  $B_n$ 's. The boundary conditions are the same as in the lumped parameter solution: continuity and periodicity. We require that

$$\mathcal{J}(t_d^-) = \mathcal{J}(t_d^+) \quad \text{a)}$$

(A2.5B-26)

$$\mathcal{J}(0^+) = \mathcal{J}(24 \text{ hr}^-) \quad \text{b)}$$

We first use condition (a) and take the scalar product of with both sides of the equation. The result is

$$A_m = \sum_{n=1}^{\infty} O_{mn} B_n e^{-\Lambda_w \ell_n'^2 t_n} + C_m \quad \text{(A2.5B-27)}$$

where

$$O_{mn} = \mathcal{J}_m \cdot \mathcal{J}_n'$$

$$C_m = (\mathcal{J}_m \cdot (\chi_A' - \chi_A)) T_A(0) - (\mathcal{J}_m \cdot \chi_S) S(0)$$

$$t_n = 24 \text{ hrs} - t_d$$

We next use condition (b) and take the scalar product of  $\mathcal{J}_m'$  with both sides of the equation, so that

$$B_m = \sum_{n=1}^{\infty} O_{mn} A_n e^{-\Lambda_w \ell_n'^2 t_d} + D_m \quad \text{(A2.5B-28)}$$

where

$$D_m = (\mathcal{J}_m' \cdot \chi_S) S(t_d) + (\mathcal{J}_m' \cdot (\chi_A - \chi_A')) T_A(t_d)$$

Combining (A.25B-27) and (28), we get expressions for  $A_m$  and  $B_m$ :

$$A_m = \sum_{\substack{n=1 \\ \ell=1}}^{\infty} O_{mn} O_{\ell n} e^{-\Lambda_w(\ell_\ell^2 t_d + \ell_n'^2 t_n)} A_\ell + \sum_{n=1}^{\infty} O_{mn} e^{-\Lambda_w \ell_n'^2 t_n} D_n + C_m \quad (\text{A2.5B-29a})$$

$$B_m = \sum_{\substack{n=1 \\ \ell=1}}^{\infty} O_{nm} O_{n\ell} e^{-\Lambda_w(\ell_n^2 t_d + \ell_\ell'^2 t_n)} B_\ell + \sum_{n=1}^{\infty} O_{mn} e^{-\Lambda_w \ell_n^2 t_d} C_n + D_m \quad (\text{A2.5B-29b})$$

### Evaluation of the Solution

To evaluate (A2.5B-25 and 29) requires the determination of three expressions:  $O_{mn}$ ,  $\chi_s \cdot \mathcal{J}_m$ ,  $\chi_A \cdot \mathcal{J}_m$ . We find equations for these three next; following that we evaluate a numerical solution based on the Sonoma house.

First,  $O_{mn} = \mathcal{J}_m \cdot \mathcal{J}'_n$

$$O_{mn} = N_m N'_n \left( C_f + C_w \int_0^1 d\xi \frac{D_2 D'_2 \sin \ell_m (1-\xi) \sin \ell'_n (1-\xi)}{(\sin \ell_m + D_1 \ell_m \cos \ell_m) (\sin \ell'_m + D'_1 \ell'_m \cos \ell'_m)} \right)$$

Since  $D_2 = D'_2$  and  $D_1 = D'_1$ , we can write this as

$$O_{mn} = N_m N'_n \left( C_f + C_w \frac{D_2 \left( \frac{\sin(\ell_m - \ell'_n)}{\ell_m - \ell'_n} - \frac{\sin(\ell_m + \ell'_n)}{\ell_m + \ell'_n} \right)}{2(\sin \ell_m + D_1 \ell_m \cos \ell_m) (\sin \ell'_n + D_1 \ell_n \cos \ell'_n)} \right)$$

As in the case of the  $N_n$ 's, this expression is very sensitive to small errors in the  $\ell$ 's. It could be expressed elegantly as

$$O_{mn} = N_m N'_n C_f (\Lambda_1 - \Lambda'_1) / \Lambda_w (\ell_m^2 - \ell_n'^2), \text{ but this is even more}$$

sensitive to errors in evaluating the  $\ell$ 's. A more useful form for

numerical work is

$$O_{mn} = N_m N'_n \left( C_f + \frac{C_w}{\Lambda_3^2} \frac{[(\Lambda_1 - \Lambda_w \ell_m^2) D_1 + \Lambda_3 D_2][(\Lambda_1' - \Lambda_w \ell_n'^2) D_1 + \Lambda_3 D_2]}{2 \sin \ell_m \sin \ell_n'} \right) \times \left[ \frac{\sin(\ell_m - \ell_n')}{\ell_m - \ell_n'} - \frac{\sin(\ell_m + \ell_n')}{\ell_m + \ell_n'} \right] \quad (\text{A2.5B-30})$$

Next we evaluate  $\chi_{\sim S} \cdot \mathcal{J}_m$ . From (A2.5B-12) we can write  $\chi_{\sim S}$  as

$$\left( \frac{\hat{h}_f \chi_S + \alpha_f}{\hat{U}_{fo} + \hat{h}_f + i\omega_1 C_f}, \frac{h_w \chi_S + \alpha_w}{D} \left( \sinh k_w d(1-\xi) \right) \right)$$

where D is defined in (A2.5B-10), and

$$k_w = \sqrt{\frac{\omega_1 (\rho C_p)_w}{2K_w}} (1+i)$$

Note that  $K_w$  is evaluated for  $\omega = \omega_1$ . Thus the expression for the scalar product of  $\chi_{\sim S}$  and  $\mathcal{J}_m$  is

$$\chi_{\sim S} \cdot \mathcal{J}_m = N_m \left( C_f \frac{\hat{h}_f \chi_S + \alpha_f}{\hat{U}_{fo} + \hat{h}_f + i\omega_1 C_f} + \frac{C_w D_2 (\chi_S \hat{h}_w + \alpha_w)}{D (\sin \ell_m + D_1 \ell_n \cos \ell_m)} \int_0^1 d\xi \right) \times \left( \frac{e^{i\ell_m(1-\xi)} - e^{-i\ell_m(1-\xi)}}{2i} \right) \left( \frac{e^{\theta(1-\xi)(1+i)} - e^{-\theta(1-\xi)(1+i)}}{2} \right)$$

where  $\theta = \frac{|k_w|}{\sqrt{2}} d = \text{Re}(k_w) \cdot d$ .

For  $\mathcal{J}'_m$  we simply substitute primed values of  $\ell_m$ . The integral, call it I, can be expressed as

$$I = -2e^{-\theta(1+i)} \frac{1}{2i} \left\{ \frac{e^{\theta(1+i)} - e^{i\ell_m}}{\theta + i(\theta - \ell_m)} - \frac{e^{\theta(1+i)} - e^{-i\ell_m}}{\theta + i(\theta + \ell_m)} - e^{2\theta(1+i)} \right. \\ \left. \times \left[ \frac{e^{-\theta(1+i)} - e^{i\ell_n}}{-\theta + i(-\theta - \ell_m)} - \frac{e^{-\theta(1+i)} - e^{-i\ell_m}}{-\theta + i(-\theta + \ell_m)} \right] \right\} \quad (\text{A2.5B-31})$$

Then

$$\chi_{\sim S} \cdot \mathcal{J}_m = N_m \left( C_f \frac{\hat{h}_f \chi_S + \alpha_f}{\hat{U}_{fo} + \hat{h}_f + i\omega_1 C_f} - \frac{C_w (\chi_S \hat{h}_w + \alpha_w) I((\Lambda_1 - \Lambda_w \ell_m^2) D_1 + \Lambda_3 D_2)}{D \Lambda_3 \sin \ell_m} \right) \quad (\text{A2.5B-32})$$

For  $\chi_{\sim S}$  we use the primed values of  $\ell_m$  and  $\Lambda_1$  (as well as I).

The final expression we need is  $\mathcal{J}_m \cdot \chi_A$

This calculation is analogous to the preceding:

$$\mathcal{J}_m \cdot \chi_A = N_m \left( C_f \frac{\hat{h}_f \chi_A + \hat{U}_{fo}}{\hat{h}_f + \hat{U}_{fo} + i\omega_0 C_f} + C_w \frac{J((\Lambda_1 - \Lambda_w \ell_n^2) D_1 + \Lambda_3 D_2)}{D \Lambda_3 \sin \ell_m} \right)$$

where

$$J = \int_0^1 d\xi \frac{(A_w K_w k_w + \hat{h}_w) e^{k_w d} - \chi_A \hat{h}_w}{2 e^{\theta(1+i)} D} \frac{e^{i\ell_m(1-\xi)} - e^{-i\ell_m(1-\xi)}}{2i} \\ \times \left( e^{\theta(1+i)\xi} - e^{2\theta(1+i)} e^{-\theta(1+i)} \right) + \int_0^1 d\xi \frac{e^{i\ell_m(1-\xi)} - e^{-i\ell_m(1-\xi)}}{2i} \\ \times \left( e^{\theta(1+i)(1-\xi)} \right)$$

Note that  $K_e$  and  $\theta_e$  are evaluated for  $\omega = \omega_0$  here.

We also note that

$$J = \frac{-(A_w K_w k_w + \hat{h}_w) e^{k_w d} + \chi_A \hat{h}_w}{2 e^{\theta(1+i)} D} I^* + \frac{1}{2i} e^{\theta(1+i)}$$

$$\times \left[ \frac{e^{-\theta(1+i)} - e^{-i\ell_n}}{\theta + i(\theta - \ell_n)} - \frac{e^{\theta(1+i)} - e^{i\ell_m}}{\theta + i(\theta + \ell_m)} \right]$$

where  $I^*$  is the result of evaluating (A2.5B-31) for  $I$  except setting  $\omega = \omega_0$  in calculating  $\theta$  and  $k_w$ .

### Numerical Solution

We base our model house loosely on the Sonoma house described in Section 3.5. That house contained some internal thermal mass (building materials) which we omit in this section. We make the following assumptions about the building parameters and materials: (Note that since we are comparing two mathematical solutions, the exact accuracy of the parameters is unimportant as long as they are consistent in both solutions):

Floor thermal mass:  $C_f = 3535 \text{ Btu/}^\circ\text{F}$

$$\hat{U}_{fo} = \begin{cases} 400 \text{ Btu/}^\circ\text{F (day)} \\ 30 \text{ Btu/}^\circ\text{F (night)} \end{cases}$$

Floor-to-room film coefficient:  $\hat{h}_f = 75 \text{ Btu/}^\circ\text{F}$

Area of walls:  $A_w = 198 \text{ ft}^2$

Thickness of walls:  $d = \frac{1}{2} \text{ ft}$

Heat capacity of walls:  $\rho C_p = 9 \text{ Btu/}^\circ\text{F ft}^3$

Total heat capacity of walls:  $\rho C_p A_w d = 891 \text{ Btu/}^\circ\text{F}$

Walls-to-room film coefficient:  $\hat{h}_w = 198 \text{ Btu/}^\circ\text{F-hr}$

Quick house heat transfer coefficient:  $\hat{U}_q = \text{Btu/}^\circ\text{F-hr}$

Fraction of sun absorbed on floor:  $\alpha_f = 952$

Fraction of sun absorbed on walls:  $\alpha_w = 048$

Solar gain during the day:  $S_1 e^{i\omega_1 t}$

(where  $S_1 = 65,000 e^{-9903i} \text{ Btu/hr}$ )

Length of day period:  $t_d = 6.5 \text{ hrs}$

Solar frequency:  $\omega_1 = 0.3415$

For simplicity, we take  $\Delta T = 0$ , steady outdoor temperature. The lumped parameters are:

$$\hat{U}_{wi} = 112 \text{ Btu/}^\circ\text{F-hr}$$

$$\hat{U}_{wo} = 35.4 \text{ Btu/}^\circ\text{F-hr}$$

$$C_w = 428 \text{ Btu/}^\circ\text{F}$$

along with the parameters  $\hat{h}_w, \hat{h}_f, C_f, \hat{U}_{fo}, \hat{U}_q$  above.

The lumped parameter solution can be derived as

$$T_w = \begin{cases} -21.1 e^{-0.2119t} + 43.5 e^{-0.1263t} + 12.128 e^{i(\omega_1 t - 2.42)} & \text{day} \\ 6.0 e^{-0.2104(t-t_d)} + 19.7 e^{-0.02312(t-t_d)} & \text{night} \end{cases}$$

$$T_f = \begin{cases} 1.3 e^{-0.2119t} + 84.8 e^{-0.1263t} + 48.38 e^{i(\omega_1 t - 2.2035)} & \text{day} \\ -0.2 e^{-0.2104(t-t_d)} + 86.2 e^{-0.02312(t-t_d)} & \text{night} \end{cases}$$

$$T_R = \begin{cases} -4.8 e^{-0.2119t} + 32.2 e^{-0.1263t} + 18.445 e^{i(\omega_1 t - 1.89)} & \text{day} \\ 1.4 e^{-0.2104(t-t_d)} + 26.7 e^{-0.2312(t-t_d)} & \text{night} \end{cases}$$

In addition, to compare this solution to the exact solution, we wish to derive a wall temperature which is analogous in both solutions.

$T_w$  is not measurable, but the wall surface temperature,  $T_{ws}$ , is.

From (1) we note that

$$T_{ws} = \left( \frac{\alpha_w S + \hat{h}_w T_R + \hat{U}_{wi} T_w}{\hat{h}_w + \hat{U}_{wi}} \right)$$

Thus

$$T_{ws} = \begin{cases} -10.69 e^{-0.2119t} + 36.28 e^{-0.1263t} + 22.480 e^{i(\omega_1(t-4.80\text{hrs}))} & \\ 3.06 e^{-0.2104(t-t_d)} + 24.17 e^{-0.02312(t-t_d)} & \end{cases}$$

We now proceed to calculate the exact solution. From (A2.5B-7 and 8) we evaluate the D's and  $\Lambda$ 's:

$$\begin{aligned}\Lambda_1 &= 0.127 \quad (\text{day}) \\ &\text{or } 0.02257 \quad (\text{night}) \\ \Lambda_3 &= 0.002562 \\ \Lambda_w &= 0.03022\end{aligned}\qquad \begin{aligned}D_1 &= 0.025675 \\ D_2 &= 0.336\end{aligned}$$

We next use (A2.5B-14) for the decay parameters  $\lambda_m$

$$\begin{aligned}\lambda_1 &= 2.0402 & \lambda'_1 &= 0.8743 \\ \lambda_2 &= 2.578 & \lambda'_2 &= 2.56754 \\ \lambda_3 &= 5.34435 & \lambda'_3 &= 5.3441 \\ \lambda_4 &= 8.2937 & \lambda'_4 &\cong \lambda_4 \\ \lambda_5 &= 11.327 & \lambda'_5 &\cong \lambda_5 \\ \lambda_6 &= 14.4015 & \lambda'_6 &\cong \lambda_6\end{aligned}$$

Then we can use (A2.5B-23) to evaluate the normalization factors

$$\begin{aligned}N_1 &= 1.6495 \times 10^{-2} & N'_1 &= 1.6756 \times 10^{-2} \\ N_2 &= 3.243 \times 10^{-3} & N'_2 &= 1.3607 \times 10^{-3} \\ N_3 &= 4.986 \times 10^{-4} & N'_3 &= 4.366 \times 10^{-4} \\ N_4 &= 2.146 \times 10^{-4} & N'_4 &= 2.037 \times 10^{-4} \\ N_5 &= 1.177 \times 10^{-4} & N'_5 &\cong N_5 \\ N_6 &= 7.47 \times 10^{-5} & N'_6 &\cong N_6\end{aligned}$$

Using (A2.5B-30) we calculate the matrix  $(O_{mn})$ . To check the calculation we note that

$$\mathcal{J}'_n = \sum_{m=1}^{\infty} \mathcal{J}_m \cdot \mathcal{J}'_n \mathcal{J}_m = \sum O_{mn} \mathcal{J}_m$$

Also

$$\mathcal{J}_m = \sum_{\ell=1}^{\infty} \mathcal{J}_m \cdot \mathcal{J}'_{\ell} \mathcal{J}'_{\ell} = \sum O_{m\ell} \mathcal{J}'_{\ell}$$

Thus

$$\mathcal{J}'_n = \sum_{m\ell} O_{mn} O_{m\ell} \mathcal{J}'_{\ell}$$

so

$$\sum O_{mn} O_{m\ell} = \delta_{n\ell} .$$

Similarly

$$\sum O_{nm} O_{\ell m} = \delta_{n\ell} .$$

So to check the matrix  $O_{mn}$ , the sums of the squares of its rows and columns should add to one. We calculate that

$O_{mn}$	=	0.99363	-0.11258	-0.00359	. . . .
		0.11295	0.99346	-0.00076	. . . .
		0.0037	0.00038	1.0017	. . . .
		.	.	.	.
		.	.	.	.
		.	.	.	.

We note that the test  $\sum_{n \neq m} O_{mn}^2 = 1$  checks to three significant figures.

We note also that except for  $O_{21}$  and  $O_{12}$ , all off-diagonal terms are very small. All diagonal terms are very close to one. We use these results to calculate  $\chi_{\sim s} \cdot \mathcal{J}_m$  from (A2.5B-31) and (32) using the result [from Appendix 2.4, Eq.(A2.4-22)] that  $\chi_s = 2.872 \times 10^{-4} e^{-0.9747i}$ .

After a very long and tedious calculation (evaluating I in (A2.5B-31) in a 98-step calculation on an HP programmable calculator), we find that

$$\begin{array}{ll}
 \chi_{\sim s} \cdot \mathcal{J}'_1 = 4.546 \times 10^{-2} e^{-1.2173i} ; & \chi_{\sim s} \cdot \mathcal{J}'_1 = 4.573 \times 10^{-2} e^{-1.2151i} \\
 \chi_{\sim s} \cdot \mathcal{J}'_2 = 5.12 \times 10^{-3} e^{-1.0323i} & \chi_{\sim s} \cdot \mathcal{J}'_2 = 9.453 \times 10^{-4} e^{0.4917i} \\
 \chi_{\sim s} \cdot \mathcal{J}'_3 = 1.453 \times 10^{-3} e^{2.7509i} & \chi_{\sim s} \cdot \mathcal{J}'_3 = 1.572 \times 10^{-3} e^{2.6727i} \\
 \chi_{\sim s} \cdot \mathcal{J}'_4 = 8.984 \times 10^{-4} e^{2.9675i} & \chi_{\sim s} \cdot \mathcal{J}'_4 = 9.138 \times 10^{-4} e^{2.9396i} \\
 \chi_{\sim s} \cdot \mathcal{J}'_5 = 5.402 \times 10^{-4} e^{3.0432i} & \chi_{\sim s} \cdot \mathcal{J}'_5 = 5.592 \times 10^{-4} e^{3.0289i} \\
 \chi_{\sim s} \cdot \mathcal{J}'_6 = 3.56 \times 10^{-4} e^{3.0765i} & \chi_{\sim s} \cdot \mathcal{J}'_6 = 3.58 \times 10^{-4} e^{3.0679i}
 \end{array}$$

Thus from (A2.5B-27) and (28), we arrive at the values of  $C_m$  and  $D_m$  that follow and are prepared to solve for the coefficients  $A_m$  and  $B_m$  in (A2.5B-25), which is the objective of the whole exercise:

$C_1 = 1673.2$	$D_1 = 2830.4$
$C_2 = 138.4$	$D_2 = -8.758$
$C_3 = 16.97$	$D_3 = -70.50$
$C_4 = 21.98$	$D_4 = -29.25$
$C_5 = 15.50$	$D_5 = -15.19$
$C_6 = 10.86$	$D_6 = -8.938$

Note that in the last several calculations, the sixth term of the series is not trivially small, so that we are potentially making an error in truncating the series so soon.

Equations (A2.5B-29a) and (29b) supply the equations for  $A_m$  and  $B_m$ . These look like complicated sums, but can be evaluated to a good approximation with only a few terms. We look first at (a):

$$A_m = \sum_{\substack{n=1 \\ \ell=1}}^{\infty} O_{mn} O_{\ell n} e^{-\Lambda_w (\ell^2 t_d + \ell'^2 t_n)} A_{\ell} + \sum_{n=1}^{\infty} O_{mn} e^{-\Lambda_w \ell'^2 t_n} D_n + C_m$$

For  $m = 1$  or  $2$ , only  $O_{11}$ ,  $O_{22}$ ,  $O_{12}$  or  $O_{21}$  can appear in the first sum. Other diagonal elements with  $m$  differing from  $n$  by two or more are essentially zero, while  $O_{KK}$  for  $K \geq 3$  is accompanied by an exponential of  $e^{-\lambda_3 t_d}$  or smaller. Since  $e^{-\lambda_3 t_d} < 0.004$ , such terms are negligibly small. For  $m \geq 3$ , all terms in the sum are small, since terms with exponentials of appreciable size involve  $O_{32}$  or  $O_{31}$  which are very small, while the exponential for the  $O_{33}^2$  term is smaller than  $10^{-8}$ .

In the second sum, the exponential kills off all terms with  $n \geq 3$ . This reduces the sum to two terms for  $m=1$  or  $2$ , and eliminates it for  $m > 3$  (since  $O_{3i} \cong 0$  for  $i \neq 3$ ). Thus we can solve for  $A_m$  as follows:

$$A_1 = O_{11}^2(0.2947)A_1 + O_{11}O_{21}(0.181)A_2 + O_{11}(0.6675)D_1 + C_1$$

where we have dropped:

$O_{12}^2 e^{-\Lambda_w(\lambda_1^2 t_d + \lambda_2^2 t_n)} A_1$	because	$O_{12}^2 \sim 0.01$
	and	$e^{-()} \sim 0.01$
$O_{12}O_{22} e^{-\Lambda_w(\lambda_2^2 t_d + \lambda_2^2 t_n)} A_2$	because	$ O_{12}O_{22}  \sim 0.1$
	and	$e^{-()} \sim 0.01$
$O_{12} e^{-\Lambda_w \lambda_2^2 t_n} D_2$	because	$ O_{12}  \sim 0.1$
	and	$e^{-()} \sim 0.03$
	and	$D_2 \ll D_1$

Thus

$$A_1 = 0.0286 A_2 + 5007$$

Next,

$$A_2 = O_{21}O_{11}(0.2947)A_1 + (O_{21}^2(0.181) + O_{22}^2(0.0083))A_2 + O_{21}(0.6675)D_1 + O_{22}(0.0306)D_2 + C_2$$

where we have dropped

$O_{22}O_{12} e^{-\Lambda_w(\lambda_1^2 t_d + \lambda_2^2 t_d)} A_1$	because	$ O_{12}  \sim 0.1$
		$e^{-()} \sim 0.01$

So,  $A_2 = 0.0312 A_1 + 355$ ,  $A_3 = -0.00238 D_1 + C_3 = 23.96$ ,  
 $A_4 = C_4 = 21.98$ ,  $A_5 = C_5 = 15.50$ ,

$$A_6 = C_6 = 10.86 \quad .$$

Having evaluated the first six terms of the series for  $A_m$ , we return to (A2.5B-29b) for  $B_m$ . As before, most terms in the expression will turn out to be trivially small.

$$B_m = \sum_{\substack{n=1 \\ \ell=1}}^{\infty} O_{nm} O_{n\ell} e^{-\Lambda_w(\ell_n^2 t_d + \ell_\ell'^2 t_n)} B_\ell + \sum_{n=1}^{\infty} O_{nm} e^{-\Lambda_w \ell_n^2 t_d} C_n + D_m$$

Thus

$$B_1 = [O_{11}^2(0.2947) + O_{21}^2(0.181)]B_1 + [O_{11}O_{12}(0.0135) + O_{21}O_{22}(0.0083)]B_2 \\ + O_{11}(0.4414)C_1 + O_{21}(0.2711)C_2 + D_1$$

or

$$B_1 = (-0.00082)B_2 + 5076$$

Next,

$$B_2 = [O_{12}O_{11}(0.2947) + O_{22}O_{21}(0.181)]B_1 + [O_{12}^2(0.0135) + O_{22}^2(0.0083)]B_2 \\ + O_{12}(0.4414)C_1 + O_{22}(0.2711)C_2 + D_2$$

or

$$B_2 = -0.01276 B_1 + -55.1$$

$$B_3 = O_{13}(0.4414)C_1 + D_3 = -73.14$$

$$B_4 = D_4 = -29.25$$

$$B_5 = D_5 = -15.19$$

$$B_6 = D_6 = -8.938$$

Since in the solution (A2.5B-25), we encounter the quantities  $A_n N_n$  rather than just  $A_n$  (the  $N_n$  is part of the expression for  $\mathcal{J}_n$ ) we solve the preceding equation for  $A_n N_n$  and list the results below:

$A_1 N_1 = 82.83^\circ\text{F}$	$B_1 N_1' = 85.06^\circ\text{F}$
$A_2 N_2 = 1.659^\circ\text{F}$	$B_2 N_2' = 0.16311^\circ\text{F}$
$A_3 N_3 = 0.01195^\circ\text{F}$	$B_3 N_3' = 0.03193^\circ\text{F}$
$A_4 N_4 = 0.004717^\circ\text{F}$	$B_4 N_4' = 0.005958^\circ\text{F}$
$A_5 N_5 = 0.001824^\circ\text{F}$	$B_5 N_5' = 0.001788^\circ\text{F}$
$A_6 N_6 = 0.0008^\circ\text{F}$	$B_6 N_6' = -0.0006587^\circ\text{F}$

We next display the numerical values of the exponential decay constants ( $\Lambda_w \lambda_n^2$ )

$\lambda_1 = 0.1258 \text{ hr}^{-1}$	$\lambda_1' = 0.02310 \text{ hr}^{-1}$
$\lambda_2 = 0.2008$	$\lambda_2' = 0.1992$
$\lambda_3 = 0.8631$	$\lambda_3' = 0.8631$
$\lambda_4 = 2.079$	$\lambda_4' = \lambda_4$
$\lambda_5 = 3.877$	$\lambda_5' = \lambda_5$
$\lambda_6 = 6.268$	$\lambda_6' = \lambda_6$

The value of  $\chi_s$  is computed to be

$$\left( 7.290 \times 10^{-4} e^{-1.2144i}, \quad 3.436 \times 10^{-4} e^{-1.6041} \left( \frac{\sinh kd(1-\xi)}{\sinh kd} \right) \right)$$

This completes the numerical work necessary to evaluate a solution which can be compared to the lumped parameter solution. To make the comparison, we shall calculate  $T_f, T_R$  and the wall surface temperature  $T_{ws}$ .

We note that wall surface temperature is  $T_w(0)$ . The room

temperature can be derived from the room heat balance (2):

$$T_R = \frac{1}{\hat{U}_q + \hat{h}_w + \hat{h}_f} (\hat{h}_f T_f + \hat{h}_w T_{ws}) .$$

For the inhomogeneous term, it is simplest to use the relation

$$T_R = \chi_s S e^{i\omega_1 t}$$

where  $\chi_s = 2.782 \times 10^{-4} e^{-0.9747i}$ . Thus we calculate (to the nearest 0.01 degree):

$$T_f = \begin{cases} 82.83 e^{-0.1258t} + 1.66 e^{-0.2008t} + 0.01 e^{-0.8631t} + 47.38 e^{i\omega_1(t-6.46 \text{ hrs})} \\ 85.06 e^{-0.02310(t-t_d)} + -0.16 e^{-0.1992(t-t_d)} + -0.03 e^{-0.8631(t-t_d)} \\ + -0.01 e^{-2.079(t-t_d)} \end{cases}$$

$$T_R = \begin{cases} 32.58 e^{-0.1258t} + -5.22 e^{-0.2008t} + -0.41 e^{-0.8631t} + -0.43 e^{-2.079t} \\ + -0.32 e^{-3.877t} + -0.23 e^{-6.268t} + \dots + 18.67 e^{i\omega_1(t-5.75 \text{ hrs})} \\ 26.47 e^{-0.02310(t-t_d)} + 1.30 e^{-0.1992(t-t_d)} + 1.254 e^{-0.8671(t-t_d)} \\ + 0.58 e^{-2.079(t-t_d)} + 0.37 e^{-3.877(t-t_d)} + 0.19 e^{-6.268(t-t_d)} \\ + \dots \end{cases}$$

$$T_{ws} = \begin{cases} 37.89 e^{-0.1258t} + -11.72 e^{-0.2008t} + -0.88 e^{-0.8631t} + -0.92 e^{-2.079t} \\ + -0.68 e^{-3.877t} + -0.49 e^{-6.268t} + \dots + 22.34 e^{i\omega_1(t-5.18 \text{ hrs})} \\ 24.03 e^{-0.2310(t-t_d)} + 2.83 e^{-0.1992(t-t_d)} + 2.68 e^{-0.8631(t-t_d)} \\ + 1.23 e^{-2.079(t-t_d)} + 0.69 e^{-3.877(t-t_d)} + 0.41 e^{-6.268(t-t_d)} \\ + \dots \end{cases}$$

This concludes the calculation. We discuss its significance next.

### Floor (Storage) Temperature

As is readily apparent from the coefficients, there is excellent agreement between the lumped solution and the exact solution. The inhomogeneous terms agree in phase and are 2% apart in magnitude; in general, the lumped and exact temperatures agree within about 2%. This agreement is to be expected since the floor is an inherently lumped material which is described identically in both models.

Note the fast convergence of the coefficients  $(A_n N_n)$ . This convergence should go as  $1/n^3$  in the limit of large  $n$ . This is because by (A2.5B-29),  $A_n$  goes proportionally to  $\mathcal{J}_m \cdot \chi_s$ , which in turn goes as  $1/n$  (since  $\ell_n \sim n\pi$  for large  $n$  and  $\mathcal{J}_n \cdot \chi_s \propto \ell^2 I/N$  while  $I \propto 1/\ell_n$ ). Thus since  $N_n \propto 1/n^2$ ,  $A_n N_n \propto 1/n^3$ . Thus only the first one or two terms are important.

### Room Temperature

Since the room has no thermal mass, and is coupled to the solar-receiving wall surface, which also has no thermal mass in the lumped model, it can change temperature discontinuously. It does so when the collector panel is opened or closed.

In the real world temperatures do not change discontinuously. Thus we would expect to "round off the corners" on the graph of temperature versus time for the lumped model. When one does this, it looks quite similar to the exact solution (see Fig. 2.11).

This is apparent looking at the equations for room temperature. The coefficients of the slowest decaying exponential at night are 26.7

in the lumped model and 26.5 in the exact solution. The second coefficients are within 1°F of each other, while in the exact solution, the third and higher terms decay to less than ¼°F after 2 hrs. For the daytime period the agreement is also close: about 1% for the first term and 0.4°F, or 10%, for the second. The decay times are also in agreement; the slow decay constants differ by less than 0.1% at night and 0.5% in the day, while the second decay constants agree to within 6%. (The direction of disagreement is also as expected. The lumped model is trying to simulate a series of faster decays with one "fast" term -- so one would expect its decay constants to be faster (larger). This is indeed the result of the calculations.)

The inhomogeneous terms are of comparable magnitude in both models. However, the phase delay in the lumped model is about ½-hour too small. This error in phase lag is to be expected from the response function analysis of the lumped parameter method discussed in Appendix 2.5A.

The reader should note the behavior of the coefficients for room temperature. For both day and night, the coefficients decrease rapidly from  $n=1$  to  $n=2$  or  $3$ , but beyond this the convergence is slow. This result is expected because room temperature is a weighted average of storage temperature and wall-surface temperature; and the latter can be seen by (A2.5B-15), (25), and (22) or (23) to converge only as  $1/n$ . (Note that  $N_n \propto 1/n^2$  but  $D_2 \sin \ell_n / (\sin \ell_n + D_1 \ell_n \cos \ell_n)$  diverges with  $n^2$ ; thus the only convergence of the wall surface temperature is due to the convergence of  $A_n$ . As discussed under floor temperature, this is only a  $1/n$  convergence).

Because of the slow convergence it can be seen that some nontrivial

terms are left out by truncating the series at  $n = 6$ . This can also be seen by calculating  $T_R$  ( $t = 0$  or  $t = t_d$ ) with both the night and day equations. By (A2.5B-26),  $T_R$  should not change discontinuously, but the truncated solution jumps by about  $1^\circ\text{F}$  at sunset and  $1\frac{1}{2}^\circ\text{F}$  at sunrise. These truncation errors die off quickly, of course, since the seventh term decays to 0.01% of its original magnitude after one hour.

#### Wall Surface Temperature

Wall surface temperature is the most sensitive comparison of the lumped parameter model with the exact solution, since it is a variable which refers to the continuum which is being approximated in the lumped model. In the continuum solution, the wall behavior is characterized by a function  $T_w(x,t)$ , while the lumped model approximates this with a wall-storage temperature  $T_w(t)$ , which is *not* the average of  $T_w(x,t)$ , but rather is chosen to simulate the response of the wall surface to excitations.

Wall surface temperature is analogous in both solutions so it is a good variable to compare. In this case the wall surface temperature comparison checks the validity of the thick-wall model for 6"-thick wood.

As in the case with room temperature, the wall surface temperature in the lumped parameter model can change discontinuously because the wall surface has no thermal mass as idealized in that model. Large (5 - 8°F, or 15 - 50%) jumps in wall surface temperature are in fact calculated in the lumped parameter model.

The exact solution requires continuous surface temperature; however the change from day to night generates a series of relatively important,

quickly decaying terms which smooth out the discontinuities, as shown in Fig. A2.5B-1. The figure illustrates the generally good agreement between the lumped model and the exact solution (except at the discontinuities). Agreement is within 5% for all times beyond 2 hours after sunrise or sunset. In addition, the form of the expressions is similar, with the slow decay terms differing by 4½% in the day and by less than .1% at night, and the second terms differing by 10% and 8% respectively. The inhomogeneous terms are alike in magnitude but differ in phase lag by 25 minutes; again, the lumped model has insufficient phase lag.

As discussed in the section on room temperature, convergence is relatively slow ( $\propto 1/n$ ) after the first two terms: this results in truncation errors, for stopping the sum at  $n = 6$ , of up to 3.3°F or 15%.

This section has shown that the thick-wall lumped parameter method agrees with the exact solution to within about 3 to 5%. How does a more simplistic lumped parameter model compare?

Suppose we choose lumped parameter for the wall naively, by simply setting  $\hat{U}_{wi} = \hat{U}_{wo}$  and requiring that the series conductance of the wall still come out to  $\hat{U}_w$  or  $A_w K_w / d$ . We set  $C_w$  equal to the heat capacity of the wall:  $(\rho C_p) d A_w$ . Then numerically,

$$\hat{U}_{wi} = \hat{U}_{wo} = 53.9 \text{ Btu/}^\circ\text{F-hr}$$

and

$$C_w = 891 \text{ Btu/}^\circ\text{F}.$$

We solve the lumped parameter model with these values and all other parameters unchanged; the results for wall surface temperature are:

$$T_{ws} = \begin{cases} 18.42 e^{-0.09891t} + 5.36 e^{-0.1299t} + 25.828 e^{i(\omega_1 t - 4.26 \text{ hrs})} & \text{day} \\ 24.19 e^{-0.2312(t-t_d)} + -0.06 e^{-0.10104(t-t_d)} & \text{night} \end{cases}$$

This solution yields decay constants which are substantially different than either of the previous cases. While the slow night decay constant is unchanged, the faster decay constant differs from the previous models by a factor of 2. The slow day decay constant is 20% smaller than before, while the fast constant is 35% smaller.

The coefficients are also different, with the exception of the dominant night coefficient. The faster night decay has a coefficient of essentially zero in this model, compared to  $3^\circ$  in the previous cases. While before the first two day coefficients had opposite signs, the present model gives coefficients of the same sign. The inhomogeneous term is also different from the previous models, with 15% ( $3.5^\circ\text{F}$ ) larger amplitude and about 1 hour less phase lag than the exact solution.

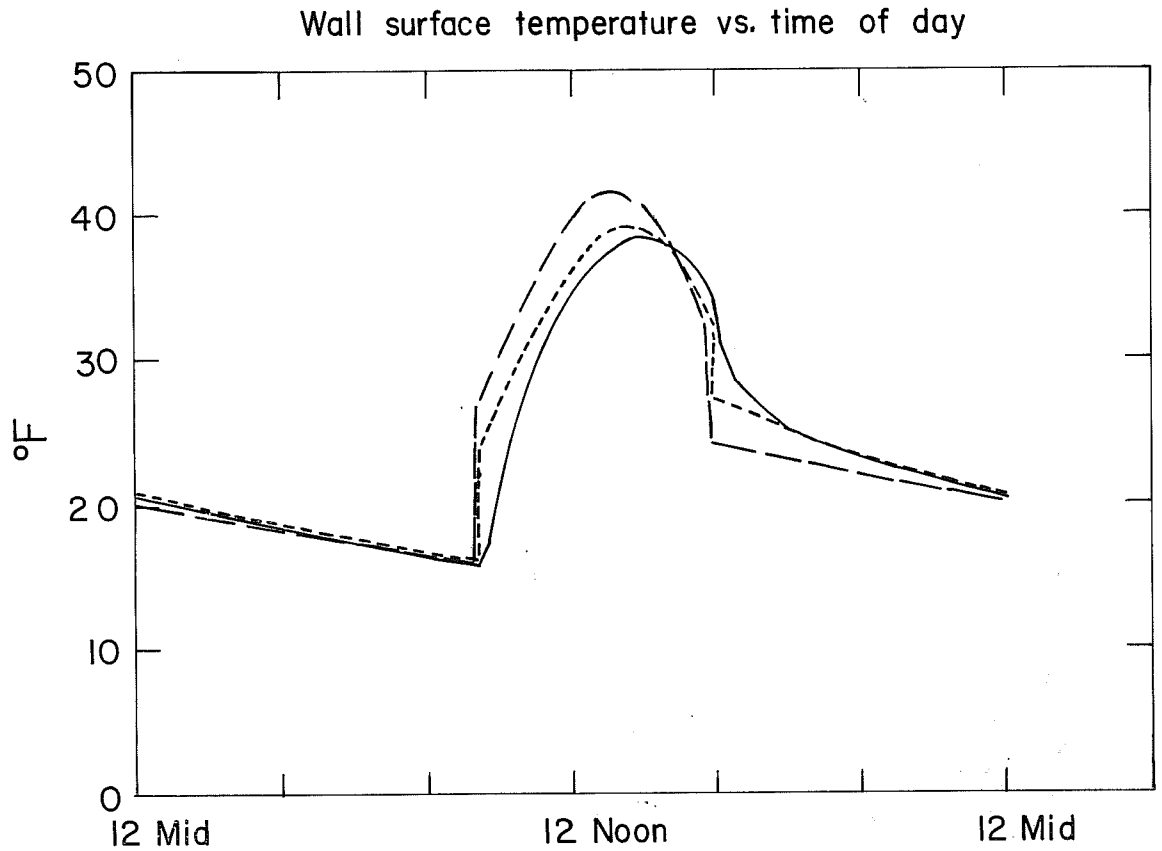
The results of this model compared to the other two are graphed in Fig.A2.5B-1. As seen in the figure, agreement is generally worse than for the "optimal" lumped parameters. All three models converge on the same temperature in the early morning hours, but the rest of the time the "dumb" lumped parameter model disagrees with the exact model by two or three times as much as the "optimal" lumped parameter model (and in the same direction). That is, during the day, the "dumb" lumped parameter model is off by 10 to 14% (not counting the first 2 hours), while during the night, the agreement is within 8%, improving to better than 3% by midnight. The "dumb" lumped parameter model also has larger day/night discontinuities of  $10.7^\circ$  (or 65%) at sunrise and  $6.5^\circ\text{F}$  (27%) at sunset.

It should be recalled at this point that any lumped parameter representation which has  $\hat{U}_{wo}$  and  $\hat{U}_{wi}$  adding in series to the correct wall U-value will get the steady-state response of the wall-surface right -- what we are comparing is the difference in modeling the daily (and faster) fluctuations.

### Conclusions

This section has shown how the simplified equations of heat transfer for a passive solar house can be solved exactly, even when house parameters change as a function of time. This calculation is extremely time-consuming and tedious to evaluate compared to the other calculations described in this paper, even for the simplified case of one distributed material ("wall") and one physically lumped material ("floor").

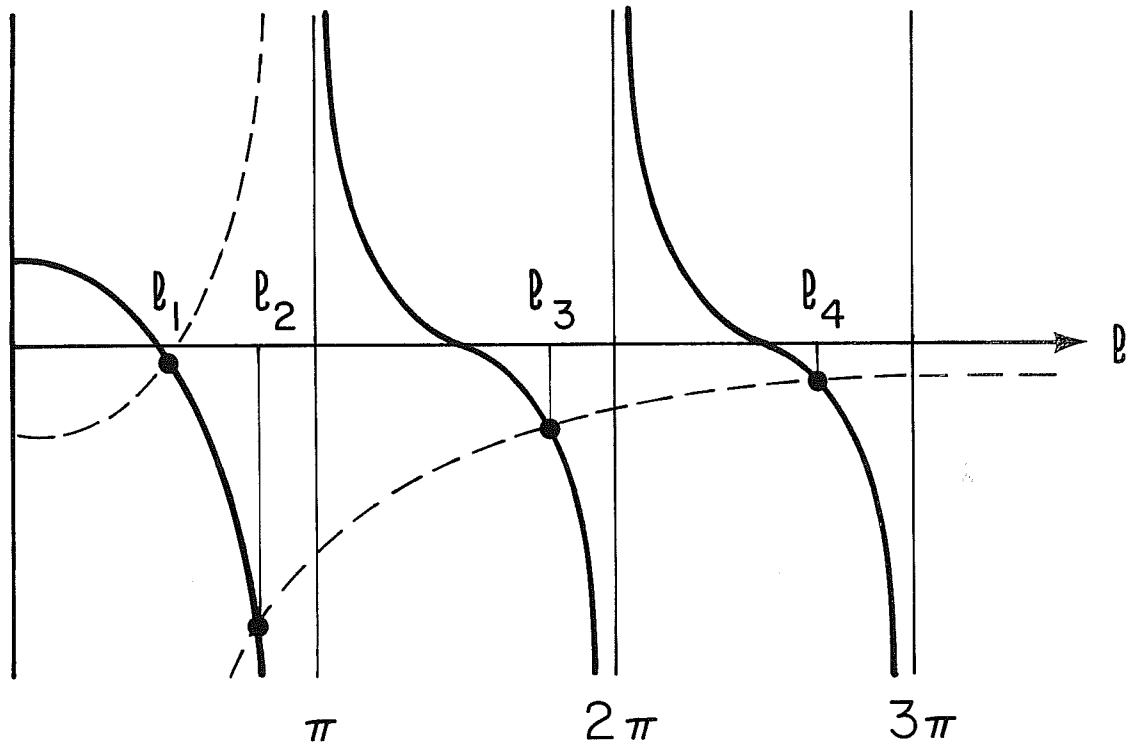
For the numerical example developed in this section, the lumped parameter approximation agrees reasonably well with the exact solution. Further numerical examples could test the range of validity of the lumped parameter models. A more demanding test would involve a smaller lumped heat capacity and a continuum wall which was further into the "thick wall" domain. Alternately, one might extend the solution to cover two distributed materials, so that the basic vectors would look like  $(T_f(y,t), T_w(x,t))$ .



XBL 786- 1102

Fig. A2.5B-1. Comparison of wall-surface temperature elevations for the lumped parameter model and an exact solution of the problem. The solid line represents the exact solution, while the light dotted line describes the lumped parameter approximation. The heavy dashed line describes the performance of a naive lumped parameter approach.

### Graphical solution of Eq. A2.5B-14



XBL 786-1111

Fig. A2.5B-2. A graphical solution of Eq. A2.5B-14. The left-hand side is graphed with solid lines and the right is shown by dashed lines. Intersections of these lines represent solutions; they are labelled  $\rho_1, \rho_2, \dots$ .